

«Dynamics of Hydrogen Bonds in the Melt-State of Supramolecular Polymers»

Dissertation

zur Erlangung des Doktorgrades der Naturwissenschaften (Dr. rer. nat.)

der

Naturwissenschaftlichen Fakultät II

der Martin-Luther-Universität Halle-Wittenberg,

vorgelegt

von Florian Herbst

geb. am 10.12.1984 in Halle (Saale)

Gutachter:

1. Prof. Dr. Wolfgang H. Binder
2. Prof. Dr. Laurent Bouteiller

Datum der Verteidigung: 19.02.2014

“Don’t ask the barber whether you need a haircut”

Daniel S. Greenberg

Contents

1. Introduction	1
2. Aim of the work	21
3. Concept	22
4. General part	24
4.1. Synthesis of azide-functionalized poly(isobutylene)s	24
4.2. Synthesis of functionalized PIBs bearing hydrogen bonding moieties via the azide/alkyne-“click” reaction	26
4.4. Synthesis of azide-functionalized poly(<i>n</i> -butyl acrylate)s	31
4.5. Synthesis of functionalized PnBAs bearing hydrogen bonding moieties via the azide/alkyne-“click” reaction	33
4.6. “Capped” thymine-functionalized poly(<i>n</i> -butyl acrylate)s – PnBA-THY ₂ -Cap	36
4.7. Investigation of the association/aggregation of hydrogen bonding moieties in supramolecular polymers	36
4.7.1. Association of hydrogen bonding motifs in solution	41
4.7.2. Association/aggregation of hydrogen bonding motifs in the melt state	42
4.7.3. Influence of the molecular weight for PIB and the THY-DAT-system	42
4.7.4. Time-temperature superposition (TTS)	48
4.7.5. Effect of the functionality on PIB and the THY-DAT-system	50
4.7.6. Effect of the polarity of the matrix on bifunctional polymers and the THY-DAT-system	53
4.7.7. Effect of the molecular weight for PIB and the BA-HW-system	57
4.7.8. Effect of the functionality on PIB and the BA-HW-system	64
4.7.9. Effect of the hydrogen bonding group on bifunctional PIBs	66
4.7.10 Influence of the molecular weight on bifunctional PIBs bearing barbituric acid (BA) groups	67
4.8. Self-healing studies of bifunctional PIBs bearing barbituric acid (BA) groups	72
5. Experimental Part	75
5.1. Chemicals	75
5.2. Materials	75
5.3. Methods	76
5.4. Synthesis	80
5.4.1. 1,3,5-Triethyl-5-(pent-4-yn-1-yl)pyrimidine-2,4,6(1 <i>H</i> ,3 <i>H</i> ,5 <i>H</i>)-trione (23)	80
5.4.2. 6-(4-Ethynylbenzyl)-1,3,5-triazine-2,4-diamine – variety 1	81
5.4.3. 2-(4-(3-Hydroxy-3-methylbut-1-yn-1-yl)phenyl)acetonitrile	82
5.4.4. 6-(4-Ethynylbenzyl)-1,3,5-triazine-2,4-diamine – variety 2	83
5.4.5. 2-(4-(Prop-2-yn-1-yloxy)phenyl)acetonitrile	84
5.4.6. 6-(4-(Prop-2-yn-1-yloxy)benzyl)-1,3,5-triazine-2,4-diamine	84
5.4.7. 2,6-Diaminotriazine-functionalized PIBs (PIB-DAT)	85
5.4.8. Barbituric acid-functionalized PIBs (PIB-BA) and PIB-BA-Cap	87
5.4.8. Hamilton wedge-functionalized PIBs (PIB-HW)	89
5.4.9. Pyrene-functionalized PIB (PIB-Pyrene)	91
5.4.10. Thymine-functionalized PnBAs (PnBA-THY)	92

Contents

5.4.11. “Capped” thymine-functionalized PnBAs (PnBA-THY-Cap)	94
5.4.12. 2,6-Diaminotriazine-functionalized PnBAs (PnBA-DAT)	95
5.4.13. Barbituric acid-functionalized PnBAs (PnBA-BA)	97
5.4.14. Hamilton wedge-functionalized PnBAs (PnBA-HW)	99
6.1. Summary	102
7. Literature	108
8. Appendix	I
8.1. Synthesis	I
8.1. NMR-titration experiments	VIII
8.2. Evaluation of MALDI-TOF-MS measurements & detailed synthesis tables	IX
8.3. List of publications	XXVII

Abbreviations

ATMS	- allyltrimethylsilane
BA	- barbituric acid moiety
9-BBN	- 9-borabicyclo[3.3.1.]nonane
Brine	- concentrated NaCl solution
CHCl ₃	- chloroform
CuITEP	- [CuI(P(OEt) ₃)] - copper iodide triethylphosphite
DAT	- 2,6-diaminotriazine moiety
DCM	- dichloromethane
DIPEA	- <i>N,N</i> -diisopropylamine
Dithranol	- 1,8-dihydroxy-10 <i>H</i> -anthracen-9-on
DCTB	- <i>trans</i> -2-[3-(4- <i>tert</i> -butylphenyl)-2-methyl-2-propenylidene]malononitrile
DMA	- <i>N,N</i> -dimethylacetamide
DMDBH	- dimethyl 2,6-dibromoheptanedioate
dNbpy	- 4,4'-dinonyl-2,2'-dipyridyl
DtBp	- 2,6-di- <i>tert</i> -butylpyridine
Et ₃ N	- triethylamine
FS	- frequency sweep measurement
HW	- Hamilton wedge moiety
IAA	- <i>trans</i> -indoleacrylic acid
NaAsc	- sodium ascorbate
NaTFA	- sodium trifluoroacetate
LiTFA	- lithium trifluoroacetate
MCPBA	- 3-chloroperbenzoic acid
MBPP	- methyl 2-bromopropionate
PEG	- poly(ethylene glycol)
CuBrTTPP	- [(Ph ₃ P) ₃ CuBr] - bromotris(triphenylphosphine)copper(I)
Ph ₃ P	- triphenylphosphine
PIB	- poly(isobutylene)
PnBA	- poly(<i>n</i> -butyl acrylate)
Pyr	- pyridine
TBABr	- tetrabutylammonium bromide
TBAF	- tetrabutylammonium fluoride
TBTA	- tris[(1-benzyl-1 <i>H</i> -1,2,3-triazol-4-yl)methyl]amine
THF	- tetrahydrofuran
THY	- thymine moiety
TPP	- triphenylphosphine
TMSA	- trimethylsilylazide

1. Introduction

“Chemistry can be likened to “language”. The atoms are the “letters”. The molecules are the “words”. Assemblies of molecules make up the “sentences”. The sets of assembled molecules [...] are the “paragraphs”. The ways in which the [...] assemblies [...] contain and express information are the “chapters”. The manner in which this information is conveyed [...] is the “book”.

Ultimately, chemistry has to tell a “story”.”^[1]

As expressed by Sir J. F. Stoddart literarily it is often the assembly of small simple molecules into larger complex structures which influences our everyday life, moreover, making daily “life” possible at all. For instance, four unimposing nucleobases that form base pairs, which form double-helical DNA, are the keystones of human being. The driving forces – from a chemist’s point of view – are the non-covalent intra- and intermolecular interactions usually referred to as supramolecular interactions. In comparison to covalent bonds these supramolecular bonds are dynamic, reversible and labile, allowing permanent exchange and reshuffling of the interacting components. Due to this non-covalent character the field of supramolecular chemistry is often called the “chemistry beyond the molecule”.^[2] For the “development and use of molecules with structure-specific interaction of high selectivity”, Donald J. Cram,^[3] Charles J. Pederson,^[4] and Jean-Marie Lehn^[5-6] were awarded with the Nobel-prize in chemistry in 1987.^[7]

Next to small molecules also low and medium molecular weight polymers ($M_n \approx 1000-10000$ g/mol) can be interconnected via supramolecular forces combining both the overall good mechanical properties of polymers and the outstanding characteristics of supramolecular chemistry.^[8-14] It was again J.-M. Lehn who first reported on the formation of polymer strands made via self-assembly of specifically interacting small molecules.^[15] Since these polymer analogues were made from smaller dynamically interacting building blocks, they were often called “dynamers” (dynamic polymers).^[16-17]

Figure 1 shows how different kinds of architectures like linear, crosslinked or graft-type structures can be made via self-assembly of smaller supramolecular building blocks. The resulting supramolecular polymers are linked by the aforementioned defined often directed and reversible non-covalent interactions. Since these interactions are the main structural element, the construction of polymeric architectures is possible by choosing the adequate supramolecular building block. These supramolecular polymers often resemble their covalently linked counterparts. While the supramolecular graft polymer in **Figure 1d** is formed by the reversible connection of the main-chain functionalized (black chain) and the chain-end functionalized (red chain) building blocks, the “conventional” graft-polymer in

1. Introduction

Figure 1e is formed via non-reversible, permanent chemical bonds. Due to substitution of covalent bonds by supramolecular bonds an additional element of dynamic ordering is introduced into the corresponding polymers.

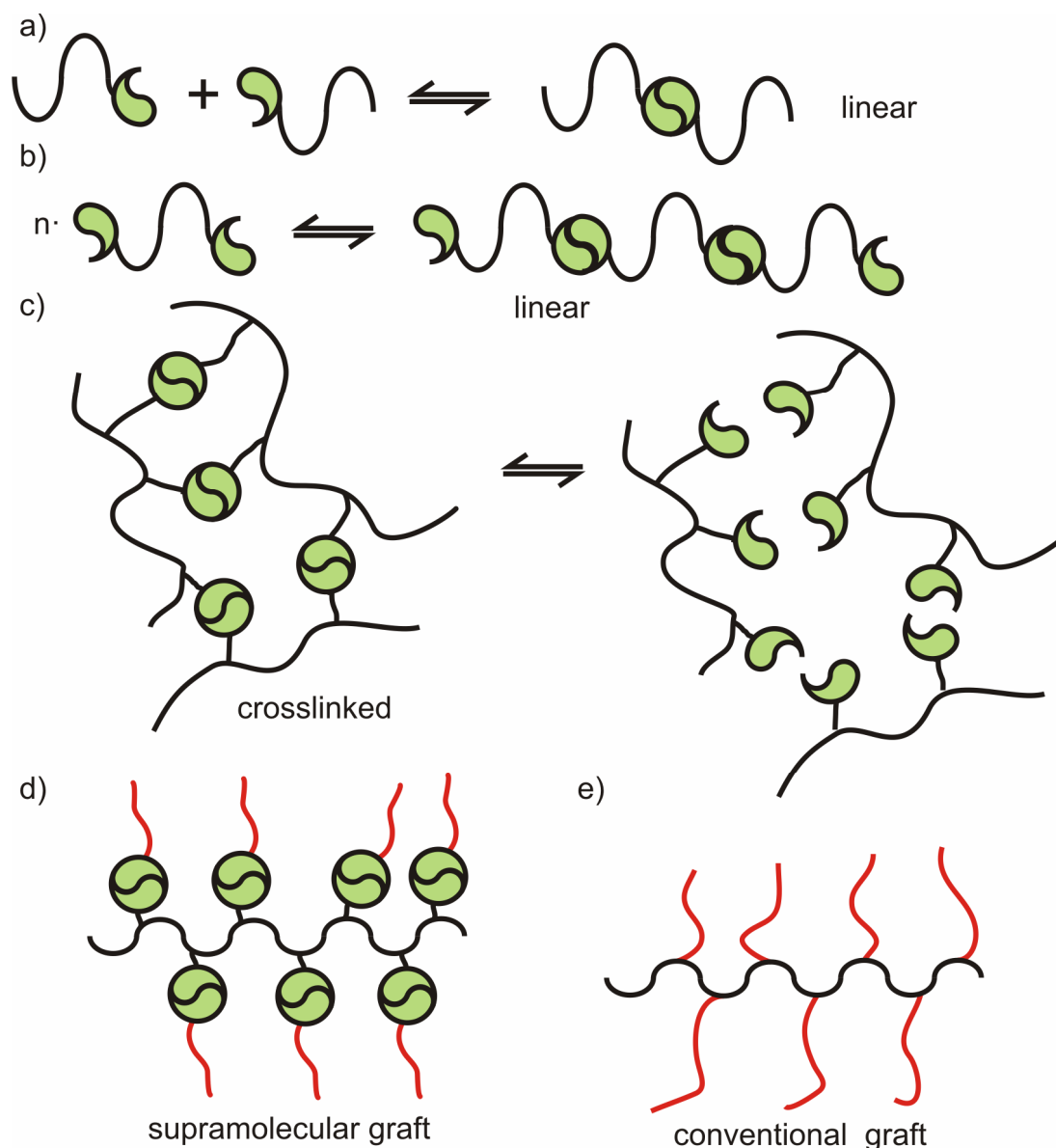


Figure 1. Different architectures (a-d) made from smaller building blocks and interconnected via reversible supramolecular forces. Figure e) shows a conventional (permanent chemical bonds) graft-type polymer.

In a most simple case two chain-end functionalized building blocks can be reversibly connected via the association of the supramolecular groups (**Figure 2**). If both building blocks have the same molecular weight, the resulting associate will have a “virtual” molecular weight which is twice the molecular weight of the single building block. Such an effect can be easily monitored via GPC measurements (**Figure 2a**).^[18] The underlying equilibrium between the associate and the bare building blocks can be expressed by an equilibrium (or association) constant K (**Figure 2b**), which can be effected by temperature, pH, concentration, polarity of

1. Introduction

the surrounding matrix, strength of the association or a force (**Figure 2c**). Due to the inherent dynamic character of this equilibrium, or in other words, the inherent dynamic between associate and single building block it is also a matter of time which species is observed.

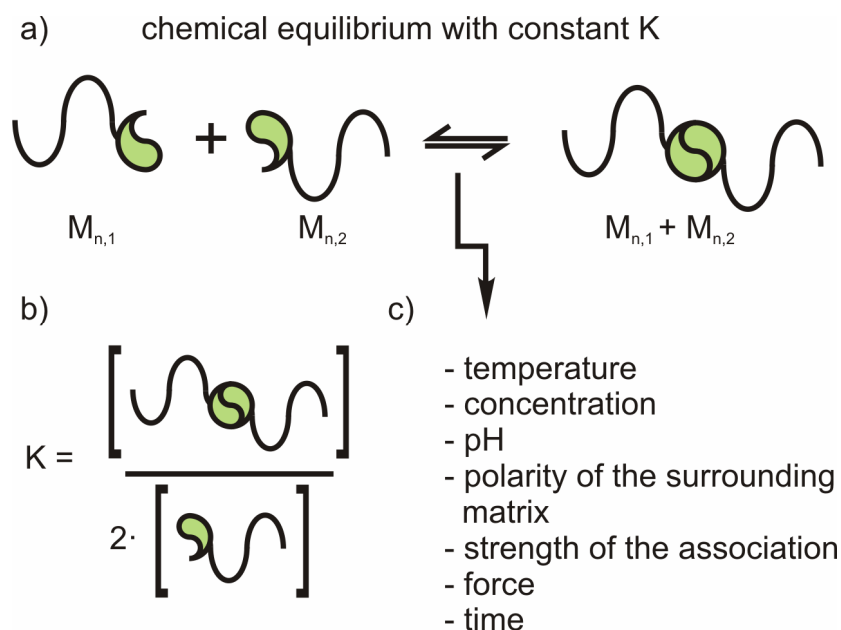


Figure 2. a) The chemical equilibrium between the single building blocks and the corresponding associate expressed by b) an equilibrium constant K which can be c) effected by several stimuli.

Although all supramolecular interactions exhibit several characteristics, for instance, dynamic and reversibility, there is a multitude of different concepts applied in polymer chemistry using various supramolecular forces to achieve, e.g., self-assembly. Mostly applied in supramolecular polymer chemistry are π - π -interactions,^[18-23] ionic forces,^[24-30] metal-ligand complexes,^[31-40] host-guest systems,^[41-53] and hydrogen bonding.^[54-57] Besides the utilization of a single supramolecular force the combination of two or more different forces is possible, allowing the link of diverse strengths and dynamics.^[58-64] Among the above mentioned interactions/systems, hydrogen bonding is the most prominent applied in supramolecular polymer chemistry,^[65-71] since several specifically interacting hydrogen bonding motifs (often referred as “key-lock”-systems) are easily synthetically available and the strength (in terms of the association constant) can be varied by orders of magnitude from 10^3 - 10^{12} M^{-1} .

Figure 3 shows various examples for hydrogen bonding motifs including Meijer’s 2-ureido-4-pyrimidone (UPy) dimers,^[72-73] Zimmerman’s 2,7-diamido-1,8-naphthyridine/urea of guanosine motif (DAN/UG),^[74-78] Meijer’s UPy/2,7-diamido-1,8-naphthyridine system,^[78-81] Bouteiller’s 2,4-bis(2-ethylhexylureido)toluene (EHUT) motif,^[82-85] Hamilton’s Hamilton wedge/barbituric acid (HW/BA) motif,^[86-87] the thymine/2,6-diaminotriazine (THY/DAT)

1. Introduction

interaction as an example for nucleobase based systems,^[88-92] and a quadruple motif reported by Blight *et al.*^[78, 93]

The hydrogen bonding motif displayed in **Figure 3d** (Blight *et al.*^[93]) is probably the strongest “key-lock” system reported so far.^[78] Besides a strong association constant ($K_{\text{assn.}}$) of $\sim 10^{12} \text{ M}^{-1}$ in CH_2Cl_2 , it exhibits a binding free energy (ΔG°) of $-71 \text{ kJ}\cdot\text{mol}^{-1}$. Although this motif binds extremely strong in comparison to other reported hydrogen bonding motifs,^[78] it only covers $\sim 20\%$ of the thermodynamic stability of an ordinary carbon-carbon bond, highlighting that for materials containing both, supramolecular and covalent bonds, it is the weaker supramolecular bond that limits the overall mechanical strength.

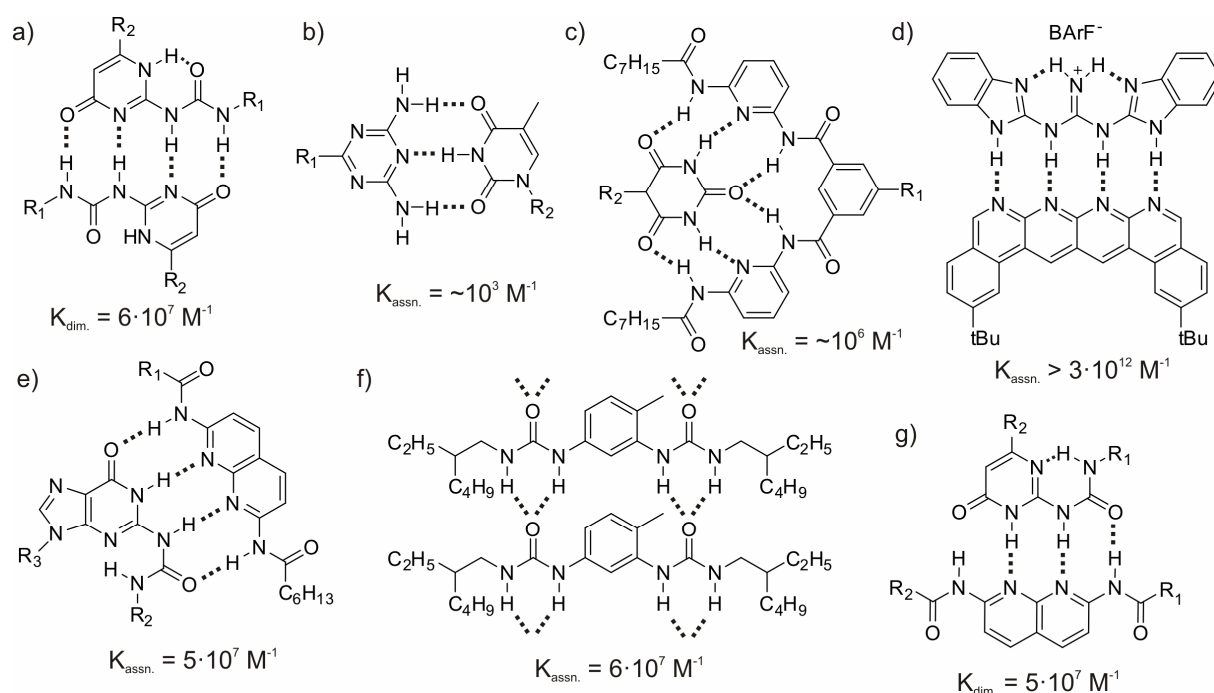


Figure 3. Different hydrogen bonding motifs with the corresponding association/dimerization constants measured in CDCl_3 : a) 2-ureido-4-pyrimidone (UPy); b) thymine/2,6-diaminotriazine (THY/DAT); c) Hamilton wedge/barbituric acid; d) quadruple motif according to Blight *et al.*^[93]; e) 2,7-diamido-1,8-naphthyridine/urea of guanosine (DAN/UG); f) 2,4-bis(2-ethylhexylureido)toluene (EHUT); g) UPy/2,7-diamido-1,8-naphthyridine.

The unusual strength of Blight’s motif arises from the combination of a quadruple hydrogen bonding acceptor (AAAA) and a quadruple hydrogen bonding donor (DDDD) (see **Figure 4a**). In addition to the primary D-A interaction it is the secondary hydrogen bonding interaction that has a significant impact on the overall thermodynamic stability. These secondary interactions can either be attractive (**Figure 4c**) or repulsive (**Figure 4b**). For example, Meijer’s quadruple UPy motif (AADD-DDAA) has an association constant of $\sim 10^7 \text{ M}^{-1}$,^[72] while the quadruple ureidotriazine system (ADAD-DADA) reported by Hirschberg *et al.* only has an orders of magnitude lower association constant of $\sim 10^4 \text{ M}^{-1}$, due to repulsive instead of attractive secondary forces.^[94]

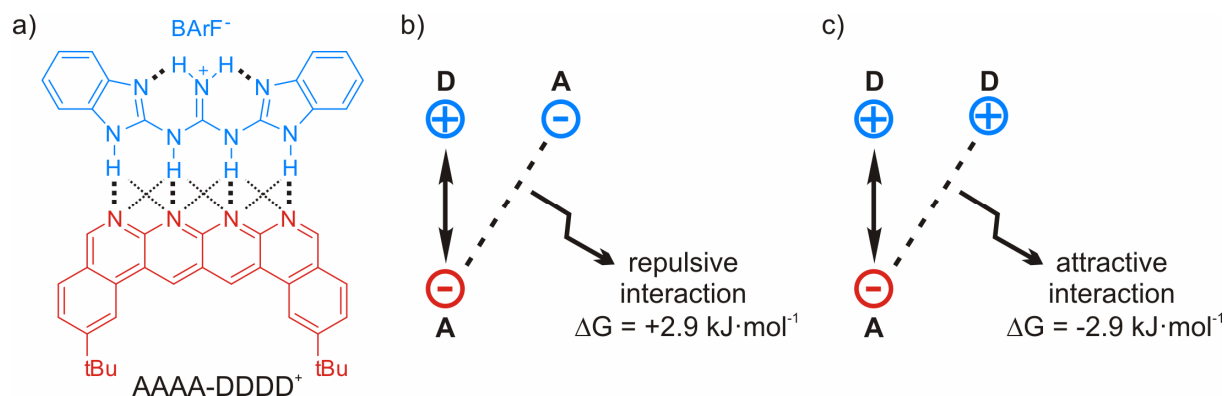


Figure 4. a) A quadruple AAAA-DDDD⁺ hydrogen bonding motif according to Blight *et al.*^[93]; b) secondary repulsive interaction; c) secondary attractive interaction.

Sartorius and Schneider reported on an empirical increment system for hydrogen bonding arrays.^[95] While the primary interaction has an energy (ΔG°) of $7.9 \text{ kJ}\cdot\text{mol}^{-1}$ per D-A pair, the secondary interaction contributes $\pm 2.9 \text{ kJ}\cdot\text{mol}^{-1}$. A good agreement of theoretically calculated and experimentally determined values further clarifies the advantages of hydrogen bonds as supramolecular interaction due to their relatively predictable strength and directory.

However, for the formation of supramolecular polymers it is further important to understand the time-dependent dynamics of association. While the dynamics are already well understood in solution, because here the association can be described by simple models, less is known for gels (concentrated solution) and especially for polymer melts. In gels and melts, besides the association of two supramolecular groups, also the aggregation of several supramolecular groups is possible (see **Figure 5**), making the description of the association/aggregation dynamics much more complex.



Figure 5. Besides the defined association of two supramolecular groups also the aggregation into larger aggregates with different shape and dynamics is possible.

For an arbitrary set of specifically interacting hydrogen bonding groups **A** and **B** (“key-lock” system), the possible modes of association in solution are as simple as displayed in **Figure 6**. Besides the favored A-B formation the dimerization of each group (A-A and B-B) is possible.

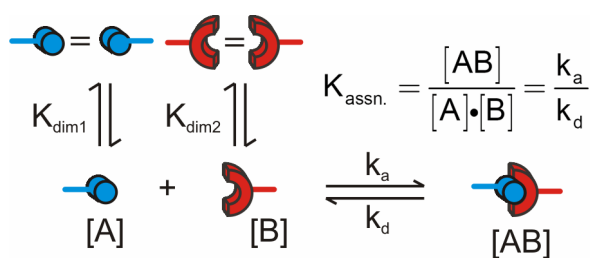


Figure 6. Possible modes of aggregation for an arbitrary set of specifically interacting hydrogen bonding groups **A** and **B** in solution.

Each species is in a permanent dynamic equilibrium which is expressed by the association constant $K_{\text{assn.}}$ (for the formation of A-B) or the dimerization constant $K_{\text{dim.}}$ (A-A or B-B). Since $K_{\text{assn.}}$ is usually large (see **Figure 3**) in comparison to K_{dim} (usually in the range of $K_{\text{dim}} < 100 \text{ M}^{-1}$), the dimerization can be neglected in solution. According to this model, the association constant $K_{\text{assn.}}$ is defined by the ratio of the rate of association (k_a)/rate of dissociation (k_d). Already in 1968 it was shown by Hammes and Park for triple hydrogen bonding arrays that the rate of association k_a is a diffusion controlled process and independent from the hydrogen bonding motif.^[96] For three different systems the rate of association k_a was found to be in the range of $1.5\text{-}4.0 \cdot 10^9 \text{ M}^{-1} \cdot \text{s}^{-1}$. As a consequence, the rate of dissociation k_d ($k_d = k_a/K_{\text{assn.}}$) is a direct measure for the strength of the hydrogen bond. This model holds true for all hydrogen bonding arrays, except Meijer's UPy motif, since here three different tautomers were involved (see **Figure 7**).^[97]

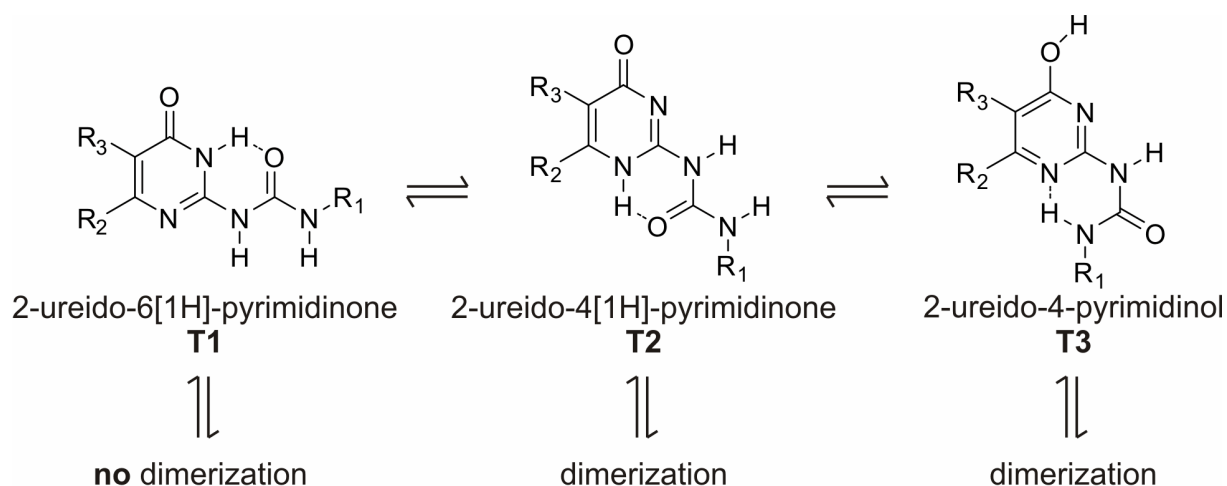


Figure 7. Association of different tautomers of Meijer's 2-ureido-4-pyrimidinone (UPy) motif.

While the two tautomers **T2** and **T3** form the quadruple hydrogen bonding dimer, tautomer **T1** is unable to undergo dimer formation. As a result, the rate of association ($k_a = 5.0 \cdot 10^8 \text{ M}^{-1} \cdot \text{s}^{-1}$ in CHCl_3) is one order of magnitude lower compared to other systems. Nevertheless, the UPy motif with a dimerization constant ($K_{\text{dim.}}$) of $\sim 5.7 \cdot 10^7 \text{ M}^{-1}$ is among the

1. Introduction

strongest hydrogen bonding motifs with a slow exchange rate and a long bond lifetime τ_d of 120 ms, which is the inverse rate of dissociation ($\tau_d = 1/k_d$).^[97]

Due to the adequate bond lifetime in solution, bifunctional building blocks bearing the hydrogen bonding motif on both chain ends are, therefore, able to form long supramolecular polymer chains. As a result, the solution shows e.g. an increase of the viscosity. A corresponding example was reported by Bouteiller and coworkers utilizing functionalized poly(dimethylsiloxane)s (PDMSs) bearing either benzoic acid or benzoic ester functional groups (see **Figure 8a**).^[98]

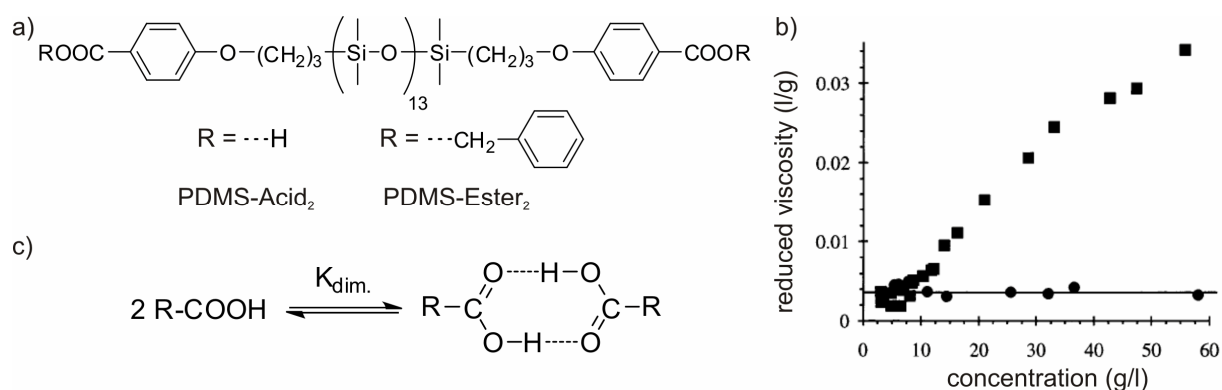


Figure 8. a) Functionalized linear PDMSs; b) influence of attractive hydrogen bonding on the solution's viscosity (● = PDMS-Ester₂ and ■ = PDMS-Acid₂); c) dimerization of two carboxylic acid groups. Figure b) taken from Abed *et al.*^[98]

While the addition of the PDMS-Ester₂ to a solution of *n*-hexane has no influence on the reduced viscosity (within a concentration range of 0-60 g/l), the addition of the PDMS-Acid₂ causes an remarkable increase of the reduced viscosity due to the linear extension of the PDMS chains via attractive hydrogen bonding of the acid groups (see **Figure 1b**). Similar observations were also made by Lillya *et al.*^[99]

The extent of association can be expressed by a “virtual” degree of polymerization (DP) which depends on the association constant $K_{\text{assn.}}$, temperature and the concentration (*c*) of the building block. The association constant can be easily determined via e.g. NMR,^[100-101] UV-VIS,^[102] ultrasound^[96] or atomic force microscopy (AFM).^[103-106]

In order to calculate the relation between DP and $K_{\text{assn.}}$ and thus to predict the viscosity of a supramolecular solution it is necessary to adjust the DP independently from the monomer concentration for a particular system. Cohen-Stuart and coworkers solved this problem by utilizing “chain stoppers” which are monofunctional buildings blocks that lead to a decrease of the virtual DP upon a critical stopper concentration.^[83-84, 107]

1. Introduction

They showed that the linear extension of bifunctional building blocks can be described similar to Flory's meanfield theory of condensation polymerization:^[108]

$$DP = 2 \cdot [K_{assn.} \cdot c]^{0.5}$$

If the virtual DP is sufficiently high, the supramolecular chains can entangle bestowing the solution (sol) viscoelastic properties thus transforming it into a gel (network) (**Figure 9a**). The corresponding transition is called sol-gel transition and can be achieved via different supramolecular architectures. Besides the already mentioned linear chain extension,^[13, 98] the usage of multivalent building blocks^[109-110] or polymers that were functionalized along their chains^[61, 111] can lead to the formation of a supramolecular network (see **Figure 9c**).

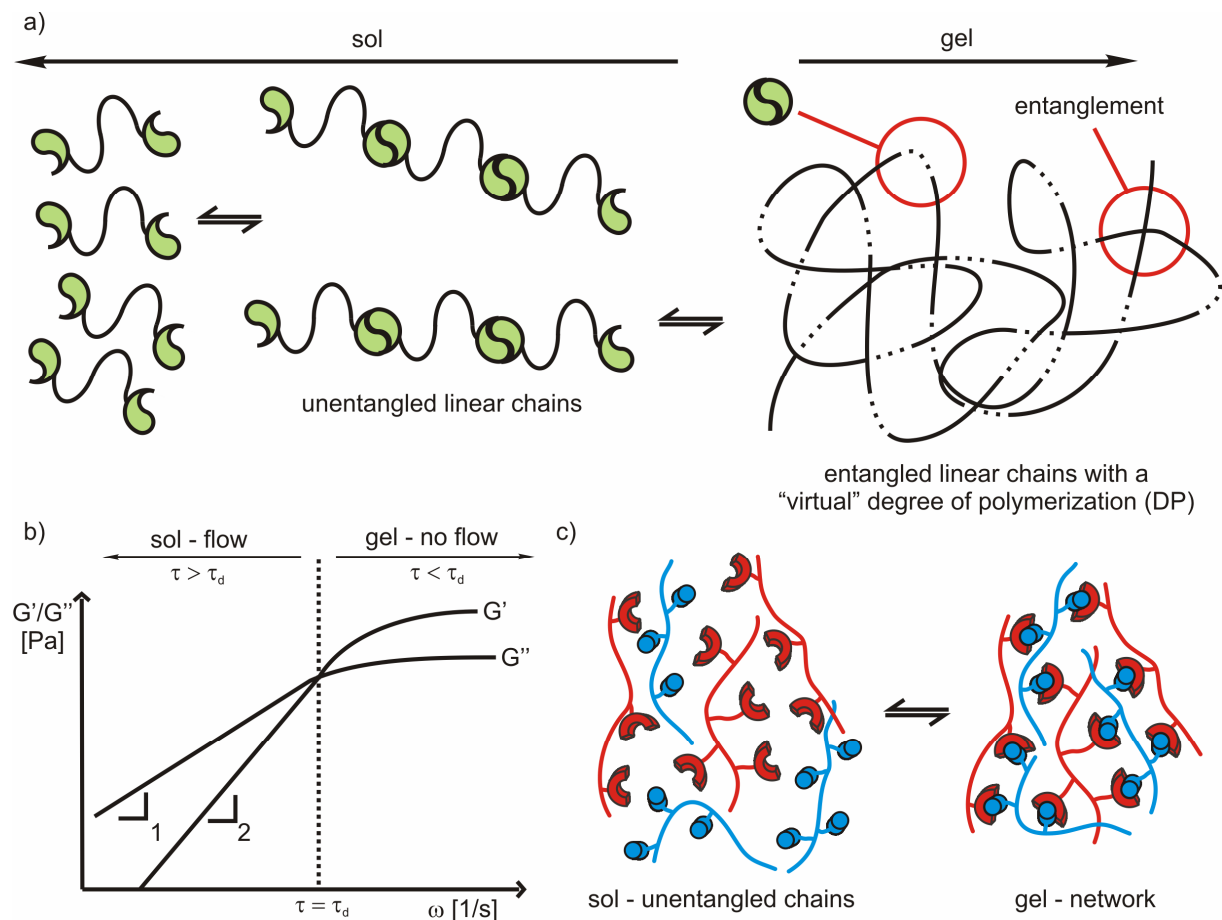


Figure 9. a) Network-formation of entangled linear chains, due to the supramolecular association of small building blocks; b) typical frequency sweep measurement of a supramolecular network; c) formation of a supramolecular network due to functionalization along the polymer chain.

A suitable tool to investigate the time- and temperature-dependent association in supramolecular polymers are frequency (time) dependent, oscillatory rheology measurements. A typical frequency-sweep measurement is sketched in **Figure 9b** and will be explained by an example reported by Craig and coworkers. They utilized poly(4-vinylpyridine) (P4VP) which is reversibly crosslinked via specific metal-ligand coordination between bifunctional

1. Introduction

organometallic cross-linkers and the pyridine moiety of P4VP (see **Figure 10a**).^[32, 112-114] At high frequencies (short times) the bond lifetime τ_d is long in comparison to the applied frequency ($\tau_d > \tau$) and the supramolecular bonds were monitored in the closed state. As a result, the mechanical properties resemble those of a permanent (physical) cross-linked network on short timescales and, thus, a rubbery plateau is observed (**Figure 9a**). At lower frequencies (long times) the supramolecular bonds were monitored in the open state ($\tau_d < \tau$) and the mechanical properties were dominated by the bare P4VP chains. They found that the mechanism of ligand exchange in the polymer network is the same solvent-assisted pathway observed for low molecular weight model complexes. Therefore, the gel-point ($\tau_d = \tau$), the transition between the two states, corresponds to the bond lifetime τ_d of the metal-ligand complex.

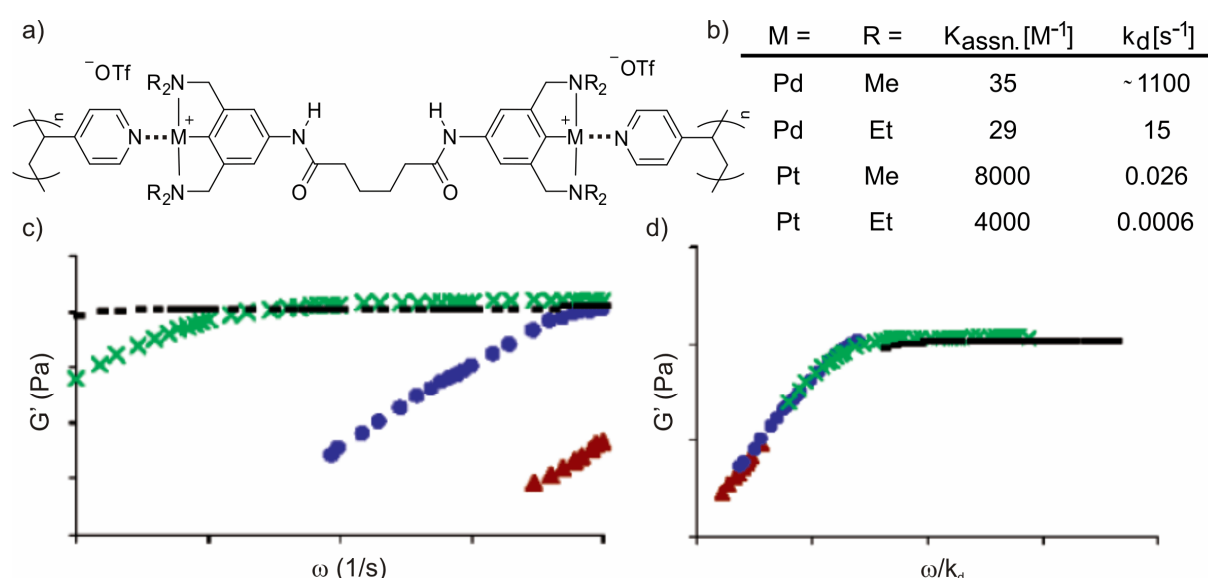


Figure 10. Supramolecular bond formation between bifunctional organometallic cross-linkers and the pyridine moiety of P4VP; b) bond characteristics for different motif compositions; c) storage modulus (G') vs. frequency plot; d) G' vs. normalized frequency (ω/k_d) plot – all curves superpose. Figure c) and d) taken from Yount *et al.*^[113]

For these particular complexes the association constant $K_{\text{assn.}}$ and the rate of dissociation can be easily varied by doing only minor changes on the chemical structure of the metal-ligand system (see **Figure 10b**), an approach impossible to apply for hydrogen bonding moieties (to this extent).^[85] Therefore, the bond lifetimes vary from ~ 1 ms to tens of minutes, although the equilibrium structures of the complexes were effectively identical. If the individual frequency sweep measurements (see **Figure 10c**) were now scaled by the rate of dissociation k_d , all curves perfectly superpose (see **Figure 10d**), evidencing the dissociation dynamics dominating the dynamic mechanical properties of the network. Due to the simple scaling behavior of this system the viscoelastic properties can be easily predicted and tailored.

1. Introduction

Unfortunately, Craig's system is one of the very few that can be described in such a simple manner. In order to do so with other systems it is essential to get a deeper understanding of the formation and the dynamics of supramolecular (polymer) networks and to describe their behavior with general valid models. Although several well accepted models are known to describe ordinary polymer solutions (gels) and melts, e.g., the Rouse^[115-116] or the Reptation model,^[117] they do not consider the presence of reversible transient bonds, which play an important role in supramolecular polymers. As a consequence, several attempts were reported, which take the reversible association into account. Cates's "living" reptation model is,^[118] among others,^[119-120] one of the most prominent since it was found to be applicable and valid for various systems.^[83, 121-126] It was later advanced by Granek and Cates,^[127] Cates and Candau^[128] and himself.^[129] It describes the dynamics of a linear entangled polymer solution (**Figure 9a**), assuming that the chains can break with equal probability per unit, time and length, and that chain recombination occurs at a rate proportional to the concentration of the chain fragments. According to Cates, stress relaxation can proceed via reptation or reversible scission and recombination. **Figure 11a** displays the elementary steps of stress relaxation according to scission and recombination.

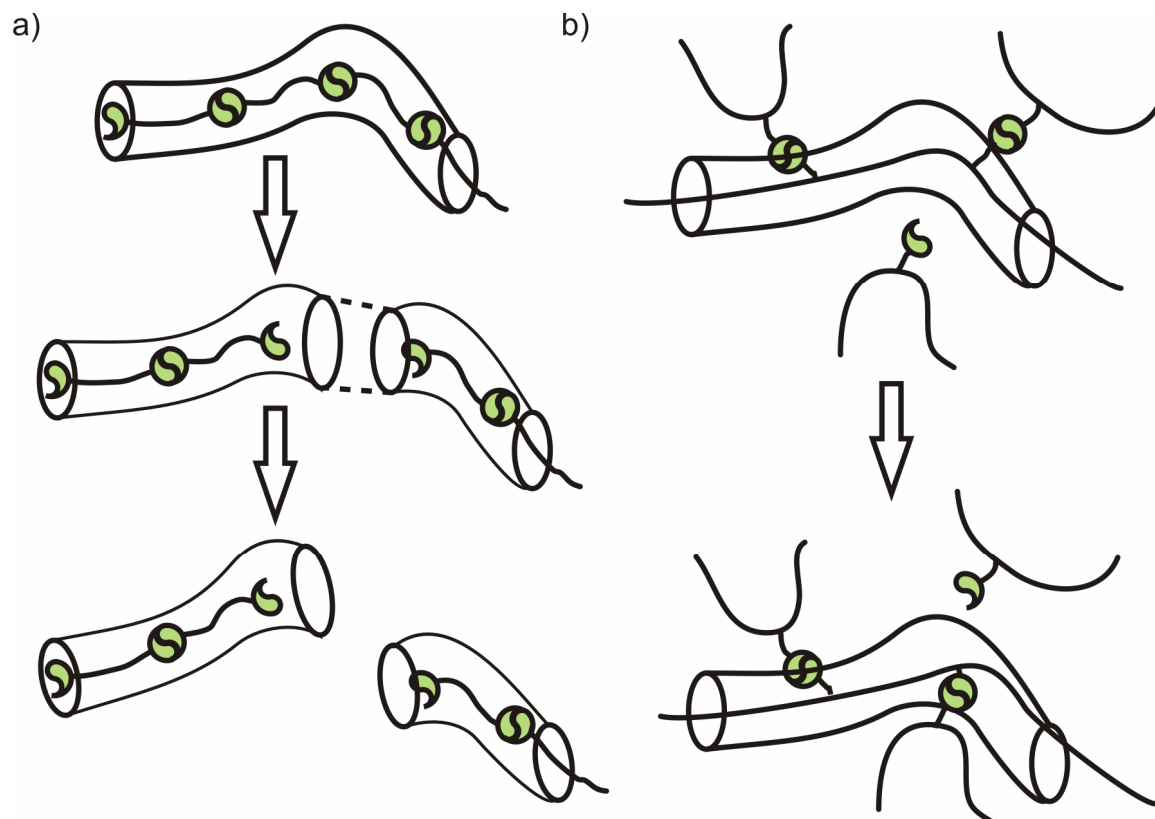


Figure 11. Relaxation mechanism according to the a) the "living" reptation and b) the "sticky" reptation model.

1. Introduction

Considering one particular transient polymer chain, consisting of linear bifunctional building blocks, it is trapped in a tube. The tube can be seen as movement restrictions caused by the surrounding polymer matrix. Relaxation of the chain can occur when a supramolecular bond breaks and one or two of the resulting new chain ends can pass through the tube, due to now possible local movement, before they can recombine. As a result, the chain ends can recombine with chain ends of the surrounding matrix. However, the “living” reptation model only describes the stress relaxation of linear transient chains. Since network formation can also be observed via covalently jointed (permanent) chains, which were interconnected by reversible association of “sticky” side groups, Leibler, Rubinstein, and Colby developed the “sticky” reptation model,^[130] which is an extension of de Gennes’s classical reptation model.^[131]

Figure 11b shows the elementary steps of the “sticky” reptation. In the initial situation the considered chain, which is functionalized along the chain, has two supramolecular tie-points with surrounding chains (top). These supramolecular tie-points are reversible, dynamic and in a permanent equilibrium between the open and closed state. When a tie-point is in the open state also the combination with other supramolecular groups from the matrix is possible under formation of a new supramolecular tie-point (bottom).

Rubinstein and Semenov later refined the “sticky” reptation model for application to dilute, semidilute unentangled and semidilute entangled solutions.^[132-133] A main outcome of the Rubinstein and Semenov theory is that for supramolecular polymer networks one rather has to consider the effective bond lifetime τ_d^* than the bare bond lifetime τ_d ($\tau_d < \tau_d^*$) of one particular supramolecular bond, which is usually determined for model systems in solution. The origin of the effective bond lifetime τ_d^* is explained by means of **Figure 12**. Two chains were interconnected via three supramolecular transient tie-points each of them in dynamic reversible equilibrium between the open and closed state. If only one or two of the three tie-points are in the open state no relaxation of stress is possible since the two chains are still hold together by the third closed tie-point. In order to release an applied stress or to monitor the network in the sol-state (see **Figure 9a**), all three transient tie-points have to be in the open state. Otherwise, the two polymer chains were not able to depart from each other. Therefore, the process of unbinding and ease is limited by the mobility of the polymer chains and by the presence of adjacent tie-points, making the release of one tie-point dependent from other binding events. As a result, e.g., the onset of the terminal flow region (crossover of G'/G'') is shifted towards lower frequencies (longer timescales) (see **Figure 9a**). A similar effect is reasonable for multicenter aggregates (aggregates of three or more supramolecular groups).

1. Introduction

As a further result of the Rubinstein and Semenov theory it is important to clearly distinguish the theoretical description of solutions (sols) and gels. While for sols the experimental data can be related to the single supramolecular bond, for gels it is the density of the resulting network and thus the mobility of the polymers itself which influences the lifetime of the reversible supramolecular bond.

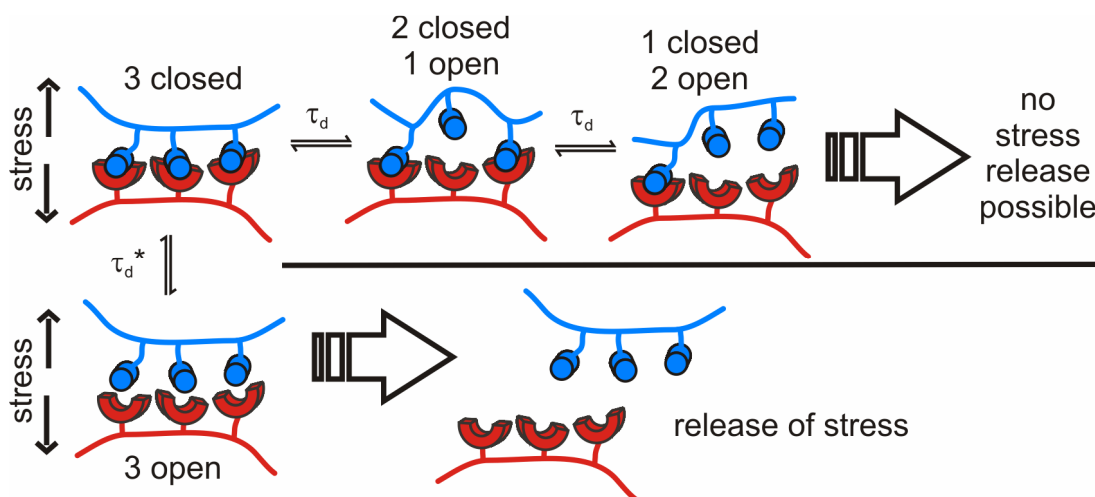


Figure 12. Origin of the renormalized tie-point lifetime, which is usually expressed by the effective bond lifetime τ_d^* .

The effect of concurrent binding and unbinding events on the lifetime of a supramolecular bond in polymer melts was shown by Feldman *et al.*, utilizing amorphous poly(*n*-butyl acrylate)s (PnBAs) bearing various amounts of Meijer's UPy group distributed along the polymer chain (see **Figure 13a**).^[134]

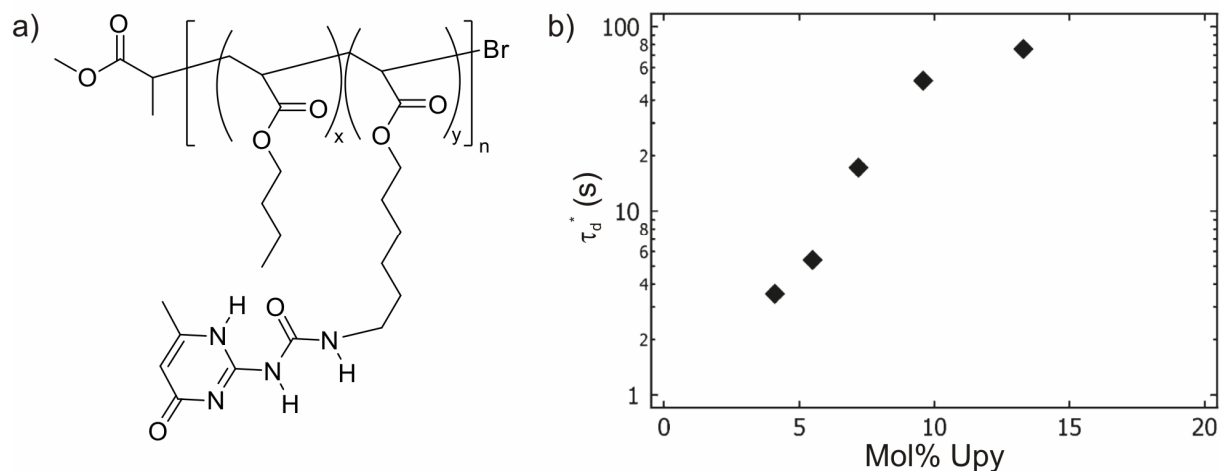


Figure 13. a) Poly(*n*-butyl acrylate)s (PnBAs) functionalized with different amounts of UPy; b) dependence of the effective bond lifetime τ_d^* on the Mol% of UPy groups. Figure b) taken from Feldman *et al.*^[134]

1. Introduction

Although the synthesis of similar polymers was reported earlier by Long and coworkers,^[135] only the combination of controlled radical polymerization (ATRP) and postpolymerization functionalization reported by Feldman *et al.* allows the synthesis of more defined polymers. It was shown for random copolymers with a similar molecular weight that an increase of the mole fraction of the UPy groups (mol% UPy) leads to a drastic increase of the effective bond lifetime since concurrent unbinding of more and more tie-points becomes less likely (see **Figure 13b**). The effective bond lifetime τ_d^* was calculated from the frequency at which the storage modulus has dropped to 90 % of its plateau value. While the bare bond lifetime in solution is in the range of 80 ms (polar solvent) to 1.7 s (nonpolar solvent), τ_d^* was found to be in the range of 1.2 s up to ~80 s in the relative polar PnBA environment depending on the mol% UPy groups.

Although the experimental (rheological) results can be predicted by the Rubinstein and Semenov theory, it only works well for random copolymers with very low UPy content but not for high UPy incorporation or blocky copolymers. Furthermore, the PnBA polymers were still relatively undefined since the postpolymerization functionalization reaction only has a yield of ~75-85 % and, e.g., a copolymer with an average of ~4 % incorporation consists of chains with zero up to four UPy groups per chain. Nevertheless, this example shows that it is rather the dynamic of unbinding and binding (τ_d^*) than the association constant K_{assn} that dominates the macroscopic response.

However, only a few systems were reported which can be described by the above discussed models. Many systems suffer from the formation of aggregates (see **Figure 5**) which are formed via the aggregation of several supramolecular groups. Unfortunately, the mentioned theories do not consider such aggregation and a general model for the precise prediction of network formation and network dynamics of a supramolecular polymer is not available till now. Although a few samples can be discussed in a simple manner, a detailed analysis often suffers from the formation of complex aggregates or phase separation of the supramolecular group for instance the formation of fibers,^[136-139] stacks,^[62, 140-141] clusters^[28, 70] or crystalline domains.^[90, 142-143] These phenomena are particularly dominant in polymeric melts since here the often polar supramolecular groups are not solvated by a solvent rather they are surrounded by the often less polar polymer itself (polymer matrix).

As a result, one does not necessarily need strong interacting groups because for instance also the combination of (weak) hydrogen bonding (effective bond lifetime) and phase separation can be applied for the formation of a self-supporting supramolecular material as well. Noro *et al.* reported in a series of papers that supramolecular networks can be build up by mixing two low T_g polymers, carboxyl-terminated telechelic poly(ethyl acrylate) (PEA-(COOH)₂) and

1. Introduction

poly(ethyleneimine) (PEI) (see **Figure 14b+c**).^[144-145] The resulting polymer blends are based on simple molecular design since PEA-(COOH)₂ is easily accessible via controlled radical polymerization (RAFT) while PEI is even commercially available. Although only one hydrogen bond is formed between two interacting groups (small association constant), strong solvent free rubbers were obtained by combination of hydrogen bonding (long effective bond lifetime due to improbable concurrent unbinding) and phase separation of the functional groups within the polymer matrix (see **Figure 14a**).^[144]

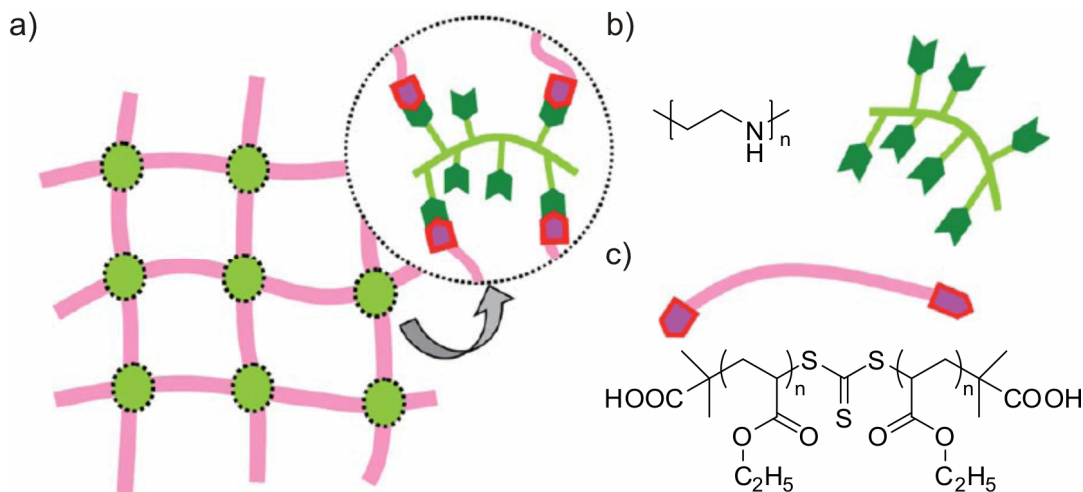


Figure 14. Formation of a supramolecular network between PEA-(COOH)₂ and PEI via combination of hydrogen bonding and phase separation. Figure according to Noro *et al.*^[144]

Additionally to the mentioned obstacles above towards the precise prediction of network formation and network dynamics, even small changes in the chemical structure can cause radical changes of the material microstructure and thus the macroscopic response.

Stadler and coworkers investigated main chain functionalized poly(butadiene)s (PBDs) bearing hydrogen bonding side groups namely the 4-phenyl-1,2,4-triazolidine-3,5-dione (urazole) (**Figure 15a**) and 4-urazoylbenzoic acid group (**Figure 15d**).^[142, 146-153] Although both groups are chemically related, their impact on the thermo-rheological behavior and the microphase structure of the linear PBDs is extremely different. PBDs with urazole groups show e.g. a broadening of the rubbery plateau zone and an increase of the zero-shear viscosity in comparison to the unfunctionalized PBDs precursor, due to formation of two hydrogen bonds between a pair of urazole groups (**Figure 15b**).^[147-148, 153]

For the urazole-PBDs a thermo-rheological simple behavior was observed and their temperature dependence of $\log a_T$ (shift factor) can be described by the Williams-Landel-Ferry (WLF) equation.^[154] In contrast, PBDs bearing urazoylbenzoic acid groups show a considerable more complex behavior due to phase separation of the urazoylbenzoic acid

1. Introduction

groups by cooperative aggregation (see **Figure 15c**).^[142, 150] As a result, no time-temperature superposition is possible. Although the urazole group merely differs from the urazole group by the presence of the carboxyl moiety, additional secondary forces introduced by the carboxyl groups lead to the formation of extended aggregates of the 4-urazolebenzoic acid groups. These groups phase separate from the polymer matrix while the urazole groups are homogeneously distributed within the polymer matrix.^[155] Similar effects were reported by Meijer and coworkers for linear poly(caprolactone)s (PCLs) bearing the UPy motif.^[139]

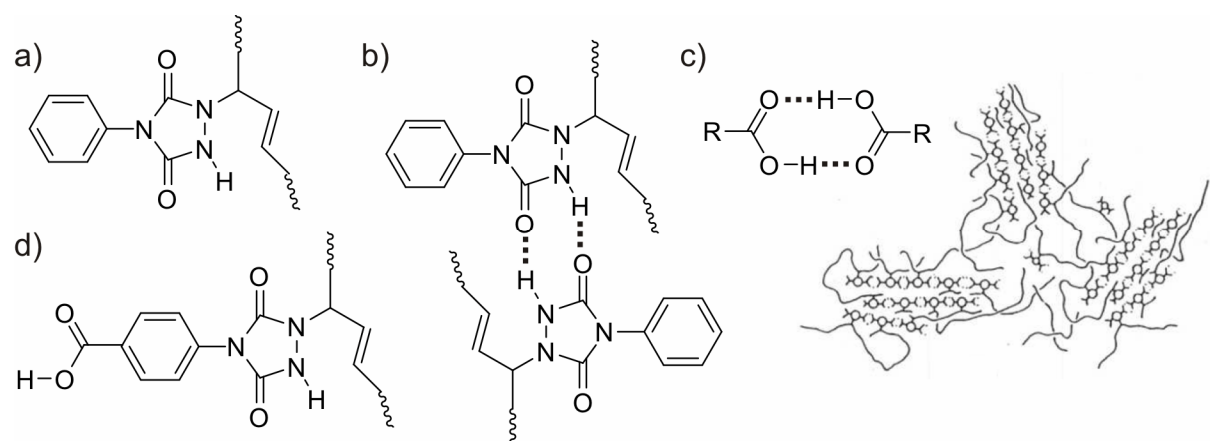


Figure 15. Formation of a supramolecular network via functionalized linear poly(butadiene)s (PBDs) bearing either a) 4-phenyl-1,2,4-triazolidine-3,5-dione (urazole) or d) 4-urazolebenzoic acid groups; b) each group can form two hydrogen bonds; c) 4-urazolebenzoic acid groups can form two additional hydrogen bonds, which leads to the formation of phase separated domains. Figure c) taken from Hilger *et al.*^[150]

As the theoretical description of such supramolecular systems is often complicated due to complex modes of association/aggregation, why is it important to get a deeper understanding of the dynamics of supramolecular bonds in such systems? The need of a deeper understanding arises from the broad variety of different applications of such systems. Furthermore, these kinds of polymers have several advantages over conventional polymers. For instance, conventional polymers were often processed by injection molding or injection embossing from the melt state. Due to the long entangled polymer chains (with a molecular weight of hundreds of thousands g/mol) the polymer melts exhibit very high viscosities, thus which limits the range of applications and increase the complexity of the processing step. As the association/aggregation in supramolecular polymers can be easily affected by temperature, such polymers can be processed at elevated temperatures as low viscous melts (viscosity is affected by the low molecular weight building blocks). Upon molding and cooling the supramolecular bonds are reformed due to their inherent dynamic character. Therefore, such supramolecular polymers can be processed as low viscous melts (at elevated temperatures), but applied as high molecular weight materials at ambient temperatures.^[156]

1. Introduction

Several supramolecular forces are known, numerous combinations of different forces and architectures are possible and there are also manifold of other applications of supramolecular materials. A selection of possible applications is listed in **Table 1**.

Table 1. Summary of recently reported applications of supramolecular chemistry.

entry	application	literature
1	self-healing	[14, 22, 26, 157-166]
2	microelectronics/nanotechnology	[138, 167-173]
3	superamphiphiles	[174-175]
4	biomimetic	[73, 159, 176-179]
5	functional behavior	[9, 44, 64, 180-184]
6	functionalization of surfaces	[181, 185-188]
7	capsules/cages/vesicles	[188-192]
8	stimuli responsive materials	[14, 193-195]
9	fibers/wires/rods	[138, 158, 172, 196]
10	controlled self-assembly	[8, 10, 15, 35, 179, 183, 197-198]
11	catalysis	[199]
12	stabilization	[186, 200-201]
13	shape memory	[202-203]
14	miscibility in polymer blends	[77, 204-208]

According to Moore's law, the number of transistors on integrated circuits doubles approximately every 18 months - a prediction made in 1965 and still valid in 2013.^[209] Integrated circuits were usually manufactured by photolithographic techniques, however nowadays the limits for further miniaturization are almost reached. For further improvements (smaller circuit size) new techniques are necessary. One example could be block copolymer lithography. Tang *et al.* reported on the fabrication of highly ordered square arrays based on the assembly of supramolecular polymers.^[173] Diblock copolymers of poly(ethylene oxide)-*b*-poly(styrene-*r*-4-hydroxystyrene) (PEO-*b*-P(S-*r*-4HS) and poly(styrene-*r*-4-vinylpyridine)-*b*-poly(methyl methacrylate) (P(S-*r*-4VP)-*b*-PMMA) (see **Figure 16a**) were prepared by living polymerizations. Due to hydrogen bonding between the 4-hydroxystyrene and 4-vinylpyridine, the block copolymers form highly ordered nanostructures after a spin-coating process.

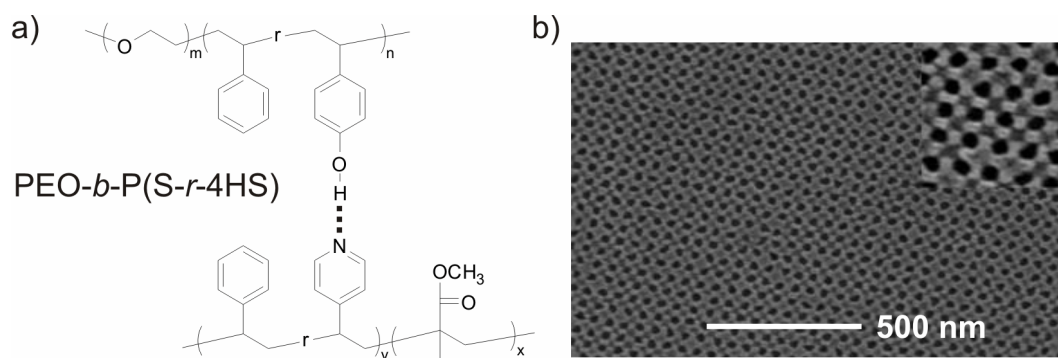


Figure 16. a) Supramolecular diblock copolymers forming b) high defined square arrays (SEM top view). Figure b) is taken from Tang *et al.*^[173]

After photodegradation of the PMMA block square arrays of ~ 20 nm were obtained (cylindrical pores; see **Figure 16b**), much smaller than with standard photolithographic methods (~ 30 nm), putting this concept on the frontline for further microelectronic applications.

From the variety of different applications of supramolecular (polymer) chemistry (**Table 1**), self-healing applications are among the most important and fascinating. The inherent dynamic character of a supramolecular bond allows the creation of materials that often autonomously heal micro- and even macroscopic defects, thus increasing the material's lifetime and safety (for literature see **Table 1**).

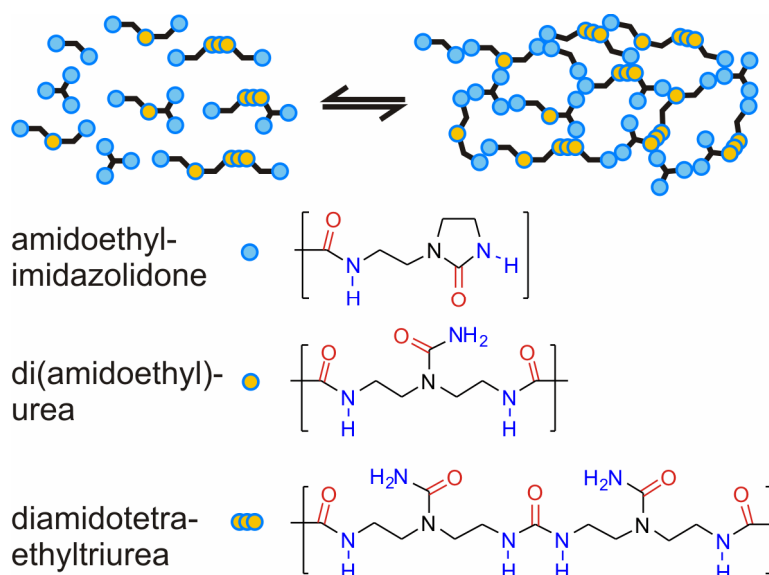


Figure 17. Low molecular weight building blocks, based on multivalent fatty acids, form a supramolecular network due to hydrogen bonding.

One of the most prominent examples was developed by Leibler and coworkers utilizing functionalized fatty di- and triacids which were first reacted with diethylene triamine and then with urea (see **Figure 17**).^[157, 163-164] The resulting compound contains several functionalized

1. Introduction

low molecular weight molecules that are able to form hydrogen bonds between the building blocks. Plasticizing with 11 wt% dodecane (to lower the T_g) bestows the material sufficient internal mobility ($T_g < T_{25^\circ\text{C}/\text{RT}}$) and it was (macroscopically) obtained as a rubbery material. The resulting material was not crystalline, easily synthesized on a 100 g scale, capable to be molded or extruded at high temperatures and further reveals rheological and mechanical properties typical for ordinary rubbers.

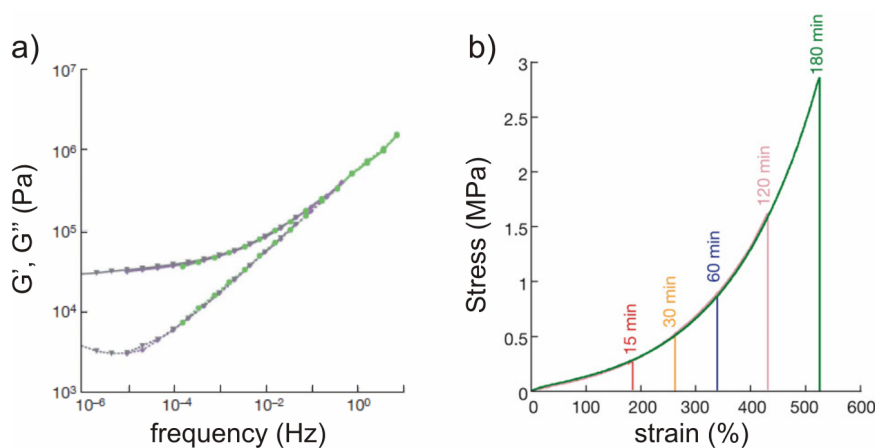


Figure 18. Mechanical measurements of a supramolecular rubber reported by Cordier *et al.*: a) frequency sweep measurement; b) stress-strain experiments after different healing times. Figure according to Cordier *et al.*^[163]

Figure 18a shows the frequency dependence of storage (G') and loss (G'') modulus, revealing a rubbery plateau at low frequencies and the close proximity to the glass transition at high frequencies. However, in comparison to an ordinary rubber this material exhibits some unique properties. When the rubber is cut into two parts with a scalpel, it is assumed that the weak supramolecular hydrogen bonds were “cut” preferentially while the building blocks itself (stronger covalent bonds) were not affected. Due to the inherent dynamic reversible character of the supramolecular bonds, the now “free” hydrogen bonds remain active for a certain period of time. When the two fractured surfaces were brought into contact and slightly pressed together, the material autonomously recovers its mechanical properties as exemplified by the stress-strain behavior in **Figure 18b** whereby longer healing times lead to a higher extent of healing.

Guan and coworkers reported on the synthesis of a supramolecular PS-*b*-PnBA diblock copolymer bearing Meijer’s UPy motif on the PnBA chain end.^[162] The incompatibility of the two polymer blocks leads to phase separation into hard PS cores and a soft amorphous PnBA matrix (see **Figure 19a**). Due to the formation of UPy dimers via hydrogen bonding, the PS cores were interconnected via a supramolecular PnBA network. Similar to the behavior of Leibler’s rubber, a macroscopic damage probably leads to the rupture of the weaker hydrogen

1. Introduction

bonds between the UPy dimers within the PnBA matrix. Upon recombination of the fractured surfaces, the UPy dimers were reformed due to the dynamic reversible character of the hydrogen bonds, leading to a recovery of the mechanical properties (see **Figure 19b**).

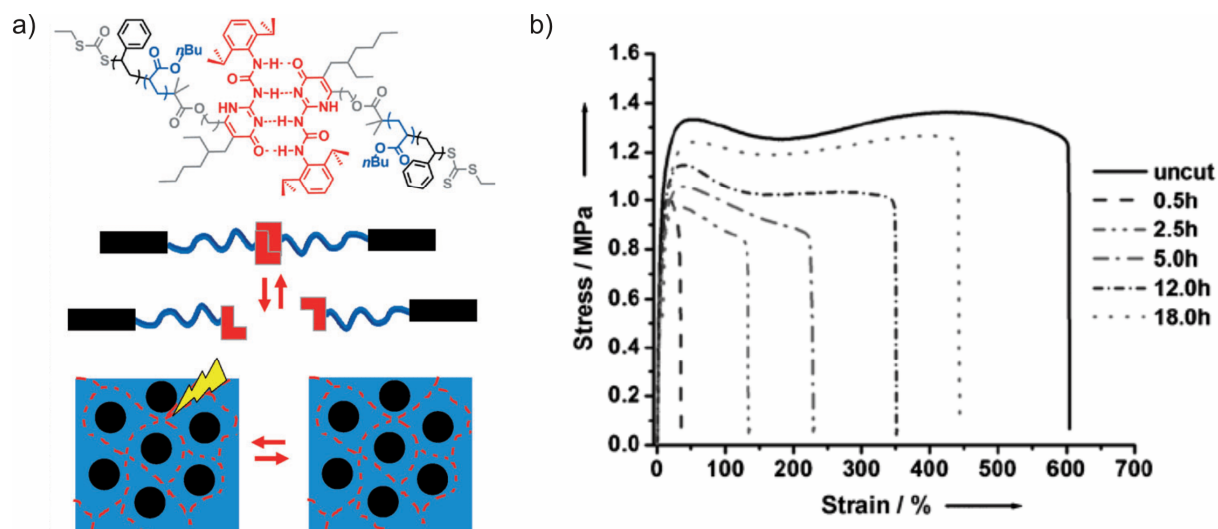


Figure 19. a) Phase separation of a supramolecular block copolymer bearing Meijer's UPy groups; b) stress-strain behavior after different healing times. Figure according to Hentschel *et al.*^[162]

Guan's material exhibits better mechanical properties (strength) than Leibler's, due to the combination hydrogen bonding and thermoplastic elastomeric behavior (TPE approach^[161]). On the other hand it suffers from long healing times and incomplete healing efficiency because of the lower volume fraction of hydrogen bonding groups. This interplay (strength vs. healing efficiency) will be a challenge for further scientific investigations.^[166]

Another challenge is to get a deeper and general understanding of the dynamics of the hydrogen bonds either within the polymer matrix or within the fractured surface. The importance of sufficient dynamics of the hydrogen bonding groups (or the surrounding matrix) was shown by Leibler and coworkers for their famous self-healing rubber.^[163] While the pristine compound was observed as a brittle non-self-healing material, it needs the plastification with 11 wt% dodecane, which causes a decrease of the T_g below room temperature, to enable sufficient dynamics and, thus the outstanding self-healing properties.

Supramolecular polymers are promising candidates for several high-end applications most of all as self-healing materials. A broad variety of non-covalent interactions are available to form such materials also via different molecular architectures. While supramolecular gels often suffer from the presence of the solvent due to low mechanical strength, limitation of the application temperature by the boiling point of the solvent, or evaporation of the solvent in long-term applications, supramolecular bulk materials do not. However, the precise prediction

1. Introduction

and theoretical description of solvent free supramolecular polymers in most cases suffers from the formation of a magnitude of different complex aggregates. As a result, at the latest research, the investigation of the structure-dynamic relation essentially needs the experimental proof. Therefore, it especially needs highly defined, amorphous, supramolecular polymers to achieve a deeper understanding of the formation and the dynamics in supramolecular materials for future applications.

2. Aim of the work

Aim of this work was to systematical investigate the association and/or aggregation behavior of specific interacting hydrogen bonding moieties (“key-lock-systems”) in the polymer melt. Since a multitude of applications arise from the characteristics of the hydrogen bonds it is important to get deeper insight in the dynamics of the hydrogen bonds in the melt state. Therefore, suitable amorphous polymers with a low glass transition temperature ($T_g \ll T_{RT}$) had to be synthesized in order to achieve “simple” model systems without additional contributions of crystalline polymer domains typically present in partially crystalline polymers. Highly defined polymers in terms of complete functionalization and molecular weight distribution were needed to directly relate the mechano-physical properties of the corresponding supramolecular polymers to the extent of hydrogen bonding. Furthermore, the influence of chain length (molecular weight), architecture (linear monofunctional and linear bifunctional chains), strength of the hydrogen bonding interaction (in terms of $K_{\text{assn.}}$), temperature and polarity of the polymer melt was investigated.

3. Concept

For the detailed investigation of the hydrogen bonding dynamics in the polymer melt the corresponding polymer(s) must necessarily fulfill several requirements. Beside a small as possible molecular weight distribution ($PDI < 1.2$) and a complete end group functionalization with the corresponding hydrogen bonding groups, high thermal (and chemical) stability and an adjustable molecular weight was desirable. Furthermore, the polymers should be different in polarity and exhibit a low glass transition temperature. Therefore, poly(isobutylene) (PIB) was chosen as a low polarity polymer (**Figure 20a**) while poly(*n*-butyl acrylate) (PnBA) was chosen as a polymer with medium polarity (**Figure 20b**). Both polymers were accessible via “living” polymerization techniques, allowing the synthesis of polymers with a low PDI and a defined end group, being either mono- or bifunctional.

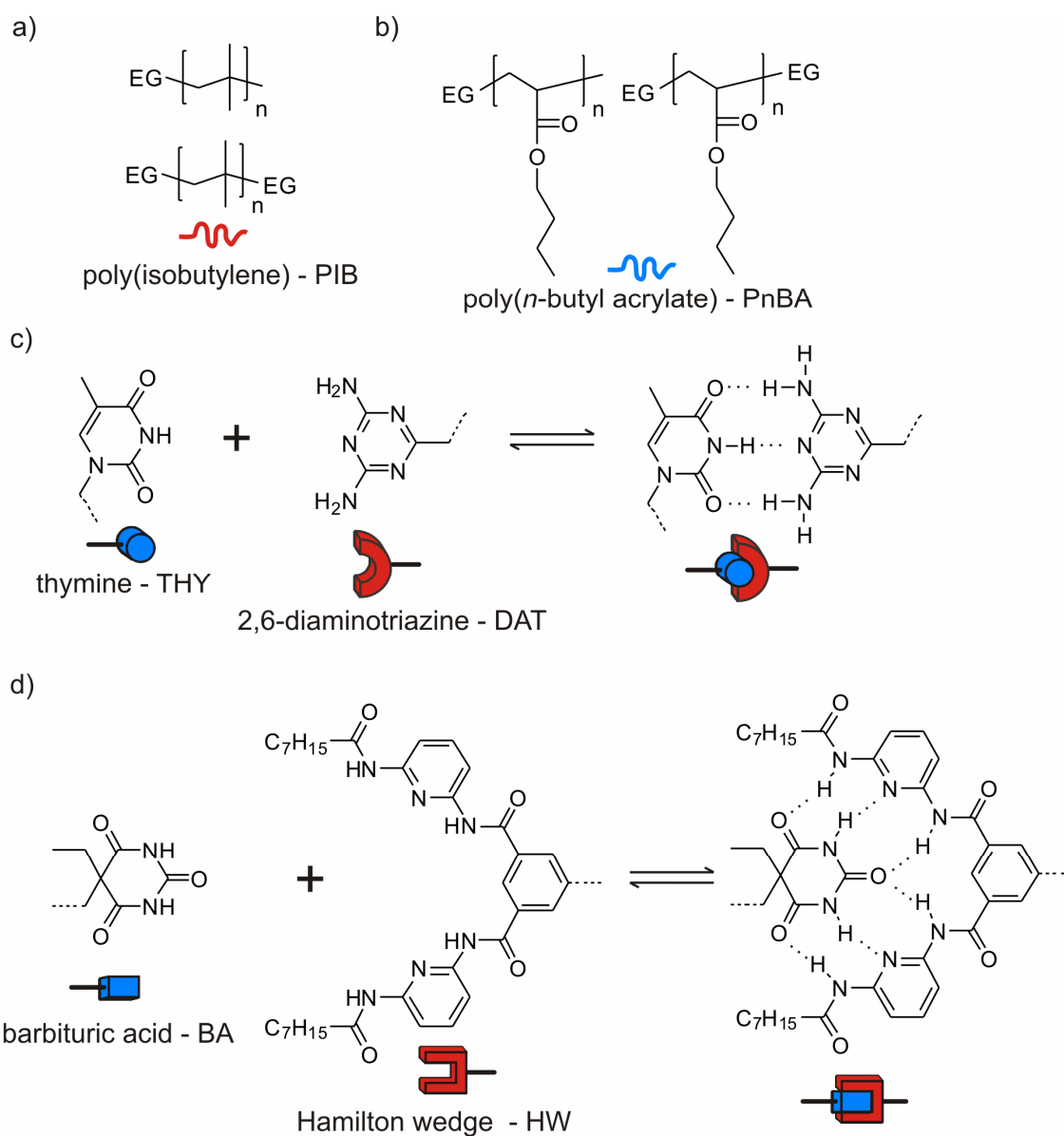


Figure 20. Concept for the investigation of the dynamics of hydrogen bonding in the polymer melt.

3. Concept

While PIB could be synthesized via living carbocationic polymerization (LCCP), PnBA was available via atom transfer radical polymerization (ATRP). For the combination of both, polymer and hydrogen bonding moiety, the azide-alkyne-“click” reaction was chosen since it is very compatible with polar groups (hydrogen bonding moieties) and both polymers were accessible as azides via post-polymerization modification reactions (**Figure 20**). This modular approach allowed the synthesis of the functionalized polymers from the very same batch of azide-functionalized polymers allowing a good comparison of the mechanical investigations.

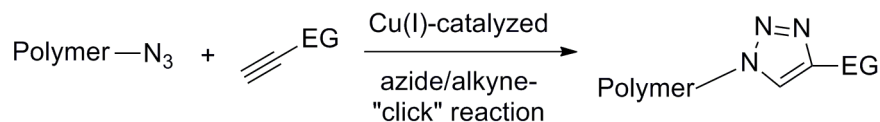


Figure 21. Azide/alkyne-“click” reaction of azide-functionalized polymers and alkyne functionalized hydrogen bonding moieties (EG = end group).

Therefore, the hydrogen bonding groups were needed as the corresponding alkynes. The strength of the hydrogen bonding motif was varied by utilizing either the triple hydrogen bonding motif thymine/2,6-diaminotriazine (THY-DAT) (**Figure 20c**) or the sextuple hydrogen bonding motif Hamilton wedge/barbituric acid (HW-BA) (**Figure 20d**). All groups (THY, BA and HW) were synthetically available as alkynes, while for DAT the development of a synthetic route was necessary. The association of the hydrogen bonding motifs was investigated in solution via ¹H-NMR titration experiments, since literature values for low molecular weight compounds were available for comparison. In the melt state the association/aggregation was investigated via oscillatory melt rheology, since it allows the time (frequency) and temperature dependent measurement of the amorphous polymers. Furthermore, melt rheology is very sensitive towards the structure (linear chains), the functionality (complete functionalization of all chains; telechelic polymers) and the molecular weight distribution (PDI). Small-angle X-ray scattering (SAXS) is a commonly used tool to explore the microstructure of block copolymers or supramolecular assemblies on the nanometer scale. Since the functionalized polymers bearing hydrogen bonding moieties can be seen as block copolymers with a long non- or medium-polar (the PIB or PnBA chain) and a very short highly polar block (hydrogen bonding end group) SAXS measurements were performed to gain a deeper insight into the nanostructure of these polymers.

4. General part

4.1. Synthesis of azide-functionalized poly(isobutylene)s

The common pathway towards poly(isobutylene) is the carbocationic polymerization.^[210] Under specific conditions (temperature,^[211] initiator, Lewis acid co-initiator, solvent etc.) side reactions, especially β -H-elimination, can be suppressed to a minimal extend. When specific initiator systems were applied, all polymer chains can be initiated at the very same time at the beginning of the polymerization process. Therefore, the final chain length (molecular weight) can be calculated by the monomer/initiator ratio and the polymer exhibits a small PDI (< 1.2). The so called “living carbocationic polymerization”^[212-213] (LCCP) was developed by Iván and Kennedy^[214] and is the advancement of their “inifer” method.^[215-217]

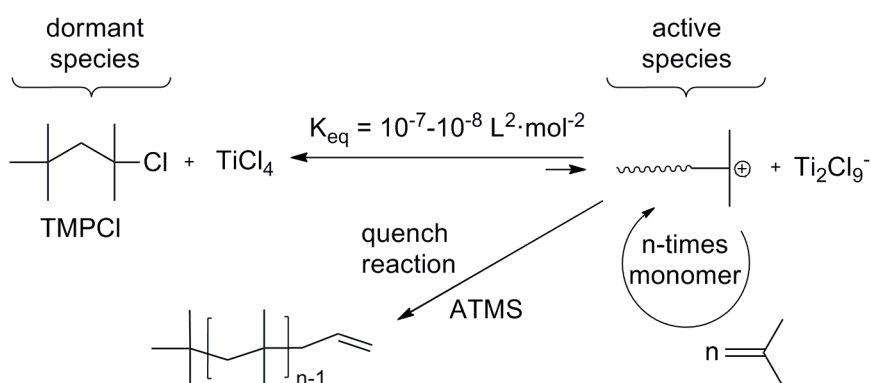


Figure 22. Concept of the living carbocationic polymerization (LCCP).

The basic concept of the LCCP is shown in **Figure 22**. Besides the monomer (isobutylene) and an initiator (e.g. TMPCl^[218] - a tertiary chloride), the addition of an Lewis (e.g. TiCl₄,^[219-220] BCl₃,^[221-223] FeCl₃^[224] or GaCl₃^[225]) acid is necessary to establish the equilibrium displayed in **Figure 22**. Only the “free” carbocation (“free” depends on the solvatization) can react with an additional monomer, while the tertiary chloride species can not. Therefore, these species are referred as dormant- (left side) and active species (right side). For an arbitrary LCCP this equilibrium lies far on the side of the dormant species (left side), with typical values for the equilibrium constants of $K_{eq.} = 10^{-7} - 10^{-8} \text{ L}^2 \cdot \text{mol}^{-2}$.^[210] One drawback of the LCCP is the sensitivity of the Lewis acid towards nucleophiles. As result a LCCP is not only extremely sensitive towards water, furthermore, the direct introduction of functional groups is limited to nucleophiles which exclusively react with the carbocation, but do not affect the Lewis acid (and thus the equilibrium).

However, several end groups can selectively introduced by end quenching the LCCP,^[217, 226-245] whereby at the beginning of this work only the quenching with allyltrimethylsilane

4. General Part

(ATMS)^[246-247] and subsequent multistep postpolymerization transformation allowed the defined synthesis of azide-functionalized PIBs. The resulting PIBs were either mono-^[218] or the bifunctional.^[248] Functionality was introduced by using allyltrimethylsilane (ATMS) as π -nucleophile quenching agent for the LCCP,^[246-247] resulting in allyl-functionalized PIBs – a polymer which can conveniently be transformed into the azide-functionalized polymer (**Figure 23**).^[215, 246, 249-254]

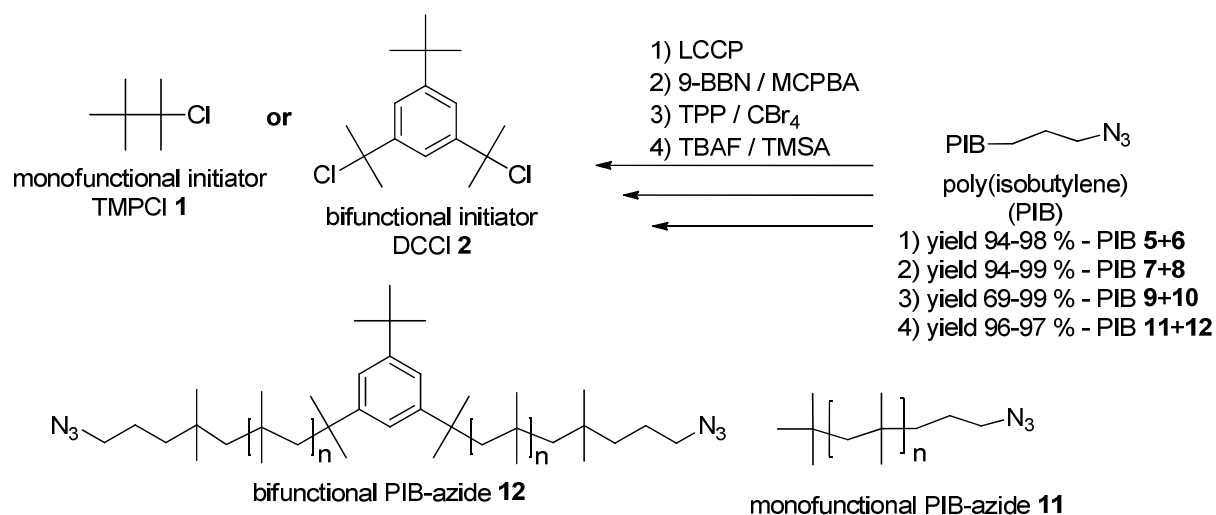


Figure 23. Synthetic route towards mono- and bifunctional azide-functionalized PIBs.

The synthesized allyl- and azide-functionalized PIBs are summarized in **Table 2** revealing a perfect match between the calculated ($M_{n(th)}$) and experimental ($M_{n(GPC)}$ and $M_{n(NMR)}$) molecular weight(s) for the allyl-functionalized PIBs (**5+6**), evidencing the living character of the polymerization.

4. General Part

Table 2. Allyl-functionalized poly(isobutylene)s (PIB-allyl) (**5+6**) synthesized via LCCP and azide-functionalized PIBs (PIB-azide) (**11+12**) synthesized via multi-step end group transformation.

entry	PIB	mono ^a or bi ^b	M _{n(th)} [g·mol ⁻¹]	[M]/[I]	characterization				
					M _{n(GPC)} ^c [g·mol ⁻¹]	PDI ^c	M _{n(NMR)} [g·mol ⁻¹]	yield [g]	yield [%]
1	5a	m	3000	51.6	3100	1.13	3000	14.4	96.0
2	5b	m	10000	175.3	8500	1.10	8700	14.2	94.6
3	6a	b	3000	48.2	2400	1.12	2400	12.4	95.4
4	6b	b	10000	173.1	8600	1.16	8700	6.4	98.6
5	11a	m	2800 ^d	—	2600	1.12	2900	12.0	96.1 ^e
6	11b ^f	m	2700 ^d	—	2800	1.23	3000	1.6	69.7 ^e
7	11c	m	7700 ^d	—	7700	1.11	7800	15.3	97.3 ^e
8	11d ^f	m	29600 ^d	—	28600	1.10	— ^g	6.4	89.9 ^e
9	12a ^f	b	3400 ^d	—	3400	1.23	3500	0.5	82.8 ^e
10	12b ^f	b	3200 ^d	—	3100	1.29	3300	3.7	81.7 ^e
11	12c ^f	b	8100 ^d	—	7600	1.24	8400	4.2	91.1 ^e
12	12d ^f	b	13900 ^d	—	13800	1.23	14800	2.2	90.0 ^e
13	12e ^f	b	27400 ^d	—	29200	1.18	29300	3.4	97.0 ^e

^a Initiator = TMPCl (**1**); ^b initiator = DCCl (**2**); ^c external calibration with PIB standards; ^d molecular weight of the bromine-functionalized precursor; ^e yield of the last transformation step from PIB-Br to PIB-N₃; ^f these polymers were already synthesized within the framework of my diploma thesis^[255]; ^g not possible due to poor resolution of the initiator fragment.

4.2. Synthesis of functionalized PIBs bearing hydrogen bonding moieties via the azide/alkyne-“click” reaction

In order to investigate the influence of specifically interacting hydrogen bonding groups on the mechano-rheological behavior of PIB it was necessary to attach the corresponding motifs onto the chain end(s) of the PIB. For a precise comparison of the resulting data it was further necessary to synthesize the functionalized polymers, bearing our selection of hydrogen bonding motifs (THY, DAT, HW, BA and other groups), from the very same batch of polymer (same molecular weight). A few synthetic routes were reported to attach one of these groups onto PIB chains,^[88] e.g., monofunctional PIB-THY can be synthesized via Michael addition of a PIB-acrylate precursor and thymine (2-step reaction)^[240] or (mono- and bifunctional) via nucleophilic substitution reaction with activated chloromethyl ethers.^[250]

A suitable route to attach our selection of H-bonding motifs is only given by the azide/alkyne-“click” reaction. Based on the work of Huisgen,^[256-258] it was Sharpless and coworkers who rediscovered this versatile reaction.^[259-260] Since the 1,3-dipolar cycloaddition between terminal acetylenes and azides is a highly effective (high yields) reaction, which

4. General Part

additionally has a high tolerance towards solvents and functional groups, it is nowadays one of the basic tools for the attachment of functional groups in polymer chemistry.^[261-269] Starting from the azide-functionalized PIBs the corresponding alkyne functionalized hydrogen bonding groups were attached via Cu^I catalysis to form regioselective the 1,4 triazole (see **Figure 24**).^[270]

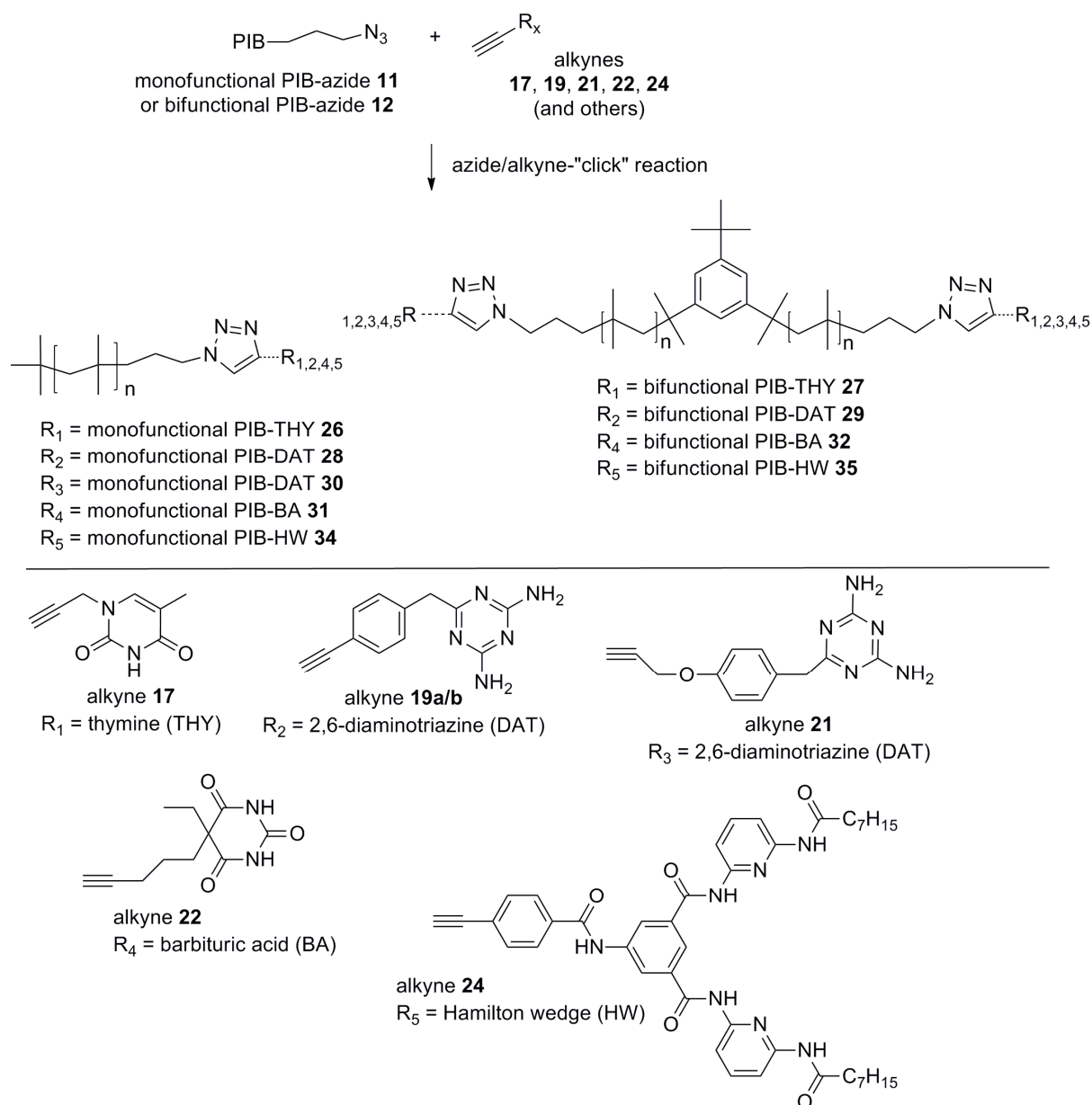


Figure 24. Synthetic concept for the synthesis of PIBs bearing different hydrogen bonding moieties.

PIB bearing hydrogen bonding moieties were successfully synthesized via a microwave assisted azide/alkyne-"click" reaction under common reaction conditions (see experimental part). It turned out, that with increasing molecular weight of the starting polymer, the yield decreases markedly for alkynes **19** and **24** (see **Table 3**). This effect can be attributed to the

4. General Part

sensibility of alkyne **19** and **24** (aromatic terminal alkyne group) towards Glaser-like coupling reactions. Even a 10-fold excess of alkyne **19** (see entry 7) did not lead to improved results. Starting from bifunctional PIB-N₃, an incomplete functionalization can lead to a mixture of non-, mono-, and bifunctionalized PIB chains. Unfortunately PIB does not give clear spots in TLC, therefore, no separation of mono- and bifunctionalized chains was possible. As a consequence only low molecular weight PIB-DAT₂ and PIB-HW₂ could be synthesized with complete functionalization. A later refinement applying alkyne **21** revealed a better yield for a high molecular weight PIB (entry 6) compared to alkyne **19** (entry 4+5). This observation indicates a reduced sensitivity of the aliphatic terminal alkyne **21** towards oxidative coupling reactions.

Critical for the following rheological investigations was the synthesis of the pure polymeric material, truly containing the hydrogen bonding end group(s) quantitatively. Therefore, the structure was confirmed via ¹H- and ¹³C-NMR spectroscopy, as well as MALDI-TOF-MS measurements for all functionalized PIBs. The proof for complete functionalized is exemplarily described for a bifunctional PIB bearing BA end groups. A comparison of the resonance of the initiator fragment at 7.17 ppm (3H for PIB-BA₂ **32a-e**) and the characteristic resonance of the end group at 2.74 ppm (4H for PIB-BA₂ **32a-e**) revealed a perfect match of the integrals, evidencing a complete (bi-)functionalization. ¹³C-NMR revealed the appearance of the signals of the end group and the initiator fragment in the low field region (**Figure 25a**).

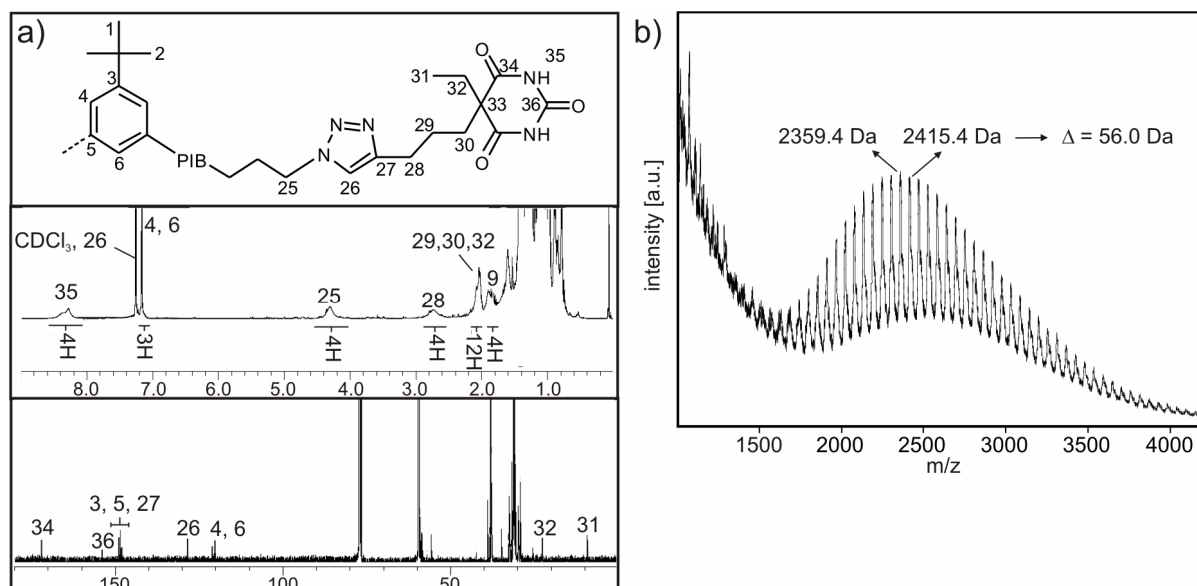


Figure 25. a) ¹H- and ¹³C-NMR spectra and b) MALDI-TOF-MS spectrum of PIB-BA₂ **32a**.

In addition to the expected resonances in NMR, the structure was confirmed by MALDI-TOF-MS measurements. The MALDI-TOF-MS spectrum of PIB-BA₂ **32a** is shown in **Figure**

4. General Part

25b, displaying two main series. Each series of ions is separated by 56.1 Da, reflecting the mass of the monomer repeating unit. In agreement with earlier observations for PIB-polymers reported by Binder *et al.*,^[250] the most intensive signal of the main series can be assigned to an $[\text{M}\cdot\text{Na}_3\text{Li}_1]^+$ -ion, assuming the exchange of three of the acidic CO–NH–CO protons of the barbituric acid groups. For a species $[\text{M}\cdot\text{Na}_3\text{Li}_1]^+$ ($n = 26$) the theoretical m/z value of 2360.034 Da is in good agreement with the experimental value of 2359.4 Da ($\Delta m = 294$ ppm). For the second series, the most intensive peak at 2427.6 Da can be assigned to a species $[\text{M}\cdot\text{Na}_1\text{Li}_1]$ ($n = 28$), in good agreement with the theoretical m/z value of 2428.255 Da ($\Delta m = 269$ ppm). Therefore, the combination of NMR and MALDI-TOF-MS measurements proved the complete functionalization of the PIBs.

4. General Part

Table 3. 2,6-Diaminotriazine-functionalized PIBs (PIB-DAT) (**28+29**; entry 1-8), barbituric acid-functionalized PIBs (PIB-BA) (**31-33**; entry 9-18) and Hamilton wedge-functionalized PIBs (PIB-HW) (**34+35**; entry 19-24) synthesized via azide/alkyne-“click” reactions.

entry	PIB	mono or bi	alkyne	$M_{n(\text{azide})}^a$ [g·mol ⁻¹]	catalyst-system	characterization					
						T_{decay}^e [°C]	$M_{n(\text{NMR})}$ [g·mol ⁻¹]	$M_{n(\text{GPC})}^b$ [g·mol ⁻¹]	PDI ^b	yield [mg]	yield [%]
1	28a	m	19	2800	CuITEP	–	3200	– ^f	– ^f	74	39.0
2	28b	m	19	2600	CuITEP	–	4000	– ^f	– ^f	1030	42.6
3	28c	m	19	2600	CuSO ₄ / NaAsc	–	2700	– ^f	– ^f	36	52.9
4	28d	m	19	7800	CuITEP	–	7900	– ^f	– ^f	180	11.9
5	28e	m	19	7700	CuITEP	–	7600	– ^f	– ^f	729	55.9
6	30a	m	21	7800	CuITEP	–	8200	6300 ^a	1.1	654	92.1
7	28f	m	19	28600	CuITEP/ CuBr	–	– ^d	23500 ^a	1.1	6	6.7
8	29a	b	19	3400	CuITEP	–	3700	– ^f	– ^f	45	90.9
9	31a	m	22	2800	CuBrTTPP	–	3800	2700	1.2	11	23.9
10	31b	m	22	2600	CuBrTTPP /CuBr ^c	368	3800	2400	1.1	316	52.7
11	31c	m	22	7700	CuBrTTPP/ CuBr ^c	357	7000	6500	1.1	554	55.4
12	31d	m	22	28600	CuBrTTPP /CuBr ^c	359	– ^d	27200	1.1	479	50.7
13	32a	bi	22	3200	CuBrTTPP /CuBr	–	4700	4900	1.6	33	16.4
14	32b	bi	22	3200	CuBrTTPP /CuBr	362	3900	4000	1.3	443	58.6
15	32c	bi	22	13800	CuBrTTPP /CuBr	362	14000	13800	1.2	357	74.8
16	32d	bi	22	7600	CuBrTTPP /CuBr ^c	355	8700	7900	1.2	466	79.1
17	32e	bi	22	~30000	CuBrTTPP /CuBr ^c	345	28400	26700	1.1	256	54.2
18	33	bi	23	3100	[(Ph ₃ P) ₃ CuBr /CuBr	342	3800	3700	1.3	180	80.8
19	34a	m	24	2800	CuBrTTPP /CuBr ^c	–	3330	3200	1.2	49	94.2
20	34b	m	24	2600	CuBrTTPP /CuBr ^c	346	3470	2400	1.1	463	63.0
21	34c	m	24	7700	CuBrTTPP /CuBr	372	8500	8300	1.1	390	39.1
22	34d	m	24	28600	CuBrTTPP/ CuBr	363	27700	25900	1.1	71	7.0
23	35a	bi	24	3200	CuBrTTPP/ CuBr	343	4900	4700	1.2	384	43.3 ^g
24	35b	bi	24	13800	CuBrTTPP /CuBr ^c	–	functionalization max. 50 %			99	34.0

^a Molecular weight of the azide-functionalized precursor; ^b external calibration with PIB standards; ^c excess of CuBr was used, which means ≥ 10 equivalents with respect to the amount (mmol) of polymer; ^d not possible due to poor resolution of the initiator fragment; ^e determined at 5 % weight loss; ^f M_n -values determined via GPC-measurements are considerably underestimated, probably due to interaction of the 2,6-diaminotriazine group with the column material; ^g NMR integration reveals a functionalization of minimum 94 %.

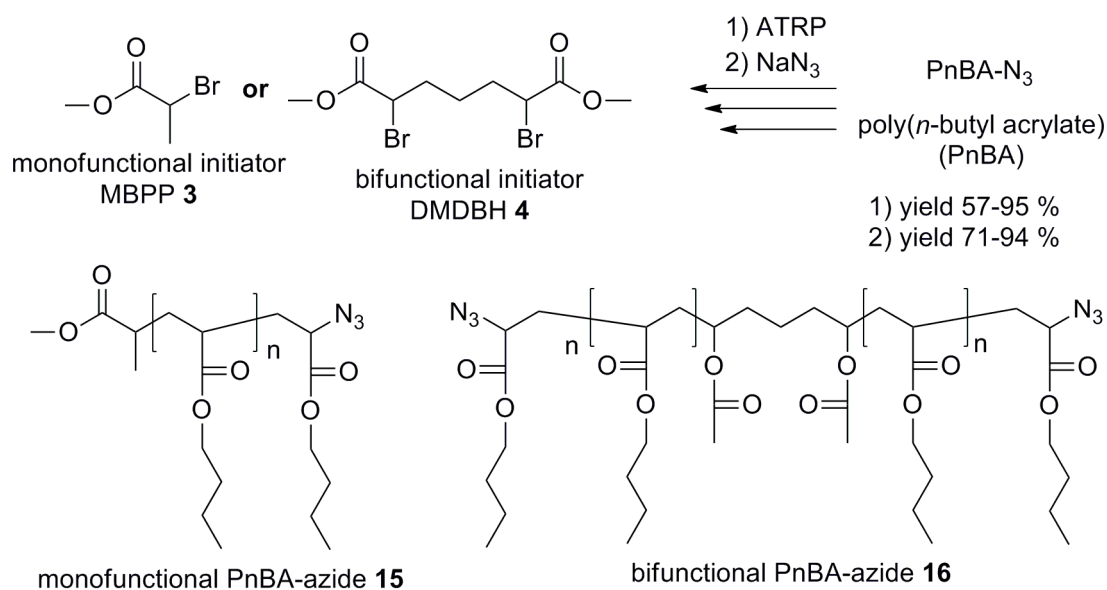
4.4. Synthesis of azide-functionalized poly(*n*-butyl acrylate)s

Figure 26. Synthetic concept for the synthesis of azide-functionalized PnBAs.

The synthesis of azide-functionalized poly(*n*-butyl acrylate)s (PnBAs) was accomplished via a combination of atom transfer radical polymerization (ATRP) and postpolymerization transformation reaction according to Coessens *et al.* (Figure 26).^[271-272] Since this approach allowed the synthesis of the azide-functionalized PnBA via a convenient 2-step route, it is advantageous over the approach via living anionic polymerization of *tert*-butyl acrylate, transesterification with butanol and subsequent end group transformation.^[273-274] Furthermore, several attempts were reported to directly introduce different hydrogen bonding groups via a combination of functionalized initiators and controlled radical polymerization (ATRP, NMP or RAFT).^[71, 91-92, 275-279] However, these strategies are limited by the availability of the corresponding functional initiators. Therefore, only the route via the azide/alkyne-“click” reaction allowed the projected synthesis of supramolecular mono- and bifunctional PnBAs bearing the four selected hydrogen bonding groups (THY, DAT, BA and HW) from the very same batch of polymer. After the literature workup the polymers contained significant amounts of the dNbpy-ligand that crystallized as white needles within the final polymers. Therefore, the corresponding polymers were efficiently purified via dialysis in THF (MWCO of the dialysis tubes was 1000 Da). Mono- and bifunctional polymers were synthesized utilizing either the monofunctional initiator MBPP or the bifunctional initiator DMDBH. The molecular weight could be tailored via the [M]/[I] ratio, proving the controlled character of the ATRP. Polymers up to a molecular weight of ~22000 g/mol were synthesized with good yields and narrow chain distributions (Table 4).

4. General Part

Table 4. Azide-functionalized PnBAs (PnBA-N₃) synthesized via ATRP and subsequent end group transformation.

entry	PnBA	mono or bi	M _{n(GPC)} ^a [g·mol ⁻¹]	characterization					
				T _{decay} ^e [°C]	M _{n(GPC)} ^b [g·mol ⁻¹]	PDI	M _{n(NMR)} [g·mol ⁻¹]	yield ^c [g]	yield ^c [%]
1	15a	m	1800	245	2100	1900	1.2	2.00	71.9 ^d
2	15b	m	3200	323	3400	3300	1.2	8.40	88.9
3	15c	m	8000	337	9800	8000	1.1	7.61	88.5
4	16a	bi	3800	335	4300	3500	1.2	8.12	94.8
5	16b	bi	22500	342	24500	22800	1.1	4.30	94.3

^a Molecular weight of the bromine-functionalized precursor; ^b external calibration with PS standards; ^c yield of the last transformation step from PnBA-Br to PnBA-N₃; ^d purified via dialysis after transformation into the azide; ^e measured at 5% weight loss.

In order to prove the complete functionalization with azide groups, MALDI-TOF-MS measurements were performed. While the initial PnBA-Br also revealed a small series of chains bearing a chloride as halogen atom, the PnBA-N₃ polymers were proven to be fully functionalized, also via ¹H-NMR (see appendix).

Therefore, mono- and bifunctional PnBAs with different molecular weights could be efficiently synthesized via combination of atom transfer radical polymerization and subsequent end group transformation.

4.5. Synthesis of functionalized PnBAs bearing hydrogen bonding moieties via the azide/alkyne-“click” reaction

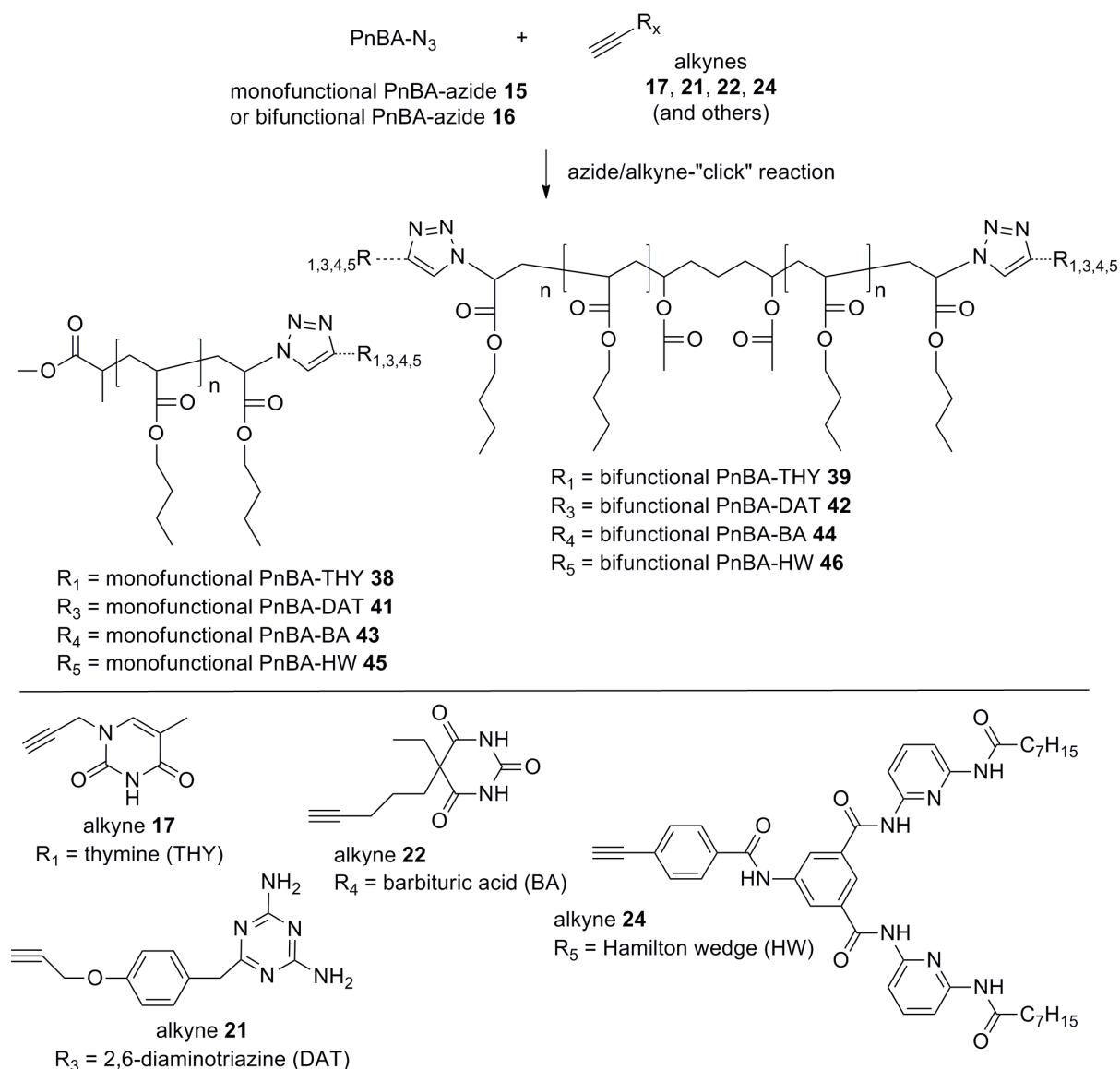


Figure 27. Synthetic concept for the synthesis of PnBAs bearing different hydrogen bonding moieties.

PnBAs with hydrogen bonding moieties were synthesized via microwave assisted azide/alkyne-“click” reactions. Freeze-pump-thaw cycles were performed in order to remove even traces of oxygen and different Cu(I)-catalysts were applied, but in each case a fraction of the starting material had to be isolated via column chromatography. Fortunately, in the case of bifunctional PnBAs the separation of the mono- and bisubstituted product was hardly possible. Therefore, even high molecular weight bifunctional PnBAs could be synthesized. **Table 5** summarizes the synthesized PnBAs bearing hydrogen bonding motifs. For HW-functionalized PnBAs the yields decrease with increasing molecular weight of the PnBA (**Table 5**; entry 15-17). Since the reactions were performed after three freeze-pump-thaw cycles in a sealed Schlenk-flask, the presence of significant amounts of oxygen can be

4. General Part

excluded. Therefore, also other unknown side-reactions, despite the already mentioned Glaser-type coupling reactions, are feasible.

Table 5. Thymine-functionalized PnBAs (PnBA-THY) (**38+39**; entry 1-6), 2,6-diaminotriazine-functionalized PnBAs (PnBA-DAT) (**41+42**; entry 7-11), barbituric acid-functionalized PnBAs (PnBA-BA) (**43+44**; entry 12-14) and Hamilton wedge-functionalized PnBAs (PnBA-HW) (**45+46**; entry 15-17) synthesized via azide/alkyne-“click” reactions.

entry	PnBA	mono or bi	alkyne	$M_{n(\text{azide})}^a$ [g·mol ⁻¹]	catalyst-system	characterization					
						T_{decay}^c [°C]	$M_{n(\text{NMR})}$ [g·mol ⁻¹]	$M_{n(\text{GPC})}^b$ [g·mol ⁻¹]	PDI ^b	yield [mg]	yield [%]
1	38a	m	17	1900	CuBrTTPP	306	1800	2250	1.2	293	87.4
2	38b	m	17	3200	CuBr	303	3900	3300	1.2	695	65.6
3	38c	m	17	8000	CuITEP	317	10300	8700	1.1	566	55.1
4	38d	m	17	3200	CuITEP	303	3900	3100	1.2	473	44.5
5	39a	b	17	3500	CuBr	323	4600	3000	1.2	753	61.9
6	39b	b	17	22800	CuBr	310	26900	24100	1.1	259	12.9
7	41a	m	21	1900	CuBr	315	2300	1400	1.2	194	55.2
8	41b	m	21	3300	CuITEP	315	3800	2000	1.2	490	47.5
9	41c	m	21	8000	CuITEP	316	10900	8600	1.1	600	54.3
10	42a	b	21	3500	CuBr	333	4600	1700	1.3	796	61.1
11	42b	b	21	22800	CuBr	345	29600	25500	1.1	490	24.0
12	43a	m	22	3300	CuBr	322	3400	2700	1.2	651.0	60.0
13	43b	m	22	8000	CuBr	336	10200	9400	1.2	790.0	72.5
14	44a	bi	22	3500	CuBr	327	4700	4700	1.2	590.0	53.2
15	45a	m	24	9800	CuBr	335	10800	10200	1.1	152.0	23.7
16	45b	m	24	3400	CuBr	340	4000	4200	1.1	412.0	36.4
17	46a	bi	24	4300	CuBr	342	5500	5800	1.1	610.0	57.0

^a Molecular weight of the azide-functionalized precursor; ^b external calibration with PS standards; ^c measured at 5% weight loss.

Since the complete functionalization with the corresponding hydrogen binding motif is crucial for subsequent rheological investigations, ¹H- and ¹³C-NMR measurements as well as MALDI-TOF-MS measurements were performed. NMR-investigations revealed the appearance of all expected resonances and integration of the resonances of initiator- and end group evidenced the complete functionalization in each case. For a more detailed analysis MALDI-TOF-MS measurements were performed, revealing only species of the desired product in each case. A representative MALDI-TOF-MS spectrum is shown in **Figure 28** and described exemplarily. For PnBA-THY₂-4k (**39a**) the best spectrum was obtained by

4. General Part

ionization with Na-ions (matrix: IAA:NaTFA:Analyte = 100:10:1), showing four important series, where each series of ions is separated by ~ 128.1 Da, the mass of the repeating unit (calculated 128.1 Da).

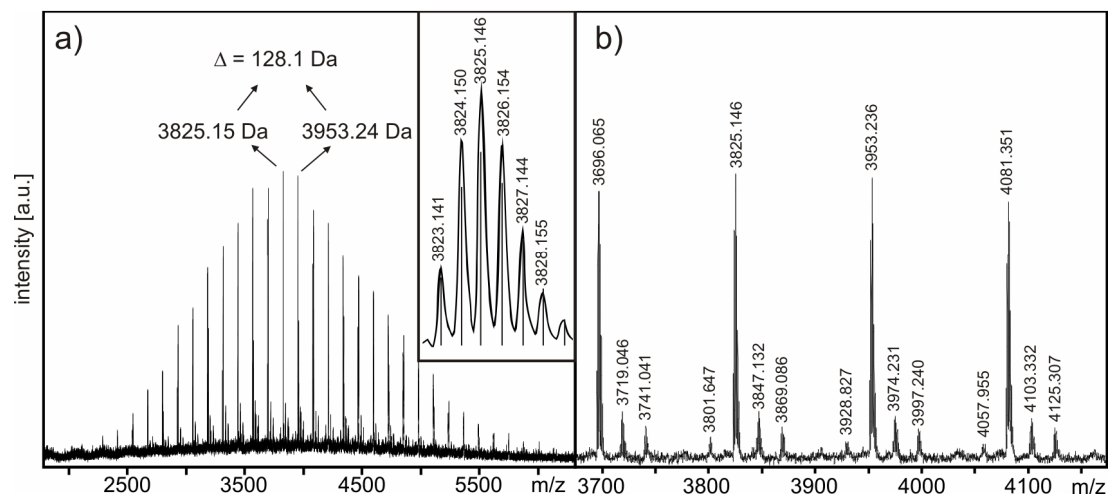


Figure 28. MALDI-TOF-MS spectrum of PnBA-THY₂-4k (**39a**) with $M_n \approx 4000$ Da.

The most intensive signal of the main series at 3825.146 Da can be assigned to a species $[M \cdot Na]^+$ ($C_{200}H_{330}N_{10}O_{58}Na_1$; $n = 24$), a value that agrees well with the theoretical m/z value for a species $[M \cdot Na]^+$ ($n = 24$) of 3825.314 Da ($\Delta m = 44$ ppm). For the first and second minor series the acidic proton(s) of the thymine group was exchanged by an ion. The most intensive signal of the first minor series at 3847.132 Da can be assigned to a species $[M \cdot Na_2]^+$ ($C_{200}H_{329}N_{10}O_{58}Na_2$; $n = 23$), in good agreement with the theoretical m/z value for a species $[M \cdot Na_2]^+$ ($n = 23$) of 3847.296 Da ($\Delta m = 43$ ppm). The most intensive signal of the second minor series at 3869.278 Da can be assigned to a species $[M \cdot Na_3]^+$ ($C_{200}H_{328}N_{10}O_{58}Na_3$; $n = 23$), a value that agrees well with the theoretical m/z value for a species $[M \cdot Na_3]^+$ ($n = 23$) of 3869.086 Da ($\Delta m = 50$ ppm). For the most intensive signal of the third minor series at 4057.955 Da the species can be assigned to $[M \cdot H]^+$ ($C_{214}H_{355}N_{10}O_{62}Na_3$; $n = 25$), in good match with the theoretical m/z value for a species $[M \cdot H]^+$ ($n = 25$) of 4059.499 Da ($\Delta m = 380$ ppm). The calculated isotopic patterns of the main and first minor series match well with the observed patterns (only visible for low molecular weight peaks).

Therefore, mono- and bifunctional PnBAs with different molecular weights bearing various hydrogen bonding motifs (THY, DAT, BA and HW) could be efficiently synthesized via azide/alkyne-“click” reactions.

4.6. “Capped” thymine-functionalized poly(*n*-butyl acrylate)s – PnBA-THY₂-Cap

In order to investigate the influence of hydrogen bonding in melt rheology measurements the synthesis of analogues of the supramolecular PnBA devoid of hydrogen bonding was necessary (**Figure 29**). A feasible concept for this attempt is the capping of the –CO–NH–CO– proton of the thymine groups via methylation with iodomethane after deprotonation with sodium hydride in dry DMF.

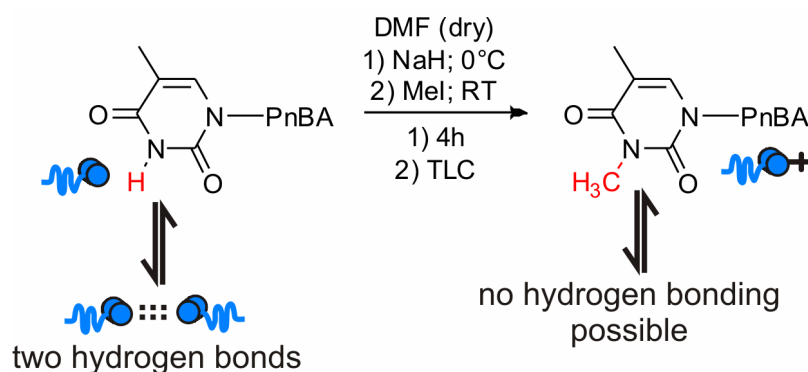


Figure 29. Synthesis of “capped” THY-functionalized PnBA **40**.

Reaction conditions were adapted from Cortial *et al.* and tested to be applicable with a low molecular weight model substance (product of dodecylazide and **17**). Due to the methylation of the hydrogen bonding acceptor (–CO–NH–CO–) there is a significant difference between the R_F -value of starting material and product. Therefore, the conversion can be easily monitored via thin layer chromatography. After work-up the complete conversion was evidenced by the appearance of the additional resonance at 3.34 ppm in ¹H-NMR spectroscopy of the –CO–NCH₃–CO– group (see chapter 5.4.11.).

4.7. Investigation of the association/aggregation of hydrogen bonding moieties in supramolecular polymers

Due to the successful synthesis of the corresponding supramolecular polymers bearing different hydrogen bonding moieties, the analysis of the association or aggregation regarding different polymer-parameters was possible. Besides the strength of the hydrogen bonding motif (THY-DAT vs. BA-HW), the polarity of the polymer(-matrix) (PIB vs. PnBA), the functionality of the polymer (mono- vs. bifunctional) and the molecular weight could be varied within these investigations.

4. General Part

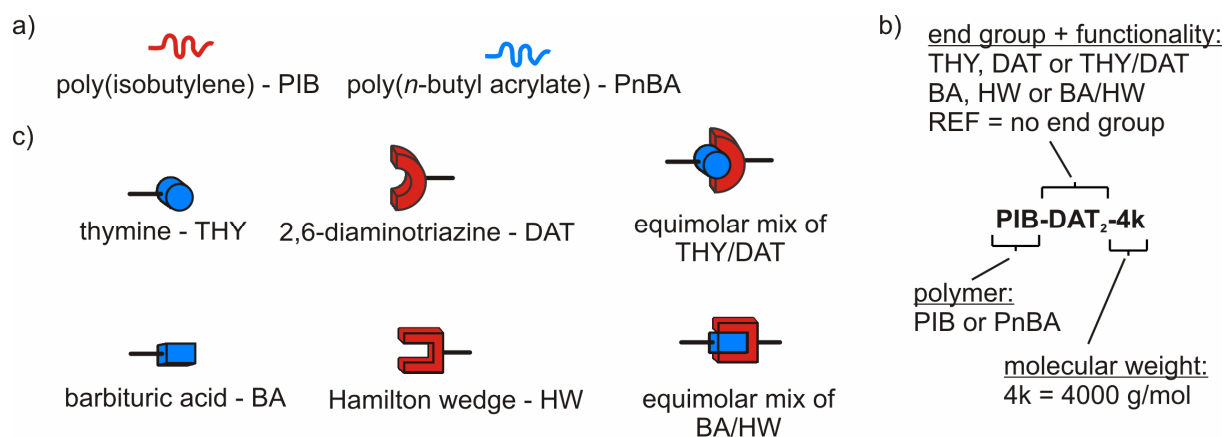


Figure 30. a+c) Comic-abbreviations for the applied supramolecular polymers and b) sample-code for the corresponding samples.

Figure 30a+c shows the used comic-abbreviations for the investigated supramolecular polymers, while **Figure 30b** explains the used sample-code. For example: “PIB-DAT₂-4k” means the polymer is poly(isobutylene) (PIB) which is bifunctional and bears DAT-groups (“DAT₂”). The molecular weight of this sample is 4000 g/mol (“4k”). If the term “THY/DAT” or “BA/HW” is used, the sample contains an equimolar mixture of both polymers. For example: “PnBA-THY/DAT-4k” is an equimolar mixture of a monofunctional PnBA bearing THY-groups and a monofunctional PnBA bearing DAT-groups. Both polymers have a molecular weight of 4000 g/mol (“4k”).

The investigations included the analysis of the association/aggregation in solution and in the polymer melt. For solution studies several methods are known to determine $K_{\text{assn.}}$ including ultrasonic attenuation measurements,^[96] the UV-Vis dilution method^[102] and NMR-titration experiments.^[100, 280] The latter were applied in this work. For an arbitrary binding motif A and B the association in solution is as simple as displayed in **Figure 31**. The rate of association is usually a diffusion controlled process (k_a is identical for most of the hydrogen bonding motifs). Only a few systems are known where e.g. tautomers^[97] or an energetic conformation bias^[281] are significant, here the rate of association is not diffusion controlled.

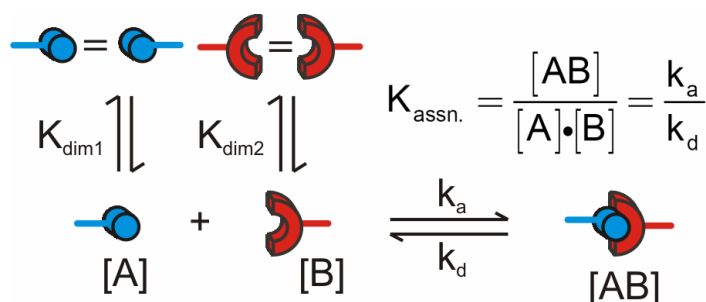


Figure 31. Association modes for the THY-DAT-motif in solution.

4. General Part

For a so called “key-lock-system” (e.g. THY-DAT or BA-HW) the formation of the A–B associate is strongly favored, since the association constant $K_{\text{assn.}}$ ($K_{\text{assn.}} > 1000 \text{ M}^{-1}$) is much higher than the dimerization constant(s) $K_{\text{dim.}}$ ($K_{\text{dim.}} < 100 \text{ M}^{-1}$). Although these studies were usually performed with low molecular weight model substances, no significant impact of the higher molecular weight or the polarity of the applied polymers was expected, since their concentration is too small (to have a significant impact on the viscosity of the solution) and the polarity of the matrix is mainly dictated by the solvent. Additionally, for the investigated systems (THY-DAT and BA-HW) no aggregation in diluted solutions was reported. Therefore, we expect the corresponding $K_{\text{assn.}}$ and $K_{\text{dim.}}$ values to be in the range of the values reported for low molecular weight model substances. However, the polarity of the solvent should influence these values in the way that they will increase with decreasing polarity of the solvent. In this case the association is favored.

Unfortunately, at the beginning of this work only less was known about the association/aggregation behavior of the here applied hydrogen bonding motifs in the melt-state of amorphous polymers. Therefore, the combination of melt rheology studies and SAXS measurements allowed the identification of potential aggregates (SAXS) and their impact on the rheological properties (viscosity, rubbery plateau). Especially rheology measurements are very sensitive towards changes of the microstructure of the polymer (due to association/aggregation). Assuming the simple association of two polymer chains via the supramolecular interaction, the viscosity should be increased by a factor of 2, as long as the chains are below the entanglement molecular weight of the polymer (**Figure 32a**). Otherwise, the relation between viscosity and molecular weight is expected to be $\eta \sim M_n^{3,4}$ (**Figure 32c**).

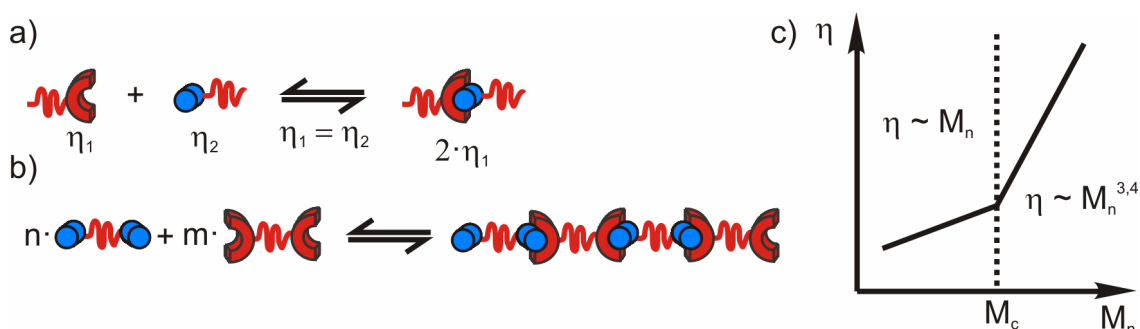


Figure 32. a+b) Possible modes of association of the THY-DAT-motif attached to PIB; c) relation between viscosity and molecular weight of the supramolecular associate.

Especially for bifunctional polymers the formation of long supramolecular chains is possible (**Figure 32b**). In this case, depending on the strength of the interaction, also the formation of a network and, thus, a rubbery plateau in frequency sweep (FS) is possible (see again

4. General Part

introduction **Figure 9**). In the case of a simple association of two groups, the effect on the viscosity should be proportional to the strength of association (determined in solution). However, Rowan *et al.* reported on the formation of stacks of THY-groups in the medium polar poly(THF) matrix (see again introduction **Figure 5**). Such a microphase separation (stacks) of the end group should be visible in SAXS measurements and should cause furthermore a drastic increase of the viscosity. Later, Cortese *et al.* (2011 and 2012) reported on the formation of crystalline domains of THY-groups in a poly(ethylene oxide) matrix.^[90, 143] In this case the polymer might be observed as a solid, with an additional melting peak in DSC measurements. Such effects are expected to be more significant for PIB (low polarity matrix), while the polar PnBA matrix should prevent the THY groups of aggregation or crystallization. However, due to the high polarity of the hydrogen bonding groups similar effects (crystallization or microphase separation) are feasible for all investigated groups (THY, DAT, BA and HW). Besides the formation of cylindrical stacks, also the formation of spherical aggregates (also called “clusters”) is possible (**Figure 33**). Such clusters are expected to be visible in SAXS measurements due to the electron density difference between the cluster and the polymer matrix. Due to additional friction such clusters might increase the viscosity significantly.

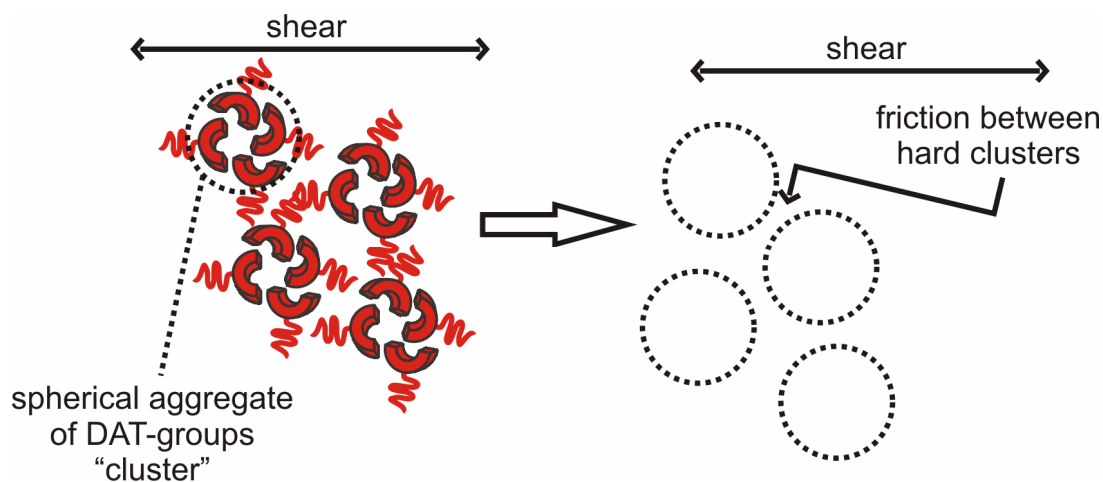


Figure 33. Formation of spherical aggregates (“clusters”) of DAT-groups attached to monofunctional PIBs.

If they have a certain size the clusters might hinder each other, bestowing the sample an elastic portion (in terms of a rubbery plateau), although the polymer chains itself might be far below the entanglement molecular weight. A similar effect was reported by Antonietti *et al.* for PS-microgels.

For bifunctional polymers the formation of long linear entangled chains is possible, whereby the extent of association should be dependent on the strength of the hydrogen bonding

4. General Part

interaction. On the other hand, the formation of aggregates can lead to the formation of a network, usually evidenced by a pronounced rubbery plateau in FS measurements. In this case two different kinds of elastically active entanglements are possible: supramolecular tie-points formed by the hydrogen bonding groups and conventional entanglements. The latter are formed since the chain ends are trapped in the aggregates, although the molecular weight of the chain itself might be below the entanglement molecular weight (**Figure 34**).

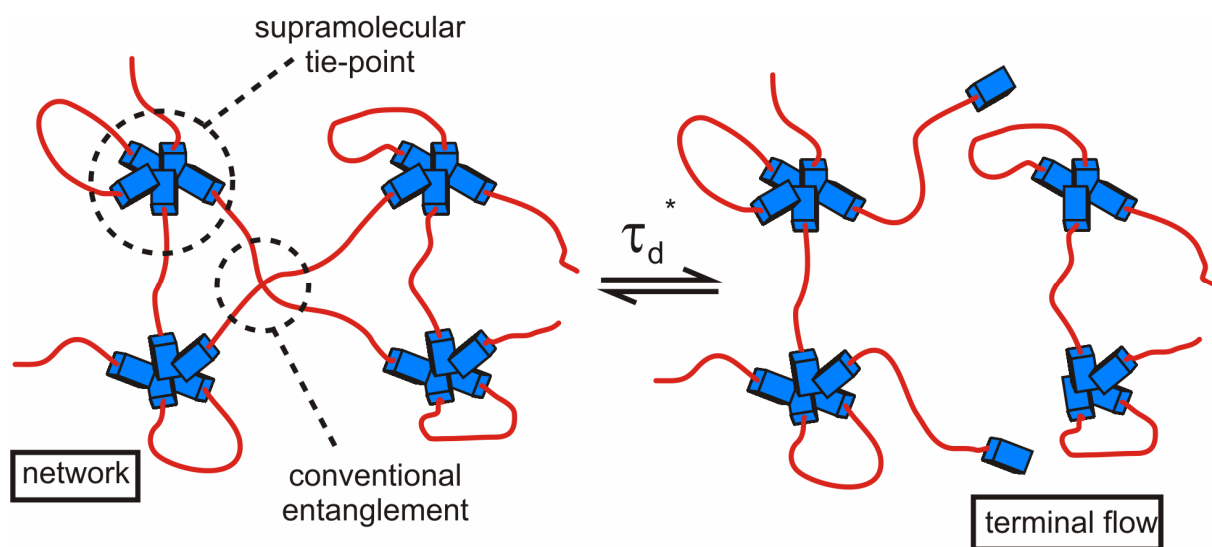


Figure 34. Network formation of a bifunctional PIB bearing BA-groups due to aggregation of the BA-groups.

The resulting network density should be dependent on the number and size of the aggregates. The compared samples have a similar molecular weight and, thus, a similar number of end groups per volume fraction. Smaller aggregates should lead to more elastically active tie-points compared to larger (less) aggregates. As a result the rubbery plateau for small/more aggregates should be higher. Nothing is known about the life-time of these clusters, but it is expected that, e.g., the lifetime of a BA-aggregate (τ_d^*) is significant longer than the lifetime of a BA-BA-associate in solution.

Additionally to the discussed structural effects of the hydrogen bonding groups, also effects on the chain itself are feasible. While the THY, DAT and BA groups have a similar size, the HW is large compared to them. Therefore, also an effect on the glass transition temperature (T_g) is possible, since a change in T_g effects the viscosity of the polymer.

Furthermore, secondary effects, which do not play a role in solution, might become significant in the melt state. For example, for the DAT-group additional π - π -stacking is possible and for the HW-groups a second hydrogen-bonding site is present (**Figure 35**).

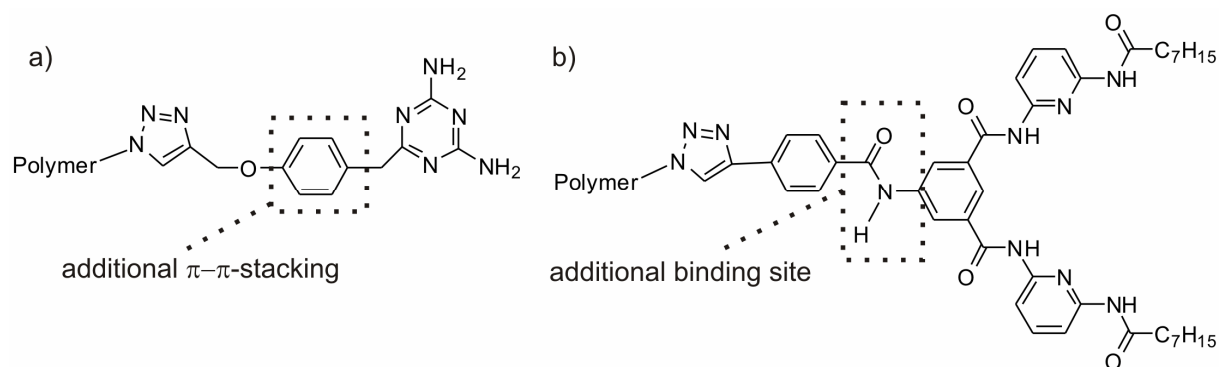


Figure 35. Possible secondary interactions for a) the DAT group and b) the HW group.

4.7.1. Association of hydrogen bonding motifs in solution

The determined dimerization and association for the THY-DAT and the BA-HW system attached to either PIB or PnBA are listed in **Table 6**. As expected the association ($K_{\text{assn.}}$) is much stronger for the “key-lock”-interactions (THY-DAT and BA-HW) than for the dimerization of the individual groups by orders of magnitude. Since for the BA-HW-motif six hydrogen bonds were formed it is stronger than the THY-DAT-motif (3 hydrogen bonds) by two orders of magnitude. All measured values fit with the values reported in the literature, assuming an uncertainty of 10-20 % which is typical for NMR-titration experiments. Only the dimerization constant ($K_{\text{dim.}}$) measured for the HW-HW-association is significant stronger compared to the literature (entry 5 in **Table 6**). This effect can be attributed to the slightly different chemical structure of the Hamilton wedge (HW) in the cited literature.

Table 6. Association ($K_{\text{assn.}}$) and dimerization ($K_{\text{dim.}}$) constant for the THY/DAT and BA/HW system for PIB and PnBA determined via NMR-titration experiments at 25 °C.

entry	interaction	quantity	PIB ^a		PnBA ^b		reference
			value	lifetime [μs]	value	lifetime [μs]	
1	THY-THY	$K_{\text{dim.}}$ [M^{-1}]	3.8 ± 0.49 ^c	$1.9 \cdot 10^{-3}$	70 ± 14 ⁱ	0.04	4.3 ± 0.65 [282]
2	DAT-DAT	$K_{\text{dim.}}$ [M^{-1}]	1.65 ± 0.58 ^d	$8.3 \cdot 10^{-4}$	22 ± 7 ^j	0.01	2.2 ± 0.33 [282]
3	THY-DAT	$K_{\text{assn.}}$ [M^{-1}]	1087 ± 142 ^e	0.54	2.6 ± 1.3 ^k	1.3	870 ± 130 [282]
4	BA-BA	$K_{\text{dim.}}$ [M^{-1}]	12 ± 3 ^f	$6 \cdot 10^{-3}$	— ^l	— ^l	4.0 ± 0.6 [283]
5	HW-HW	$K_{\text{dim.}}$ [M^{-1}]	62 ± 19 ^g 32 ± 11 ^g	0.03	— ^l	— ^l	16 [284] 8 [284]
6	BA-HW	$K_{\text{assn.}}$ [M^{-1}]	$0.6 \pm 0.2 \cdot 10^5$ ^h	30	— ^l	— ^l	0.63 ± 0.06 [109]

^a solvent = $CDCl_3$; ^b solvent = toluene- d_6 ; ^c PIB-THY **38a**; ^d PIB-DAT **41a**; ^e **38a+41a**; ^f PIB-BA **31b**; ^g PIB-HW **34b**; ^h **31b+34b**; ⁱ PnBA-THY **38a**; ^j PnBA-DAT **41a**; ^k **38a+41a**; ^l not possible due to overlapping with the solvent residual peak.

Moreover, the constants measured for PnBA are slightly higher compared to PIB (entry 1-3 in **Table 6**), an observation which can be attributed to the polarity difference of the used

solvents. Therefore, the values measured in toluene- d_6 are higher than in $CDCl_3$ due to the higher polarity of $CDCl_3$. Nevertheless, there is no significant difference of the values measured for the polymeric compounds compared to low molecular weight model substances, evidencing that there is no influence of the molecular weight in NMR-titration experiments under the applied conditions. Assuming a simple diffusion controlled process ($k_a \approx 2 \cdot 10^9 \text{ M}^{-1} \cdot \text{s}^{-1}$ [96]) the bond lifetimes ($\tau_d = 1/k_d$ and $k_d = k_a/K_{\text{assn.}}$ (or $K_{\text{dim.}}$)) can be easily calculated. As expected the bond lifetimes are high for the “key-lock” interactions (entry 3+6). Therefore, the dimerization in solution can be neglected due to the strong directional THY-DAT and BA-HW association.

4.7.2. Association/aggregation of hydrogen bonding motifs in the melt state









Any change of the chain architecture or of the molecular weight leads to a strong effect on the thermo-rheological properties. Since PIB and PnBA have a low T_g ($T_g \ll 0 \text{ }^\circ\text{C}$) both are in the melt state at room temperature and thus ideal candidates to study the association or aggregation of hydrogen bonding motifs in a solvent free (melt) state. Therefore, frequency-dependent melt rheology is a suitable tool to investigate the time- and temperature-dependent association in the melt state^[285] and is also often used for similar studies in solution.^[286-289]

4.7.3. Influence of the molecular weight for PIB and the THY-DAT-system

As a model experiment monofunctional PIBs (**Table 7**) and equimolar mixtures (with respect to the end groups) of PIB-THY and PIB-DAT were utilized to investigate the association/aggregation of the end groups and the effect of the molecular weight in the melt state.

4. General Part

Table 7. Abbreviations for the in this chapter discussed samples.

entry	sample comic	sample code	compounds	molecular weight series
1		PIB-REF-4k	– ^a	4000 g/mol ∩
2		PIB-THY-4k	26b ^b	
3		PIB-DAT-4k	28b	
4		PIB-THY/DAT-4k	26b + 28b	
5		PIB-REF-10k	– ^c	10000 g/mol ∩
6		PIB-THY-10k	26c	
7		PIB-DAT-10k	28d	
8		PIB-THY/DAT-10k	26c + 28d	

^a PIB-REF-4k is a monofunctional PIB-Allyl with $M_n(\text{GPC}) = 3700 \text{ g/mol}$, $M_n(\text{NMR}) = 3700 \text{ g/mol}$ and $\text{PDI} = 1.2$; ^b synthesized via the chloromethyl ether method;^[250] ^c PIB-REF-10k is a monofunctional PIB-Allyl with $M_n(\text{GPC}) = 10600 \text{ g/mol}$, $M_n(\text{NMR}) = 10900 \text{ g/mol}$ and $\text{PDI} = 1.25$.

Since the molecular weights of the samples of the 4k-series are below the entanglement molecular weight ($M_c(\text{PIB}) = \sim 16020 \text{ g/mol}$),^[290] one would expect in the case of an effective connection of two polymer chains due to the supramolecular interaction an increase of the viscosity by a factor of ~ 2 (see **Figure 32a**).^[285] One has to note that it was reported that PIB shows a small deviation from the general theory where $\eta \sim M^1$ is valid for unentangled polymers.^[291] Besides the directed THY-DAT interaction, the dimerization THY-THY and DAT-DAT is possible. On the basis of the association studies in solution one would expect a significant effect of the complementary THY-DAT interaction. Furthermore, the formation of aggregates due to the aggregation of several THY or DAT groups is possible.

None of the functionalized samples shows an additional melting peak in DSC measurements, indicating the absence of any crystalline domains. Furthermore, there is no significant impact of the end group on the T_g of the polymer. For the unfunctionalized PIB-REF-4k a glass transition temperature of $T_g = -69 \text{ }^\circ\text{C}$ was measured which is in agreement with the literature.^[292] The attachment of either a THY (PIB-THY-4k) or a DAT (PIB-DAT-4k) group has only an insignificant effect on T_g which can be assigned to the dependence of the T_g on the molecular weight of the polymer,^[292-293] which slightly increases due to the attachment of the functional group. It was reported that a chain end functionalized poly(ethylene oxide) (PEO) bearing the THY group was obtained as a solid due to crystallization of the THY groups, evidenced by an additional melting peak in DSC measurements.^[90, 143] Although PIB is much less polar than PEO, an effect which should favor the crystallization of the highly polar THY group, no crystallinity was observed. This observation can be attributed to the effect of the molecular weight. The investigated PIBs ($\approx 4000 \text{ g/mol}$) have approximately

4. General Part

double the molecular weight than the PEOs (≈ 2000 g/mol). Therefore, the influence of the THY group is less pronounced and prevents the THY groups from crystallization.

Table 8. Rheology data of the THY/DAT system for monofunctional PIBs with $M_n \approx 4000$ g/mol (entry 1-4) and $M_n \approx 10000$ g/mol (entry 5-9).

entry	sample code	T_g [°C] ^c	T_m [°C]	η' [Pa·s] for T [°C] ^a			
				20	40	60	80
1	PIB-REF-4k	-69	–	299	61	17	6
2	PIB-THY-4k	-67	–	1610	201	37	9
3	PIB-DAT-4k	-67	–	9980 ^b	2110 ^b	574 ^b	254 ^b
4	PIB-THY/DAT-4k	-65	–	11800	1420	241	56
5	PIB-REF-10k	-67.1	–	2430	504	149	65
7	PIB-THY-10k	-65.3	–	154000	3300	527	119
8	PIB-DAT-10k	-65.2	–	42400	7670	1890	407
9	PIB-THY/DAT-10k	-64.6	–	55000	8410	1050	188

^a Values for the zero-shear rate viscosity; ^b sample shows “flowlike” behavior, but the terminal flow is not yet reached; the viscosity is not the true zero shear rate viscosity; instead the viscosity at 0.1 s⁻¹ is displayed; ^c T_g at the midpoint of the transition.

The thermo-rheological data are summarized in **Table 8** and displayed in **Figure 36a**. As anticipated the viscosity decreases with increasing temperature for all samples and the unfunctionalized sample PIB-REF-4k shows the lowest viscosity at each temperature.

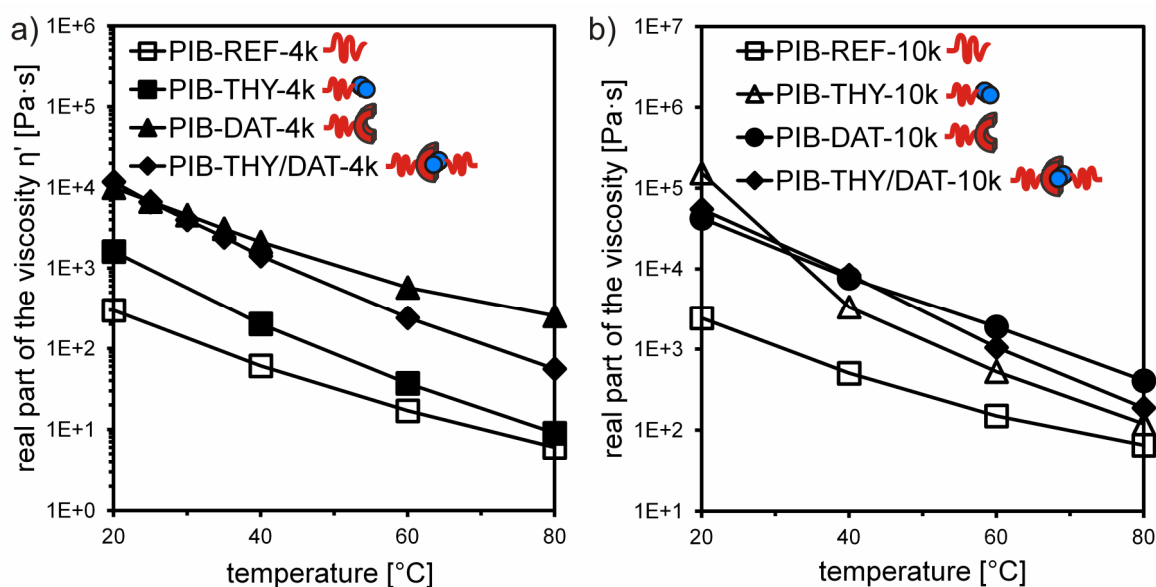


Figure 36. a) Viscosity vs. temperature plot for monofunctional PIBs with $M_n \approx 4000$ Da and b) for monofunctional PIBs with a molecular weight of ~ 10000 g/mol.

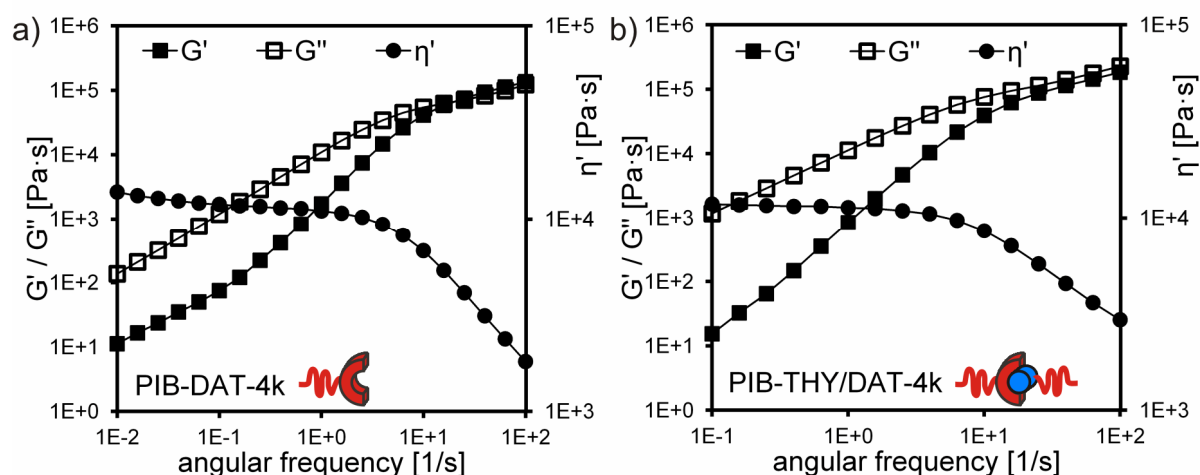


Figure 37. Frequency sweep measurements at 20 °C of a) PIB-DAT-4k and b) PIB-THY/DAT-4k.

The introduction of the THY moiety at the PIB chain end (PIB-THY-4k) results in an increase of the viscosity by a factor of ~ 5.3 at 20 °C. This effect diminishes with increases temperature (at 80 °C the factor is only 1.5) and can be attributed to the interaction of the THY groups.

A similar or weaker effect was expected for PIB-DAT-4k related from the solution studies. However, PIB-DAT-4k reveals a huge increase of the viscosity at 20 °C in comparison to PIB-REF-4k (factor ~ 33) and even in comparison to PIB-THY-4k (factor ~ 6). Additionally, a constant shear rate viscosity was not reached for PIB-DAT-4k (see **Figure 37a**). In both cases the increase of the viscosity can not be explained by the association of two chains via dimerization of two THY or two DAT groups. Since effective entanglement can be excluded, this observation can only be attributed to the formation of aggregates of the hydrogen bonding groups.

It is known that melamine-based systems (which are similar to DAT) undergo a strong aggregation in the solid state.^[294] Furthermore, the thermoreversible formation of supramolecular stacks of THY groups within a poly(THF) matrix was reported,^[70] as well as other systems showing aggregation in the solid or melt state.^[295-296] Therefore, one can assume a similar aggregation of the DAT and THY groups within the PIB melt. In the case of PIB-DAT-4k this assumption could be proven via SAXS measurements.

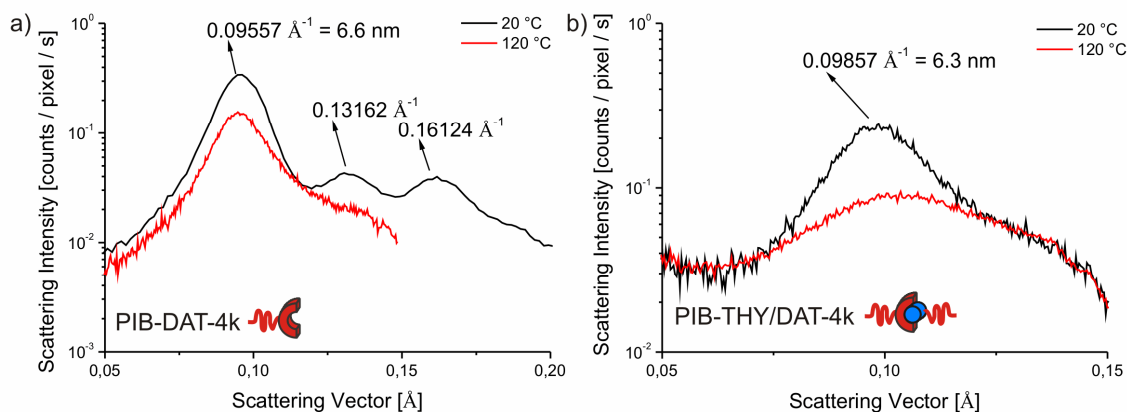


Figure 38. SAXS measurements of a) PIB-DAT-4k and b) PIB-THY/DAT-4k at 20 °C (black curve) and 120 °C (red curve).

Figure 38a shows the SAXS measurement of PIB-DAT-4k (**28b**) revealing a body-centered cubic (BCC) microstructure (ratio of the peaks is $1:\sqrt{2}:\sqrt{3}$) at 20 °C.^[297] The BCC lattice is stable up to 90 °C and destroyed at 120 °C, showing only a broad peak for a less ordered polymer melt. When the sample is cooled from 120 °C to 20 °C the BCC-lattice is reformed within 20 minutes, demonstrating the reversible dynamic character of the hydrogen bonds. Due to the high polarity difference between the DAT group and PIB chain, the DAT groups phase separate from the PIB matrix in a way (BCC structure) typical for BCPs with a very short block.^[298] The thermal stability of the BCC grid up to > 80 °C is in excellent agreement with the unusual high viscosity measured for PIB-DAT-4k and the lack of a (true) terminal flow region, due to sterical hindrance of the aggregates (see again **Figure 33**). Furthermore, the measured periodicity of $d = 2\pi/q_{\text{max}} \sim 6.3 \text{ nm}$ is in good agreement with the persistence length of the PIB chain (with $M_n \sim 3.500 \text{ Da}$) which is $\sim 2 \text{ nm}$ as calculated with the ideal chain model and literature values for PIB bond lengths.^[299]

For the equimolar mixture PIB-THY/DAT-4k the SAXS measurement reveals no well-ordered microstructure. Due to the presence of THY groups in PIB-THY/DAT-4k, which can specifically interact with the DAT groups, the formation of a defined BCC lattice is suppressed. As a result, PIB-THY/DAT-4k shows a terminal flow region in the frequency sweep measurements (see **Figure 37b**). Therefore, the results from the SAXS measurements additionally prove the selective DAT-THY binding. Unfortunately, no excess scattering was observed for PIB-THY-4k which can be attributed to insufficient electron density between PIB chain and THY group. Moreover, potential present THY aggregates might be too small to be detected in conventional SAXS measurements. However, the presence of THY aggregates was proven for bifunctional PIBs (see chapter 4.7.5.). Although the association for THY-THY

4. General Part

and DAT-DAT is comparable in solution, the viscosity increase in the melt state reveals a much stronger aggregation of the DAT groups in the PIB melt.

For sample PIB-THY/DAT-4k containing specifically interacting THY and DAT groups the viscosity in comparison to PIB-REF-4k increased by a factor of ~ 39.5 (at 20 °C). Although the viscosity values of PIB-THY/DAT-4k and PIB-DAT-4k are similar at lower temperatures (20 °C), there are some striking differences in the frequency dependent measurements and at higher temperatures. While PIB-DAT-4k does not show terminal flow at low frequencies, sample PIB-THY/DAT-4k does. Due to the equimolar presence of THY and DAT groups in PIB-THY/DAT-4k the formation of larger aggregates like in PIB-DAT-4k is suppressed by the specific THY-DAT interaction. This fact limits the number and/or size of the DAT self-aggregates. Since these large aggregates have a huge influence on the rheological behavior, PIB-DAT-4k reveals larger values for the viscosity than PIB-THY/DAT-4k.

Since for PIB-THY/DAT-4k the viscosity increase in comparison to PIB-REF-4k is large (factor of ~ 39.5 at 20 °C), even for the sample with specifically interacting THY and DAT groups one has to consider the aggregation of the functional groups to a significant extent. Nevertheless, a small contribution can be assigned to the nonlinear increase of the viscosity for low molecular weight PIB, as demonstrated by Flory *et al.*^[291]

To investigate the influence of the molecular weight on monofunctional PIBs a series of PIBs with a higher molecular weight were measured in order to determine the influence of the hydrogen bonding group upon dilution (smaller volume fraction of the end group within the PIB matrix). While the individual polymer chains are still below the entanglement molecular weight M_c ,^[290-291] the supramolecular connection of two (or more) chains can lead to entanglements and, thus, to the appearance of a rubber plateau.

However, for none of the samples (see **Table 8**; entry 5-9) a rubbery plateau was observed, probably because M_c is only slightly exceeded to form (rheological) effective entanglements. In comparison to the low molecular weight analogues the absolute values for the viscosities are about one order of magnitude higher due to the overall higher molecular weight of the polymer chains. Despite the higher viscosities, the curves for PIB-REF-10k, PIB-THY-10k, PIB-DAT-10k and PIB-THY/DAT-10k have a similar shape compared to their low molecular weight analogues (see **Figure 36b**).

All functionalized PIBs with a higher molecular weight (10k-series) again reveal the presence of aggregates since the increase of the viscosity compared to the corresponding PIB-REF is far larger than ~ 2 (for association of two chains). This effect is (at 20 °C) again significant strong for, e.g., PIB-DAT-10k (factor ~ 17) and PIB-THY/DAT-10k (factor ~ 23).

4. General Part

A Significant difference was observed for pure PIB-THY-10k at 20 °C, where the highest viscosity within this series was measured. However, a huge drop of the viscosity was caused by an increase of the temperature to 40 °C (see **Figure 36b**). This might indicate the presence of weak THY-THY stacks, which break at elevated temperatures (above 20 °C). The formation of THY-stacks was reported by Sivakova *et al.* for linear poly(THF).^[70] Unfortunately, no excess scattering was observed for this sample.

As a result, the decrease of the volume fraction of the hydrogen bonding groups (due to the higher molecular weight of the PIB chains) does not lead to an (significant) enhanced compatibility of the hydrogen bonding groups and the nonpolar PIB matrix. On the other hand, for the same reason (volume fraction) the SAXS measurement of PIB-DAT-10k does not show an ordered BCC microstructure compared to its low molecular weight analogue PIB-DAT-4k (see **Figure 39**).

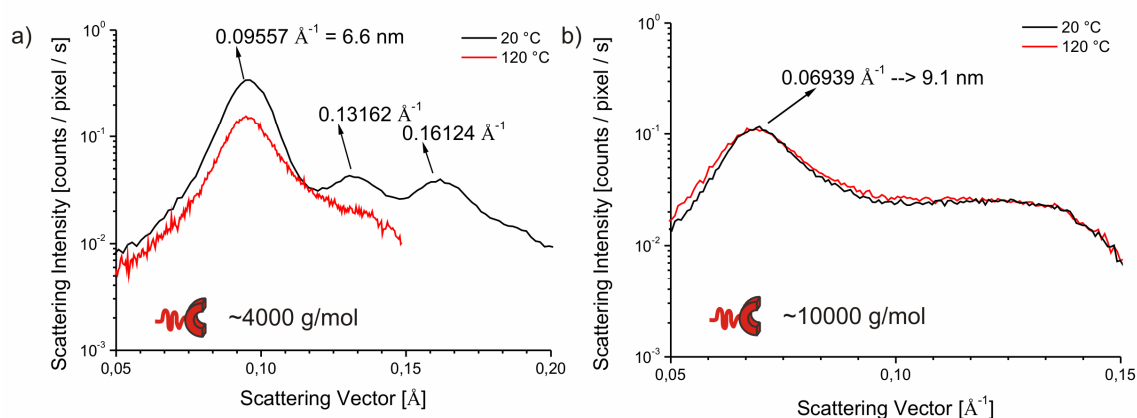


Figure 39. SAXS measurements of PIB-DAT with a molecular weight of a) ~4000 g/mol and b) ~10000 g/mol.

4.7.4. Time-temperature superposition (TTS)

Besides the formation of aggregates the formation of crystalline domains is possible. It was, e.g., reported that the THY moiety can crystallize within a polymer matrix, as reported by Cortese *et al.* for THY functionalized poly(propylene oxide) (PPO).^[90, 143]

For small amplitude oscillatory shear (SAOS) measurements the storage modulus G' and the loss modulus G'' are independent from the strain amplitude (also called the regime of linear viscoelasticity – LVE).^[300] For these types of settings the data obtained via frequency sweep measurements at different temperatures can be superposed (time-temperature-superposition - TTS) by a horizontal shift of the individual curves by the so called shift factor a_T .^[119]

4. General Part

However, this method is only applicable for polymers, polymer blends or polymer solutions showing “thermo-rheologically simple” behavior, meaning that there are only changes in the rate of relaxation but no change of the microstructure (e.g. melting) with change of the temperature.^[301] It is often applied for solutions of supramolecular polymers as well.^[302] De Lucca Freitas *et al.* reported that TTS is possible for urazole functionalized PBD rubbers,^[148, 153] while TTS fails for 4-urazoylbenzoic acid functionalized PBDs due the crystallization of the functional group within the polymer matrix.^[149-150] Therefore, TTS is a suitable tool to exclude the presence of crystalline domains.

For all PIBs listed in **Table 8** (and all samples investigated in this thesis) TTS was possible and the results are exemplarily explained for the 4k-series of PIB and the THY/DAT system (**Table 8**; entry 1-4). The shift factors (a_T) vs. temperature plot is displayed in **Figure 40**.

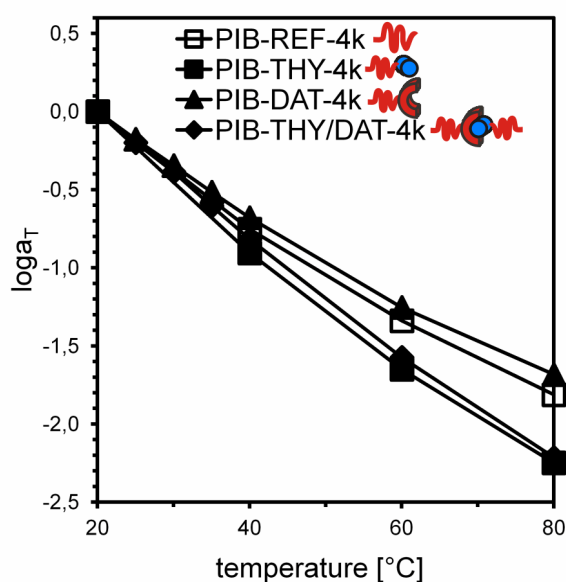


Figure 40. Horizontal shift factors vs. temperature plot for monofunctional PIBs.

The successful application of TTS proves the absence of any crystalline domains, a result which was additionally evidenced by DSC measurements. Furthermore, PIB-REF-4k and PIB-DAT-4k show a comparable temperature dependence of the shift factor a_T (slope), indicating that the aggregates formed in PIB-DAT-4k are stable over the studied temperature range (20-80 °C) and that the temperature dependence is governed by the chain dynamics. The thermal stability of the aggregates in PIB-DAT-4k was additionally evidenced by SAXS measurements, revealing a stable BBC-structure till $T > 80$ °C (see **Figure 39**). Contrarily, PIB-THY-4k and PIB-THY/DAT-4k reveal an enhanced temperature dependence (steeper slope in **Figure 39**) in comparison to PIB-REF-4k. Hence, the dynamics of the supramolecular interaction (temperature dependent aggregation) plays a significant role for





4. General Part

these two samples. For these two samples the aggregating hydrogen bonding motifs undergo an exchange of their counterparts on the same time scales as the external mechanical perturbation. Therefore, the viscosity is additionally decreased due to the deaggregation of the hydrogen bonding moieties.

4.7.5. Effect of the functionality on PIB and the THY-DAT-system

A series of bifunctional PIBs (see **Table 9**) was investigated since it is known that bifunctional building blocks can form long supramolecular chains due to linear chain extension.^[98] On the other hand in the case of aggregation of the hydrogen bonding groups these aggregates were interconnected due to the end-end-functionalization of the chains, leading to the formation of a network.

Table 9. Abbreviations for the in this chapter discussed samples.

entry	sample comic	sample code	compounds	molecular weight series
1		PIB-REF ₂ -4k	– ^a	4000 g/mol ∞
2		PIB-THY ₂ -4k	27a	
3		PIB-DAT ₂ -4k	29a	
4		PIB-(THY/DAT) ₂ -4k	27a + 29a	

^a PIB-REF₂-4k is a bifunctional PIB-Allyl₂ with $M_n(\text{GPC}) = 2700$ g/mol, $M_n(\text{NMR}) = 2900$ g/mol and PDI = 1.27.

Measurements on monofunctional PIBs revealed the presence of aggregates of the hydrogen bonding groups within the polymer matrix, but all samples were obtained as liquids at room temperature.

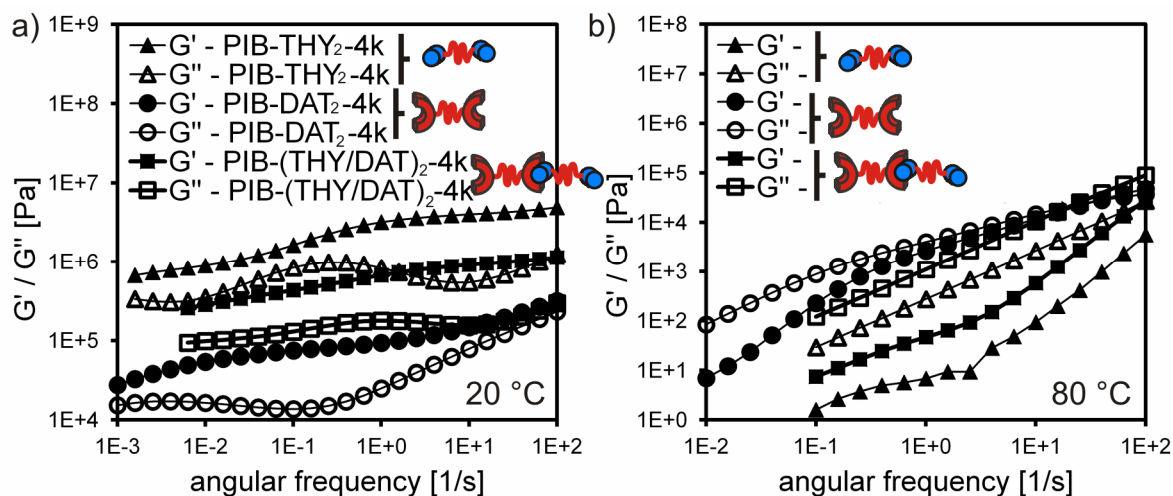


Figure 41. Frequency sweep measurements of bifunctional PIBs bearing the THY/DAT motif at a) 20 °C and b) 80 °C.

4. General Part

However, all bifunctional PIBs within this series (see **Table 9**) were obtained as rubbery materials, each of them revealing a pronounced rubbery plateau in frequency dependent rheology measurements at 20 °C (see **Figure 41a**). Owing to the presence of two functional groups per chains and the tendency to form aggregates, bifunctional PIBs can form a supramolecular network, whereby the aggregates act as a supramolecular tie-points (see **Figure 42** left).

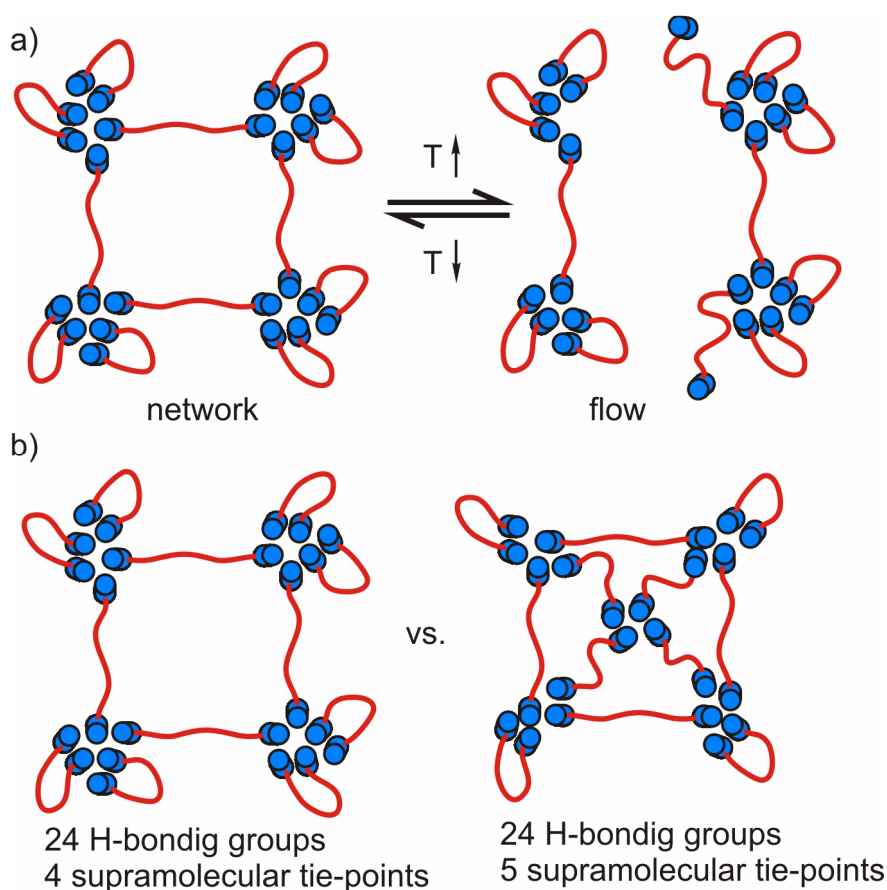


Figure 42. a) Thermo-reversible network formation by supramolecular aggregates of PIB-THY₂; b) smaller aggregates (right side) form more elastically active tie-points than larger aggregates (left side) in the same volume of matrix, leading to a higher plateau modulus for the network on the right side.

The resulting networks reveal different strength (in terms of the plateau modulus G_N^0) indicating different amounts of elastically active tie-points (see **Table 10**). A comparison of the plateau modulus of high molecular weight linear PIBs ($G_N^0 \approx 2.5\text{-}3.2 \cdot 10^5 \text{ Pa}$ ^[290, 303]) with PIB-THY₂-4k and PIB-(THY/DAT)₂-4k, reveals a much higher plateau for the functionalized polymers, further evidencing the presence of a denser network formed by supramolecular tie-points. Therefore, the formation of linear chains via simple association can be excluded. Since all polymers bear two functional groups and have the same molecular weight, thus, have the same volume fraction of functional groups, differences of the plateau modulus arise from a change in the number/size-ratio of the clusters (**Figure 42b**). Therefore, PIB-THY₂-4k

4. General Part

has smaller and more tie-points compared to PIB-DAT₂-4k, which has larger but less tie-points. Consequently, the resulting mixture PIB-(THY/DAT)₂-4k lies in between. These results indicate a stronger self-aggregation tendency of DAT-groups than THY-groups within the PIB matrix, although the association in solution is similar. SAXS measurements were performed to investigate the microstructure of the functionalized polymers. While for PIB-THY₂-4k no excess scattering was observed, PIB-DAT₂-4k and PIB-(THY/DAT)₂-4k show an unordered microstructure with different domain sizes (see **Figure 43**). Since both samples have the same chain length (same M_n), the difference in the domain size can be attributed to larger clusters for PIB-DAT₂-4k than for PIB-(THY/DAT)₂-4k. This observation is in agreement with the rheology measurements since smaller clusters lead to a higher number of elastically active tie-points, evidenced by a higher plateau value for PIB-(THY/DAT)₂-4k (compared to PIB-DAT₂-4k).

Table 10. Rheological data of the THY/DAT system for bifunctional PIBs with $M_n \approx 4000$ g/mol.

entry	sample code	G_N^0 [MPa]	T_g [°C] ^a	η' [Pa·s] for T [°C] ^b			
				20	40	60	80
1	PIB-REF ₂ -4k ^e	– ^d	-70.1	306	59	15	6
2	PIB-THY ₂ -4k	4.0	-58	– ^c	– ^c	2370	292
3	PIB-DAT ₂ -4k	0.08	-61	– ^c	– ^c	– ^c	8450
4	PIB-(THY/DAT) ₂ -4k	0.95	-60	– ^c	– ^c	25000	1210

^a T_g at the midpoint of the transition; ^b values for the zero shear rate viscosity; ^c no terminal flow at this temperature in our frequency range; ^d no plateau; ^e PIB-REF₂-4k is a bifunctional PIB-Allyl₂ with $M_n(\text{GPC}) = 2700$ g/mol, $M_n(\text{NMR}) = 2900$ g/mol and PDI = 1.27.

At elevated temperatures (60 °C or 80 °C) all samples shows terminal flow (**Figure 41b** and **Table 10**), revealing the breakup of the supramolecular tie-points upon heating. Subsequent cooling to 20 °C leads to the reformation of the network. Frequency measurements after 20 min annealing at 20 °C reveal the same results compared to the measurements before heating. Therefore, bifunctional PIBs reveal the typical behavior as reported for thermoplastic elastomers (TPEs) due to the formation of a thermo-reversible supramolecular network (see **Figure 42**).^[304] While PIB-THY₂-4k and PIB-(THY/DAT)₂-4k already show terminal flow at 60 °C, PIB-DAT₂-4k first shows flow at 80 °C, at which it has the highest viscosity within this series of polymers. This observation again indicates the strong thermal stability of the DAT aggregates in the melt state.

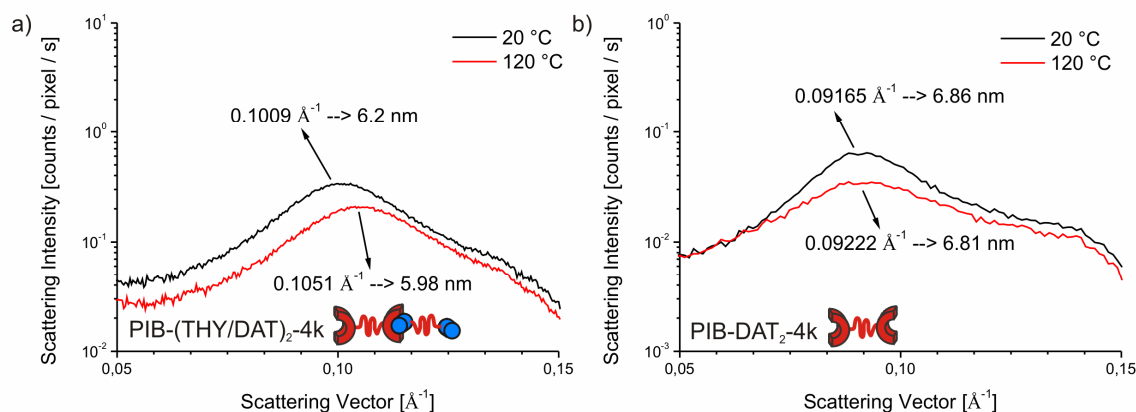


Figure 43. SAXS measurements of a) PIB-(THY/DAT)₂-4k and b) PIB-DAT₂-4k at 20 °C (black curve) and 120 °C (red curve).

4.7.6. Effect of the polarity of the matrix on bifunctional polymers and the THY-DAT-system

The polarity of the surrounding matrix is expected to have a significant impact on either the association or the aggregation of the hydrogen bonding motifs. Therefore, for the more polar PnBA a less pronounced aggregation compared to PIB was expected. In fact, all bifunctional PnBAs were obtained as low viscous liquids, while the corresponding PIBs were obtained as brittle rubbers.

Table 11. Abbreviations for the in this chapter discussed samples.

entry	sample comic	sample code	compounds	molecular weight series
1		PnBA-REF ₂ -4k	16a	4000 g/mol
2		PnBA-THY ₂ -4k	39a	
3		PnBA-DAT ₂ -4k	42a	
4		PnBA-THY-Cap ₂ -4k	40	
5		PnBA-(THY/DAT) ₂ -4k	39a + 42a	
6		40+42a	40 + 42a	
7		PnBA-REF ₂ -25k	16b	25000 g/mol
8		PnBA-THY ₂ -25k	39b	
9		PnBA-DAT ₂ -25k	42b	
10		PnBA-(THY/DAT) ₂ -25k	39b + 42b	

This macroscopic observation already indicated a significant decrease of the aggregation of the hydrogen bonding groups within the polar PnBA matrix. The behavior of the bifunctional

4. General Part

PnBAs is, therefore, also discussed in terms of the molecular weight of the PnBAs (see **Table 11**).

In a first step, low molecular weight bifunctional PnBAs (see **Table 11**; entry 1-6) and equimolar mixtures (with respect to the end group) (PnBA-(THY/DAT)₂-4k and **40+42a**) were investigated since one expects here the melt behavior being dominated by the effect of the end group due to linear chain extension of the bifunctional chains.

The viscosity vs. temperature plot is displayed in **Figure 44** (also see **Table 12**), revealing a strong increase of the viscosity by orders of magnitude for all functionalized PnBAs (PnBA-THY₂-4k, PnBA-DAT₂-4k, PnBA-THY-Cap₂-4k, PnBA-(THY/DAT)₂-4k and **40+42a**) in comparison to the native PnBA-REF₂-4k (devoid of a bulky end group). None of the samples shows a rubbery plateau at any accessible temperature. They rather already show the onset of the transition to the glass at temperatures around -10 °C due to the relatively high glass transition temperatures of the functionalized PnBA (**Table 12**). For instance, the attachment of the DAT group (PnBA-DAT₂-4k) on both chain ends of PnBA leads to an increase of the T_g by 31.8 °C. For a similar pair of PIBs the increase of the T_g is only 9 °C.

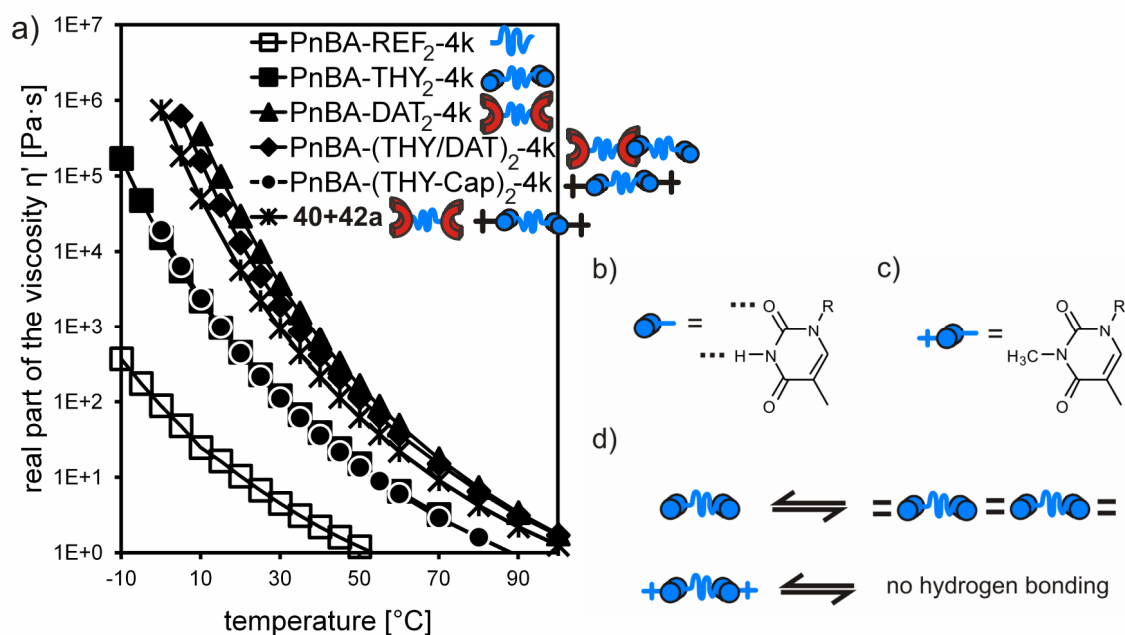


Figure 44. Viscosity vs. temperature plot for bifunctional PnBAs with a molecular weight of ~4000 g/mol; b) the THY group is capable to form two hydrogen bonds, while c) the “capped” THY group is not able to form hydrogen bonds; d) linear chain extension is only possible for bifunctional PnBAs bearing THY groups.

Therefore, one expects for functionalized PnBAs an impact on the viscosity by both, the attractive hydrogen bonding between the supramolecular groups (chain extension) and the increase of the glass transition temperature. For PIB it was shown by competitive experiments

4. General Part

(see chapter 4.7.7. and 4.7.10.) that the end group itself only has a small influence on the thermo-rheological properties.

Table 12. Rheological data of the THY/DAT system for bifunctional PnBAs with $M_n \approx 4000$ g/mol (entry 1-6) and $M_n \approx 25000$ g/mol (entry 7-10).

entry	sample code	T_g [°C] ^a	η' [Pa·s] for T [°C] ^b						
			-10	0	10	20	40	60	80
1	PnBA-REF ₂ -4k	-58.2	369	88	– ^d	10	2	0.7	– ^d
2	PnBA-THY ₂ -4k	-39.1	$1.7 \cdot 10^5$	$1.5 \cdot 10^4$	– ^d	453	39	7	2
3	PnBA-DAT ₂ -4k	-26.4	– ^c	– ^c	– ^d	$2.9 \cdot 10^4$	681	49	7
4	PnBA-THY-Cap ₂ -4k	-30.1	– ^c	$1.9 \cdot 10^4$	– ^d	440	36	6	2
5	PnBA-(THY/DAT) ₂ -4k	-38.0	– ^c	– ^c	– ^d	$1.3 \cdot 10^4$	410	37	7
6	40+42a	-27.4	– ^c	$7.4 \cdot 10^5$	– ^d	$5.6 \cdot 10^4$	215	22	4
7	PnBA-REF ₂ -25k	-48.8	$9.6 \cdot 10^3$	$2.0 \cdot 10^3$	540	182	33	9	3
8	PnBA-THY ₂ -25k	-51.7	$1.7 \cdot 10^4$	$3.3 \cdot 10^3$	831	266	45	12	4
9	PnBA-DAT ₂ -25k	-44.4	$1.3 \cdot 10^5$	$1.6 \cdot 10^4$	$3.3 \cdot 10^3$	734	94	22	7
10	PnBA-(THY/DAT) ₂ -25k	-46.5	$2.0 \cdot 10^5$	$2.0 \cdot 10^4$	$3.7 \cdot 10^3$	909	108	24	7

^a T_g at the midpoint of the transition; ^b values for the zero shear rate viscosity; ^c sample too glassy; ^d not measured.

Owing to the absence of a rubbery plateau one can exclude both, the presence of aggregates formed by nonspecific aggregation of several hydrogen bonding moieties (as found for PIBs) and the lack of chain entanglements due to linear chain extension. Furthermore, no excess scattering was observed for all PnBA samples, indicating the absence of aggregates. As a result, the lack of a rubbery plateau also evidences an only weak contribution of attractive hydrogen bonding and, thus, weak hydrogen bonding of the THY-DAT system within the PnBA matrix. Consequently, the strong increase of the zero shear viscosity can be mainly attributed to the significant increase of the T_g - an effect which often has been neglected in comparable rheological investigations of poly(*n*-butyl acrylate)s.^[134] A comparative experiment of a PnBA-THY₂-4k bearing THY groups and its analogue PnBA-THY-Cap₂-4k, a PnBA where the CO–NH–CO proton of the THY group is exchanged by a methyl group, was performed. For PnBA-THY-Cap₂-4k hydrogen bonding between the THY-Cap groups is not possible (see **Figure 44d**) thus the viscosity without effective hydrogen bonding can be measured. It is shown in **Figure 44a** that there is no difference between these two polymers regarding the melt viscosity. Since there is only a small difference between the T_g values ($\Delta T_g = 9.0$ °C), these experiments reveal that there is only a very small impact of the THY-THY association on the rheological properties and, thus, no significant association of chains due to

4. General Part

hydrogen bonding in the melt state. This observation is in agreement with the low dimerization constant measured in solution. Surprisingly, PnBA-DAT₂-4k (DAT-DAT interaction) shows a slighter higher viscosity than PnBA-(THY/DAT)₂-4k (THY-DAT interaction). Although PnBA-DAT₂-4k displays a higher T_g ($T_g = -26.4$ °C) than PnBA-(THY/DAT)₂-4k ($T_g = -38.0$ °C), the THY-DAT association in solution is stronger by three orders of magnitude compared to the DAT-DAT interaction. As a result, contrary to the observations in solution, the DAT-DAT association displays a similar strength as the THY-DAT association in the melt state. Furthermore, the equimolar mixture PnBA-(THY/DAT)₂-4k was compared to a similar mixture (**40+42a**), containing a PnBA with capped THY groups (**40**). Thus, for **40+42a** no triple hydrogen bonding between THY and DAT is possible. **Figure 44** (and **Table 12**) shows that PnBA-(THY/DAT)₂-4k has a higher viscosity than the mixture **40+42a** by a factor of ~ 2 at 20 °C, proving a small contribution of THY-DAT interaction in PnBA-(THY/DAT)₂-4k. One has to keep in mind that in **40+42a** the DAT-DAT association is of course possible and might additionally contribute to the absolute viscosity value. Moreover, attractive π - π -stacking of the DAT group can attribute as a secondary force to the association of PnBA. However, although the THY-DAT interaction was proven to undergo a strong association in solution, the effect on the thermo-rheological properties in the melt state is much smaller. As a consequence, the increase of the viscosity caused by the attachment of the hydrogen bonding groups is mainly caused by the significant increase of the glass transition temperatures.

Additionally, bifunctional high molecular weight PnBAs ($M_n \approx 25000$ g/mol) were investigated (**Table 11**; entry 7-10), since for this series of polymers we expected more precise information of the association strength in the melt state, due to the reduced effect of the hydrogen bonding motifs on the T_g of the polymer. Furthermore, this series of polymers is just below the M_c of PnBA ($M_c \approx 20000$ g/mol^[305-306]). Therefore, even the linear extension of only a few PnBA chains can lead to supramolecular chains with sufficient length for rheological effective entanglements.

The viscosity vs. temperature data are displayed in **Figure 45**, showing that the attachment of any functional group (PnBA-THY₂-25k, PnBA-DAT₂-25k, PnBA-(THY/DAT)₂-25k) onto the native PnBA-REF₂-25k exerts a less drastic affect on the viscosity in comparison to the low molecular weight analogues. This affect can be attributed to a less pronounced increase of the T_g 's (see **Table 12**). A comparison of the viscosity of PnBA-REF₂-25k (no functional group) with PnBA-THY₂-25k, which only has a slightly higher viscosity than PnBA-REF₂-25k, again evidences the weak THY-THY interaction in the PnBA melt state. PnBA-DAT₂-25k

4. General Part

and PnBA-(THY/DAT)₂-25k show a much higher viscosity than the reference PnBA-REF₂-25k (and PnBA-THY₂-25k as well).

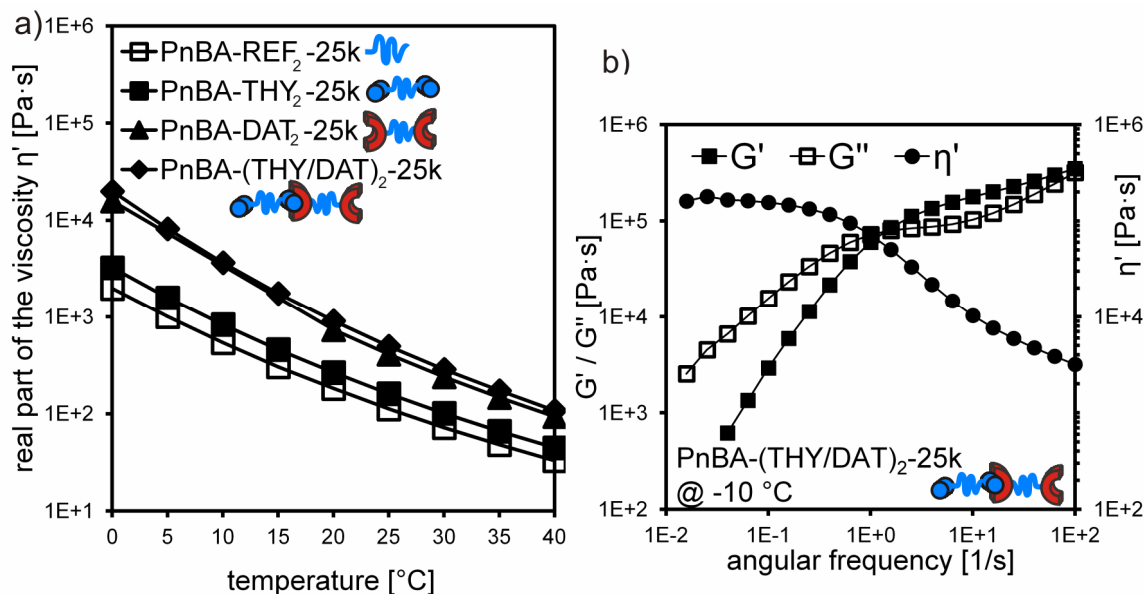


Figure 45. a) Viscosity vs. temperature plot for bifunctional PnBAs with a molecular weight of ~25000 g/mol; b) frequency sweep measurement of PnBA-(THY/DAT)₂-25k at -10 °C showing a rubbery plateau due to linear chain extension.













Comparing the viscosity of PnBA-DAT₂-25k and PnBA-(THY/DAT)₂-25k at 20 °C, a 1.2-fold higher viscosity of PnBA-(THY/DAT)₂-25k was observed, again proving a similar strength of the DAT-DAT and THY-DAT interaction in the melt state. Additionally, these two samples show a small rubbery plateau at -10 °C (see **Figure 45b**), which PnBA-REF₂-25k and PnBA-THY₂-25k do not show, evidencing the presence of sufficiently long entangled supramolecular chains due to association of the bifunctional chains. Additionally, for bifunctional PnBAs no microphase separation was evidenced in SAXS measurements, indicating the absence of aggregates. For some samples a weak maximum was found, which can be attributed to the correlation hole effect due to the electron density difference of the end group and the polymer chain.^[134]

4.7.7. Effect of the molecular weight for PIB and the BA-HW-system

As a model experiment monofunctional PIBs as well as equimolar mixtures (with respect to the end groups) of PIB-BA and PIB-HW were utilized to investigate the association/aggregation of the end groups and the effect of the molecular weight. The in this chapter discussed samples are listed in **Table 13**.

4. General Part

Table 13. Abbreviations for the in this chapter discussed samples.

entry	sample comic	sample code	compounds	molecular weight series
1		PIB-REF-4k	11a	≈ 4000 g/mol
2		PIB-BA-4k	31b	
3		PIB-HW-4k	34b	
4		PIB-BA/HW-4k	31b + 34b	
5		PIB-REF-10k	11c	≈ 10000 g/mol
6		PIB-BA-10k	31c	
7		PIB-HW-10k	34c	
8	—	PIB-Pyrene	36	
9		PIB-BA/HW-10k	31c+34c	≈ 30000 g/mol
10		PIB-REF-30k	11d	
11		PIB-BA-30k	31d	
12		PIB-HW-30k	34d	
13		PIB-BA/HW-30k	31d + 34d	≈

In solution the association of the BA and the HW is stronger by orders of magnitude compared to the dimerization of both groups. Nevertheless, the HW-dimerization is slightly stronger than the BA-dimerization. Due to the high polarity of both groups also the formation of aggregates is possible. Here one also has to keep in mind that the HW group is much larger than the BA group and might also link via secondary interactions (see **Figure 35**). Due to any connection of two chains for the 30k-series the formation of elastically effective entanglements is possible.

4. General Part

Table 14. Rheological data of the HW/BA system for monofunctional PIBs with $M_n \approx 4000$ g/mol (entry 1-4); $M_n \approx 10000$ g/mol (entry 5-9) and $M_n \approx 30000$ g/mol (entry 10-13).

entry	sample code	T_g [°C] ^a	η' [Pa·s] for T [°C] ^b					
			20	40	60	80	100	120
1	PIB-REF-4k	-72.8	409	82	22	7	– ^d	– ^d
2	PIB-BA-4k	-68.4	7528	1133	205	50	– ^d	– ^d
3	PIB-HW-4k	-66.4	– ^c	– ^c	– ^c	– ^c	40003	4748
4	PIB-BA/HW-4k	-68.4	– ^c	36500	1480	207	48	– ^d
5	PIB-REF-10k	-67.1	1200	222	59	21	8	3
6	PIB-BA-10k	-67.5	16738	2795	595	149	44	13
7	PIB-HW-10k	-66.1	– ^c	– ^c	27890	2077	348	89
8	PIB-Pyrene	-66.3	1268	242	62	20	10	3
9	PIB-BA/HW-10k	-67.3	28290	4544	975	271	95	35
10	PIB-REF-30k	-68.8	8716	1952	571	222	79	37
11	PIB-BA-30k	-66.5	510039	67135	10732	2052	478	139
12	PIB-HW-30k	-66.4	– ^c	230451	40471	9400	2709	950
13	PIB-BA/HW-30k	-68.9	643495	9975	19167	4723	1437	489

^a T_g at the midpoint of the transition; ^b values for the zero shear rate viscosity; ^c no terminal flow at this temperature in our frequency range; ^d not measured due to very low viscosity.

In a first step, monofunctional PIBs of the 4k-series (**Table 13**; entry 1-4), were investigated by frequency dependent measurements at different temperatures (see **Table 14**). The reference sample PIB-REF-4k shows the expected behavior for an unentangled polymer which is devoid of hydrogen bonding. Terminal flow is observed at all temperatures, while the absolute values of the viscosity decrease with increasing temperature. The attachment of the barbituric acid group in PIB-BA-4k leads to a remarkable increase of the viscosity compared to PIB-REF-4k (at 20 °C by a factor of ~18) and terminal flow at each investigated temperature was observed. Theoretically, the connection of two unentangled chains via attractive BA-BA-type hydrogen bonding should lead to an increase of the viscosity by a factor of 2. Therefore, the viscosity increase of PIB-BA-4k compared to PIB-REF-4k (**11a**) again indicates the formation of larger aggregates, formed by more complex modes of aggregation than a simple BA-BA-type dimerization. This argument gains evidence when sample PIB-HW-4k is considered. Here, the polymer does not show terminal flow below temperatures of 100 °C, instead the sample is obtained as a brittle rubbery material. This effect is probably caused by the formation of large aggregates (of the Hamilton wedge), which can only slide over each other at elevated temperatures (higher chain mobility and partial

4. General Part

deaggregation) (see **Figure 33**). Similar effects were observed for aggregates formed in PIB-based polymeric ionic liquids.^[30]

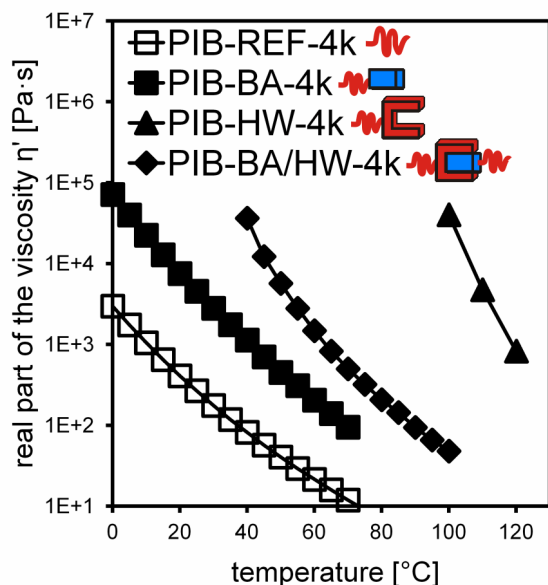


Figure 46. Viscosity vs. temperature plot for monofunctional PIBs bearing the BA/HW motif with a molecular weight of ~4000 g/mol.

For the equimolar mixture PIB-BA/HW-4k terminal flow was already observed at 40 °C, but the viscosity is drastically increased in comparison to PIB-REF-4k (and PIB-BA-4k), again indicating the formation large supramolecular aggregates. However, in comparison to PIB-HW-4k, the mixture PIB-BA/HW-4k flows at much lower temperatures, proving the partial deaggregation of large HW-clusters due to attractive HW-BA interaction.

SAXS measurements revealed the presence of a microstructure for all functionalized PIBs within this series (PIB-BA-4k, PIB-HW-4k and PIB-BA/HW-4k). **Figure 47a** displays the SAXS measurements of PIB-HW-4k showing one sharp peak and a broad shoulder. Both are stable up to 120 °C indicating the presence of large temperature stable aggregates – an observation which is on good agreement with the rheological investigation, where for PIB-HW-4k terminal flow was only observed at high temperatures.

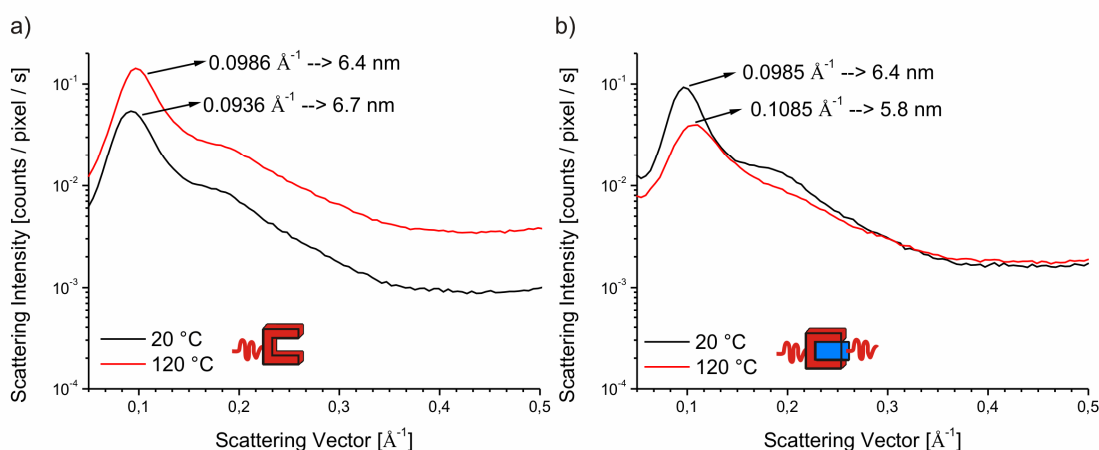


Figure 47. SAXS measurements of a) PIB-HW-4k and b) the supramolecular mixture PIB-BA/HW-4k at 20 °C (black curve) and 120 °C (red curve).

The corresponding mixture PIB-BA/HW-4k shows a similar curve at 20 °C (see **Figure 47b**) but, in contrast to PIB-HW-4k, at higher temperatures the shoulder vanishes, indicating a less pronounced stability of the aggregates due to the specific HW-BA interaction. These results are again in agreement with the rheological investigations, where terminal flow for PIB-BA/HW-4k was observed at lower temperatures compared to PIB-HW-4k.

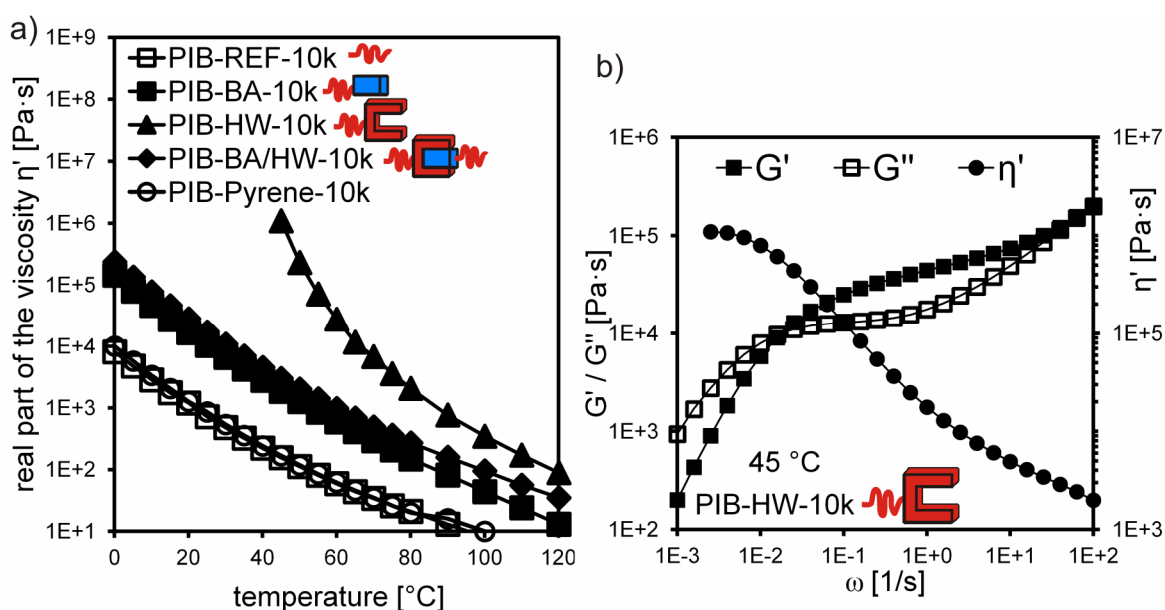


Figure 48. a) Viscosity vs. temperature plot for monofunctional PIBs bearing the BA/HW motif with a molecular weight of ~10000 g/mol; the figure includes the PIB-Pyrene-10k (**36**) control experiment for the influence of a bulky end group; b) frequency sweep measurement of the unentangled monofunctional PIB-HW-10k at 45 °C showing a plateau.

Increasing the molecular weight and, thus, decreasing the volume fraction of the hydrogen bonding group, one expects a reduced influence of the end group on the rheological properties of the PIB polymers. As a result, PIB-HW-10k already shows terminal flow at 60 °C

(PIB-HW-4k above 100 °C). However, the attachment of any end group still causes a strong increase of the viscosity compared to the PIB-REF-10k sample (see **Figure 48**), indicating the presence of supramolecular aggregates. For example, the attachment of the BA group (PIB-BA-10k) leads to an increase of the viscosity by a factor of ~14. **Figure 48b** shows the frequency sweep measurement of PIB-HW-10k at 45 °C. Although the polymer is far below the entanglement molecular weight ($M_c \approx 16.900 \text{ g/mol}^{[290-291]}$), the measurement reveals a pronounced rubbery plateau. Also the single supramolecular association of two chains ($M_{n(\text{virtual})} = 2 \cdot 10000 \text{ g/mol} = 20000 \text{ g/mol}$) can not lead to such a pronounced plateau at this temperature, as evidenced by measurements with high molecular weight PIBs ($M_n \approx 30000 \text{ g/mol}$; see **Figure 49a**). Antonietti *et al.* reported for poly(styrene) microgels consisting of a hard spherical core and unentangled chains at the outer rim, the appearance of a rubbery plateau in frequency dependent rheology measurements.^[307] The corresponding plateau is caused by the hard spheres which can not slide over each other, thus, giving a strong contribution to the elastic portion (storage modulus). Therefore, such an effect is dominant in PIB-HW-10k again evidencing the presence of large aggregates of the hydrogen bonding groups. These aggregates do not necessarily need to have a spherical shape. In order to investigate the bare presence of the end group(s) (without “active” hydrogen bonding) on the thermo-rheological properties of PIB, a corresponding PIB bearing the bulky pyrene group was investigated. PIB-Pyrene (**36**) is devoid of hydrogen bonding and, thus, the bare influence of the end group could be studied. **Figure 48a** also shows the viscosity vs. temperature plot for PIB-REF-10k and PIB-Pyrene-10k revealing that there is no difference of the viscosity arising from the presence of the bulky pyrene end group. Therefore, the drastic effects observed for functionalized PIBs bearing hydrogen bonding moieties can be attributed to the aggregation due to hydrogen bonding.

A series high molecular weight functionalized polymers were investigated to study the influence of hydrogen bonding on linear already entangled PIBs. Therefore, functionalized PIBs with a molecular weight of ~30000 g/mol were investigated, since they were synthetically available with complete end group functionalization and the polymer chains are slightly above the entanglement molecular weight ($M_c \approx 16.900 \text{ g/mol}^{[290-291]}$) to form rheological effective entanglements (see **Table 14**; entry 10-13). This set of polymers has the lowest volume fraction of the hydrogen bonding group due to the high molecular weight. As a result, PIB-HW-30k already shows terminal flow at 40 °C (PIB-HW-10k 60 °C; PIB-HW-4k only above 100 °C). Although this series of polymers exhibits the lowest volume fraction of end groups, the attachment of any end group has the strongest affect on the viscosity compared to the PIB-REF. Since the bare polymer chains are already slightly entangled ($M_n >$

4. General Part

M_c), the formed supramolecular aggregates (by aggregation of the end groups) have a significant higher virtual M_n (virtual $M_n \gg M_c$), thus, being significant more entangled. Assuming the simple association of two chains one would expect an increase of the viscosity by a factor of ~ 10 due to the relation $\eta \sim M_n^{3,4}$ (see again **Figure 32c**). However, the attachment of the BA group leads to an increase of the viscosity by a factor of ~ 59 at 20°C (factor of ~ 14 for the 10k series) (see **Table 14**). Therefore, the formation of aggregates takes place even in high molecular weight PIBs. **Figure 49** displays the temperature sweep measurements of PIB-REF-30k and PIB-BA-30k, revealing a small plateau up to 20°C for the unfunctionalized polymer and an extended plateau, up to 55°C , for the BA-functionalized polymer. These observations again proof the presence of aggregates and indicate that the supramolecular aggregates strongly influence the rheological behavior, even at high molecular weights, due to the increase of effective entanglements.

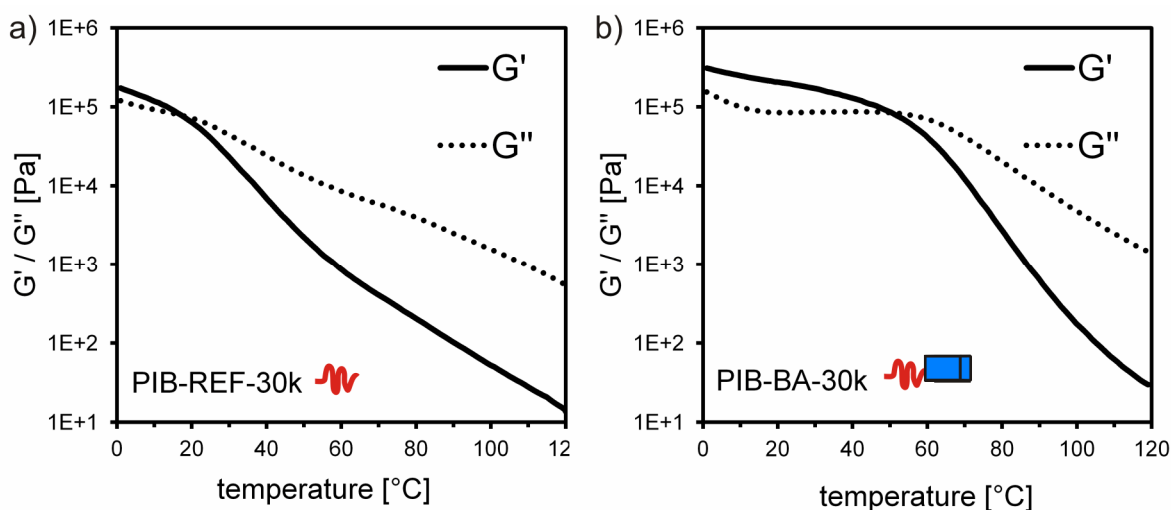






Figure 49. Temperature sweep measurements for a) PIB-REF-30k and b) PIB-BA-30k.

4.7.8. Effect of the functionality on PIB and the BA-HW-system

In addition to the preceding investigations for monofunctional polymers also bifunctional polymers were studied (see **Table 15**), because only these polymers can form extended supramolecular chains or networks either via association or aggregation.

Table 15. Abbreviations for the in this chapter discussed samples.

entry	sample comic	sample code	compounds	molecular weight series
1		PIB-REF ₂ -4k	12b	4000 g/mol ≈
2		PIB-BA ₂ -4k	32b	
3		PIB-HW ₂ -4k	35a	
4		PIB-(BA/HW) ₂ -4k	32b+35a	

The samples PIB-HW-4k and PIB-(BA/HW)₂-4k were obtained as brittle rubbers at room temperature, whereas PIB-BA₂-4k was a strong, bendy rubber with a high plateau modulus of $4.4 \cdot 10^5$ Pa (**Figure 50b**). For linear high molecular weights PIBs a plateau modulus of $2.5\text{--}3.2 \cdot 10^5$ Pa was reported.^[290, 303] Thus, one can conclude that a network formed by tie-points of BA-aggregates is present in PIB-BA₂-4k (see again **Figure 34**). Interestingly, PIB-BA₂-4k shows terminal flow at 20 °C if it is probed at very low frequencies, revealing an astonishing high viscosity of $20 \cdot 10^6$ Pa·s. This is more than 93000 times higher than the viscosity of PIB-REF₂-4k. This observation can be explained by the formation of a transient network due to dynamic supramolecular tie-points consisting of three or more barbituric acid groups. At high frequencies the material behaves like a rubber, because the lifetime of such an aggregate is long compared to the frequency, thus, the sample properties are dominated by the “closed” network. At low frequencies these aggregates are monitored in a “semi-closed” or “open” state, leading to a dynamic response of the whole supramolecular network. As a result, terminal flow is observed. Although aggregates of the BA-groups were formed, the supramolecular groups retain their reversibility and dynamic, evidenced by the presence of both a plateau and terminal flow region. At detailed discussion of the corresponding lifetimes of the BA-aggregates is given in chapter 4.7.10.

4. General Part

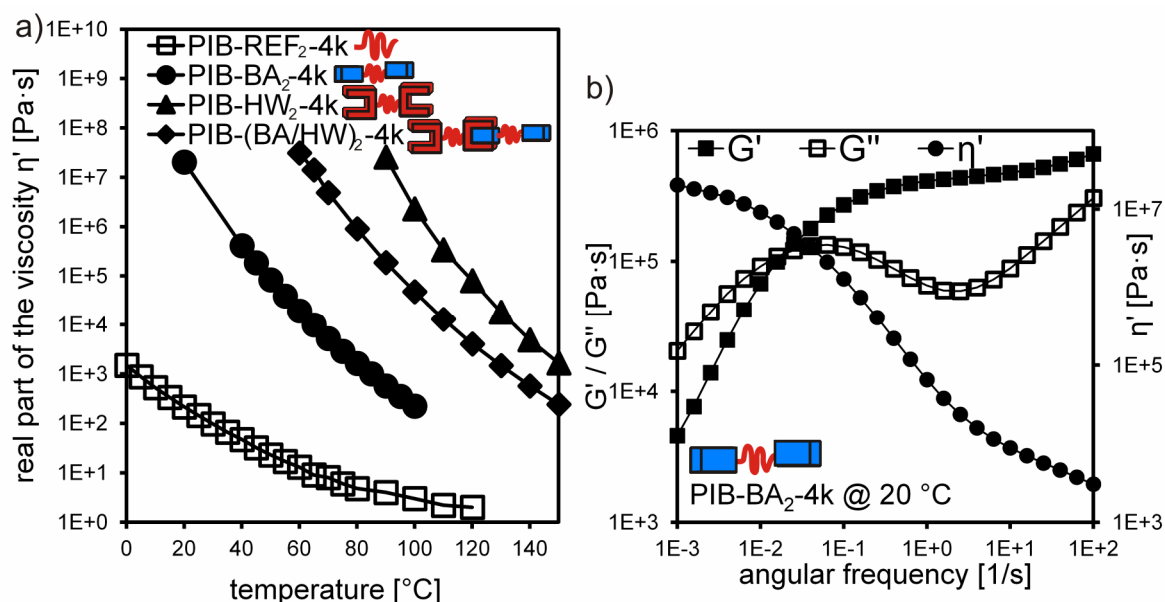


Figure 50. a) Viscosity vs. temperature plot for bifunctional PIBs bearing the BA/HW system with a molecular weight of ~ 4000 g/mol; b) frequency sweep measurement of the bifunctional PIB-BA₂-4k at 20 °C showing a plateau and a terminal flow region.

In general, all functionalized polymers show a remarkable increase of the viscosity compared to the reference sample (see **Table 16**).

Table 16. Rheological data of the HW/BA system for bifunctional PIBs with $M_n \approx 4000$ g/mol.

entry	sample code	T_g^a [°C]	η' [Pa·s] for T [°C] ^b					
			20	40	60	80	100	120
1	PIB-REF ₂ -4k	-70.1	215	47	13	5	3	2
2	PIB-BA ₂ -4k	-59.2	$20 \cdot 10^6$	$4.1 \cdot 10^5$	19177	1640	223	– ^d
3	PIB-HW ₂ -4k	-60.1	– ^c	– ^c	– ^c	– ^c	$2.2 \cdot 10^6$	80277
4	PIB-(BA/HW) ₂ -4k	-60.0	– ^c	– ^c	$31 \cdot 10^6$	$9.0 \cdot 10^5$	47573	4070

^a T_g at the midpoint of the transition; ^b values for the zero shear rate viscosity; ^c no terminal flow at this temperature in our frequency range; ^d not measured.

PIB-HW₂-4k does not reveal terminal flow below a temperature of 90 °C, even at very low frequencies ($\omega = 0.001$ rad/s), indicating the presence of clusters with a higher thermo-stability compared to the clusters in PIB-BA₂. At 90 °C PIB-HW₂-4k reveals a similar behavior as PIB-BA₂-4k at 20 °C, showing a high rubbery plateau of $3.1 \cdot 10^6$ Pa and a high viscosity of $2.2 \cdot 10^6$ Pa·s (6 orders of magnitude higher than PIB-REF₂-4k at this temperature), due to at this temperature still present supramolecular tie-points. For the corresponding mixture PIB-(BA/HW)₂-4k the resulting properties are in between the two extremes (pure PIB-BA₂-4k and pure PIB-HW₂-4k), indicating also here the presence of large aggregates, but also the partially deaggregation of HW-clusters due to the BA-HW






4. General Part

interaction. Although the BA- and HW-dimerization is similar in solution, the aggregation of the HW is much stronger in the melt state, an observation which can be attributed to the larger size of the HW-group compared to the BA-group, or to the additional binding site of the HW.

4.7.9. Effect of the hydrogen bonding group on bifunctional PIBs

Although the hydrogen bonding motifs applied in this work are so called “key-lock” systems, each of the individual groups shows a small tendency towards dimerization in solution. For the THY, DAT, and BA group the dimerization is similar, only the HW shows a slightly higher dimerization (see again chapter 4.7.1.). To investigate the influence of these groups on the melt behavior of PIB a series of bifunctional PIBs is discussed here (**Table 17**).

Table 17. Rheological data of the HW/BA and THY/DAT system for bifunctional PIBs with $M_n \approx 4000$ g/mol.

entry	sample comic	sample code	compounds	molecular weight series
1		PIB-REF ₂ -4k	12b	4000 g/mol ≈
2		PIB-BA ₂ -4k	32b	
3		PIB-HW ₂ -4k	35a	
4		PIB-THY ₂ -4k	27a	
5		PIB-DAT ₂ -4k	29a	

All of these samples were obtained as rubbers at room temperature due network formation via aggregates of the end groups.

Table 18. Rheological data of bifunctional PIBs with $M_n \approx 4000$ g/mol bearing different hydrogen bonding groups.

entry	sample code	T_g^a [°C]	η' [Pa·s] for T [°C] ^b					
			20	40	60	80	100	120
1	PIB-REF ₂ -4k	-70.1	215	47	13	5	3	2
2	PIB-BA ₂ -4k	-59.2	$20 \cdot 10^6$	$4.1 \cdot 10^5$	19177	1640	223	– ^d
3	PIB-HW ₂ -4k	-60.1	– ^c	– ^c	– ^c	– ^c	$2.2 \cdot 10^6$	80277
4	PIB-THY ₂ -4k	-58,0	– ^c	– ^c	2370	292	– ^d	– ^d
5	PIB-DAT ₂ -4k	-61,0	– ^c	– ^c	– ^c	8450	– ^d	– ^d

^a T_g at the midpoint of the transition; ^b values for the zero shear rate viscosity; ^c no terminal flow at this temperature in our frequency range; ^d not measured.

The onset of the terminal flow was observed at different temperatures for these samples, indicating a different strength of aggregation compared to the situation in solution (**Table 18**).

4. General Part

Only PIB-BA₂-4k shows terminal flow at 20 °C indicating the lowest tendency of the BA-groups towards aggregation in the PIB melt. PIB-THY₂-4k and PIB-DAT₂-4k reveal terminal flow at 60 °C and 80 °C, respectively. Although their dimerization is quite similar in solution, their aggregation in the PIB melt is strikingly different. This observation can be explained by the effect of secondary forces in the case of DAT-groups. For the same reason also the strong aggregation of the HW can be explained since here the additional binding site might favor aggregation in the melt state. Only the main reason for the strong aggregation of the THY-group remains unclear, although this observation is in agreement with the literature.^[70] As a result it is not possible to derive the aggregation tendency of hydrogen bonding groups in the melt state from their demerization in solution, since here several other effect have a significant influence.

4.7.10 Influence of the molecular weight on bifunctional PIBs bearing barbituric acid (BA) groups

A series of bifunctional BA-functionalized PIBs was investigated to study the effect of the molecular weight. Therefore, the molecular weight was varied between 3000 g/mol and 30000 g/mol. Since the volume fraction of the BA groups decreases with increasing molecular weight of the polymer chain, one would expect a noticeable effect on the supramolecular network and, thus, on the thermo-rheological properties. However, this is not the case for the series of bifunctional PIBs bearing barbituric acid groups.

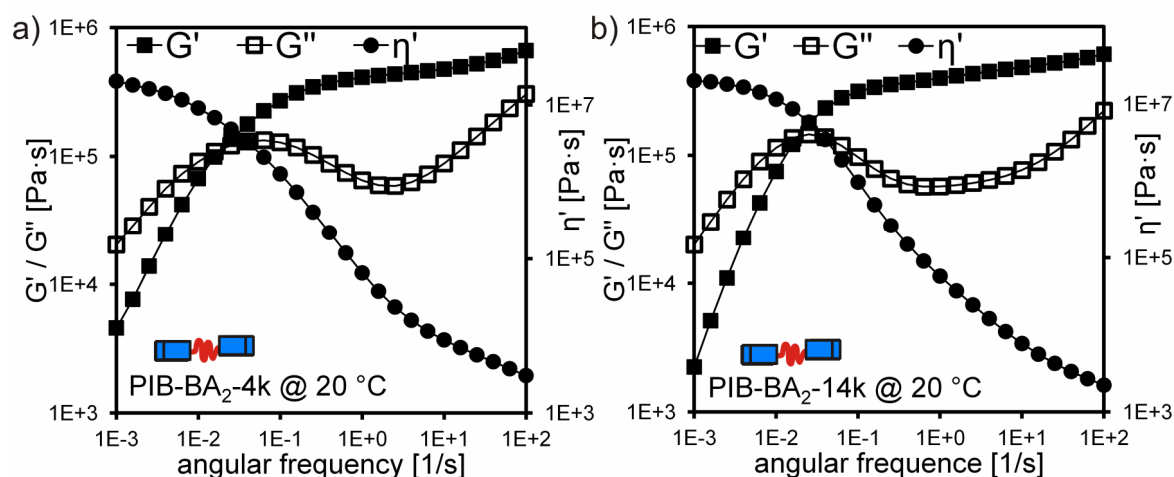


Figure 51. Frequency sweep measurement of a) the PIB-BA₂-4k and b) PIB-BA₂-14k at 20 °C, both showing a plateau of the same height and the onset of the terminal flow region at the same frequency although the molecular weight is different by 10000 g/mol.

4. General Part

At room temperature all four polymers were obtained as bendy rubbers and show the same trend for the storage and loss modulus in frequency dependent measurements (see **Figure 51**), revealing almost the same values for the zero shear viscosity and the plateau modulus (**Table 19** and **Figure 52**).

These results are in striking contrast to the expectations, but can be explained by considering the molecular weight between the entanglements (M_e). M_e can be calculated via the following formula:^[134]

$$\frac{1}{M_e} = \frac{G_N^0}{\rho \cdot R \cdot T} + \frac{2}{M_n}$$

The last term ($2/M_n$), the correction for dangling chain ends (which can not form an entanglement) according to Flory, can be omitted since all polymers are chain-end functionalized.

Table 19. Rheological data for bifunctional barbituric acid modified PIBs (PIB-BA₂) with different molecular weights.

entry	PIB	sample code	T _g ^a [°C]	τ _d ^{*b} [s]	G _N ^{0c} [MPa]	M _e [g/mol]	η' [Pa·s] for T [°C] ^d				
							20	40	60	80	100
1	32b	PIB-BA ₂ -4k	-59.2	1.6	0.44	5041	20·10 ⁶	4.1·10 ⁵	1.9·10 ⁴	1640	223
2	32d	PIB-BA ₂ -8k	-64.5	2.5	0.59	3760	19·10 ⁶	5.3·10 ⁵	2.8·10 ⁴	2598	420
3	32c	PIB-BA ₂ -14k	-64.2	1.6	0.42	5281	20·10 ⁶	7.4·10 ⁵	4.5·10 ⁴	4346	582
4	32e	PIB-BA ₂ -30k	-65.7	0.25	0.31	7155	8·10 ⁶	4.5·10 ⁵	4.0·10 ⁴	5236	976
5	33a	PIB-BA ₂ -Cap-4k	-54.8	–	–	–	3081	425	85	21	7

^a T_g at the midpoint of the transition; ^b τ_d^{*} is measured at the frequency where G' is 90% of G_N⁰; ^c G_N⁰ is measured at 20 °C at the minimum of tanδ; ^d values for the zero shear rate viscosity.

For PIB-BA₂-4k M_e is ~5000 g/mol and, therefore, larger than the end to end distance of the polymer chains given by the molecular weight. This observation might originate from the fact that a certain amount of functional groups (chain ends) are not bound in a transient supramolecular tie-point (since M_e > M_n). Although the amount of free chain ends can hardly be quantified, one can state qualitatively that the amount of free chain ends is relatively small, since a higher content of free chain ends would lead to an additional relaxation, evidenced by another maximum of G'' within the frequency range of the plateau.^[308] The absence of such a secondary relaxation (**Figure 51**) further proves the absence of unbound dangling chain ends in the polymer melt. Thus, in contrast to the cited literature, the samples were in an equilibrated state.^[308] Therefore, the mismatch between M_n and M_e can be attributed to the uncertainty of the determination of the G_N⁰ values.^[309]

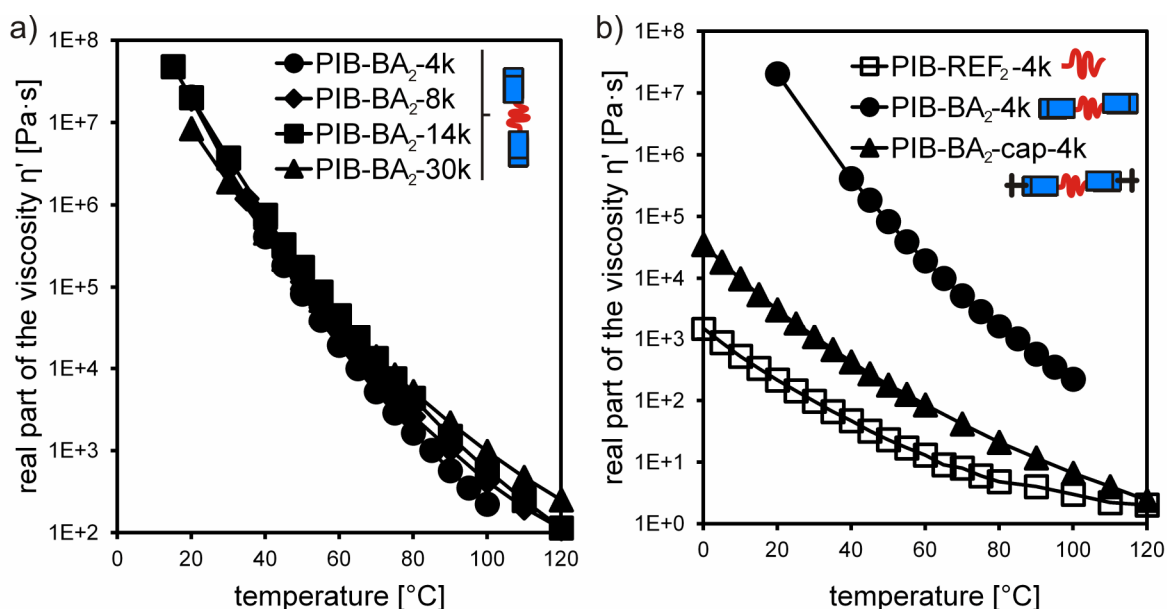


Figure 52. a) Viscosity vs. temperature plot for bifunctional PIBs bearing the BA group with different molecular weights; b) Viscosity vs. temperature plot for bifunctional PIB-BA₂-4k (**32b**) in comparison to PIB-BA₂-cap-4k (**33a**) which is devoid of hydrogen bonding but has a similar structure.

With increasing molecular weight (M_n) of the samples the values for M_e remain in the range of ~ 3000 to ~ 7000 g/mol. Since for, e.g., PIB-BA₂-14k the minimum distance between to supramolecular tie-points is given by the molecular weight (due to the chain end functionalization), the small value for M_e ($M_e < M_n$) indicates the presence of a significant additional amount of conventional entanglements. These kind of entanglements are formed by the entanglement of chains which are trapped with their chain ends in a supramolecular tie-point (see **Figure 34**). Therefore, conventional entanglements were formed although M_n is below the entanglement molecular weight (M_c). Since transient supramolecular networks are formed in bifunctional PIB-BAs, owing to the formation of multicenter tie-points of several BA groups, the lifetime of such an aggregate can be measured from the frequency at which the storage modulus has dropped to 90% of its plateau value.^[134] The resulting lifetimes are in the range of ~ 2 s for polymers with $M_n < M_c$ and 0.25 s for the already entangled sample PIB-BA₂-30k ($M_n > M_c$). These values are significant larger than the lifetime τ_d of the single bond in solution ($6 \cdot 10^{-3}$ μ s for single BA-BA dimerization in CDCl₃ at 25 °C), evidencing the presence of multicenter aggregates, where the release of one group is dependent from other binding events. As a result, the calculated lifetimes in the melt state have to be seen as effective bond lifetimes τ_d^* . One has to state that the τ_d^* values have an assured uncertainty since they were calculated from a logarithmic frequency scale with only 5 points per decade. For PIB-BA₂-30k the smaller values for τ_d^* (and G_N^0 ; see **Table 19**) originate from the smallest volume fraction of the supramolecular end group within this series. Furthermore, the presence of chain entanglements ($M_n > M_c$) in PIB-BA₂-30k might prevent the formation of

4. General Part

supramolecular tie-points with the same size or shape, as in PIB-BA₂-14k, -8k, and -4k, to a certain extent. Since for smaller aggregates concurrent unbinding is more likely, a smaller aggregate size results in a lower effective bond lifetime τ_d^* .

The underlying supramolecular tie-points can be easily affected by temperature, whereby an increase of the temperature causes a deaggregation of the supramolecular tie-points. Indeed, at 80 °C the rheological properties are dominated by the chain dynamics, therefore, for the highest molecular weight (PIB-BA₂-30k) the highest viscosity was observed and vice versa (see **Table 19**), evidencing the impact of the supramolecular interactions only at low temperatures.

In order to qualitatively prove this impact a modified barbituric acid functionalized PIB was synthesized bearing the “capped” BA-moiety which is devoid of hydrogen bonding since the $-N-H$ protons were exchanged by ethyl groups ($-N-CH_2-CH_3$) (see **Figure 52b**). In comparison to its supramolecular analogue, PIB-BA₂-Cap-4k was obtained as a low viscous liquid at each accessible temperature. Therefore, this comparative experiment proves that the astonishing rheological behavior of barbituric acid-functionalized PIBs (PIB-BA₂) is caused by the formation of supramolecular tie-points via hydrogen-bonding. The underlying hydrogen-bonding interactions are significantly stronger in the melt state (in terms of the effective bond lifetime τ_d^*) compared to the situation in solution.

However, PIB-BA₂-Cap-4k has a higher viscosity compared to the corresponding reference (see **Figure 52b**), an effect which can be attributed to the higher molecular weight of PIB-BA₂-Cap-4k due to the attachment of the end groups. This observation is in agreement with the investigations on functionalized PIBs bearing bulky pyrene groups (see chapter 4.7.7.).

For all four polymers within the series of bifunctional BA-functionalized PIBs master curve construction via horizontal shift of the storage- and loss modulus until optimal superposition was possible,^[119, 310] revealing the shift factors a_T . **Figure 53a** shows the corresponding shift factor vs. temperature plot for the different polymers. The resulting curves for all BA-functionalized polymers reveal a steeper slope compared to PIB-REF₂-14k (or any other PIB-REF₂). In other words the rheological properties of PIB-BA₂ have a stronger temperature dependence than unfunctionalized PIBs, since the temperature dependent supramolecular aggregation (network formation) adds a significant additional contribution to the thermo-rheological properties.

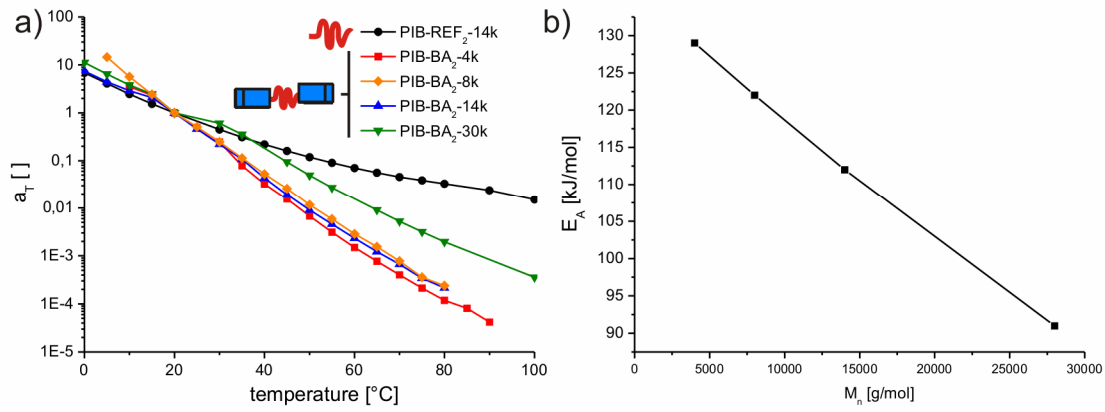


Figure 53. a) Horizontal shift factors (a_T) vs. temperature plot for PIB-BA₂ with different molecular weights; b) activation energy for viscous flow (E_A) vs. molecular weight plot für PIB-BA₂. PIB-REF₂-14k is a bifunctional PIB-OH₂ with $M_n(\text{GPC}) = 14100 \text{ g/mol}$, $M_n(\text{NMR}) = 14700 \text{ g/mol}$ and $\text{PDI} = 1.24$.

Since the absence of crystalline domains with a particular melting temperature has been proven via DSC measurements and the master curve construction was possible due to rheological simple behavior, one can assume a simple temperature dependence of the supramolecular aggregation following the Arrhenius equation:

$$\log(a_T) = \frac{E_A \cdot 0.43}{R} \cdot \left(\frac{1}{T} - \frac{1}{T_0} \right)$$

Therefore, the activation energy for viscous flow E_A can be derived from the $\log(a_T)$ vs. $(1/T - 1/T_0)$ plot. **Figure 53** shows the E_A vs. molecular weight (M_n) plot for the series of bifunctional BA-functionalized PIBs revealing a linear relation between E_A and M_n , indicating a linear decrease of supramolecular clusters with increasing molecular weight of the PIB, an observation which is in agreement with the corresponding SAXS data. Since the aggregation of barbituric acid groups lead to the formation of aggregates, which are areas with enhanced electron density contrast with respect to the poly(isobutylene) matrix, SAXS measurements were performed to investigate the microstructure of PIB-BA₂. Each sample reveals a broad first order maximum accompanied by a less pronounced second order intensity maximum (visible as a shoulder), evidencing the formation of supramolecular aggregates of several BA groups (for PIB-BA-30k no excess scattering was observed due to the low amount of end groups per volume unit). The size of the first intensity maximum can be considered as the distance between nearest neighboring aggregates of functional groups. While for PIB-BA-4k the distance is 6.8 nm, PIB-BA-13k reveals a much larger distance of 8 nm (see **Figure 54**).

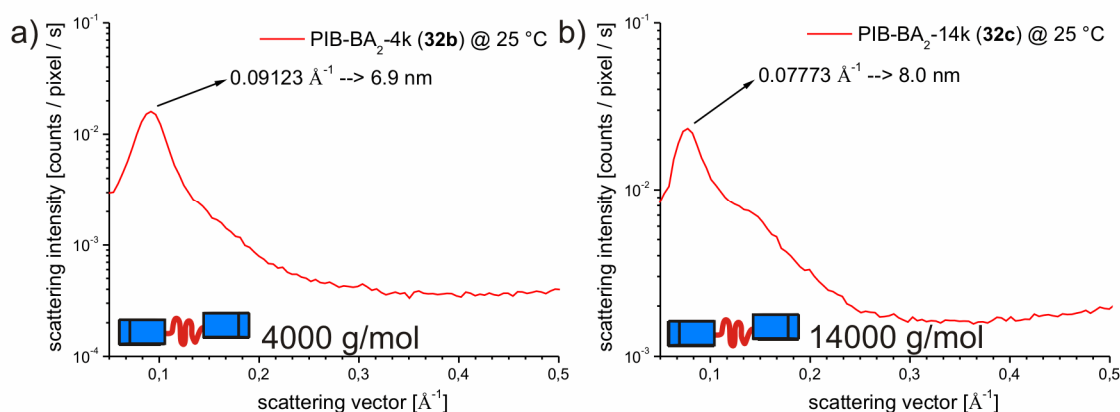


Figure 54. SAXS measurements of a) PIB-BA₂-4k and b) PIB-BA₂-14k at 25 °C.

This observation is in agreement with the higher molecular weight for PIB-BA-13k and, thus, the lower volume fraction of BA groups within the PIB matrix. Therefore, the samples exhibit a different amount of aggregates per volume fraction. Although these supramolecular aggregates act as elastically effective tie-points, all samples reveal a similar behavior in rheological measurements. Therefore, the different distance of aggregates in samples with the same rheological behavior can be seen as the evidence for the presence of ordinary entanglements due to entanglement of chains with trapped chain ends (see **Figure 34**).

4.8. Self-healing studies of bifunctional PIBs bearing barbituric acid (BA) groups

The bifunctional barbituric acid-functionalized PIBs (PIB-BA₂) show a rubbery plateau in combination with the ability of dynamic rearrangement of their supramolecular aggregates under force at long timescales (low frequencies in rheology measurements). These samples are, therefore, suitable to be investigated in more detail with respect to their self-healing behavior. In comparison to the rheology experiments, no external force is applied during these macroscopic tests. **Figure 55** shows the time-dependent evolution of a macroscopic self-healing experiment on PIB-BA₂-30k. In this test, a discoidal piece of the material is cut into two halves. Then, these two halves are immediately brought into contact again, whereupon the bright crack partially heals after 24 h. After a time of 48 h the crack vanishes (heals) completely. One can assume that the supramolecular bonds were ruptured preferentially when cutting the sample with a scalpel. The supramolecular groups remain unassociated (“sticky”) within the fractured surface for a certain period of time (see **Figure 56a** middle). When the two halves were brought into contact again, the supramolecular clusters can reform, thus, healing the crack (right).

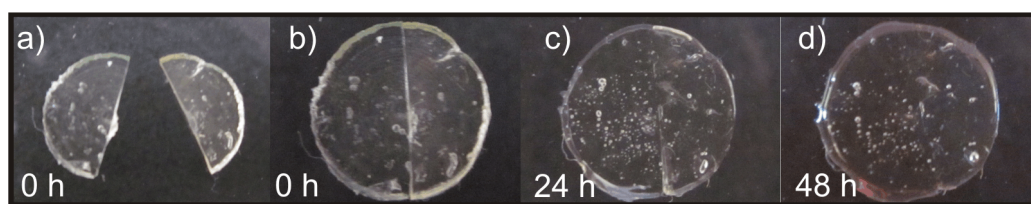


Figure 55. Self-Healing experiment of PIB-BA₂-30k.

In order to quantify the mechanical properties of the pristine and the healed materials, DMA measurements of small rectangles of the samples were performed (see **Figure 56b**). All samples were not shape persistent on a very long time scale, as evidenced by the terminal flow region in rheology measurements and the loss of a sharp contour of the discs prepared for macroscopic tests (compare **Figure 56a** and **d**). Furthermore, each sample exhibits a pronounced rubbery plateau and a very high viscosity. A similar behavior was reported by Wathier *et al.* for polymeric ionic liquids, made from poly(acrylic acid) and dicationic phosphonium salts.^[29]

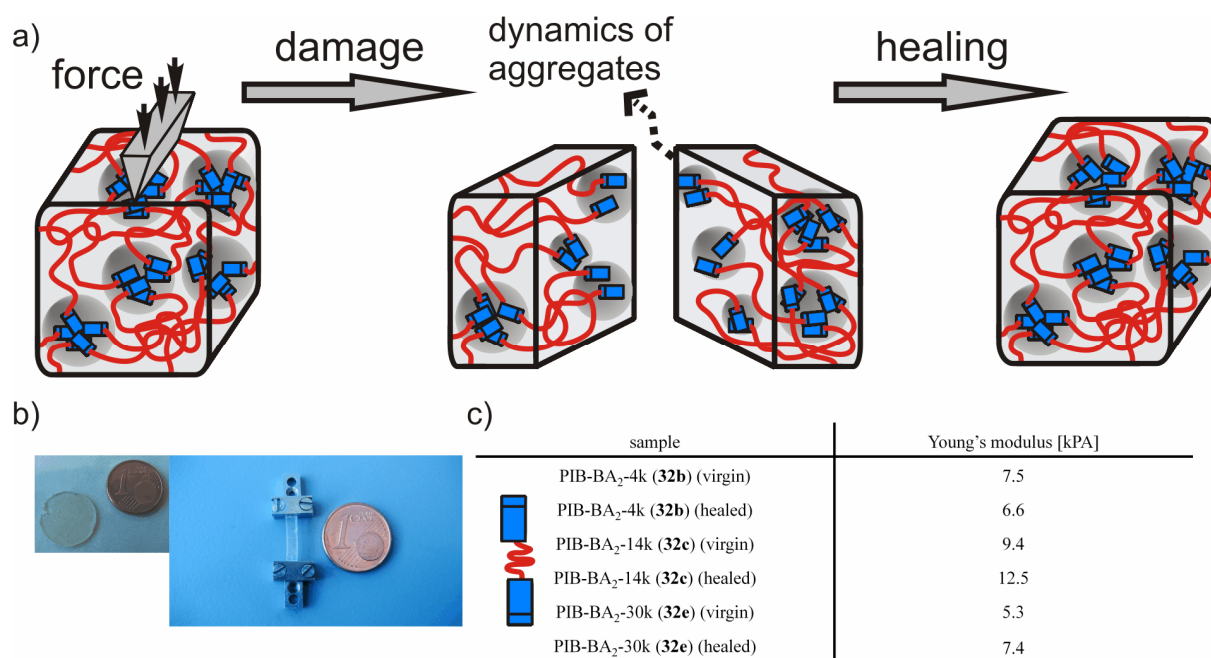


Figure 56. a) Proposed mechanism of the self-healing observed for PIB-BA₂ due to reformation of the supramolecular aggregates of BA groups; b) dimension of the DMA-samples compared to a 1 cent coin; c) Young's modulus of the virgin and healed samples (determined at 1% strain) for different molecular weights.

Therefore, in a first step a creep experiment was performed to investigate the time-dependent shape persistence of PIB-BA₂-4k under a constant load of 400 mN. **Figure 57a** shows the corresponding creep test, revealing that there is no elongation within a period of 10 h. In contrast to the work of Wathier *et al.*, PIB-BA₂ samples are shape persistent within this period

4. General Part

of time and the observed terminal flow (rheology experiments) and loss of contour (macroscopic self-healing tests) correspond to time-scales longer than 10 h. As a consequence, self-healing on shorter time-scales can be attributed to the above proposed supramolecular mechanism (see **Figure 56a**).

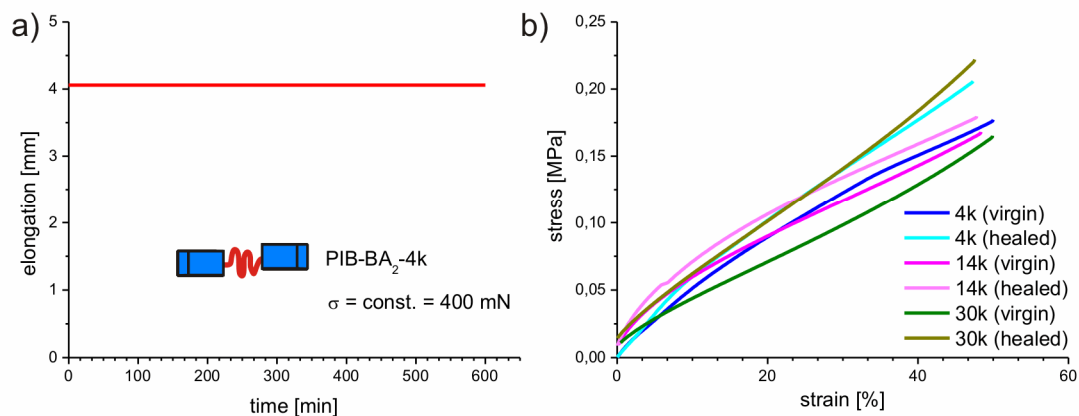


Figure 57. a) Creep test of PIB-BA₂-4k under constant load; b) stress-strain experiments of PIB-BA₂ with different molecular weights before (virgin) and after healing (healed).

Due to the small available amount of sample (several 100 mg), stress-strain measurements were only possible up to a maximal strain of 50 % (instrument constraints). **Figure 57b** shows the corresponding curves of the virgin PIB-BA₂s (-4k, -14k and -30k), revealing that all polymers within this series exhibit the same stress-strain behavior, which is in agreement with the rheological investigations. Upon cutting and healing for 15 min, each sample reveals the same behavior as the virgin material. Since one expects faster healing for PIB-BA₂-4k compared to PIB-BA₂-30k, due to a higher amount of supramolecular tie-points per volume fraction, complete healing (up to a strain of 50 %) after 15 min indicates, that autonomous self-healing in these particular rubbers is significant faster. Unfortunately, measurements after shorter healing time and up to larger strains were not possible, owing to the limits of the instrument setup. Additionally, the Young's modulus (E-modulus) can be calculated from the DMA measurements at very small strains (< 1%). The resulting E-modulus values are displayed in **Figure 56c** revealing relatively small values in the range of several kPa. The difference between virgin and healed sample can be attributed to the instrument setup. Although a comprehensive mechanical analysis was not possible with the available amounts, the mechanical properties are very promising for further investigations, since the Young's moduli are higher than for Leibler's famous self-healing rubber,^[163] which is already produced on an industrial scale by *Arkema* under the brand name *Reverlink*.^[311]

5. Experimental Part

5.1. Chemicals

All chemicals were purchased from Sigma-Aldrich and used as received if not mentioned otherwise. Methyl 2-bromopropionate (MBPP; **3**) and dimethyl 2,6-dibromoheptanedioate (DMDBH; **4**) were purchased from Sigma-Aldrich, distilled in high vacuum and stored under an atmosphere of argon. Tetrahydrofuran (THF) was predried over potassium hydroxide and freshly distilled from sodium and benzophenone under a dry argon atmosphere before use. Isopropanol, triethylamine, dichloromethane (DCM), chloroform, dimethylsulfoxide (DMSO), benzene, *n*-butyl acrylate and pyridine were freshly distilled from CaH₂ under a dry argon atmosphere before use. *n*-Hexane was heated under reflux conditions with concentrated H₂SO₄ and H₂SO₄·(SO₃)_n for 48 h in order to remove olefins. The organic layer was washed with concentrated sodium hydrogen carbonate solution and distilled water, dried over NaSO₄ and stored over CaCl₂. It was freshly distilled from KOH/Na under a dry argon atmosphere before use. 2,6-Diaminopyridine was purchased from Sigma-Aldrich and was recrystallized from boiling chloroform. Magnesium chips were activated by washing them in the following order: diluted hydrochloric acid, distilled water, two times acetone and two times diethyl ether. Finally, the magnesium chips were dried in high vacuum. Potassium hydroxide was dried in vacuum at 120 °C for 24 h. Sodium hydride (NaH) was washed with dry *n*-hexane prior use. Commercial copper(I)bromide (CuBr) was purified by washing with saturated SO₂-water followed by the procedure reported by Keller *et al.*^[312]

5.2. Materials

[CuI(P(OEt)₃)] was synthesized according to Langille *et al.*^[313] 2-Ethyl-2-(1-pentyn-5-yl)malonate (**22**) (barbituric acid (BA) alkyne) was synthesized according to Srivastava *et al.*^[314] 5-(4-ethynyl-benzoylamino)-*N*-*N'*-bis-(6-octanoylamino-pyridin-2-yl)-isophthalamide (**24**) (Hamilton wedge (HW) alkyne) was synthesized according to Binder *et al.* (procedure was improved; please see lab-journal for details).^[315] 5-Methyl-1-(prop-2-ynyl)-1*H*-pyrimidine-2,4-dione was synthesized according to Lindsell *et al.*^[316] 1-*tert*-Butyl-3,5-bis-(1-chloro-1-methyl-ethyl)-benzol (DCCl; **2**) was synthesized according to Gyor *et al.*^[248] 2-Chloro-2,4,4-trimethyl-pentane (TMPCl; **1**) was synthesized according to Kaszas *et al.*^[218] Thymine-functionalized PIBs (**26** + **27**) were synthesized within the framework of my diploma thesis.^[255]

5.3. Methods

GPC spectra were recorded on a *Viscotek GPCmax VE 2002* Solvent/Sample Module using a H_{HRH} Guard-17369 and GMH_{HR} -N-18055 column in THF or DMF. Sample concentration was 1 mg/1 ml; injection volume was 100 μ l; column temperature was 22 °C (60 °C for DMF); detector (refractive index) temperature was 35 °C and flow rate was 1 ml/min. Measurements were stopped after 16 min. Poly(isobutylene) standards were obtained from PSS (Polymer Standards Service) and used for conventional external calibration. Standards with a molecular weight of 340, 1650, 7970, 26300, 61800 and 87600 g/mol were used for calibration. Poly(styrene) standards were obtained from PSS (Polymer Standards Service) and used for conventional external calibration. Standards with a molecular weight of 1050, 2790, 6040, 13400 and 29600 g/mol were used for calibration. Recalibrations were performed every 6 months.

NMR spectra were recorded at 27 °C on a *Varian Gemini 2000* (200 MHz), *Varian Gemini 2000* (400 MHz) and *Varian Unity Inova 500* (500 MHz) spectrometer in $CDCl_3$ (Armar AG, 99.8 Atom%D), toluene- d_8 (Armar AG; 99.5 Atom%D) and $DMSO-d_6$ (Armar AG; 99.8 Atom%D). Chemical shifts were recorded in ppm (δ ; parts per million) and referred to the solvent residual peak ($CDCl_3$ 7.26 ppm (1H) and 77.0 ppm (^{13}C); $DMSO-d_6$ 2.54 ppm (1H) and 40.45 ppm (^{13}C); toluene- d_8 7.19 (1H)). MestReC (v4.9.9.6) was used for data interpretation. Carbon atoms were listed in descending order starting from the highest (^{13}C). Hydrogen atoms were listed in descending order starting from the highest. For their coupling pattern abbreviations were used: s = singulett, bs = broad singulett, d = dublett, t = triplett, q = quadruplet, m = multipllett.

Molecular weights of the poly(isobutylene)s (PIBs) via NMR ($M_{n(NMR)}$) were determined as follows: For monofunctional PIBs the integral of the initiator at 1.00 ppm was set to 15 H (two overlapping signals with 9 and 6 H). For bifunctional PIBs the integral of the initiator at 7.17 ppm was set to 3 protons. The resonance of the $-CH_2-$ groups of the polymer chain was integrated and the resulting value was divided by 2 to yield the degree of polymerization DP.

The DP was multiplied by 56.1 g/mol, the molecular weight of the repeat unit, and the molecular weights of the initiator fragment and the introduced end group(s) were added. The added molecular weights of the fragments are (in g/mol): 148.5 for TMPCl (without Cl), 287.30 for DCCl (without Cl), 41.00 for allyl, 59.00 for hydroxyl, 121.99 for bromine, 84.10 for azide, 248.3 for THY, 309.40 for DAT (alkyne **19**), 339.38 for DAT (**21**), 306.35 for BA, 362.45 for “capped” BA and 828.00 for HW. Complete functionalization of the PIBs was proven by integrating the signal of the initiator at 1.00 ppm (7.10 ppm for bifunctional PIBs) and setting this value to 15 H (bifunctional: 3 H). The integration of the characteristic

5. Experimental Part

resonance of the THY group at 7.80 ppm leads to a value of 1 H (bifunctional: 2 H), thus, indicating a complete functionalization. The integration of the characteristic resonance of the DAT group at 3.79 ppm leads to a value of 2 H (bifunctional: 4 H) and indicates a complete functionalization. The integration of the characteristic resonance of the HW group at 0.86 ppm leads to a value of 6 H (bifunctional: 12 H) and indicates a complete functionalization. The integration of the characteristic resonance of the BA group at 0.74 ppm leads to a value of 3 H (bifunctional: 6 H) and indicates a complete functionalization.

Molecular weights of the poly(*n*-butyl acrylate)s (PnBAs) via NMR ($M_{n(NMR)}$) were determined as follows: It was assumed that all chains were initiated by the initiator, thus, all chains were bearing the initiator fragment. For monofunctional PnBAs the integral of the initiator at 3.60 ppm was set to 3 H (singulett). For bifunctional PnBAs the integral of the initiator at 3.61 ppm was set to 6 H (singulett). The resonance (triplett) of the $-CH_3-$ groups of the *n*-butyl chains of the repeating unit was integrated and the resulting value was divided by 3 to yield the degree of polymerization DP. The DP was multiplied by 128.17 g/mol, the molecular weight of the repeat unit, and the molecular weights of the initiator fragment and the introduced end group(s) were added. The added molecular weights of the fragments are (in g/mol): 167.00 for MBPP (with bromide), 87.11 for MBPP (without bromide), 346.00 for DMDBH (with bromine), 186.21 for DMDBH (without bromine), 42.02 for azide, 206.18 for THY, 220.11 for “capped” THY, 309.38 for DAT (**19a/b**), 339.38 for DAT (**21**), 264.26 for BA and 771.93 for HW. Complete functionalization of the monofunctional PnBAs was proven by integrating the signal of the initiator at 3.60 ppm and setting this value to 3 H (bifunctional: 3.61 ppm; 6 H). For bromine- and azide-functionalized PnBAs (**9-12**) this proof was not possible due to overlapping of the resonances of the end group (last repeat unit) with the resonances of the polymer chain. The integration of the characteristic resonance of the THY group at 4.95 ppm leads to a value of 2 H (bifunctional: 4 H), indicating a complete functionalization. The integration of the characteristic resonance of the DAT group (**21**) at 7.21 ppm leads to a value of 2 H (bifunctional: 4 H), indicating a complete functionalization. The integration of the characteristic resonance of the BA group at 2.67 ppm leads to a value of 2 H (bifunctional: 4 H), indicating a complete functionalization. The integration of the characteristic resonance of the HW group at 7.69 ppm leads to a value of 2 H (bifunctional: 4 H), indicating a complete functionalization.

NMR titration experiments of PIBs were (in part) performed on a *Bruker Avance III* spectrometer. The proton frequency was 600.13 MHz, and a BBI probe head was used. Temperature was controlled via a BVT3200 controller. The flip angle was 40°, relaxation delay (RD) was 5 s, and 32 scans were performed for each sample. Temperature calibration

5. Experimental Part

was performed using neat methanol and a calibration formula published by Merbach *et al.*^[317] Experiments with PnBA were performed on the above mentioned 500 MHz device at 27 °C. The NMR titration experiments were performed and evaluated according to Macomber *et al.*^[100] Additional information was taken from relevant literature dealing with these kind of experiments.^[101, 280, 318]

MALDI-TOF-MS experiments were performed on a *Bruker Autoflex III* system operating in reflectron and linier modes. Data evaluation was carried out on *flexAnalysis* software (vers. 3.0) or *Wsearch32* (vers. 1.6.2005). Ions were formed by laser desorption (smart beam laser at 355 nm, 532 nm, 808 nm and 1064 nm \pm 5 nm; 3 ns pulse width; up to 2500 Hz repetition rate), accelerated by voltage of 20 kV and detected as positive ions. Baseline subtraction and smoothing of the recorded spectra were performed using a *Savitzky-Golay* algorithm. The instrument was calibrated with poly(ethylene glycol) (PEG) standards ($M_n = 2000$ g/mol or $M_n = 4000$ g/mol) applying a quadratic calibration method with an error of 1-2 ppm. PEG standards (analyte) were dissolved in THF at a concentration of 20 mg/ml. *Trans*-2-[3-(4-*tert*-butylphenyl)-2-methyl-2-propenyldene] malononitrile (DCTB) (matrix) and lithium trifluoroacetate (LiTFA) (salt) were dissolved in THF at a concentration of 20 mg/ml. For PEG standards the ratio of matrix:analyte:salt was 100:10:1 and 1 μ l of the solution was spotted on the MALDI-target plate.

Samples of mono- and bivalent 2,6-diaminotriazine-functionalized PIBs (PIB-DATA)) were prepared by dissolving the polymer in THF at a concentration of 20 mg/ml. Dithranol was used as matrix and dissolved in THF at a concentration of 20 mg/ml. LiTFA was used as salt and dissolved in THF at a concentration of 10 mg/ml. The ratio of matrix:analyte:salt was 100:10:1. The measurements were performed in deflection or linear mode using HPC (high precision calibration) method (RP_0-4kDa_HPC.par) and PEG standards with a molecular weight of 2000 or 4000 g/mol for calibration. Ions were detected as positive ions. Samples of mono- and bivalent barbituric acid-functionalized PIBs (PIB-BA), Hamilton wedge-functionalized PIBs (PIB-HW) and “capped” barbituric acid-functionalized PIBs (PIB-BA₂-Cap) were prepared analogously using DCTB as matrix and LiTFA or AgTFA as salt. Samples of functionalized PnBAs were prepared by dissolving the polymer in THF at a concentration of 20 mg/ml.^[319] IAA was used as matrix and dissolved in acetone at a concentration of 20 mg/ml. NaTFA was used as salt and dissolved in THF at a concentration of 10 mg/ml. The ratio of matrix:analyte:salt was 100:10:1. The measurements were performed in deflection or linear mode using HPC (high precision calibration) method (RP_0-4kDa_HPC.par) and PEG standards with a molecular weight of 2000 g/mol for calibration. Ions were detected as positive ions.

5. Experimental Part

ESI-TOF-MS were performed on a *Bruker Daltonics microTOF* (time-of-flight) system via direct injection. Spectra were recorded in the positive mode with an acceleration voltage of 4.5 kV, a transfer line with 190 °C, and a scan range of 50-1000 m/z. The spectra were processed on *Bruker Daltonics ESI compass 1.3* for *microTOF* (Data Analysis 4.0). Samples were prepared by dissolving 10 mg of the sample in 1 ml methanol. Then, 100 µL of this solution were diluted with 1 ml methanol and used for the ESI-TOF-MS measurements.

Microwave irradiation experiments were performed in a *Discovery System* (model 908010) from *CEM* using the SPS method.

Small-angle X-ray scattering (SAXS) experiments were performed using a *Rigaku* rotating anode. The X-ray beam was monochromated with an Osmic X-ray optics ($\lambda = 1.54 \text{ \AA}$). The size of the beam on the sample was approximately 300 µm. The samples were placed in a chamber that was evacuated to a pressure of approximately 10^{-1} mbar. A Siemens area detector of 1024×1024 channels was used to count the scattered intensity. Typical measurements took some 10 minutes. Before a measurement was started the temperature was equilibrated for 15 min.

Rheology measurements were performed on an *Anton Paar (Physica) MCR 101-DSO* using a parallel-plate measuring system (PIB samples) (diameter 8 mm) or a cone-plate measuring system (diameter 25 mm; angle 1°) (PnBA samples). The samples were tempered by thermoelectric cooling/heating in a Peltier-chamber. Atmosphere was nitrogen or dry air. The samples were tempered for 20 min at each temperature before the measurement was started. Samples (and mixtures) were prepared by dissolving/suspending the compounds in chloroform. Afterwards, the sample was filtered through a 0.2 µm PTFE-filter and the solvent was removed. The sample was dried in high vacuum to constant weight and equilibrated at 70 °C for minimum 48 h. All measurements were performed within the LVE of the polymer. In frequency sweep measurements 5 points per decade were measured. RheoPlus/32 V3.40 was used for data evaluation. MasterCurves were created by horizontal shift of the corresponding frequency sweep curves with an error tolerance of usually 25 %.

DMA measurements were performed on a *Perkin-Elmer PYRIS[®] Diamond TMA* using polymer film extension clamps. Rectangles of the samples with a dimension of 15 mm x 2 mm and a thickness of approximately 800 µm were prepared. Creep experiments were performed on the virgin samples at a constant stress of 400 mN. Stress-strain experiments were performed with a loading rate of 100 mN/min. The corresponding measurements were performed by Ranjita Bose, Ph.D., in the Novel Aerospace Materials Group (group of Prof. Sybrand van der Zwaag; Faculty of Aerospace Engineering) at the Delft University of Technology.

5. Experimental Part

DSC (differential scanning calorimetry) thermograms were measured on a *Shimadzu DSC-60* or a *Netzsch Phoenix[®] DSC 204 F1*. Indium and mercury were used for temperature calibration. Samples with a mass of about 10 mg were encapsulated in standard aluminum pans. Nitrogen was used as purge gas. Measurements were performed at a heating rate of 10 K/min in a temperature range of -120-150 °C. Glass transition temperatures were determined at the midpoint of the transition.

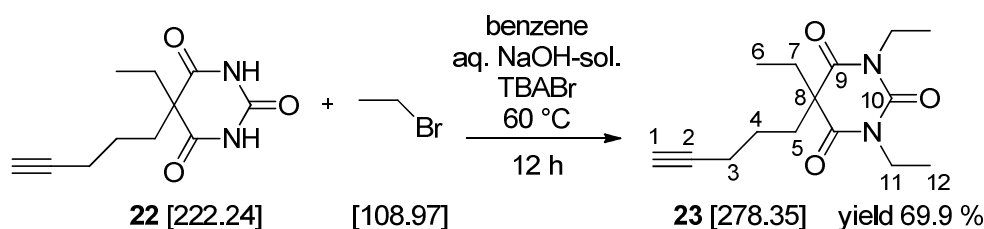
Thin layer chromatography (TLC) was performed with TLC aluminum sheets (silica gel 60 F₂₅₄) obtained from *Merck KGaA*. The following oxidation reagents for TLC were used: type 1 “blue stain”: Ce(SO₄)₂·4H₂O (1 g), (NH₄)₆Mo₇O₂₄·4H₂O (2.5 g), concentrated H₂SO₄ (6 ml) and distilled water (90 ml); type 2: „brown stain“ Ce(SO₄)₂·4H₂O (1 g), concentrated H₂SO₄ (2.75 ml) and distilled water (47 ml); type 3: KMnO₄ (3 g), K₂CO₃ (10 g) and distilled H₂O (300 ml).

Dialysis of poly(*n*-butyl acrylate)s (PnBAs) was performed using *ZelluTrans* (ROTH) regenerated cellulose dialysis tubings with a molecular weight cut-off (MWCO) of 1000 Da (nominal), 45 mm width and 27 µl thickness. The tubings were soaked in THF for 20 min prior use. The polymer was dialyzed (minimum) for 2, 4 and 12 h in THF.

TGA (thermogravimetric analysis) measurements were performed using a *Netzsch Tarsus TG 209 F3*. Typical measurements were performed using Al₂O₃-crucibles, a heating rate of 10 °C/min and an atmosphere of air (flow rate 20 ml/min). Data evaluation was accomplished using *Netzsch Proteus – Thermal Analysis* (version 5.2.1.) software.

5.4. Synthesis

5.4.1. 1,3,5-Triethyl-5-(pent-4-yn-1-yl)pyrimidine-2,4,6(1*H*,3*H*,5*H*)-trione (**23**)



In an one-neck round-bottom flask (50 ml), **22** (2.25 mmol, 500.0 mg) and NaOH (4.5 mmol, 180.0 mg) were dissolved in distilled water (3.5 ml). A solution of bromoethane (11.25 mmol, 1.23 g) and TBABr (0.9 mmol, 290.0 mg) in benzene (7 ml) was added. The resulting mixture was vigorously stirred for 12 h. Water was added and the aqueous phase was extracted two times with benzene. Both organic layers were combined, dried over NaSO₄ and filtered. After removal of the solvent the crude product was purified by

5. Experimental Part

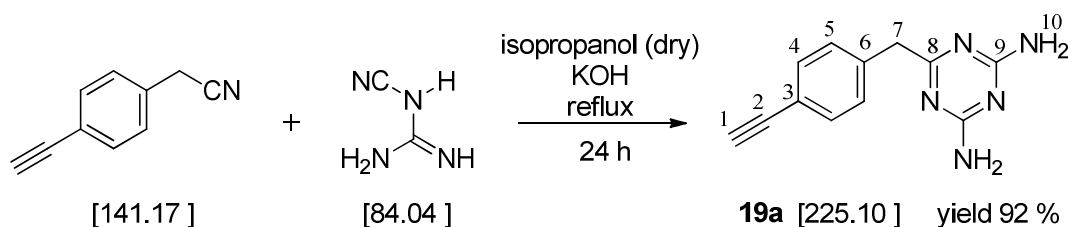
column chromatography (SiO₂, chloroform) to yield 438.0 mg (1.57 mmol, 69.9 %) of **23** as a colorless, viscous liquid.

TLC: CHCl₃ = 1; R_f((**22**) = 0.05; R_f(**23**) = 0.52

¹H-NMR (400 MHz, CDCl₃): δ 3.95 (dq, 4H, H₁₁, ²J_{H,H} = 1.7 Hz, ³J_{H,H} = 7.0 Hz), 2.13 (dt, 2H, H₃, ³J_{H,H} = 7.1 Hz, ⁴J_{H,H} = 2.6 Hz), 2.08-1.98 (m, 4H, H_{5,7}), 1.90 (t, 1H, H₁, ⁴J_{H,H} = 2.6 Hz), 1.3 (m, 2H, H₄), 1.20 (t, 6H, H₁₂, ³J_{H,H} = 7.1 Hz), 0.76 (t, 3H, H₆, ³J_{H,H} = 7.5 Hz).

¹³C-NMR (100 MHz, CDCl₃): δ 171.2 (C₉), 150.2 (C₁₀), 82.9 (C₂), 69.0 (C₁), 56.7 (C₈), 38.3 (C₁₁), 37.2 (C₇), 33.7 (C₅), 24.1 (C₄), 18.4 (C₃), 13.3 (C₁₂), 9.2 (C₆).

5.4.2. 6-(4-Ethynylbenzyl)-1,3,5-triazine-2,4-diamine – variety 1



The synthesis was done under a dry atmosphere of argon. All glassware was heated under vacuum and flushed with argon several times before chemicals were weighed in. In a two-neck round-bottom flask (100 ml), equipped with reflux condenser (with gas inlet tap), magnetic stir bar and glass stopper, 4-ethynylphenylacetonitrile (4.41 mmol, 600 μl), dicyandiamide (17.70 mmol, 1.49 g), sodium hydroxide (2.21 mmol, 124.0 mg) and isopropanol (60 ml) were added. The isopropanol was sparged with nitrogen for 10 min prior use and the mixture was heated under reflux conditions for 24 h, whereby the formation of a precipitate was observed. Subsequently, the mixture was cooled in a freezer (-24 °C) and the excess of isopropanol was decanted. Then, the residue was heated two times under reflux conditions with isopropanol (70 ml) for 10 min, suspended and filtered on a glass frit. Finally, the product was dried in high vacuum to yield 919 mg (4.08 mmol; 92.5 %) of 6-(4-ethynylbenzyl)-1,3,5-triazine-2,4-diamine (**19a**) as a beige solid.

TLC: CHCl₃/MeOH = 8/1; R_f(4-ethynylphenylacetonitrile) = 1; R_f(**19a**) = 0.15

5. Experimental Part

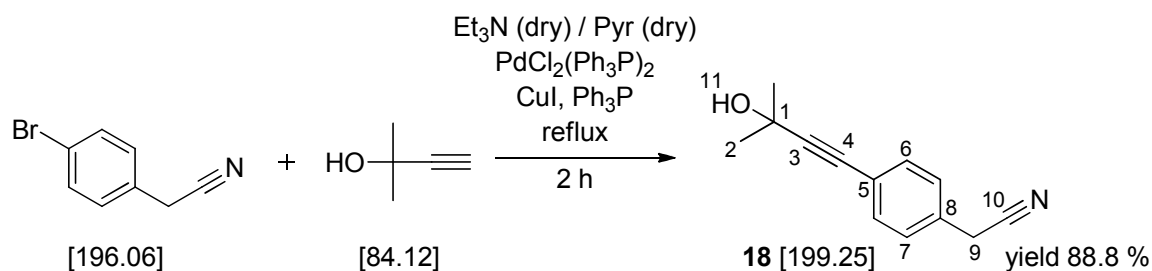
$^1\text{H-NMR}$ (400 MHz, DMSO-d_6): δ 7.39 (d, 2H, H_4 , $^3J_{\text{H,H}} = 8.02$ Hz), 7.27 (d, 2H, H_5 , $^3J_{\text{H,H}} = 8.09$ Hz), 6.62 (bs, 4H, H_{10}), 4.10 (s, 1H, H_1), 3.65 (s, 2H, H_7).

$^{13}\text{C-NMR}$ (100 MHz, DMSO-d_6): δ 175.6 (C_8), 166.9 (C_9), 139.0 (C_6), 131.3 (C_4), 129.1 (C_5), 119.4 (C_3), 83.3 (C_2), 80.1 (C_1), 44.2 (C_7).

ESI-TOF-MS measurement of **19a** via direct injection:

$[\text{M}+\text{H}]^+$ (exp.) = 226.1030 Da; $[\text{M}+\text{H}]^+$ (calc.) = 226.1093 Da; $\Delta m = 28$ ppm

5.4.3. 2-(4-(3-Hydroxy-3-methylbut-1-yn-1-yl)phenyl)acetonitrile



The Synthesis was done under a dry atmosphere of nitrogen. All glassware was heated under vacuum and flushed with argon several times before chemicals were weighed in. In a three-neck round-bottom flask (500 ml), equipped with reflux condenser (with gas inlet tap), glass stopper, magnetic stir bar and rubber septum, 4-bromophenyl acetonitrile (74.00 mmol, 14.50 g), 2-methyl-3-butyn-2-ol (88.80 mmol, 8.6 ml), triphenylphosphine (0.81 mmol, 212.5 mg), copper(I) iodide (0.30 mmol, 57.1 mg), dry triethylamine (150 ml) and dry pyridine (75 ml) were added. Subsequently, bis(triphenylphosphine)palladium(II) dichloride (0.089 mmol, 62.5 mg) was added and the mixture was heated under reflux conditions for 2.5 h, whereby the formation of a white precipitate was observed. The mixture was filtered and the filter was washed with triethylamine (2x 50 ml) and diethyl ether (3x 50 ml). Then, the filtrate and the washings were combined and the solvent was removed. After dissolving the residue was in diethyl ether (300 ml) it was washed with distilled water (500 ml), 3 wt% hydrochloric acid (300 ml) and two times distilled water (2x 500 ml). The organic phase was dried over Na_2SO_4 and filtered. After purification via column chromatography (SiO_2 , n -hexane/ethyl acetate = 2/1), the product was dried in high vacuum to yield 13.09 g (65.70 mmol, 88.8 %) of **18** as an orange/yellow powder.

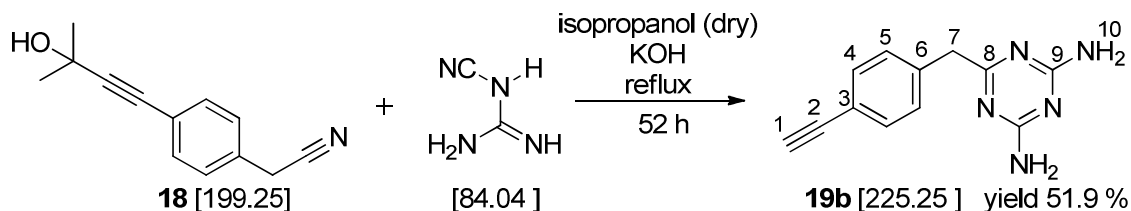
TLC: CHCl_3 ; R_f ((4-bromophenyl acetonitrile) = 0.52; R_f (**18**) = 0.25

5. Experimental Part

$^1\text{H-NMR}$ (400 MHz, CDCl_3): δ 7.42 (d, 2H, H_7 , $^3J_{\text{H,H}} = 8.27$ Hz), 7.26 (d, 2H, H_6 , $^3J_{\text{H,H}} = 8.29$ Hz), 3.74 (s, 2H, H_9), 2.08 (bs, 1H, H_{11}), 1.62 (s, 6H, H_2).

$^{13}\text{C-NMR}$ (100 MHz, CDCl_3): δ 132.3 (C_6), 129.8 (C_5), 127.8 (C_7), 122.8 (C_8), 117.3 (C_{10}), 94.7 (C_3), 81.3 (C_4), 65.6 (C_1), 31.5 (C_2), 23.5 (C_9).

5.4.4. 6-(4-Ethynylbenzyl)-1,3,5-triazine-2,4-diamine – variety 2



The Synthesis was done under a dry atmosphere of nitrogen. All glassware was heated under vacuum and flushed with argon several times before chemicals were weighed in. In a three-neck round-bottom flask (100 ml), equipped with reflux condenser (with gas inlet tap), glass stopper, magnetic stir bar and rubber septum, **18** (5.02 mmol, 1.00 g), dicyandiamide (20.08 mmol, 1.67 g), waterless potassium hydroxide (8.53 mmol, 478.6 mg) and dry isopropanol (70 ml) were added. The resulting mixture was heated under reflux conditions for 48 h, whereby the formation of a precipitate was observed. Waterless potassium hydroxide (1.00 mmol, 56.3 mg) was added and the reaction was stirred for more 4 h under reflux conditions. The reaction was allowed to cool down to room temperature and filtered. After stirring the solid residue two times with methanol (70 ml) under reflux conditions for 15 min, the mixture was cooled in a freezer (-18 °C) and filtered. Finally, the product was dried in high vacuum to yield 587.0 mg (2.61 mmol, 51.9 %) of 6-(4-ethynylbenzyl)-1,3,5-triazine-2,4-diamine **19b** as a pale beige solid.

TLC: $\text{CHCl}_3/\text{MeOH} = 8/1$; $\text{Rf}(\mathbf{18}) = 0.73$; $\text{Rf}(\text{side product}) = 0.41$; $\text{Rf}(\mathbf{19b}) = 0.27$

$^1\text{H-NMR}$ (400 MHz, DMSO-d_6): δ 7.39 (d, 2H, H_4 , $^3J_{\text{H,H}} = 8.02$ Hz), 7.27 (d, 2H, H_5 , $^3J_{\text{H,H}} = 8.09$ Hz), 6.62 (bs, 4H, H_{10}), 4.10 (s, 1H, H_1), 3.65 (s, 2H, H_7).

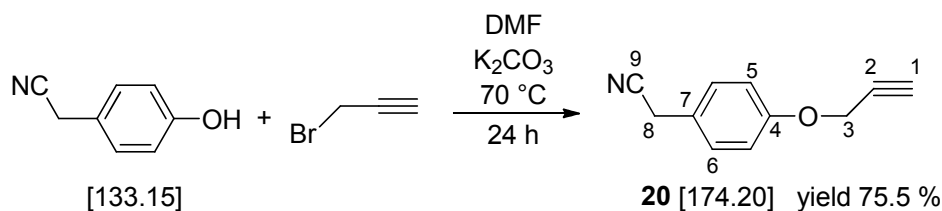
$^{13}\text{C-NMR}$ (100 MHz, DMSO-d_6): δ 175.6 (C_8), 166.9 (C_9), 139.0 (C_6), 131.3 (C_4), 129.1 (C_5), 119.4 (C_3), 83.3 (C_2), 80.1 (C_1), 44.2 (C_7).

ESI-TOF-MS measurement of **19b** via direct injection:

$[\text{M}+\text{H}]^+$ (exp.) = 226.1078 Da; $[\text{M}+\text{H}]^+$ (calc.) = 226.1093 Da; $\Delta m = 7$ ppm

5. Experimental Part

5.4.5. 2-(4-(Prop-2-yn-1-yloxy)phenyl)acetonitrile



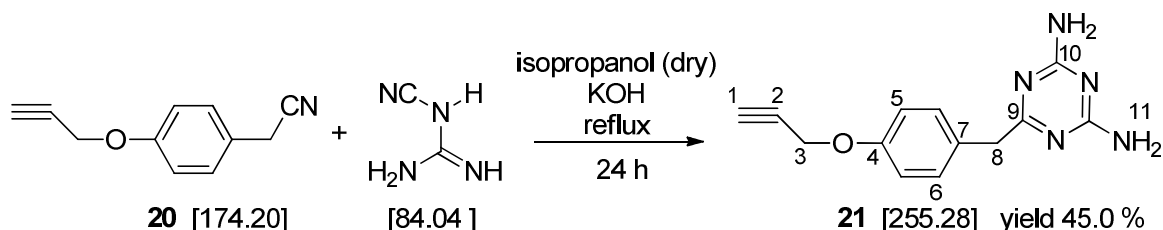
In an one-neck round-bottom flask (250 ml), equipped with magnetic stir bar, 4-hydroxyphenylacetonitrile (35.3 mmol, 4.70 g), potassium carbonate (70.6 mmol, 9.76 g), propargyl bromide (80 wt%-solution in toluene, 70.6 mmol, 10.5 g) and DMF (120 ml) were added. The mixture was stirred for 24 h at 70 °C. Afterwards, the mixture was poured into 1200 ml cold water, the precipitate was removed by filtration, and the filtrate was washed two times with chloroform. The precipitate was dissolved in chloroform and combined with the organic layers. After washing one time with brine and two times with distilled water, the combined organic layers were dried over sodium sulfate and filtered. Pure **20** was obtained via column chromatography (SiO₂, DCM). Finally, the product was dried in high vacuum to yield 4.65 g of **20** (26.64 mmol; 75.5 %) as a yellow oil, which crystallized within several minutes. Reaction conditions were adapted from Ryu *et al.*^[320]

TLC: DCM; R_f((4-hydroxyphenylacetonitrile) = 0.16; R_f(**20**) = 0.65

¹H-NMR (400 MHz, CDCl₃): δ 7.26 (d, 2H, H₆, ³J_{H,H} = 8.5 Hz), 6.98 (d, 2H, H₅, ³J_{H,H} = 8.6 Hz), 4.70 (d, 2H, H₃, ⁴J_{H,H} = 2.3 Hz), 3.69 (s, 2H, H₈), 2.53 (t, 1H, H₁, ⁴J_{H,H} = 2.4 Hz).

¹³C-NMR (100 MHz, CDCl₃): δ 157.3 (C₄), 129.1 (C₆), 122.8 (C₇), 118.0 (C₉), 115.6 (C₅), 78.2 (C₂), 75.8 (C₁), 55.9 (C₃), 22.8 (C₈).

5.4.6. 6-(4-(Prop-2-yn-1-yloxy)benzyl)-1,3,5-triazine-2,4-diamine



The Synthesis was done under a dry atmosphere of nitrogen. All glassware was heated under vacuum and flushed with argon several times before chemicals were weighed in. In a two-neck round-bottom flask (100 ml), equipped with reflux condenser (with gas inlet tap), magnetic stir bar and glass stopper, **20** (5.74 mmol; 1.00 g), dicyandiamide (11.48 mmol;

5. Experimental Part

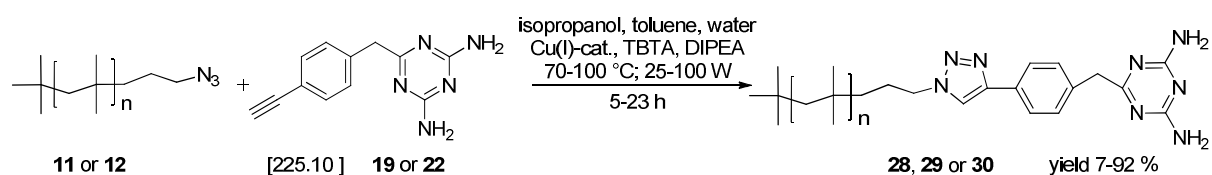
964.8 mg), KOH (1.15 mmol; 64.0 mg) and 40 ml dry isopropanol were added. The mixture was heated under reflux conditions for 24 h, whereby the formation of a white precipitate was observed. Afterwards, the mixture was cooled to 0 °C and filtered through a glass frit. After stirring the solid with distilled water (50 ml) it was filtered again. The neat solid was washed with a small amount of cold methanol (5 ml) and cold diethyl ether (5 ml). Finally, the product was dried in high vacuum to yield 667.0 mg (2.61 mmol, 45.0 %) of **21** as a pale beige solid.

TLC: CHCl₃/MeOH = 8/1; Rf(**20**) = 0.9; Rf(**21**) = 0.29

¹H-NMR (400 MHz, DMSO-d₆): δ 7.19 (d, 2H, H₆, ³J_{H,H} = 8.6 Hz), 6.90 (d, 2H, H₅, ³J_{H,H} = 8.6 Hz), 6.59 (bs, 4H, H₁₁), 4.74 (d, 2H, H₃, ⁴J_{H,H} = 2.3 Hz), 3.56 (s, 2H, H₈), 3.52 (t, 1H, H₁, ⁴J_{H,H} = 2.3 Hz).

¹³C-NMR (100 MHz, DMSO-d₆): δ 176.4 (C₉), 167.0 (C₁₀), 155.6 (C₄), 130.8 (C₆), 129.8 (C₇), 114.5 (C₅), 79.3 (C₂), 78.0 (C₁), 55.2 (C₃), 43.6 (C₈).

5.4.7. 2,6-Diaminotriazine-functionalized PIBs (PIB-DAT)

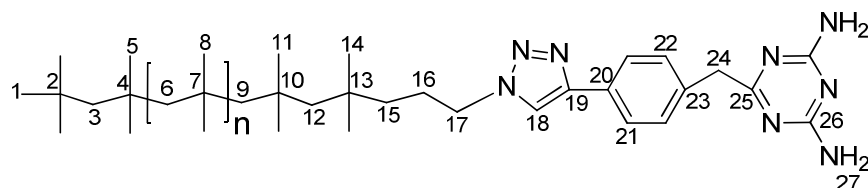


In an one-neck round-bottom flask (100 ml), azide-functionalized PIB (**11** or **12**) was dissolved in toluene. Isopropanol, water, DIPEA and TBTA were added. The mixture was sparged with nitrogen for 20 min. Subsequently, the Cu^I-catalyst and 6-(4-ethynylbenzyl)-1,3,5-triazine-2,4-diamine **19** (or alkyne **21**) were added. Then, the flask was closed with a rubber septum and placed in a microwave oven. Microwave irradiation was started immediately. After reaction was finished the solvent was removed in vacuum and the residue was dissolved in chloroform. Then, the organic layer was washed with saturated ammonium chloride solution, twice with distilled water, dried over Na₂SO₄ and filtered. Chloroform was removed in vacuum and the crude product was purified by column chromatography (SiO₂; see **Table 20**), whereby the unreacted chains were eluted first, before changing the solvent to a more polar mixture to elute the DAT-functionalized product. Finally, the polymer was dissolved in a small amount of *n*-hexane, precipitated in 10-fold excess of methanol and dried in high vacuum to yield 2,6-diaminotriazine-functionalized PIB (**28-30**; PIB-DAT) as a clear, colorless, viscous liquid. For experimental details see **Table 33** (appendix).

5. Experimental Part

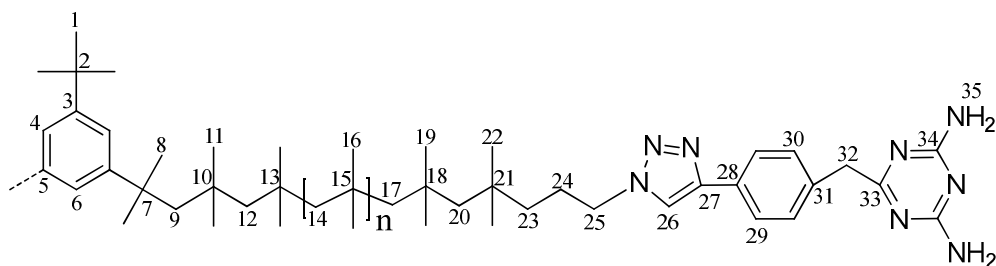
Table 20. Details for column chromatography of DAT-functionalized PIBs.

entry	PIB	start	R _F (prod.)	R _F (educt)	change to	R _F (prod.)
1	28a	CHCl ₃	0	1	CHCl ₃ /MeOH = 10/1	0.8-0.5
2	29a	CHCl ₃	0	1	CHCl ₃ /MeOH = 20/1	0.29
3	28d+e	CHCl ₃	0	1	CHCl ₃ /MeOH = 10/1	0.65
4	28c	CHCl ₃	0	1	CHCl ₃ /MeOH = 30/1	0.17
5	28f	Hex	0	1	CHCl ₃ /MeOH = 100/1	1
6	30a	CHCl ₃	0	1	CHCl ₃ /MeOH = 100/1	0.37



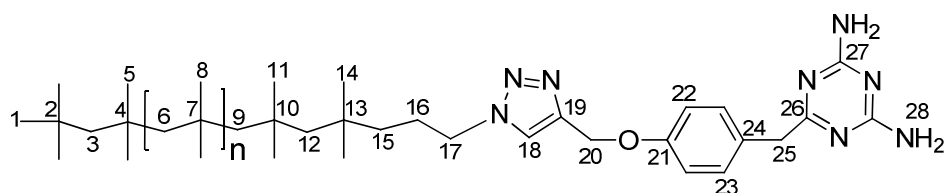
¹H-NMR (500 MHz, CDCl₃): δ 7.78 (d, 2H, H₂₁, ³J_{H,H} = 6.12 Hz), 7.71 (s, 1H, H₁₈), 7.39 (d, 2H, H₂₂, ³J_{H,H} = 6.55 Hz), 5.31 (bs, 4H, H₂₇), 4.34 (t, 2H, H₁₇, ³J_{H,H} = 7.02 Hz), 3.79 (s, 2H, H₂₄), 1.44 (s, n·2H, H₆), 1.11 (s, n·6H, H₈), 0.99 (s, 15 H, H₁₊₅).

¹³C-NMR (125 MHz, CDCl₃): δ 177.5 (C₂₅), 167.0 (C₂₆), 147.4 (C₁₉), 136.9 (C₂₃), 129.6 (C₂₂), 129.2 (C₂₁), 125.7 (C₂₀), 119.2 (C₁₈), 59.6 (C₆), 58.9 (C₉), 58.3 (C₉), 55.8 (C₁₂), 51.3 (C₁₇), 44.8 (C₂₄), 42.4 (C₁₅), 38.2 (C₇), 37.9 (C₄), 37.9 (C₁₀), 34.9 (C₁₃), 32.7 (C₂), 32.5 (C₁), 31.3 (C₈), 30.9 (C₅), 30.9 (C₁₁), 29.3 (C₁₄), 25.7 (C₁₆).



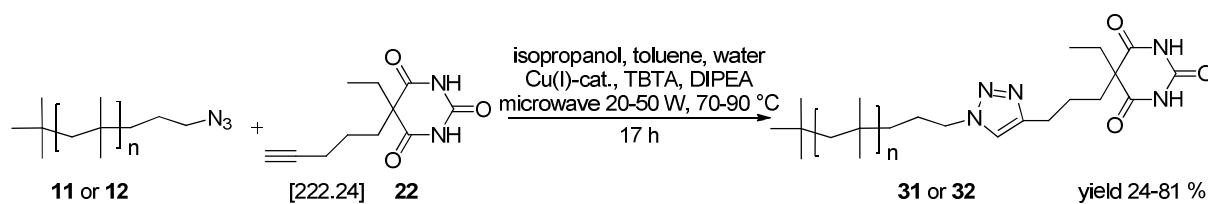
¹H-NMR (400 MHz, CDCl₃): δ 7.77 (d, 4H, H₂₉, ³J_{H,H} = 6.10 Hz), 7.71 (s, 2H, H₂₆), 7.37 (d, 4H, H₃₀, ³J_{H,H} = 6.57 Hz), 7.17 (s, 3H, H₄₊₆), 5.29 (bs, 8H, H₃₅), 4.34 (t, 4H, H₂₅, ³J_{H,H} = 7.08 Hz), 3.80 (s, 4H, H₃₂), 1.83 (s, 4H, H₉), 1.42 (s, n·2H, H₁₄), 1.10 (s, n·6H, H₁₆).

¹³C-NMR (100 MHz, CDCl₃): δ 177.5 (C₃₄), 167.0 (C₃₃), 149.0 (C₃), 148.5 (C₅), 147.4 (C₂₇), 135.2 (C₃₁), 129.6 (C₃₀), 129.2 (C₂₉), 125.8 (C₂₈), 121.2 (C₆), 120.1 (C₄), 119.2 (C₂₆), 59.5 (C₁₄), 58.6 (C₁₇), 55.7 (C₂₀), 51.2 (C₂₅), 44.8 (C₃₂), 42.3 (C₂₃), 38.1 (C₁₅), 37.9 (C₁₃), 37.8 (C₁₈), 34.8 (C₂₁), 31.2 (C₁₆), 30.8 (C₁₁), 30.7 (C₁₉), 29.2 (C₂₂), 26.6 (C₂₄).



$^1\text{H-NMR}$ (400 MHz, CDCl_3): δ 7.58 (s, 1H, H_{18}), 6.93 (d, 2H, H_{22} , $^3J_{\text{H,H}} = 8.6$ Hz), 5.20 (s, 2H, H_{20}), 5.09 (bs, 4H, H_{28}), 4.30 (t, 2H, H_{17} , $^3J_{\text{H,H}} = 7.4$ Hz), 3.76 (s, 2H, H_{25}), 1.44 (s, n·2H, H_6), 1.11 (s, n·6H, H_8), 0.99 (s, 9H, H_1). (resonance H_{23} is overlapping with the solvent residual peak).

5.4.8. Barbituric acid-functionalized PIBs (PIB-BA) and PIB-BA-Cap

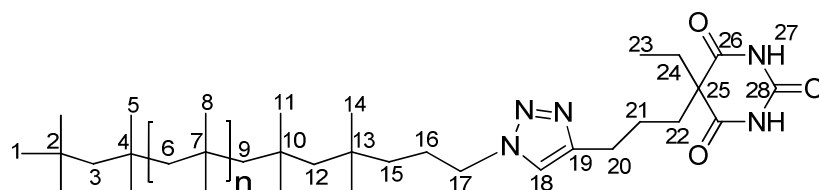


In an one-neck round-bottom flask (100 ml), azide-functionalized PIB (**11** or **12**) was dissolved in toluene. Isopropanol, water, DIPEA and TBTA were added. The mixture was sparged with nitrogen for 40 min. Subsequently, the Cu^{I} -catalyst and **22** (or **23**) were added, the flask was sealed with a rubber septum and placed in the microwave oven. Microwave irradiation was started immediately. After the reaction was complete, CHCl_3 was added and the organic phase was washed two times with saturated NH_4Cl -solution, one time with distilled water, dried over Na_2SO_4 and filtered. Chloroform was removed in vacuum and the crude product was purified by column chromatography (SiO_2 ; see **Table 21**), whereby the unreacted chains were eluted first, before changing the solvent to a more polar mixture to elute the BA-functionalized product. Finally, the polymer was dissolved in a small amount of *n*-hexane, precipitated in 10-fold excess of methanol and dried in high vacuum to yield barbituric acid-functionalized PIB (**31** or **32**; PIB-BA) as a clear, colorless, viscous liquid or rubber. For experimental details see **Table 34** (appendix).

5. Experimental Part

Table 21. Details for column chromatography of BA-functionalized PIBs.

entry	PIB	start	R _F (prod.)	R _F (educt)	change to	R _F (prod.)
1	31a+b	CHCl ₃	0	1	CHCl ₃ /MeOH = 100/1	0.1
2	31c	CHCl ₃	0	1	CHCl ₃ /MeOH = 100/1	0.17
3	31d	Hex	0	1	Hex/CHCl ₃ /MeOH = 50/50/1	0.27
4	32a	CHCl ₃	0	1	CHCl ₃ /MeOH = 200/1	0.13
5	32b	CHCl ₃	0	1	CHCl ₃ /MeOH = 200/1	0.09
6	32c	CHCl ₃	0	1	CHCl ₃ /MeOH = 100/1	0.25
7	32e	Hex	0	1	CHCl ₃ /MeOH = 100/1	0.26
8	32d	Hex/CHCl ₃	0	1	CHCl ₃ /MeOH = 100/1	0.08
9	33a	Hex	0	1	CHCl ₃	0.13

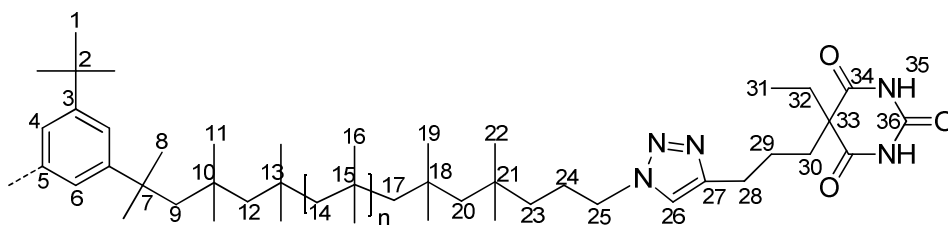


¹H-NMR (500 MHz, CDCl₃): δ 8.38 (bs, 2H, H₂₇), 7.26 (s, 1H, H₁₈), 4.36 (t, 2H, H₁₇, ³J_{H,H} = 7.3 Hz), 2.71 (t, 2H, H₂₀, ³J_{H,H} = 7.3 Hz), 2.05 (m, 6H, H₂₁₊₂₂₊₂₄), 1.42 (bs, n·2H, H₆), 1.11 (bs, n·6H, H₈), 0.99 (s, 15H, H₁₊₅), 0.92 (t, 3H, H₂₃, ³J_{H,H} = 7.4 Hz).

Note: Assignment of H₁₅₊₁₆ was not possible due to overlapping with other resonances. Integration of H₁₈ was not possible due to overlapping with the solvent residual peak of CDCl₃.

¹³C-NMR (125 MHz, CDCl₃): δ 172.0 (C₂₆), 153.4 (C₂₈), 148.1 (C₁₉), 128.4 (C₁₈), 59.5 (C₆), 58.8 (C₃), 58.2 (C₉), 57.1 (C₂₅), 55.8 (C₁₂), 42.3 (C₁₅), 38.1 (C₇), 37.8 (C₄), 37.7 (C₁₀), 34.9 (C₁₃), 32.7 (C₂₂), 32.5 (C₂), 32.4 (C₁), 31.9 (C₂₁), 31.2 (C₈), 30.8 (C₅), 30.7 (C₁₁), 29.2 (C₁₄), 26.2 (C₁₆), 9.4 (C₂₃).

Note: Assignment of C₁₇, C₂₄, C₂₀ was not possible due to overlapping with other resonances.



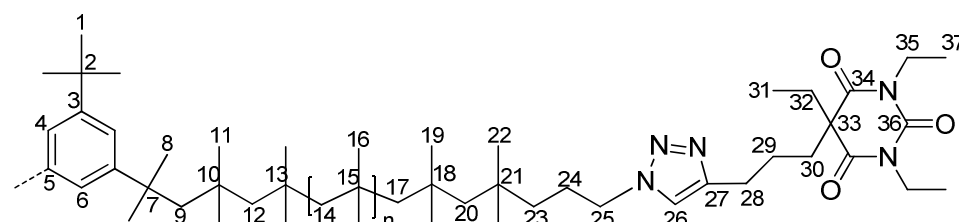
¹H-NMR (500 MHz, CDCl₃): δ 8.29 (bs, 4H, H₃₅), 7.26 (s, 2H, H₂₆), 7.17 (s, 3H, H_{4,6}), 4.30 (t, 4H, H₂₅, ³J_{H,H} = 7.4 Hz), 2.74 (t, 4H, H₂₈, ³J_{H,H} = 7.4 Hz), 2.05 (m, 12H, H_{29,30,32}), 1.85 (s, 4H, H₉), 1.42 (bs, n·2H, H₁₄), 1.11 (bs, n·6H, H₁₆), 1.02 (s, 12H, H₂₂), 0.89 (t, 6H, H₃₁, ³J_{H,H} = 7.5 Hz).

5. Experimental Part

Note: Assignment of H_{23+24} was not possible due to overlapping with other resonances. Integration of H_{26} was not possible due to overlapping with the solvent residual peak of $CDCl_3$.

^{13}C -NMR (125 MHz, $CDCl_3$): δ 171.9 (C_{34}), 153.8 (C_{36}), 149.0 (C_3), 148.5 (C_5), 148.1 (C_{27}), 128.8 (C_{26}), 121.2 (C_6), 120.1 (C_4), 59.5 (C_{14}), 59.2 (C_{12}), 59.1 (C_{17}), 58.6 (C_9), 57.1 (C_{33}), 55.8 (C_{20}), 42.4 (C_{23}), 39.0 (C_7), 38.2 (C_{15}), 38.0 (C_{13}), 37.9 (C_{18}), 37.8 (C_{10}), 34.8 (C_{21}), 34.8 (C_2), 32.7 (C_{30}), 32.3 (C_8), 31.9 (C_{29}), 31.6 (C_1), 31.2 (C_{16}), 30.8 (C_{11}), 30.7 (C_{19}), 29.2 (C_{22}), 25.5 (C_{24}), 22.7 (C_{32}), 9.4 (C_{31}).

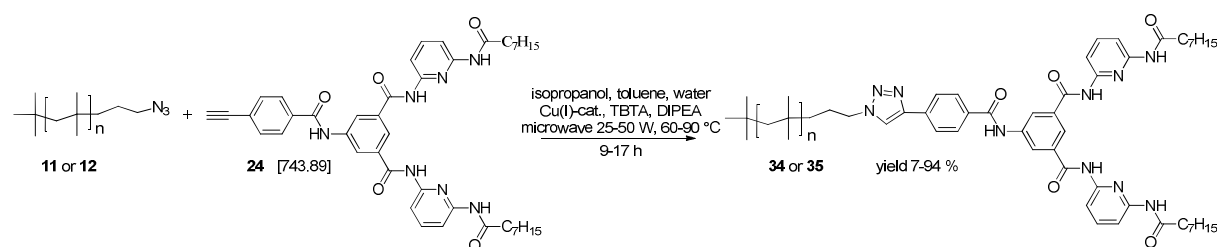
Note: Assignment of C_{32} , C_{28} , C_{25} was not possible due to overlapping with other resonances.



1H -NMR (400 MHz, $CDCl_3$): δ 7.23 (s, 2H, H_{26}), 7.12 (s, 3H, $H_{4,6}$), 4.25 (t, 4H, H_{25} , $^3J_{H,H} = 7.3$ Hz), 3.96 (dq, 8H, H_{35} , $^2J_{H,H} = 1.7$ Hz), 2.67 (t, 4H, H_{28} , $^3J_{H,H} = 7.4$ Hz), 2.04 (m, 8H, $H_{29,30}$), 1.83 (m, 8H, $H_{32,9}$), 1.42 (bs, n·2H, H_{14}), 1.11 (bs, n·6H, H_{16}), 1.02 (s, 12H, H_{22}), 0.97 (t, 18H, $H_{37,31}$).

^{13}C -NMR (100 MHz, $CDCl_3$): δ 171.4 (C_{34}), 150.2 (C_{36}), 149.0 (C_3), 148.5 (C_5), 146.9 (C_{27}), 121.2 (C_{26}), 120.3 (C_6), 120.1 (C_4), 59.5 (C_{14}), 59.2 (C_{12}), 59.1 (C_{17}), 58.6 (C_9), 56.9 (C_{33}), 55.7 (C_{20}), 51.0 (C_{25}), 42.2 (C_{23}), 39.0 (C_7), 38.6 (C_{35}), 38.2 (C_{15}), 38.0 (C_{13}), 37.8 ($C_{10,18}$), 37.2 (C_{32}), 34.8 (C_{21}), 34.7 (C_2), 34.5 (C_{30}), 34.0 (C_{28}), 32.3 (C_8), 31.6 ($C_{1,29}$), 31.2 (C_{16}), 30.8 (C_{11}), 30.7 (C_{19}), 29.2 (C_{22}), 25.3 (C_{24}), 13.4 (C_{31}), 9.2 (C_{37}).

5.4.8. Hamilton wedge-functionalized PIBs (PIB-HW)



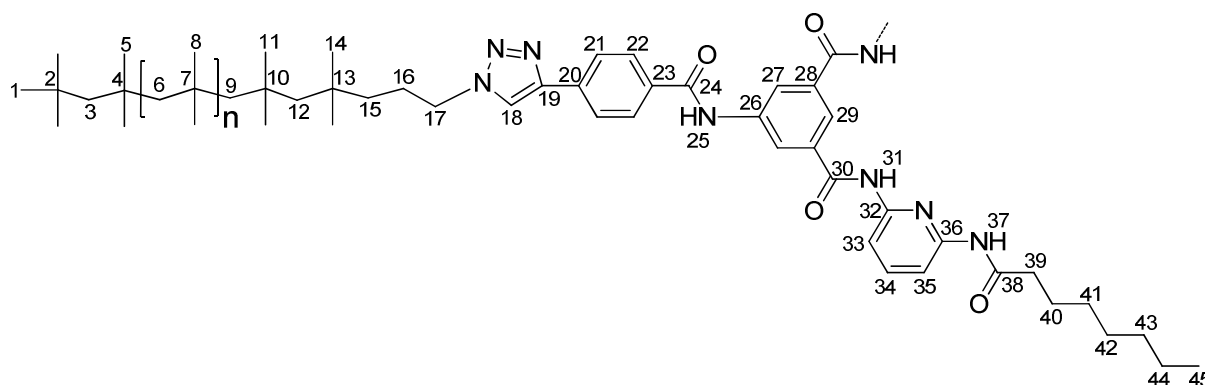
In an one-neck round-bottom flask (100 ml), azide-functionalized PIB (**11** or **12**) was dissolved in toluene. Isopropanol, water, DIPEA and TBTA were added. The mixture was sparged with nitrogen for 40 min. Subsequently, the Cu^I -catalyst and Hamilton-alkyne (**24**) were added, the flask was closed with a rubber septum and placed in the microwave oven. Microwave irradiation was started immediately. After the reaction was complete $CHCl_3$ was

5. Experimental Part

added and the organic phase was washed one time with saturated NH_4Cl solution and two times with distilled water, dried over Na_2SO_4 and filtered. Chloroform was removed in vacuum and the crude product was purified by column chromatography (SiO_2 ; see **Table 22**), whereby the unreacted chains were eluted first, before changing the solvent to a more polar mixture to elute the HW-functionalized product. Finally, the polymer was dissolved in a small amount of *n*-hexane, precipitated in 10-fold excess of methanol and dried in high vacuum to yield Hamilton wedge-functionalized PIB (**34** or **35**; PIB-HW) as a clear, colorless, viscous liquid or rubber. For experimental details see **Table 35** (appendix).

Table 22. Details for column chromatography of HW-functionalized PIBs.

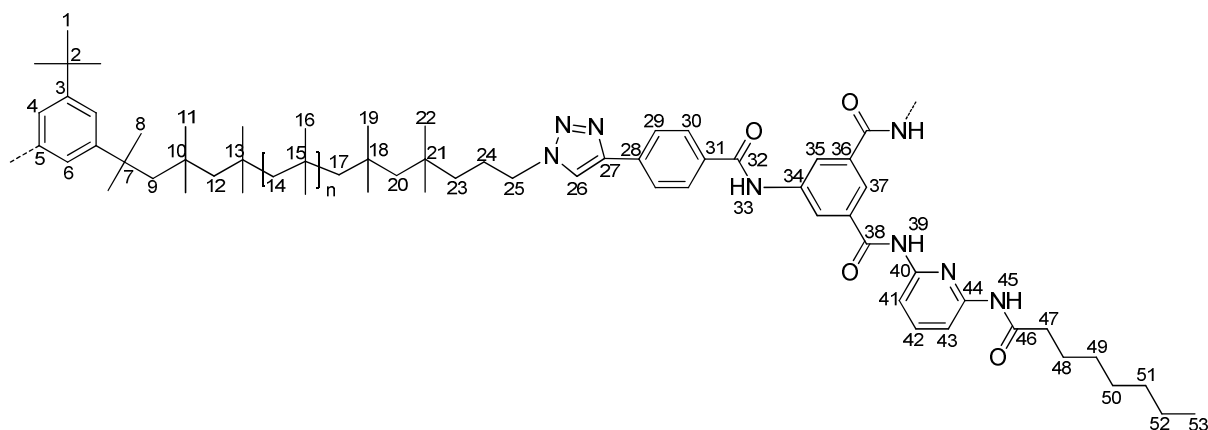
entry	PIB	start	$R_F(\text{prod.})$	$R_F(\text{educt})$	change to	$R_F(\text{prod.})$
1	34a	CHCl_3	0	1	$\text{CHCl}_3/\text{MeOH} = 100/1$	0.1
2	34b	CHCl_3	0	1	$\text{CHCl}_3/\text{MeOH} = 100/1$	0.47
3	34c	CHCl_3	0	1	$\text{CHCl}_3/\text{MeOH} = 100/1$	0.15
4	34d	Hex	0	1	$\text{CHCl}_3/\text{MeOH} = 100/1$	0.16
5	35a	CHCl_3	0	1	$\text{CHCl}_3/\text{MeOH} = 100/1$	0.17



$^1\text{H-NMR}$ (500 MHz, CDCl_3): δ 9.11 (bs, 1H, H_{25}), 8.84 (bs, 2H, H_{31}), 8.48 (s, 2H, H_{27}), 8.39 (s, 2H, H_{37}), 8.04 (s, 2H, H_{22}), 7.92-7.84 (m, 8H, $\text{H}_{18,29,33-35}$), 7.60 (s, 2H, H_{21}), 4.37 (t, 2H, H_{17}), 2.54 (s, 4H, H_{39}), 1.96 (m, 2H, H_{16}), 1.76 (m, 4H, H_{40}), 1.42 (bs, $n \cdot 2\text{H}$, H_6), ~ 1.26 (m, 16H, H_{41-44}), 1.11 (bs, $n \cdot 6\text{H}$, H_8), 0.99 (s, 15H, H_{1+5}), 0.86 (t, 6H, $^3J_{\text{H,H}} = 6.5$ Hz, H_{45}).

$^{13}\text{C-NMR}$ (125 MHz, CDCl_3): δ 172.9 (C_{38}), 166.4 (C_{30}), 163.8 (C_{24}), 150.2 (C_{32}), 148.9 (C_{36}), 145.9 (C_{19}), 140.6 (C_{34}), 139.1 (C_{26}), 135.2 (C_{28}), 135.0 (C_{23}), 130.0 (C_{21}), 128.5 (C_{22}), 128.1 (C_{20}), 126.0 (C_{27}), 122.1 (C_{29}), 120.7 (C_{18}), 110.5 (C_{33}), 109.4 (C_{35}), 59.5 (C_6), 58.8 (C_3), 58.2 (C_9), 55.9 (C_{12}), 51.4 (C_{17}), 42.3 (C_{15}), 38.2 (C_7), 37.8 (C_4), 37.8 (C_{10}), 37.6 (C_{39}), 34.9 (C_{13}), 32.6 (C_2), 32.4 (C_1), 31.7 (C_{43}), 31.2 (C_8), 30.8 (C_5), 30.8 (C_{11}), 29.3 (C_{14}), 29.2 (C_{41}), 29.1 (C_{42}), 25.6 (C_{16}), 25.5 (C_{40}), 22.6 (C_{44}), 14.1 (C_{45}).

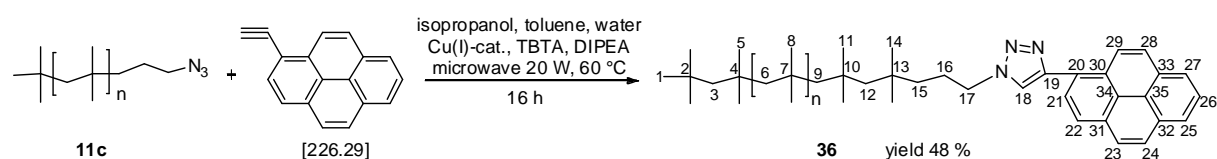
5. Experimental Part



$^1\text{H-NMR}$ (500 MHz, CDCl_3): δ 9.41 (bs, 2H, H_{33}), 9.00 (bs, 4H, H_{39}), 8.53 (bs, 4H, H_{35}), 8.33 (bs, 4H, H_{45}), 7.85 (m, 20H, $\text{H}_{30,26,37,41-43}$), 7.50 (bs, 4H, H_{29}), 7.17 (s, 3H, $\text{H}_{4,6}$), 4.33 (bs, 4H, H_{25}), 2.49 (bs, 8H, H_{47}), 1.95 (bs, 4H, H_{24}), 1.83 (s, 4H, H_9), 1.72 (bs, 8H, H_{48}), 1.42 (bs, n·2H, H_{14}), 1.32 (m, 32H, H_{49-52}), 1.11 (bs, n·6H, H_{16}), 0.85 (t, 12H, $^3\text{J}_{\text{H,H}} = 6.3$ Hz, H_{53}).

$^{13}\text{C-NMR}$ (125 MHz, CDCl_3): δ 173.0 (C_{46}), 166.4 (C_{38}), 164.2 (C_{32}), 150.2 (C_{40}), 149.0 ($\text{C}_{44,3}$), 148.5 (C_5), 146.2 (C_{27}), 140.4 (C_{42}), 139.1 (C_{34}), 135.0 (C_{36}), 134.7 (C_{31}), 130.0 (C_{29}), 128.5 (C_{30}), 128.3 (C_{28}), 125.8 (C_{35}), 122.3 (C_{37}), 121.2 (C_6), 120.0 (C_{26}), 120.1 (C_4), 110.5 (C_{41}), 109.4 (C_{43}), 59.5 (C_{14}), 58.6 (C_{17}), 56.0 (C_{20}), 51.4 (C_{25}), 42.3 (C_{23}), 39.0 (C_7), 38.2 (C_{15}), 37.9 (C_{18}), 37.8 (C_{10}), 37.5 (C_{47}), 34.9 (C_{21}), 34.8 (C_2), 32.3 (C_8), 31.7 (C_{51}), 31.7 (C_1), 31.3 (C_{16}), 30.9 (C_{11}), 30.8 (C_{19}), 29.3 (C_{22}), 29.2 (C_{49}), 29.1 (C_{50}), 25.6 (C_{24}), 25.5 (C_{48}), 22.6 (C_{52}), 14.1 (C_{45}).

5.4.9. Pyrene-functionalized PIB (PIB-Pyrene)



In an one-neck round-bottom flask (100 ml), azide-functionalized PIB (**11c**) (49 μmol ; 374 mg) was dissolved in toluene (15 ml). Isopropanol (5 ml), water (5 ml), DIPEA (0.49 mmol; 87 μl) and TBTA (9.8 μmol ; 5.2 mg) were added. The mixture was sparged with argon for 30 min. Subsequently, CuBr (49 μmol ; 7.0 mg) was added and the flask was sparged additional 10 min with argon. Then, CuBrTTPP (9.8 μmol ; 9.1 mg) and 1-ethynylpyrene (0.15 mmol; 33.3 mg) were added, the flask was closed with a rubber septum and placed in the microwave oven. Microwave irradiation was started immediately (SPS method; 20 W; 80 $^\circ\text{C}$; ΔT 10 $^\circ\text{C}$; 16 h). After reaction was complete CHCl_3 was added and the organic phase was washed one time with saturated NH_4Cl solution and two times with distilled water, dried over Na_2SO_4 and filtered. The solvent was removed and the crude

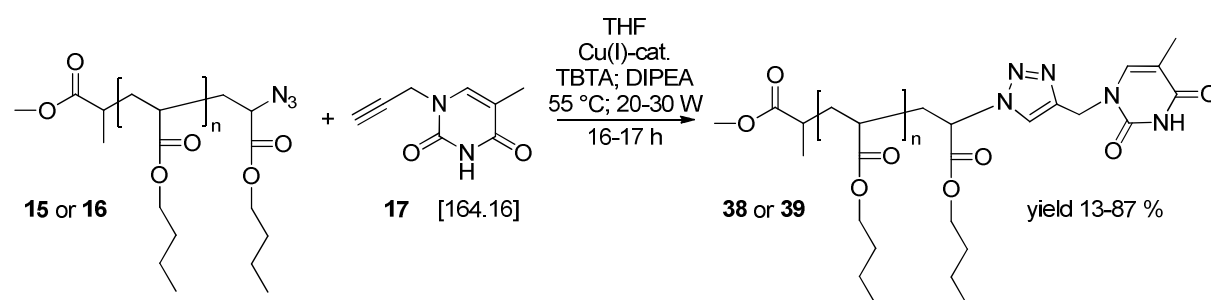
5. Experimental Part

product was purified via column chromatography (SiO₂). For purification via column chromatography of pyrene-functionalized PIB **36**, the residue was dissolved in a small amount of *n*-hexane. Non-functionalized PIB chains were separated by column chromatography using *n*-hexane ($R_f(\mathbf{36}) = 0$; $R_f(\mathbf{11c}) = 1$). After several fractions the solvent was changed to CHCl₃ and PIB **36** was eluted ($R_f(\mathbf{36}) = 1$). The solvent was removed in vacuum. Finally, the polymer was dissolved in a small amount of *n*-hexane, precipitated into 10-fold excess of methanol:acetone (v:v = 1:1) and dried in high vacuum to yield **36** (180 mg; 48 %) as a clear, slightly green glimmering liquid.

$M_n(\text{GPC}) = 8400 \text{ g/mol}$; $M_n(\text{NMR}) = 10400 \text{ g/mol}$; PDI = 1.3

¹H-NMR (400 MHz, CHCl₃): δ 8.70 (d, 2H, H₂₇, ³J_{H,H} = 9.3 Hz), 8.28-7.96 (m, 9H, H_{18,21-26,28,29}), 4.80 (t, 2H, H₁₇, ³J_{H,H} = 7.3 Hz), 1.42 (bs, n·2H, H₆), 1.11 (bs, n·6H, H₈), 0.99 (s, 15H, H₁₊₅).

5.4.10. Thymine-functionalized PnBAs (PnBA-THY)



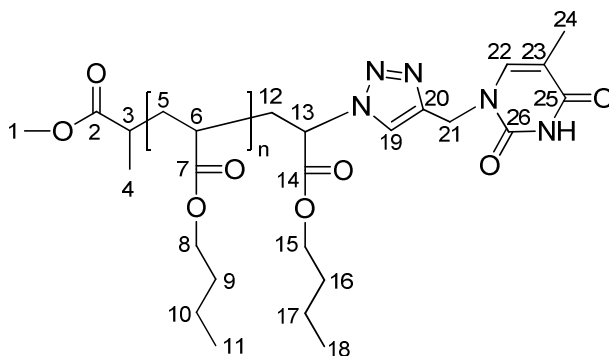
In a Schlenk flask azide-functionalized PnBA (**15** or **16**) was dissolved in THF. DIPEA, TBTA and propargylthymine (**17**) were added. Three freeze-pump-thaw-cycles were performed and the solution was allowed to reach room temperature. The Cu^I-catalyst was added and the solution was stirred for 10 min at room temperature. Then, the flask was placed in the microwave and irradiation was started. After the reaction was complete the mixture was passed through a short Al₂O₃-column (neutral), the solvent was removed in vacuum and CHCl₃ was added. The organic phase was washed one time with saturated NH₄Cl-solution, two times with distilled water, dried over Na₂SO₄ and filtered. Chloroform was removed in vacuum and the crude product was purified by column chromatography (SiO₂; see **Table 23**), whereby the unreacted and/or incomplete functionalized chains were eluted first, before changing the solvent to a more polar mixture to elute the desired THY-functionalized product. Finally, the polymer was dried in vacuum to yield thymine-functionalized PnBA as a clear, almost colorless viscous liquid. For experimental details see **Table 37** (appendix).

5. Experimental Part

Table 23. Details for column chromatography of THY-functionalized PnBAs.

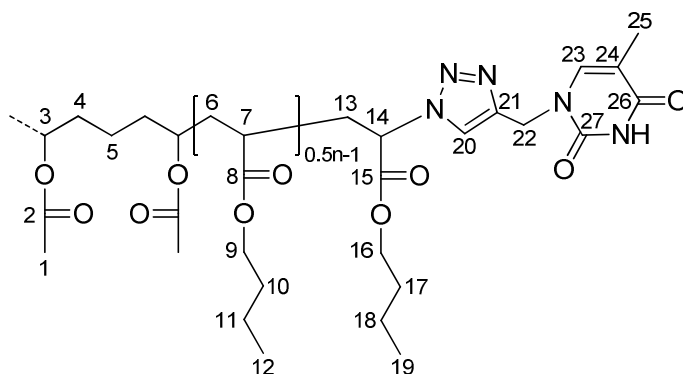
entry	PnBA	start	R _F (prod.)	R _F (educt)	R _F (mono) ^a	change to	R _F (prod.)
1	38a	CHCl ₃	0.08	?	–	CHCl ₃ /MeOH = 100/1	0.19
2	38b-d	CHCl ₃ /Hex/THF 5/5/0.1	0.16	0.25	–	–	–
3	39a	CHCl ₃ /THF 100/3	0.06	0.77	0.19	CHCl ₃ /MeOH = 100/2	0.23
4	39b	CHCl ₃ /THF 100/3	0.06	0.77	0.19	CHCl ₃ /MeOH = 100/1.4	0.18

^a R_F-value of the monofunctionalized side-product.



¹H-NMR (400 MHz, CDCl₃): δ 7.83 (s, 1H, H₁₉), 7.25 (s, 1H, H₂₂), 5.28 (m, 1H, H₁₃), 4.89 (m, 2H, H₂₁), 4.07 (t, 2H, H₁₅, ³J_{H,H} = 6.6 Hz), 3.98 (m, n·2H, H₈), 3.59 (s, 3H, H₁), 2.43 (t, 1H, H₃, ³J_{H,H} = 7.1 Hz), 2.22 (m, n·1H, H₆), 1.85-1.29 (m, n·6H, H_{5,9,10,12,16,17,24}), 1.83 (s, H₂₄), 1.06 (m, 3H, H₄), 0.87 (t, n·3H, H_{11,18}, ³J_{H,H} = 7.3 Hz).

¹³C-NMR (100 MHz, CDCl₃): δ 176.2 (C₂), 175.0-172.7 (C₇), 167.9 (C₁₄), 163.6 (C₂₅), 150.4 (C₂₆), 149.9 (C₂₀), 140.0 (C₂₂), 123.5 (C₁₉), 111.0 (C₂₃), 66.3 (C₁₅), 65.0-64.3 (C₈), 61.0 (C₁₃), 51.5 (C₁), 42.6 (C₂₁), 41.4 (C₆), 37.3 (C₃), 36.3-34.4 (C_{9,16}), 31.7 (C₁₂), 30.6-30.2 (C₅), 19.0-17.6 (C_{10,17}), 16.7 (C₄), 13.7-13.5 (C_{11,18}), 12.2 (C₂₄).



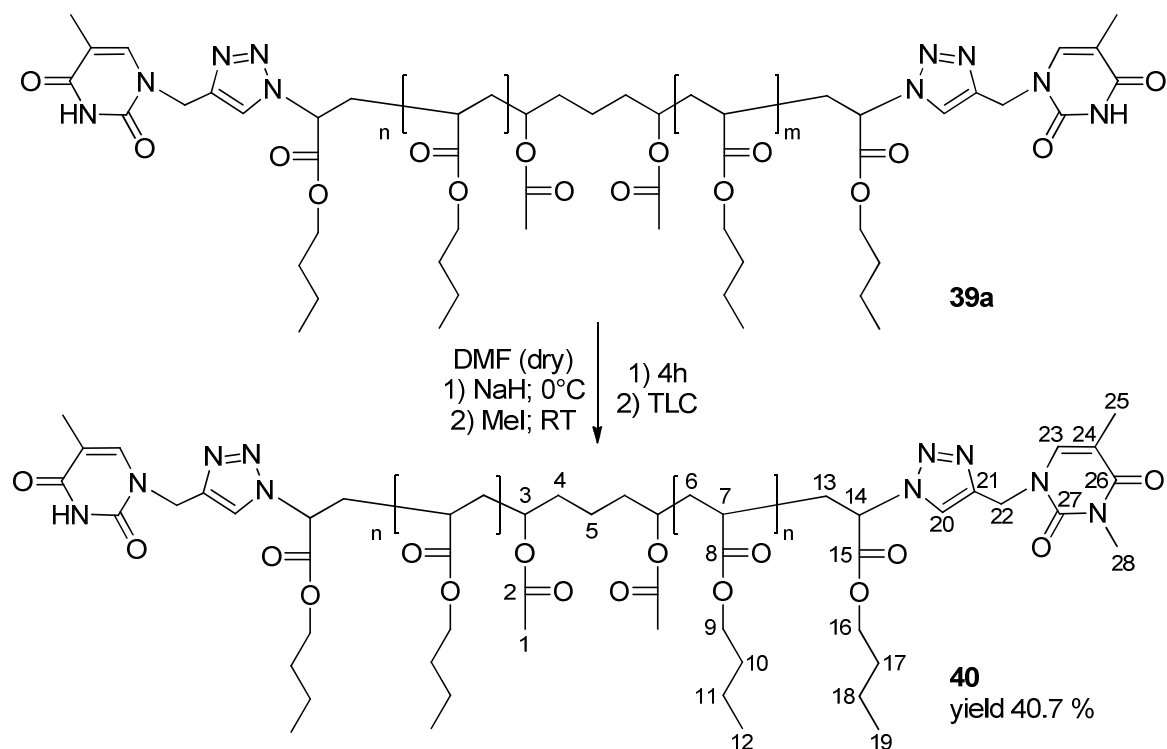
¹H-NMR (400 MHz, CDCl₃): δ 7.83 (s, 2H, H₂₀), 7.31 (s, 2H, H₂₃), 5.34 (m, 2H, H₁₄), 4.95 (s, 4H, H₂₂), 4.13 (t, 4H, H₁₆, ³J_{H,H} = 6.7 Hz), 4.03 (m, n·2H, H_{3,9}), 3.62 (s, 6H, H₁),

5. Experimental Part

2.27 (m, n·1H, H₇), 1.93-1.28 (m, n·6H, H_{4-6,10,11,13,17,18}), 1.88 (s, H₂₅),
0.92 (t, n·3H, H_{12,19}, ³J_{H,H} = 7.3 Hz).

¹³C-NMR (100 MHz, CDCl₃): δ 175.5 (C₂), 174.5 (C₈), 167.9 (C₁₅), 163.8 (C₂₆), 150.6 (C₂₇),
142.0 (C₂₁), 140.0 (C₂₃), 123.4 (C₂₀), 111.0 (C₂₄), 77.2 (C₃), 66.3 (C₁₆), 64.9-64.4 (C₉),
61.1 (C₁₄), 51.4 (C₁), 42.6 (C₂₂), 41.4 (C₇), 36.4-34.1 (C_{4,10,17}), 33.2 (C₁₃), 30.6-30.2 (C₆),
23.4 (C₅), 19.1-18.8 (C_{11,18}), 13.7-13.5 (C_{12,19}), 12.2 (C₂₅).

5.4.11. “Capped” thymine-functionalized PnBAs (PnBA-THY-Cap)



The Synthesis was done under a dry atmosphere of argon. All glassware was heated under vacuum and flushed with argon several times before chemicals were weighed in. In a one-neck round-bottom flask (10 ml), equipped with magnetic stir bar and rubber septum, mineral oil free NaH (0.63 mmol; 25.2 mg (60 wt% dispersion in mineral oil)) was added. A solution of **39a** (0.063 mmol; 290 mg) dissolved in dry DMF (5 ml) was added under ice cooling. The resulting solution was stirred at 0 °C for 4 h. Iodomethane (0.38 mmol, 23.5 μl) was added and the solution was stirred at room temperature for 12 h. Water (30 ml) was added, the aqueous phase was washed two times with chloroform and the organic layers were combined. The combined organic phases were washed four times with distilled water, dried over Na₂SO₄ and filtered. Column chromatography was performed using a CHCl₃/EA (100:6) solvent mixture. After several fractions the solvent mixture was changed to CHCl₃/MeOH (100:1) and PnBA **40** was eluted. Upon removal of the solvent by means of a rotary evaporator 118 mg (40.7 %) of **40** was obtained as a clear, pale yellow liquid.

5. Experimental Part

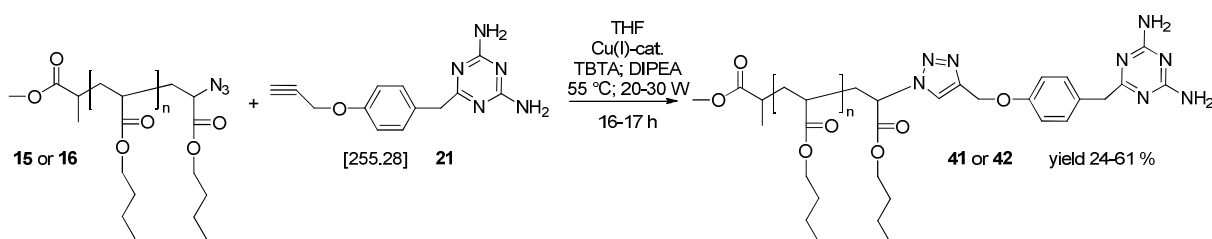
Table 24. Details for column chromatography of “capped” THY-functionalized PnBA **40**.

entry	PnBA	solvent	R _F (prod.)	R _F (educt)
1	40	CHCl ₃ /EA = 100/6	<0.1	<0.1
2	40	CHCl ₃ /MeOH = 100/1	0.56	0.31

¹H-NMR (500 MHz, CDCl₃): δ 7.82 (s, 2H, H₂₀), 7.31 (s, 2H, H₂₃), 5.35 (m, 2H, H₁₄), 4.98 (s, 4H, H₂₂), 4.03 (m, n·2H, H_{3,9,16}), 3.63 (s, 6H, H₁), 3.34 (s, 6H, H₂₈), 2.28 (m, n·1H, H₇), 1.91-1.35 (m, n·6H, H_{4-6,10,11,13,17,18}), 1.91 (s, H₂₅), 0.93 (t, n·3H, H_{12,19}, ³J_{H,H} = 7.3 Hz).

¹³C-NMR (125 MHz, CDCl₃): δ 175.5 (C₂), 174.5 (C₈), 168.5 (C₁₅), 163.9 (C₂₆), 151.5 (C₂₇), 142.4 (C₂₁), 137.9 (C₂₃), 123.1 (C₂₀), 110.1 (C₂₄), 77.2 (C₃), 65.0 (C₁₆), 64.4 (C₉), 60.9 (C₁₄), 51.4 (C₁), 43.6 (C₂₂), 41.4 (C₇), 36.4-34.3 (C_{4,10,17}), 33.1 (C₁₃), 30.6-30.5 (C₆), 28.0 (C₂₈), 24.9 (C₅), 19.1 (C_{11,18}), 13.7 (C_{12,19}), 13.0 (C₂₅).

5.4.12. 2,6-Diaminotriazine-functionalized PnBAs (PnBA-DAT)



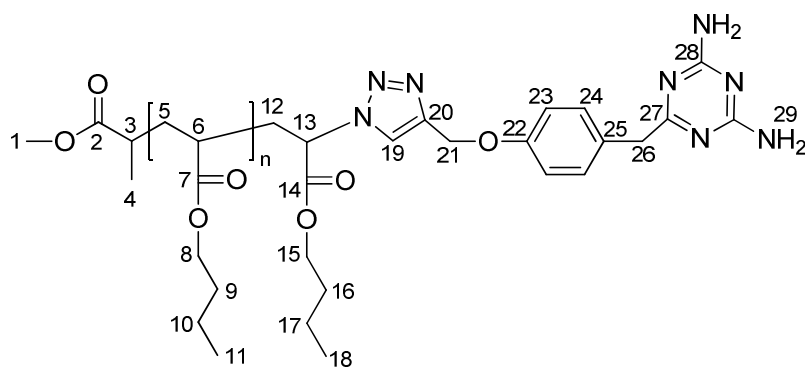
In a Schlenk flask azide-functionalized PnBA (**15** or **16**) was dissolved in THF. DIPEA, TBTA and alkyne **21** were added. Three freeze-pump-thaw-cycles were performed and the solution was allowed to reach room temperature. The Cu^I-catalyst was added and the solution was stirred for 10 min at room temperature. Then, the flask was placed in the microwave and irradiation was started. After the reaction was complete the mixture was passed through a short Al₂O₃-column (neutral), the solvent was removed and CHCl₃ was added. The organic phase was washed one time with saturated NH₄Cl-solution, two times with distilled water, dried over Na₂SO₄ and filtered. Chloroform was removed in vacuum and the crude product was purified via column chromatography (SiO₂; see **Table 25**), whereby the unreacted and/or incomplete functionalized chains were eluted first, before changing the solvent to a more polar mixture to elute the desired DAT-functionalized product. Finally, the polymer was dried in vacuum to yield DAT-functionalized PnBA as a clear, slightly yellow-orange viscous liquid. For experimental details see **Table 38** (appendix).

5. Experimental Part

Table 25. Details for column chromatography of DAT-functionalized PnBAs.

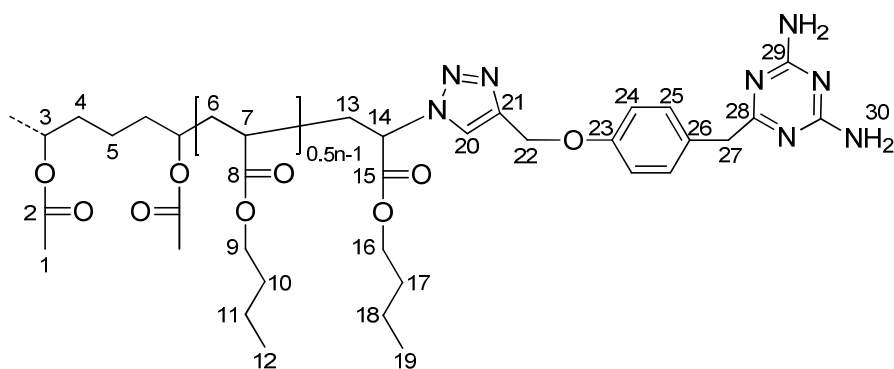
entry	PnBA	start	R _F (prod.)	R _F (educt)	R _F (mono) ^a	change to	R _F (prod.)
1	41a	CHCl ₃ /MeOH = 100/4	0.35	1	–	–	–
2	41b	CHCl ₃ /THF/Hex = 1/1/0.02	0	0.2	–	CHCl ₃ /THF = 100/2	0.14
3	41b	CHCl ₃ /THF = 100/3	0.28	0.8	–	–	–
4	42a	CHCl ₃ /THF = 100/3	0.1	>0.9	0.26	–	–
5	42b	CHCl ₃ /EA/MeOH 100/10/0.1	0.13	>0.9	>0.13	–	–
6	42b	CHCl ₃ /MeOH = 100/0.6	0.14	>0.9	0.2	–	–

^a R_F-value of the monofunctionalized side-product.



¹H-NMR (400 MHz, CDCl₃): δ 7.78 (s, H₁₉), 7.21 (d, 2H, H₂₄, ³J_{H,H} = 8.0 Hz), 6.89 (d, 2H, H₂₃, ³J_{H,H} = 8.3 Hz), 5.34 (bs, 4H, H₂₉), 5.15 (s, 2H, H₂₁), 4.11 (m, 2H, H₁₅), 4.02 (bs, n·2H, H_{8,13}), 3.71 (s, 2H, H₂₆), 3.63 (s, 3H, H₁), 2.51 (m, 1H, H₃), 2.27 (bs, n·1H, H₆), 1.90-1.26 (m, n·6H, H_{5,9,10,12,16,17}), 1.11 (m, 3H, H₄), 0.91 (t, n·3H, H_{11,18}, ³J_{H,H} = 7.4 Hz).

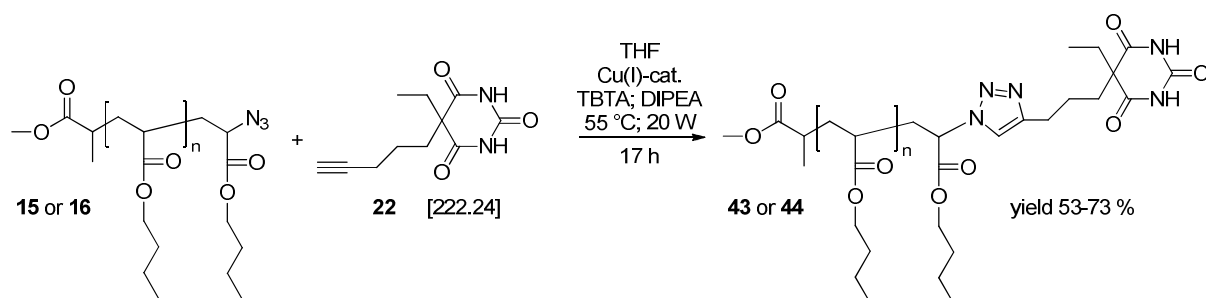
¹³C-NMR (100 MHz, CDCl₃): δ 177.9 (C₂₇), 176.2 (C₂), 174.5 (C₇), 168.1 (C₁₄), 167.2 (C₂₈), 157.1 (C₂₂), 144.5 (C₂₀), 130.2 (C₂₄), 129.9 (C₂₅), 122.5 (C₁₉), 114.7 (C₂₃), 77.2 (C₂₁), 66.2 (C₁₅), 65.0-64.3 (C₈), 62.1 (C₁₃), 51.6 (C₁), 44.1 (C₂₆), 41.4 (C₆), 37.3 (C₃), 34.5 (C_{9,16}), 31.2 (C₁₂), 30.6-30.2 (C₅), 19.0-18.6 (C_{10,17}), 16.7 (C₄), 13.7-13.5 (C_{11,18}).



$^1\text{H-NMR}$ (400 MHz, CDCl_3): δ 7.79 (m, 2H, H_{20}), 7.23 (d, 4H, H_{25} , $^3J_{\text{H,H}} = 7.2$ Hz), 6.92 (d, 4H, H_{24} , $^3J_{\text{H,H}} = 6.9$ Hz), 5.25 (bs, 8H, H_{30}), 5.16 (s, 4H, H_{22}), 4.13 (m, 4H, H_{16}), 4.03 (bs, $n \cdot 2\text{H}$, $\text{H}_{3,9,14}$), 3.74 (s, 4H, H_{27}), 3.63 (s, 6H, H_1), 2.28 (bs, $n \cdot 1\text{H}$, H_7), 1.91-1.25 (m, $n \cdot 6\text{H}$, $\text{H}_{4-6,10,11,13,17,18}$), 0.93 (t, $n \cdot 3\text{H}$, H_{12} , $^3J_{\text{H,H}} = 7.3$ Hz), 0.88 (t, 8H, H_{19}).

$^{13}\text{C-NMR}$ (100 MHz, CDCl_3): δ 178.0 (C_{28}), 175.5 (C_2), 174.6 (C_8), 168.3 (C_{15}), 167.2 (C_{29}), 157.2 (C_{23}), 144.4 (C_{21}), 130.2 (C_{25}), 129.9 (C_{26}), 122.4 (C_{20}), 114.9 (C_{24}), 77.2 ($\text{C}_{3,21}$), 66.2 (C_{16}), 64.4 (C_9), 62.2 (C_{14}), 51.4 (C_1), 44.2 (C_{27}), 41.4 (C_7), 36.3-35.4 ($\text{C}_{4,10,17}$), 31.2 (C_{13}), 30.6-30.3 (C_6), 22.6 (C_5), 19.1-18.9 ($\text{C}_{11,18}$), 13.7 (C_{12}), 13.5 (C_{19}).

5.4.13. Barbituric acid-functionalized PnBAs (PnBA-BA)



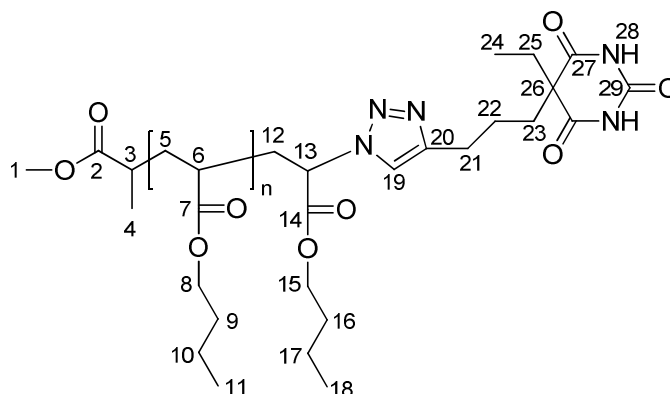
In a Schlenk flask azide-functionalized PnBA (**15** or **16**) was dissolved in THF. DIPEA, TBTA and alkyne **22** were added. Three freeze-pump-thaw-cycles were performed and the solution was allowed to reach room temperature. Then, the Cu^{I} -catalyst was added and the solution was stirred for 10 min at room temperature. The flask was placed in the microwave and irradiation was started. After the reaction was complete the solvent was removed and CHCl_3 was added. The organic phase was washed one time with saturated NH_4Cl -solution, two times with distilled water, dried over Na_2SO_4 and filtered. Chloroform was removed and the crude product was purified via column chromatography (SiO_2 ; see **Table 26**). Finally, the polymer was dried in vacuum to yield BA-functionalized PnBA as a clear, slightly yellow viscous liquid. For experimental details see **Table 39** (appendix).

5. Experimental Part

Table 26. Details for column chromatography of BA-functionalized PnBAs.

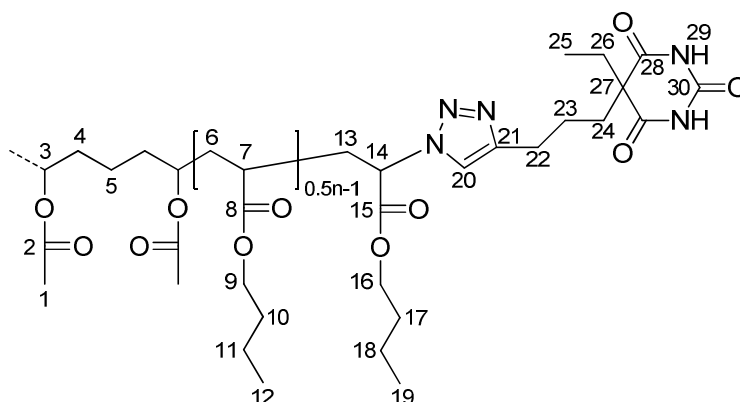
entry	PnBA	solvent mixture	R _F (prod.)	R _F (educt)	R _F (mono) ^a
1	43a	CHCl ₃ /MeOH = 100/1	0.26	>0.9	–
2	43b	CHCl ₃ /MeOH = 100/1	0.22	>0.9	–
3	44a	CHCl ₃ /MeOH = 100/2	0.15	>0.9	0.25

^a R_F-value of the monofunctionalized side-product.



¹H-NMR (500 MHz, CDCl₃): δ 8.64 (m, 2H, H₂₈), 7.47 (m, 1H, H₁₉), 5.32 (m, 1H, H₁₃), 4.12 (t, 2H, H₁₅, ³J_{H,H} = 6.6 Hz), 4.02 (m, n·2H, H₈), 3.64 (s, 3H, H₁), 2.67 (m, 2H, H₂₁), 2.27 (m, n·1H, H_{3,6}), 2.05-1.34 (m, n·6H, H_{5,9,10,12,16,17,23,25}), 1.24 (m, 2H, H₂₂), 1.11 (m, 3H, H₄), 0.92 (t, n·3H, H_{11,18}, ³J_{H,H} = 7.3 Hz), 0.87 (t, 3H, H₂₄).

¹³C-NMR (125 MHz, CDCl₃): δ 176.2 (C₂), 174.5-173.6 (C₇), 172.0 (C₂₇), 168.3 (C₁₄), 148.1 (C₂₉), 146.8 (C₂₀), 119.9 (C₁₉), 66.1 (C₁₅), 64.5-64.3 (C₈), 60.7 (C₁₃), 56.9 (C₂₆), 51.5 (C₁), 41.4 (C₆), 37.4 (C₃), 36.6-34.4 (C_{9,16}), 32.5 (C₂₃), 31.8 (C_{12,22}), 30.6 (C₅), 25.4 (C₂₁), 24.6 (C₂₅), 19.0 (C_{10,17}), 16.7 (C₄), 13.7-13.5 (C_{11,18}), 9.3 (C₂₄).

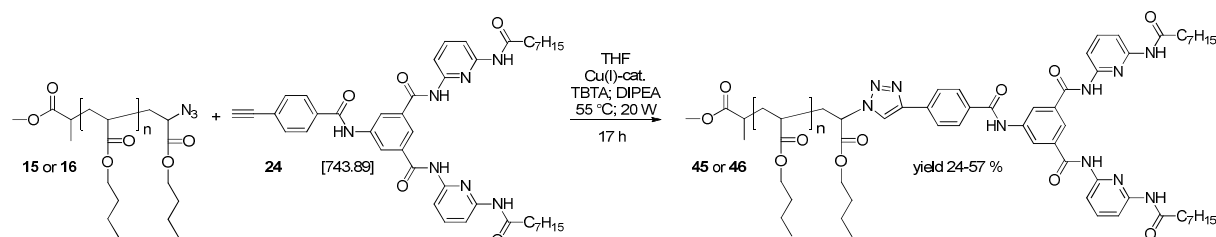


¹H-NMR (400 MHz, CDCl₃): δ 8.89 (m, 4H, H₂₉), 7.44 (m, 2H, H₂₀), 5.31 (m, 2H, H₁₄), 4.11 (m, 4H, H₁₆), 4.00 (m, n·2H, H_{3,9}), 3.61 (s, 6H, H₁), 2.66 (m, 4H, H₂₂), 2.26 (m, n·1H, H₇), 2.01-1.34 (m, n·6H, H_{4-6,10,11,13,17,18,24,26}), 1.22 (m, 4H, H₂₃), 0.90 (t, n·3H, H_{12,19}, ³J_{H,H} = 7.3 Hz), 0.87 (t, 6H, H₂₅).

5. Experimental Part

^{13}C -NMR (100 MHz, CDCl_3): δ 175.4 (C_2), 174.5-173.6 (C_8), 172.2 (C_{28}), 168.4 (C_{15}), 148.4 (C_{30}), 146.8 (C_{21}), 120.3 (C_{20}), 77.2 (C_3), 66.1 (C_{16}), 64.9-64.3 (C_9), 60.7 (C_{14}), 56.9 (C_{27}), 51.3 (C_1), 41.4 (C_7), 37.6-34.1 ($\text{C}_{4,10,17}$), 32.4 (C_{24}), 31.6 ($\text{C}_{13,23}$), 30.6 (C_6), 25.4 (C_{22}), 24.6 (C_{26}), 20.9 (C_5), 19.0-18.8 ($\text{C}_{11,18}$), 13.6-13.5 ($\text{C}_{11,19}$), 9.3 (C_{25}).

5.4.14. Hamilton wedge-functionalized PnBAs (PnBA-HW)



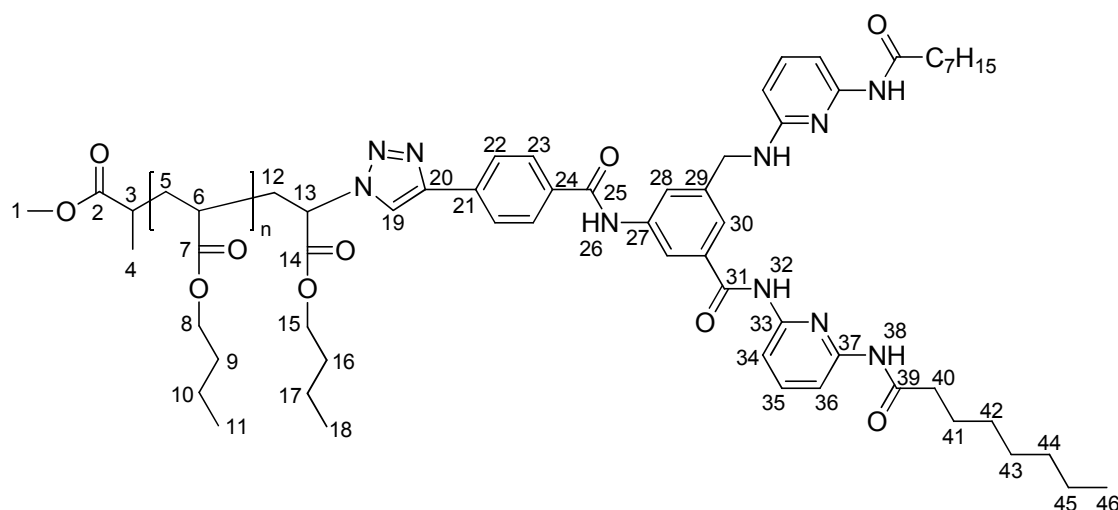
In a Schlenk flask azide-functionalized PnBA (**15** or **16**) was dissolved in THF. DIPEA, TBTA and alkyne **24** were added. Three freeze-pump-thaw-cycles were performed and the solution was allowed to reach room temperature. The Cu^{I} -catalyst was added and the solution was stirred for 10 min at room temperature. Then, the flask was placed in the microwave and irradiation was started. After the reaction was complete the mixture was passed through a short Al_2O_3 -column (neutral), the solvent was removed and CHCl_3 was added. The organic phase was washed one time with saturated NH_4Cl -solution, two times with distilled water, dried over Na_2SO_4 and filtered. Chloroform was removed in vacuum and the crude product was purified via column chromatography (SiO_2 ; see **Table 27**), whereby the unreacted and/or incomplete functionalized chains were eluted first, before changing the solvent to a more polar mixture to elute the desired HW-functionalized product. Finally, the polymer was dried in vacuum to yield HW-functionalized PnBA as a clear, slightly yellow-orange viscous liquid. For experimental details see **Table 40** (appendix).

Table 27. Details for column chromatography of HW-functionalized PnBAs.

entry	PnBA	start	R_{F} (prod.)	R_{F} (educt)	R_{F} (mono) ^a	change to	R_{F} (prod.)
1	45a	$\text{CHCl}_3/\text{MeOH} = 100/1$	0.27	>0.9	–	–	–
2	46a	$\text{CHCl}_3/\text{MeOH}/\text{THF} = 100/1/1$	0.15	>0.9	0.27	$\text{CHCl}_3/\text{MeOH} = 100/2$	0.24
3	45b	$\text{CHCl}_3/\text{EA} = 10/1$	0.27	>0.9	–	–	–

^a R_{F} -value of the monofunctionalized side-product.

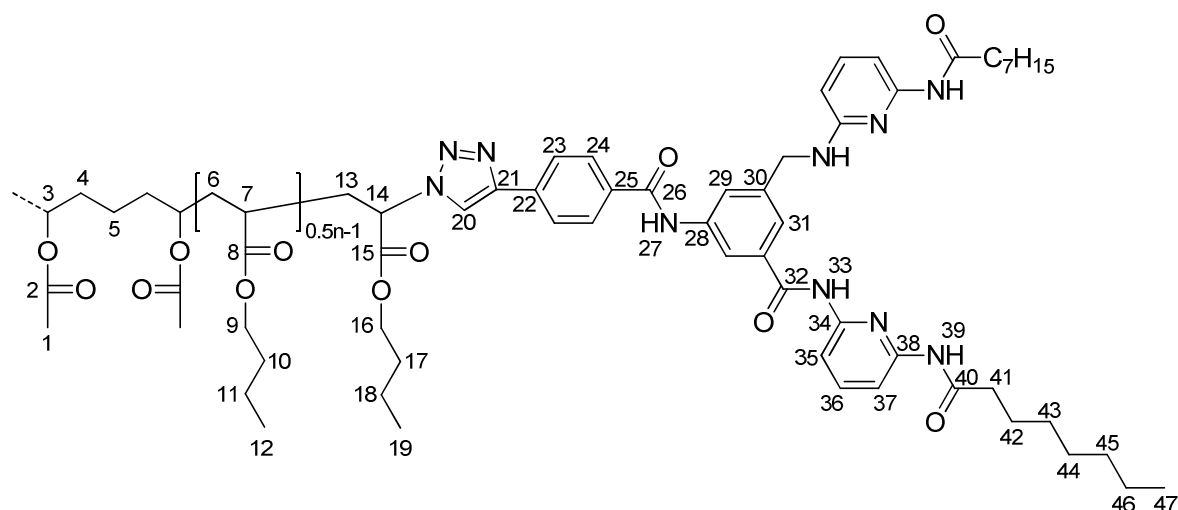
5. Experimental Part



$^1\text{H-NMR}$ (500 MHz, CDCl_3): δ 9.06 (s, 1H, H_{26}), 8.62 (m, 4H, $\text{H}_{28,32}$), 8.43 (s, 2H, H_{38}), 8.12 (m, 6H, H_{34-36}), 7.94 (m, 4H, $\text{H}_{19,23,30}$), 7.69 (m, 2H, H_{22}), 5.49 (m, 1H, H_{13}), 4.17 (t, 2H, H_{15}), 4.02 (m, n·2H, H_8), 3.64 (s, 3H, H_1), 2.54 (bs, 5H, $\text{H}_{3,40}$), 2.26 (m, n·1H, H_6), 1.89-1.12 (m, n·6H, $\text{H}_{5,9,10,12,16,17,41-45}$), 1.04 (m, 3H, H_4), 0.92 (t, n·3H, H_{11} , $^3J_{\text{H,H}} = 7.3$ Hz), 0.79 (t, 5H, H_{46}).

$^{13}\text{C-NMR}$ (125 MHz, CDCl_3): δ 176.3 (C_2), 174.5 (C_7), 172.7 (C_{39}), 171.1 (C_{14}), 166.3 (C_{25}), 163.6 (C_{31}), 150.1 (C_{33}), 149.0 (C_{37}), 147.4 (C_{20}), 140.6 ($\text{C}_{27,35}$), 135.3 (C_{29}), 134.8 (C_{24}), 133.0 (C_{22}), 128.0 (C_{23}), 126.1 (C_{21}), 122.0 (C_{28}), 121.9 (C_{30}), 120.5 (C_{19}), 109.3 (C_{34}), 107.9 (C_{36}), 66.5 (C_{15}), 64.4 (C_8), 60.4 (C_{13}), 51.5 (C_1), 41.4 (C_6), 37.6 (C_{40}), 37.3 (C_3), 36.3-34.4 ($\text{C}_{9,16}$), 31.7 (C_{12}), 30.6 ($\text{C}_{5,14}$), 29.2 (C_{42}), 29.1 (C_{43}), 25.5 (C_{41}), 22.6 (C_{45}), 19.1 ($\text{C}_{10,17}$), 17.7 (C_4), 14.0 (C_{46}), 13.7 ($\text{C}_{11,18}$).

5. Experimental Part



$^1\text{H-NMR}$ (400 MHz, CDCl_3): δ 9.29 (s, 2H, H_{27}), 8.95 (s, 4H, H_{33}), 8.57-8.41 (m, 8H, $\text{H}_{29,39}$), 8.09-7.86 (m, 20H, $\text{H}_{20,24,31,35-37}$), 7.62 (s, 4H, H_{23}), 5.45 (s, 2H, H_{14}), 4.17 (t, 4H, H_{16} , $^3J_{\text{H,H}} = 6.2$ Hz), 4.02 (bs, $n \cdot 2\text{H}$, $\text{H}_{3,9}$), 3.62 (s, 6H, H_1), 2.56 (s, 8H, H_{41}), 2.27 (m, $n \cdot 1\text{H}$, H_7), 1.90-1.26 (m, $n \cdot 6\text{H}$, $\text{H}_{4-6,10,11,13,17,18,42-46}$), 0.92 (t, $n \cdot 3\text{H}$, $\text{H}_{12,19}$, $^3J_{\text{H,H}} = 7.6$ Hz), 0.84 (t, 12H, H_{47}).

$^{13}\text{C-NMR}$ (100 MHz, CDCl_3): δ 175.4 (C_2), 174.6 (C_8), 173.1 (C_{40}), 168.2 (C_{15}), 166.4 (C_{32}), 163.8 (C_{26}), 150.2 (C_{34}), 148.9 (C_{38}), 146.3 (C_{21}), 140.6 (C_{36}), 139.3 (C_{28}), 135.1 (C_{30}), 134.7 (C_{25}), 132.9 (C_{23}), 132.4 (C_{24}), 128.1 (C_{22}), 126.0 (C_{29}), 122.0 (C_{31}), 120.8 (C_{20}), 110.5 (C_{35}), 109.5 (C_{37}), 77.2 (C_3), 66.5 (C_{16}), 64.4 (C_9), 61.0 (C_{14}), 51.5 (C_1), 41.5 (C_7), 37.5 (C_{41}), 36.1-34.2 ($\text{C}_{4,10,17}$), 31.7 ($\text{C}_{13,45}$), 30.6 (C_6), 29.2 (C_{43}), 29.1 (C_{44}), 25.5 (C_{42}), 22.6 ($\text{C}_{5,46}$), 19.1 ($\text{C}_{11,18}$), 14.0 (C_{47}), 13.7 ($\text{C}_{12,19}$).

6.1. Summary

The aim of this work was to gain a deeper understanding of the dynamics of association or aggregation of hydrogen bonds in the solvent-free melt state of amorphous polymers. Therefore, as a starting point for various investigations on the association/aggregation behavior of hydrogen bonding moieties in solution and in the melt state, poly(isobutylene)s (PIBs) and poly(*n*-butyl acrylate)s (PnBAs) were prepared. All synthesized polymers were obtained with small polydispersities and with the projected calculated molecular weights highlighting the living character of the corresponding polymerization method.

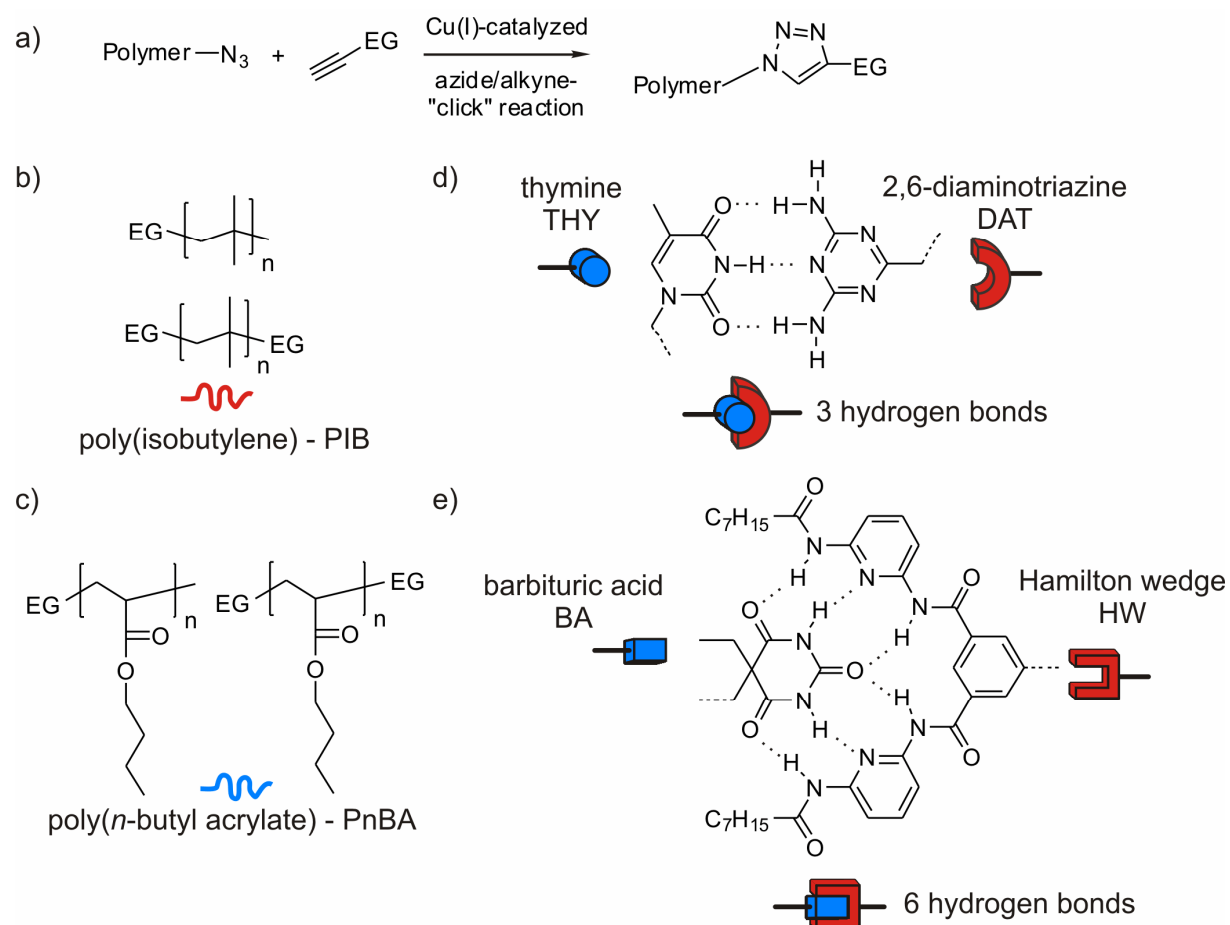


Figure 58. a) Azide/alkyne-“click” reactions were applied to attach alkyne functionalized hydrogen bonding end groups (EG) onto the azide functionalized polymers b) poly(isobutylene) (PIB) and c) poly(*n*-butyl acrylate) (PnBA) attaching d) the THY-DAT motif and e) the BA-HW motif.





Mono- and bifunctional polymers with molecular weights ranging from 3000 up to 30000 g/mol (22000 g/mol for PnBA) were successfully prepared via either living carbocationic polymerization (LCCP) or atom transfer radical polymerization (ATRP). After (multi-step) end group transformation the corresponding azides, PIB-N₃ (**11a-d** + **12a-e**) and

6. Summary and Outlook

PnBA-N₃ (**15a-c** + **16a-b**), were obtained and applied for azide/alkyne-“click” reactions to attach the various hydrogen bonding groups as shown in **Figure 58a**.

Two different motifs were investigated namely the thymine/2,6-diaminotriazine (THY/DAT) and the barbituric acid/Hamilton wedge (BA/HW) system (**Figure 58d+e**) to study the four supramolecular entities with different association strength. Therefore, mono- and bifunctional PIBs and PnBAs (**Figure 58b+c**) with molecular weights of 3000 up to 30000 g/mol (22000 g/mol for PnBA), bearing the THY-, DAT-, BA- and HW-group (and others) were synthesized (see **Table 28**) and fully characterized via ¹H-NMR, ¹³C-NMR and MALDI-TOF-MS measurements, evidencing the complete functionalization with the corresponding functional group.

Table 28. Overview on the supramolecular polymers bearing different hydrogen bonding motifs.

	 THY	 DAT	 BA	 HW
monofunctional PIBs	26a-c	28a-f	31a-d	34a-d
bifunctional PIBs	27a	29a	32a-e	35a-b
monofunctional PnBAs	38a-d	41a-c	43a-b	45a-b
bifunctional PnBAs	39a-b	42a-b	44a	46a

In a second step the synthesized library of supramolecular polymers was used to investigate the association/aggregation behavior of the hydrogen bonding groups in the polymer melt with respect to their molecular weight, the polarity of the surrounding matrix (PIB vs. PnBA), the strength of the hydrogen bonding motif (THY/DAT vs. BA/HW) and the number of supramolecular entities within the polymer (mono- vs. bifunctional). In A first step, association/aggregation of the hydrogen bonding moieties was studied in solution via NMR-titration experiments, followed by oscillatory rheology experiments and small-angle X-ray scattering (SAXS) in the melt state. In solution the order of association for the THY/DAT system was found to obey the following series: DAT-DAT ($K_{\text{dim.}} = 1.65 \pm 0.58 \text{ M}^{-1}$) \leq THY-THY ($K_{\text{dim.}} = 3.8 \pm 0.49 \text{ M}^{-1}$) \ll THY-DAT ($K_{\text{assn.}} = 1087 \pm 142 \text{ M}^{-1}$) for monofunctional PIBs in agreement with the existing literature for low molecular weight compounds (values measured in CDCl₃).

However, the association behavior in the melt state was found to be strikingly different. In PIB the THY and DAT groups form supramolecular thermo-reversible aggregates (“clusters”) within the PIB matrix, causing a huge increase of the viscosity compared to a non-functionalized reference sample (pure PIB of the same molecular weight; **Figure 59a**). In

6. Summary and Outlook

strong contrast to the behavior in solution, PIB-DAT-4k (**28b**) forms a highly ordered body-centered-cubic (BCC) lattice as determined via SAXS measurements (stable up to $> 90\text{ }^{\circ}\text{C}$). For PIB-THY-4k (**26b**) no such microphase separated structure was found although the association in solution is similar to PIB-DAT-4k (**28b**). As evidenced by DSC measurements for none of the supramolecular polymers of the library crystalline domains were found. Additionally, for all polymers time-temperature-superposition (TTS) was possible, further proving the absence of crystalline domains and revealing that the deaggregation of these clusters occurs continuous with increasing temperature and not at a specific temperature.

For a series of PIBs with a molecular weight of 30000 g/mol the formation of aggregates caused an even more drastic increase of the viscosity, since the blank polymer chains were already entangled ($M_n > M_c$).

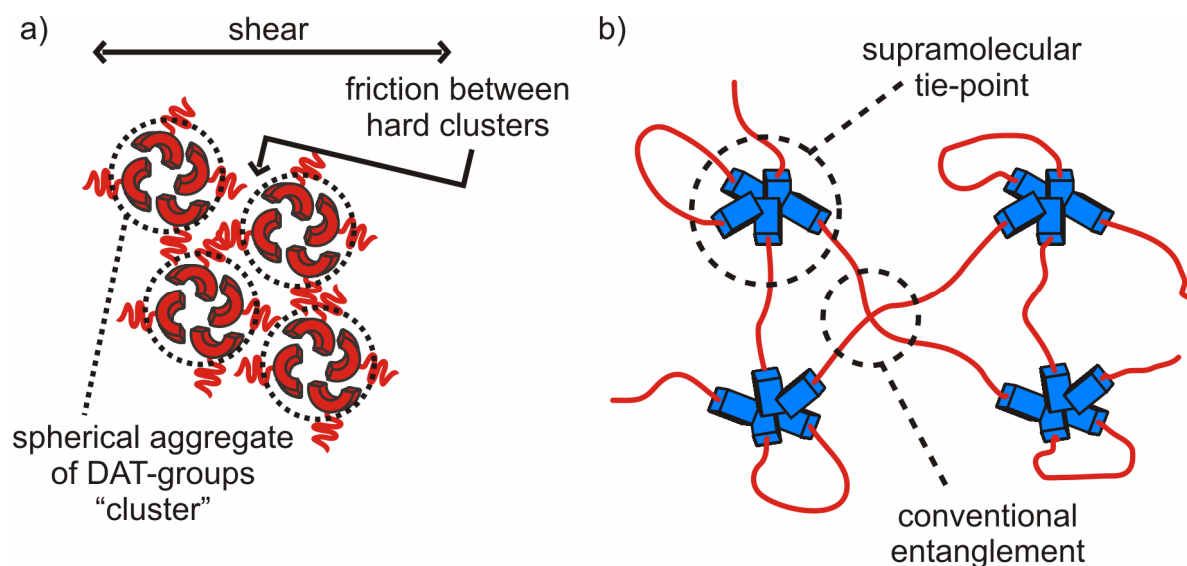


Figure 59. a) Formation of aggregates of DAT groups within the PIB matrix; b) network formation due to aggregation of bifunctional PIBs bearing hydrogen bonding groups – the network consists of supramolecular tie-points and conventional entanglements.

In the case of bifunctional PIBs the (polar) clusters were interconnected via the bifunctional PIB chains transforming the otherwise liquid polymers ($T_g \ll 20\text{ }^{\circ}\text{C}$ and $M_n < M_c$) into strong but brittle rubbers at room temperature (as shown in **Figure 59b** for PIB-BA₂). Upon heating to higher temperatures ($T > \sim 60\text{ }^{\circ}\text{C}$) a deaggregation of the clusters was observed, finally yielding the bifunctional PIBs as low viscous liquids. Therefore, these polymers behave as supramolecular thermoplastic elastomers (supramolecular TPEs). It was found for PIBs with a similar molecular weight that PIB-THY₂-4k (**27a**) reveals a higher plateau than PIB-DAT₂-4k (**29a**). In any case the plateau modulus was higher than for linear high molecular weight PIBs,

6. Summary and Outlook

proving the presence of a dense network formed via the supramolecular aggregates and not via linear chain extension.

For a series of monofunctional PIBs bearing the BA/HW motif microphase segregation of the individual hydrogen bonding group from the nonpolar PIB was detected. Especially the HW group was found to form large temperature stable aggregates. In case of PIB-HW-4k (**34b**) terminal flow was only observed at high temperatures ($T \geq 100$ °C) since otherwise the HW aggregates prevent flow of the PIB. In accordance with results from melt-rheology, these samples again displayed an intense peak in SAXS measurements, proving the formation of aggregates. For PIB-HW-10k (**34c**) a pronounced rubbery plateau was found although the chains were not entangled ($M_n < M_c$) and only monofunctional. Additionally, the bifunctional PIBs bearing the barbituric acid group (PIB-BA₂) (**32a-e**) were obtained as strong rubbers at room temperature. For PIB-BA₂-4k (**32b**) a plateau modulus of 0.44 MPa, higher than for linear high molecular weight PIBs ($G_N^0 = 0.25-0.32$ MPa), was found. Moreover, PIB-BA₂-4k (**32b**) showed a terminal flow zone at very low frequencies with an unexpectedly high viscosity of $20 \cdot 10^6$ Pa·s (93000-times higher in comparison to the unfunctionalized reference PIB-REF₂-4k; **12b**).

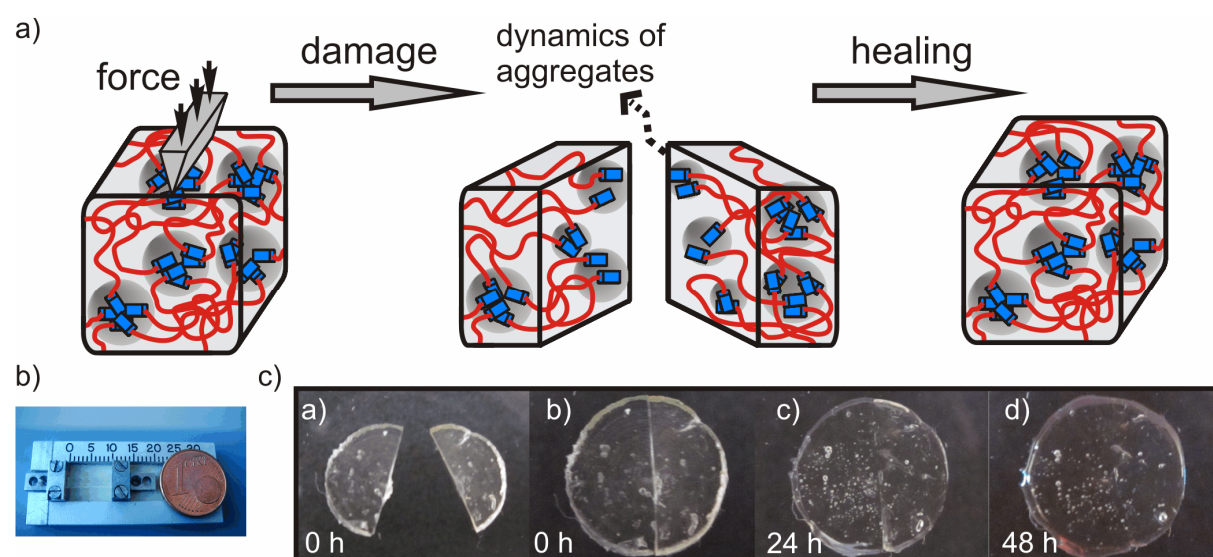


Figure 60. a) Proposed self-healing mechanism of bifunctional PIBs bearing BA groups (PIB-BA₂); b) rectangles used for DMA measurements; c) macroscopic self-healing test of PIB-BA₂-30k (**32e**).

An increase of the molecular weight for PIB-BA₂ did not affect the rheological properties, revealing almost identical rheological behavior (in terms of viscosity, plateau modulus and onset of the terminal flow region). This observation is assigned to the presence of both supramolecular tie-points (aggregates of BA groups) and physical entanglements between chains where both ends were trapped in aggregates (even if $M_n < M_c$) (see **Figure 59b**). The

6. Summary and Outlook

lifetime of the BA clusters as determined via melt-rheology was calculated to be in the range of 1.6 to 2.5 s and thus significantly higher than the bond lifetime of the BA group in solution ($6 \cdot 10^{-3}$ μ s), explaining the stability of shape (**Figure 60**).

All four investigated PIBs-BA₂ reveal a complete recovery of the mechanical properties in stress-strain experiments (up to 50 % strain) after being cut and being brought into contact again for 15 min. As the supramolecular groups remain unassociated (“sticky”) within the fractured surface for a certain period of time (see **Figure 60a+c**) they can reform the supramolecular clusters thus healing the crack. A proof that this self-healing behavior can be attributed to the internal dynamic hydrogen bonding of the BA groups was obtained with a “capped” barbituric acid PIB (PIB-BA₂-Cap; **33a**; devoid of hydrogen bonding), which displayed only liquid properties without any noteworthy elastic portion.

Investigations of the analogues, but in comparison to PIB significantly more polar, PnBAs bearing the THY/DAT system revealed that no cluster formation of the hydrogen bonding groups within the relatively polar PnBA matrix was observed. In comparison to a PnBA-REF₂ (**16a**; unfunctionalized reference PnBA) the huge increase of the viscosity of bifunctional PnBAs bearing either the THY (**39a**) or the DAT (**42a**) groups (or a mixture of both) is mainly caused by an unusual increase of the glass transition temperature. As a result the effect of hydrogen bonding on PnBAs (THY/DAT system) is relatively small. Nevertheless, for high molecular PnBAs ($M_n \approx 25000$ g/mol) a rubbery plateau was found for PnBA-DAT₂-25k (**42b**) and PnBA-(THY/DAT)₂-25k (**42b+39b**) at low temperatures, but not for PnBA-THY₂-25k (**39b**). In contrast to the order of strength in solution (DAT-DAT \leq THY-THY \ll THY-DAT; values see above), the order in the PnBA-melt was found to be THY-THY \ll DAT-DAT \leq THY-DAT. While for PIB complex temperature stable aggregates were observed for PnBA only a weak association was found.

The synthesis of a broad variety of different supramolecular polymers, also in terms of the attached group (THY, DAT, BA and HW) and functionality of the chains (mono- and bifunctional), allowed the combination of two different polymers and, therefore, two different chain dynamics (PIB+PnBA) as well. Thus a mixture of PIB-BA-4k (**31b**) and PnBA-HW-4k (**45b**) was obtained as a macroscopic homogenous liquid with a highly ordered lamellar microstructure (**Figure 61b+d**), opening the possibility to study various combinations of PnBA/PIB polymers to get a deeper insight in the dynamics of hydrogen bonding between two different liquid polymers in the melt state.

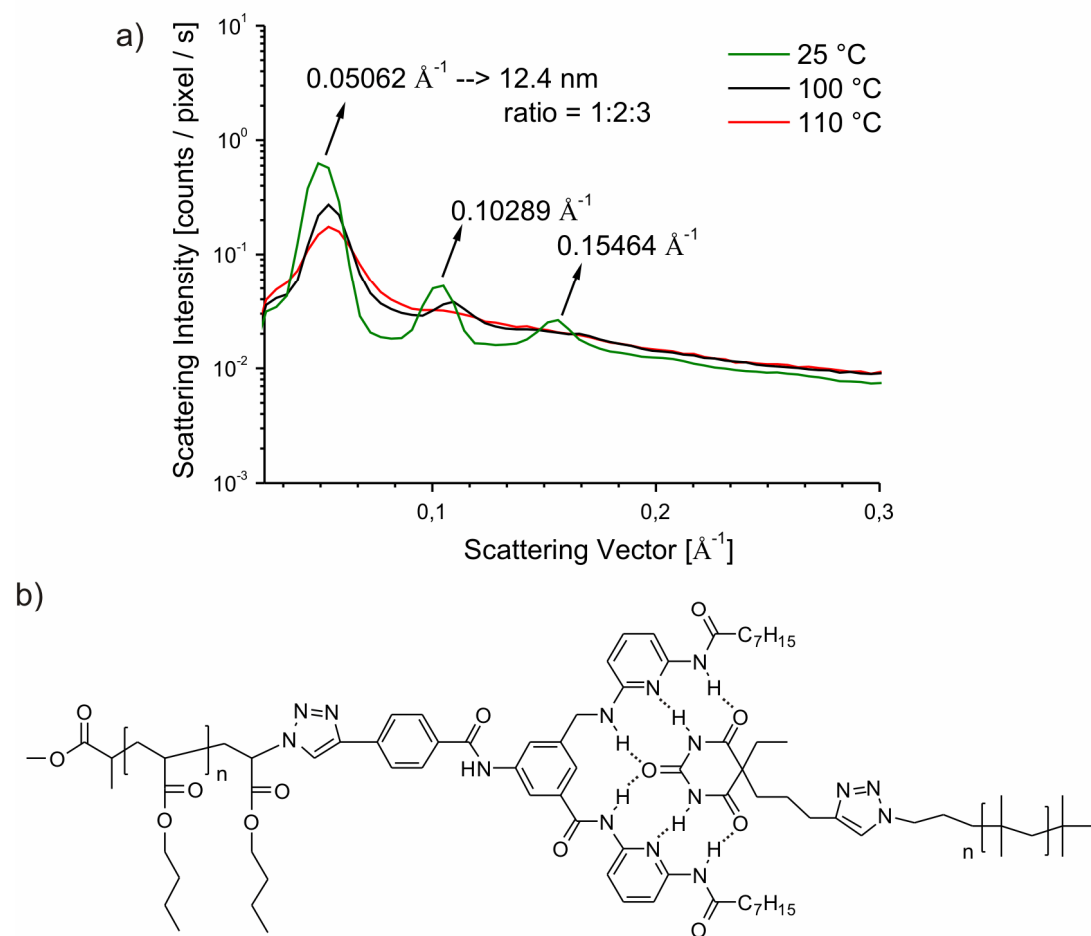


Figure 61. a) SAXS measurement indicating a lamellar microstructure of d) the supramolecular mixture of PnBA-HW-4k (**45b**; left) and PIB-BA-4k (**31b**; right).

The here conducted investigations of supramolecular polymers in the melt state reveal a deeper insight into the behavior of hydrogen bonding groups and their dynamics in polymers melts in dependence of the molecular weight of the polymers, the polarity of the polymers matrix, the strength of the hydrogen bonding motif and the functionality of the polymers. As a result, this work not only describes a broad library of investigation it further opens the possibility for continuative investigations and questions several correlations.

7. Literature

- [1] D. Philp, J. F. Stoddart, *Angew. Chem. Int. Ed.* **1996**, *35*, 1154.
- [2] G. R. Desiraju, *Nature* **2001**, *412*, 397.
- [3] D. J. Cram, *Angew. Chem. Int. Ed.* **1988**, *27*, 1009.
- [4] C. J. Pedersen, *Angew. Chem. Int. Ed.* **1988**, *27*, 1021.
- [5] J.-M. Lehn, *Angew. Chem. Int. Ed.* **1988**, *27*, 89.
- [6] J.-M. Lehn, *Angew. Chem. Int. Ed.* **1990**, *29*, 1304.
- [7] <http://www.nobelprize.org>, The Nobel Prize in Chemistry 1987, 12 Feb, **2013**.
- [8] M. M. Safont-Sempere, G. Fernández, F. Würthner, *Chem. Commun.* **2011**, *111*, 5784.
- [9] T. Aida, E. W. Meijer, S. I. Stupp, *Science* **2012**, *335*, 813.
- [10] R. Chakrabarty, P. S. Mukherjee, P. J. Stang, *Chem. Rev.* **2011**, *111*, 6810.
- [11] G. ten Brinke, J. Ruokolainen, O. Ikkala, in *Adv. Polym. Sci., Vol. 207* (Ed.: W. Binder), Springer Berlin / Heidelberg, **2007**, pp. 113.
- [12] F. Huang, O. A. Scherman, *Chem. Soc. Rev.* **2012**, *41*, 5879.
- [13] S. K. Yang, A. V. Ambade, M. Weck, *Chem. Soc. Rev.* **2011**, *40*, 129.
- [14] R. J. Wojtecki, M. A. Meador, S. J. Rowan, *Nat. Mater.* **2011**, *10*, 14.
- [15] C. Fouquey, J.-M. Lehn, A.-M. Levelut, *Adv. Mater.* **1990**, *2*, 254.
- [16] E. Kolomiets, J.-M. Lehn, *Chem. Commun.* **2005**, *12*, 1519.
- [17] J.-M. Lehn, *Prog. Polym. Sci.* **2005**, *30*, 814.
- [18] B. W. Greenland, M. B. Bird, S. Burattini, R. Cramer, R. K. O'Reilly, J. P. Patterson, W. Hayes, C. J. Cardin, H. M. Colquhoun, *Chem. Commun.* **2013**, *49*, 454.
- [19] R. Scott Lokey, B. L. Iverson, *Nature* **1995**, *375*, 303.
- [20] F. J. M. Hoeben, P. Jonkheijm, E. W. Meijer, A. P. H. J. Schenning, *Chem. Rev.* **2005**, *105*, 1491.
- [21] B. W. Greenland, S. Burattini, W. Hayes, H. M. Colquhoun, *Tetrahedron* **2008**, *64*, 8346.
- [22] S. Burattini, H. M. Colquhoun, B. W. Greenland, W. Hayes, in *Supramolecular Chemistry: From Molecules to Nanomaterials, Vol. 7* (Eds.: J. W. Steed, P. A. Gale), Wiley, **2012**, p. 3221.
- [23] S. Burattini, B. W. Greenland, D. H. Merino, W. Weng, J. Seppala, H. M. Colquhoun, W. Hayes, M. E. Mackay, I. W. Hamley, S. J. Rowan, *J. Am. Chem. Soc.* **2010**, *132*, 12051.
- [24] Y. Lei, T. P. Lodge, *Soft Matter* **2012**, *8*, 2110.
- [25] S. Roy, N. Javid, P. W. J. M. Frederix, D. A. Lamprou, A. J. Urquhart, N. T. Hunt, P. J. Halling, R. V. Ulijn, *Chem. Eur. J.* **2012**, *18*, 11723.
- [26] M. A. Aboudzadeh, M. E. Muñoz, A. Santamaría, R. Marcilla, D. Mecerreyes, *Macromol. Rapid Commun.* **2012**, *33*, 314.
- [27] M. A. Aboudzadeh, M. E. Muñoz, A. Santamaría, M. J. Fernández-Berridi, L. Irusta, D. Mecerreyes, *Macromolecules* **2012**, *45*, 7599.
- [28] G. Godeau, L. Navailles, F. Nallet, X. Lin, T. J. McIntosh, M. W. Grinstaff, *Macromolecules* **2012**, *45*, 2509.
- [29] M. Wathier, M. W. Grinstaff, *Macromolecules* **2010**, *43*, 9529.
- [30] P. Zare, A. Stojanovic, F. Herbst, J. Akbarzadeh, H. Peterlik, W. H. Binder, *Macromolecules* **2012**, *45*, 2074.
- [31] F. D. Jochum, J. Brassinne, C.-A. Fustin, J.-F. Gohy, *Soft Matter* **2013**, *9*, 2314.
- [32] D. Xu, S. L. Craig, *Macromolecules* **2011**, *44*, 5465.
- [33] D. Xu, C.-Y. Liu, S. L. Craig, *Macromolecules* **2011**, *44*, 2343.
- [34] M. Burnworth, L. Tang, J. R. Kumpfer, A. J. Duncan, F. L. Beyer, G. L. Fiore, S. J. Rowan, C. Weder, *Nature* **2011**, *472*, 334.
- [35] Y. Yan, A. de Keizer, M. Stuart, N. Besseling, in *Adv. Polym. Sci., Vol. 242* (Eds.: A. H. E. Müller, O. Borisov), Springer Berlin / Heidelberg, **2011**, pp. 91.

- [36] M. Chiper, S. Hoepfener, U. S. Schubert, C.-A. Fustin, J.-F. Gohy, *Macromol. Chem. Phys.* **2010**, *211*, 2323.
- [37] H. Danjo, K. Hirata, M. Noda, S. Uchiyama, K. Fukui, M. Kawahata, I. Azumaya, K. Yamaguchi, T. Miyazawa, *J. Am. Chem. Soc.* **2010**, *132*, 15556.
- [38] C. Mugemana, P. Guillet, C.-A. Fustin, J.-F. Gohy, *Soft Matter* **2011**, *7*, 3673.
- [39] J. B. Beck, J. M. Ineman, S. J. Rowan, *Macromolecules* **2005**, *38*, 5060.
- [40] J. B. Beck, S. J. Rowan, *J. Am. Chem. Soc.* **2003**, *125*, 13922.
- [41] Y. Yan, Y. Lin, Y. Qiao, J. Huang, *Soft Matter* **2011**, *7*, 6385.
- [42] E. A. Appel, X. J. Loh, S. T. Jones, F. Biedermann, C. A. Dreiss, O. A. Scherman, *J. Am. Chem. Soc.* **2012**.
- [43] T. Haino, A. Watanabe, T. Hirao, T. Ikeda, *Angew. Chem. Int. Ed.* **2012**, *51*, 1473.
- [44] A. Harada, R. Kobayashi, Y. Takashima, A. Hashidzume, H. Yamaguchi, *Nat. Chem.* **2011**, *3*, 34.
- [45] R. Katoono, Y. Kobayashi, M. Yamaguchi, N. Yui, *Macromol. Chem. Phys.* **2011**, *212*, 211.
- [46] C.-C. Tsai, S. Leng, K.-U. Jeong, R. M. Van Horn, C.-L. Wang, W.-B. Zhang, M. J. Graham, J. Huang, R.-M. Ho, Y. Chen, B. Lotz, S. Z. D. Cheng, *Macromolecules* **2010**, *43*, 9454.
- [47] H. Yamaguchi, R. Kobayashi, Y. Takashima, A. Hashidzume, A. Harada, *Macromolecules* **2011**, *44*, 2395.
- [48] K. Wei, J. Li, J. Liu, G. Chen, M. Jiang, *Soft Matter* **2012**, *8*, 3300.
- [49] Z.-X. Zhang, K. L. Liu, J. Li, *Macromolecules* **2011**, *44*, 1182.
- [50] Y. Xu, M. Guo, X. Li, A. Malkovskiy, C. Wesdemiotis, Y. Pang, *Chem. Commun.* **2011**, *47*, 8883.
- [51] B. Jiang, W. Tao, X. Lu, Y. Liu, H. Jin, Y. Pang, X. Sun, D. Yan, Y. Zhou, *Macromol. Rapid Commun.* **2012**, *33*, 767.
- [52] Z. Ge, H. Liu, Y. Zhang, S. Liu, *Macromol. Rapid Commun.* **2011**, *32*, 68.
- [53] T. Cai, W. J. Yang, Z. Zhang, X. Zhu, K.-G. Neoh, E.-T. Kang, *Soft Matter* **2012**, *8*, 5612.
- [54] L. Brunsveld, B. J. B. Folmer, E. W. Meijer, R. P. Sijbesma, *Chem. Rev.* **2001**, *101*, 4071.
- [55] L. Bouteiller, in *Adv. Polym. Sci., Vol. 207* (Ed.: W. Binder), Springer Berlin / Heidelberg, **2007**, pp. 79.
- [56] F. Herbst, D. Döhler, P. Michael, W. H. Binder, *Macromol. Rapid Commun.* **2013**, *34*, 203.
- [57] D. Patra, M. Ramesh, D. Sahu, H. Padhy, C.-W. Chu, K.-H. Wei, H.-C. Lin, *J. Polym. Sci. Part A: Polym. Chem.* **2011**, *50*, 967.
- [58] A. Das, M. R. Molla, B. Maity, D. Koley, S. Ghosh, *Chem. Eur. J.* **2012**, *18*, 9849.
- [59] S.-L. Li, T. Xiao, C. Lin, L. Wang, *Chem. Soc. Rev.* **2012**, *41*, 5950.
- [60] F. Grimm, N. Ulm, F. Gröhn, J. Düring, A. Hirsch, *Chem. Eur. J.* **2011**, *17*, 9478.
- [61] K. P. Nair, V. Breedveld, M. Weck, *Macromolecules* **2011**, *44*, 3346.
- [62] K. Tao, R. Bai, X. Zhao, Y. Wang, J. Li, L. Xue, *Macromol. Chem. Phys.* **2011**, *212*, 1016.
- [63] G. Gröger, W. Meyer-Zaika, C. Böttcher, F. Gröhn, C. Ruthard, C. Schmuck, *J. Am. Chem. Soc.* **2011**, *133*, 8961.
- [64] A. S. Tayi, A. K. Shveyd, A. C. H. Sue, J. M. Szarko, B. S. Rolczynski, D. Cao, T. J. Kennedy, A. A. Sarjeant, C. L. Stern, W. F. Paxton, W. Wu, S. K. Dey, A. C. Fahrenbach, J. R. Guest, H. Mohseni, L. X. Chen, K. L. Wang, J. F. Stoddart, S. I. Stupp, *Nature* **2012**, *488*, 485.
- [65] D. W. Kuykendall, C. A. Anderson, S. C. Zimmerman, *Org. Lett.* **2008**, *11*, 61.
- [66] Y. Li, T. Park, J. K. Quansah, S. C. Zimmerman, *J. Am. Chem. Soc.* **2011**, *133*, 17118.

7. Literature

- [67] C.-C. Cheng, I. H. Lin, Y.-C. Yen, C.-W. Chu, F.-H. Ko, X. Wang, F.-C. Chang, *RSC Adv.* **2012**, 2, 9952.
- [68] S. Cheng, M. Zhang, N. Dixit, R. B. Moore, T. E. Long, *Macromolecules* **2012**, 45, 805.
- [69] C.-C. Cheng, Y.-C. Yen, F.-C. Chang, *RSC Adv.* **2011**, 1, 1190.
- [70] S. Sivakova, D. A. Bohnsack, M. E. Mackay, P. Suwanmala, S. J. Rowan, *J. Am. Chem. Soc.* **2005**, 127, 18202.
- [71] O. Altintas, U. Tunca, C. Barner-Kowollik, *Polym. Chem.* **2011**, 2, 1146.
- [72] R. P. Sijbesma, F. H. Beijer, L. Brunsveld, B. J. B. Folmer, J. H. K. K. Hirschberg, R. F. M. Lange, J. K. L. Lowe, E. W. Meijer, *Science* **1997**, 278, 1601.
- [73] J. H. K. K. Hirschberg, L. Brunsveld, A. Ramzi, J. A. J. M. Vekemans, R. P. Sijbesma, E. W. Meijer, *Nature* **2000**, 407, 167.
- [74] T. Park, E. M. Todd, S. Nakashima, S. C. Zimmerman, *J. Am. Chem. Soc.* **2005**, 127, 18133.
- [75] T. Park, S. C. Zimmerman, *J. Am. Chem. Soc.* **2006**, 128, 13986.
- [76] T. Park, S. C. Zimmerman, S. Nakashima, *J. Am. Chem. Soc.* **2005**, 127, 6520.
- [77] T. Park, S. C. Zimmerman, *J. Am. Chem. Soc.* **2006**, 128, 11582.
- [78] A. J. Wilson, *Nat. Chem.* **2011**, 3, 193.
- [79] K. E. Feldman, M. J. Kade, T. F. A. de Greef, E. W. Meijer, E. J. Kramer, C. J. Hawker, *Macromolecules* **2008**, 41, 4694.
- [80] K. E. Feldman, M. J. Kade, E. W. Meijer, C. J. Hawker, E. J. Kramer, *Macromolecules* **2010**, 43, 5121.
- [81] G. B. W. L. Ligthart, H. Ohkawa, R. P. Sijbesma, E. W. Meijer, *J. Am. Chem. Soc.* **2004**, 127, 810.
- [82] L. Bouteiller, O. Colombani, F. Lortie, P. Terech, *J. Am. Chem. Soc.* **2005**, 127, 8893.
- [83] W. Knoben, N. A. M. Besseling, L. Bouteiller, M. A. Cohen-Stuart, *Phys. Chem. Chem. Phys.* **2005**, 7, 2390.
- [84] W. Knoben, N. A. M. Besseling, M. A. Cohen-Stuart, *Langmuir* **2007**, 23, 6095.
- [85] F. Lortie, S. Boileau, L. Bouteiller, *Chem.-Eur. J.* **2003**, 9, 3008.
- [86] S. K. Chang, A. D. Hamilton, *J. Am. Chem. Soc.* **1988**, 110, 1318.
- [87] S. K. Chang, D. Van Engen, E. Fan, A. D. Hamilton, *J. Am. Chem. Soc.* **1991**, 113, 7640.
- [88] W. H. Binder, S. Bernstorff, C. Kluger, L. Petraru, M. Kunz, *Adv. Mater.* **2005**, 17, 2824.
- [89] F. Herbst, K. Schröter, I. Gunkel, S. Gröger, T. Thurn-Albrecht, J. Balbach, W. H. Binder, *Macromolecules* **2010**, 43, 10006.
- [90] J. Cortese, C. Soulié-Ziakovic, S. Tencé-Girault, L. Leibler, *J. Am. Chem. Soc.* **2012**, 134, 3671.
- [91] A. Bertrand, S. Chen, G. g. Souharce, C. Ladavière, E. Fleury, J. Bernard, *Macromolecules* **2011**, 44, 3694.
- [92] O. Altintas, T. Rudolph, C. Barner-Kowollik, *J. Polym. Sci. Part A: Polym. Chem.* **2011**, 49, 2566.
- [93] B. A. Blight, C. A. Hunter, D. A. Leigh, H. McNab, P. I. T. Thomson, *Nat. Chem.* **2011**, 3, 246.
- [94] J. H. K. K. Hirschberg, A. Ramzi, R. P. Sijbesma, E. W. Meijer, *Macromolecules* **2003**, 36, 1429.
- [95] J. Sartorius, H.-J. Schneider, *Chem. Eur. J.* **1996**, 2, 1446.
- [96] G. G. Hammes, A. C. Park, *J. Am. Chem. Soc.* **1968**, 90, 4151.
- [97] S. H. M. Sontjens, R. P. Sijbesma, M. H. P. van Genderen, E. W. Meijer, *J. Am. Chem. Soc.* **2000**, 122, 7487.
- [98] S. Abed, S. Boileau, L. Bouteiller, *Macromolecules* **2000**, 33, 8479.

- [99] C. P. Lillya, R. J. Baker, S. Hutte, H. H. Winter, Y. G. Lin, J. Shi, L. C. Dickinson, J. C. W. Chien, *Macromolecules* **1992**, *25*, 2076.
- [100] R. S. Macomber, *J. Chem. Educ.* **1992**, *69*, 375.
- [101] R. E. Barrans, D. A. Dougherty, *Supramol. Chem.* **1994**, *4*, 121
- [102] M. B. Nielsen, J. O. Jeppesen, J. Lau, C. Lomholt, D. Damgaard, J. P. Jacobsen, J. Becher, J. F. Stoddart, *J. Org. Chem.* **2001**, *66*, 3559.
- [103] A. Embrechts, H. Schönherr, G. J. Vancso, *J. Phys. Chem. B* **2008**, *112*, 7359.
- [104] G. Vancso, *Angew. Chem. Int. Edit.* **2007**, *46*, 3794.
- [105] G. J. Vancso, *Angew. Chem. Int. Ed.* **2007**, *46*, 3794.
- [106] S. Zou, H. Schönherr, G. J. Vancso, *Angew. Chem. Int. Ed.* **2005**, *44*, 956.
- [107] W. Knoben, N. A. M. Besseling, M. A. Cohen-Stuart, *J. Chem. Phys.* **2007**, *126*, 024907.
- [108] P. J. Flory, *J. Am. Chem. Soc.* **1936**, *58*, 1877.
- [109] V. Berl, M. Schmutz, M. J. Krische, R. G. Khoury, J.-M. Lehn, *Chem. Eur. J.* **2002**, *8*, 1227.
- [110] K. P. Nair, V. Breedveld, M. Weck, *Soft Matter* **2011**, *7*, 553.
- [111] K. P. Nair, V. Breedveld, M. Weck, *Macromolecules* **2008**, *41*, 3429.
- [112] D. M. Loveless, S. L. Jeon, S. L. Craig, *Macromolecules* **2005**, *38*, 10171.
- [113] W. C. Yount, D. M. Loveless, S. L. Craig, *J. Am. Chem. Soc.* **2005**, *127*, 14488.
- [114] W. C. Yount, D. M. Loveless, S. L. Craig, *Angew. Chem. Int. Ed.* **2005**, *44*, 2746.
- [115] J. P. E. Rouse, *Chem. Phys.* **1953**, *21*, 1272.
- [116] B. H. Zimm, *J. Chem. Phys.* **1956**, *24*, 269.
- [117] P. G. de Gennes, *Macromolecules* **1976**, *9*, 587.
- [118] M. E. Cates, *Macromolecules* **1987**, *20*, 2289.
- [119] S. Seiffert, J. Sprakel, *Chem. Soc. Rev.* **2012**, *41*, 909.
- [120] F. Tanaka, S. F. Edwards, *Macromolecules* **1992**, *25*, 1516.
- [121] T. Vermonden, M. J. van Steenbergen, N. A. M. Besseling, A. T. M. Marcelis, W. E. Hennink, E. J. R. Sudhölter, M. A. Cohen Stuart, *J. Am. Chem. Soc.* **2004**, *126*, 15802.
- [122] J. H. K. K. Hirschberg, F. H. Beijer, H. A. van Aert, P. C. M. M. Magusin, R. P. Sijbesma, E. W. Meijer, *Macromolecules* **1999**, *32*, 2696.
- [123] R. K. Castellano, R. Clark, S. L. Craig, C. Nuckolls, J. Rebek, *PNAS* **2000**, *97*, 12418.
- [124] J. Xu, E. A. Fogleman, S. L. Craig, *Macromolecules* **2004**, *37*, 1863.
- [125] E. A. Fogleman, W. C. Yount, J. Xu, S. L. Craig, *Angew. Chem. Int. Ed.* **2002**, *41*, 4026.
- [126] T. Shikata, D. Ogata, K. Hanabusa, *J. Phys. Chem. B* **2003**, *108*, 508.
- [127] R. Granek, M. E. Cates, *J. Chem. Phys.* **1992**, *96*, 4758.
- [128] M. E. Cates, S. J. Candau, *J. Phys. Condens. Matter* **1990**, *2*, 6869.
- [129] M. E. Cates, *J. Phys. Chem.* **1990**, *94*, 371.
- [130] L. Leibler, M. Rubinstein, R. H. Colby, *Macromolecules* **1991**, *24*, 4701.
- [131] P. G. de Gennes, *J. Chem. Phys.* **1971**, *55*, 572.
- [132] M. Rubinstein, A. N. Semenov, *Macromolecules* **1998**, *31*, 1386.
- [133] A. N. Semenov, M. Rubinstein, *Macromolecules* **1998**, *31*, 1373.
- [134] K. E. Feldman, M. J. Kade, E. W. Meijer, C. J. Hawker, E. J. Kramer, *Macromolecules* **2009**, *42*, 9072.
- [135] K. Yamauchi, J. R. Lizotte, T. E. Long, *Macromolecules* **2003**, *36*, 1083.
- [136] P. Y. W. Dankers, T. M. Hermans, T. W. Baughman, Y. Kamikawa, R. E. Kieltyka, M. M. C. Bastings, H. M. Janssen, N. A. J. M. Sommerdijk, A. Larsen, M. J. A. van Luyn, A. W. Bosman, E. R. Popa, G. Fytas, E. W. Meijer, *Adv. Mater.* **2012**, *24*, 2703.
- [137] M. T. Hunley, A. S. Karikari, M. G. McKee, B. D. Mather, J. M. Layman, A. R. Fornof, T. E. Long, *Macromol. Symp.* **2008**, *270*, 1.
- [138] D. Kiriya, M. Ikeda, H. Onoe, M. Takinoue, H. Komatsu, Y. Shimoyama, I. Hamachi, S. Takeuchi, *Angew. Chem. Int. Ed.* **2012**, *51*, 1553.

7. Literature

- [139] D. J. M. van Beek, A. J. H. Spiering, G. W. M. Peters, K. te Nijenhuis, R. P. Sijbesma, *Macromolecules* **2007**, *40*, 8464.
- [140] E. Wisse, A. J. H. Spiering, F. Pfeifer, G. Portale, H. W. Siesler, E. W. Meijer, *Macromolecules* **2009**, *42*, 524.
- [141] M. M. L. Nieuwenhuizen, T. F. A. de Greef, R. L. J. van der Bruggen, J. M. J. Paulusse, W. P. J. Appel, M. M. J. Smulders, R. P. Sijbesma, E. W. Meijer, *Chem. Eur. J.* **2010**, *16*, 1601.
- [142] C. Hilger, R. Stadler, *Macromolecules* **1992**, *25*, 6670.
- [143] J. Cortese, C. Soulié-Ziakovic, M. Cloitre, S. Tencé-Girault, L. Leibler, *J. Am. Chem. Soc.* **2011**, *133*, 19672.
- [144] A. Noro, M. Hayashi, A. Ohshika, Y. Matsushita, *Soft Matter* **2011**, *7*, 1667.
- [145] A. Noro, K. Ishihara, Y. Matsushita, *Macromolecules* **2011**, *44*, 6241.
- [146] V. Abetz, A. Dardin, R. Stadler, J. Hellmann, E. T. Samulski, H. W. Spiess, *Colloid Polym. Sci.* **1996**, *274*, 723.
- [147] L. de Lucca Freitas, R. Stadler, *Colloid Polym. Sci.* **1988**, *266*, 1095.
- [148] L. L. de Lucca Freitas, R. Stadler, *Macromolecules* **1987**, *20*, 2478.
- [149] C. Hilger, R. Stadler, *Polymer* **1991**, *32*, 3244.
- [150] C. Hilger, R. Stadler, L. Liane, d. L. Freitas, *Polymer* **1990**, *31*, 818.
- [151] M. Müller, E. W. Fischer, F. Kremer, U. Seidel, R. Stadler, *Colloid Polym. Sci.* **1995**, *273*, 38.
- [152] M. Müller, U. Seidel, R. Stadler, *Polymer* **1995**, *36*, 3143.
- [153] R. Stadler, L. de Lucca Freitas, *Colloid Polym. Sci.* **1986**, *264*, 773.
- [154] M. L. Williams, R. F. Landel, J. D. Ferry, *J. Am. Chem. Soc.* **1955**, *77*, 3701.
- [155] F. Herbst, W. H. Binder, in *Self Healing Polymers* (Ed.: W. H. Binder), Wiley-VCH, **2013**.
- [156] T. F. A. de Greef, E. W. Meijer, *Nature* **2008**, *453*, 171.
- [157] F. Tournilhac, P. Cordier, D. Montarnal, C. Soulié-Ziakovic, L. Leibler, *Macromol. Symp.* **2010**, *291-292*, 84.
- [158] A. Vidyasagar, K. Handore, K. M. Sureshan, *Angew. Chem. Int. Ed.* **2011**, *50*, 8021.
- [159] A. B. W. Brochu, S. L. Craig, W. M. Reichert, *J. Biomed. Mater. Res. Part A* **2011**, *96A*, 492.
- [160] G. M. L. van Gemert, J. W. Peeters, S. H. M. Söntjens, H. M. Janssen, A. W. Bosman, *Macro. Chem. Phys.* **2012**, *213*, 234.
- [161] Y. Chen, A. M. Kushner, G. A. Williams, Z. Guan, *Nat. Chem.* **2012**, *4*, 467.
- [162] J. Hentschel, A. M. Kushner, J. Ziller, Z. Guan, *Angew. Chem. Int. Ed.* **2012**, *51*, 10561.
- [163] P. Cordier, F. Tournilhac, C. Soulie-Ziakovic, L. Leibler, *Nature* **2008**, *451*, 977.
- [164] D. Montarnal, P. Cordier, C. Soulié-Ziakovic, F. Tournilhac, L. Leibler, *J. Polym. Sci. A: Polym. Chem.* **2008**, *46*, 7925.
- [165] J. Fox, J. J. Wie, B. W. Greenland, S. Burattini, W. Hayes, H. M. Colquhoun, M. E. Mackay, S. J. Rowan, *J. Am. Chem. Soc.* **2012**, *134*, 5362.
- [166] R. Hoogenboom, *Angew. Chem. Int. Ed.* **2012**, *51*, 11942.
- [167] B. K. Kuila, M. Stamm, *Macromol. Rapid Commun.* **2010**, *31*, 1881.
- [168] E. Moulin, J.-J. Cid, N. Giuseppone, *Adv. Mater.* **2012**, *25*, 477.
- [169] K. Ariga, H. Ito, J. P. Hill, H. Tsukube, *Chem. Soc. Rev.* **2012**, *41*, 5800.
- [170] G. Song, S. M. Cho, H. J. Jung, R. H. Kim, I. Bae, H. Ahn, D. Y. Ryu, J. Huh, C. Park, *Chem. Eur. J.* **2012**, *18*, 15662.
- [171] N. Herzer, H. Guneyusu, D. J. D. Davies, D. Yildirim, A. R. Vaccaro, D. J. Broer, C. W. M. Bastiaansen, A. P. H. J. Schenning, *J. Am. Chem. Soc.* **2012**.
- [172] D. M. Bassani, *Nature* **2011**, *480*, 326.
- [173] C. Tang, E. M. Lennon, G. H. Fredrickson, E. J. Kramer, C. J. Hawker, *Science* **2008**, *322*, 429.

- [174] K. Liu, C. Wang, Z. Li, X. Zhang, *Angew. Chem. Int. Ed.* **2011**, *50*, 4952.
- [175] X. Zhang, C. Wang, *Chem. Soc. Rev.* **2011**, *40*, 94.
- [176] W. H. Binder, M. Schunack, F. Herbst, B. Pulamagatta, in *Bioinspiration and Biomimicry in Chemistry* (Ed.: G. Swiegers), Wiley-VCH, **2012**, p. 323.
- [177] S.-G. Chen, Y. Yu, X. Zhao, Y. Ma, X.-K. Jiang, Z.-T. Li, *J. Am. Chem. Soc.* **2011**, *133*, 11124.
- [178] M. Ikeda, *Bull. Chem. Soc. Jpn.* **2013**, *86*, 10.
- [179] Z.-T. Li, P. J. Stang, L. Zhao, M.-X. Wang, C.-H. Tung, in *Organic Chemistry – Breakthroughs and Perspectives*, Wiley-VCH Verlag GmbH & Co. KGaA, **2012**, pp. 477.
- [180] O. Yarimaga, J. Jaworski, B. Yoon, J.-M. Kim, *Chem. Commun.* **2012**, 48.
- [181] G. Pieters, C. Pezzato, L. J. Prins, *J. Am. Chem. Soc.* **2012**, *134*, 15289.
- [182] M. D. Ward, P. R. Raithby, *Chem. Soc. Rev.* **2013**.
- [183] C. Park, J. Lee, C. Kim, *Chem. Commun.* **2011**, *47*, 12042.
- [184] F. Rodríguez-Llansola, D. Hermida-Merino, B. Nieto-Ortega, F. J. Ramírez, J. T. L. Navarrete, J. Casado, I. W. Hamley, B. Escuder, W. Hayes, J. F. Miravet, *Chem. Eur. J.* **2012**, *18*, 14725.
- [185] A. Langner, S. L. Tait, N. Lin, R. Chandrasekar, V. Meded, K. Fink, M. Ruben, K. Kern, *Angew. Chem. Int. Ed.* **2012**, *51*, 4327.
- [186] A. Llanes-Pallas, K. Yoosaf, H. Traboulsi, J. Mohanraj, T. Seldrum, J. Dumont, A. Minoia, R. Lazzaroni, N. Armaroli, D. Bonifazi, *J. Am. Chem. Soc.* **2011**, *133*, 15412.
- [187] D. M. Loveless, N. I. Abu-Lail, M. Kaholek, S. Zauscher, S. L. Craig, *Angew. Chem. Int. Ed.* **2006**, *45*, 7812.
- [188] S. Wu, J. Huang, S. Beckemper, A. Gillner, K. Wang, C. Bubeck, *J. Mater. Chem.* **2012**, *22*.
- [189] Q.-Q. Wang, V. W. Day, K. Bowman-James, *Angew. Chem. Int. Ed.* **2012**, *51*, 2119.
- [190] D. S. Achilleos, T. A. Hatton, M. Vamvakaki, *J. Am. Chem. Soc.* **2012**.
- [191] H. Tang, C. S. de Oliveira, G. Sonntag, C. L. D. Gibb, B. C. Gibb, C. Bohne, *J. Am. Chem. Soc.* **2012**, *134*, 5544.
- [192] C. B. Aakeroy, A. Rajbanshi, J. Desper, *Chem. Commun.* **2011**, *47*, 11411.
- [193] X. Yan, F. Wang, B. Zheng, F. Huang, *Chem. Soc. Rev.* **2012**, *41*, 6042.
- [194] T. Friscic, *Chem. Soc. Rev.* **2012**, *41*, 3493.
- [195] R. Groote, B. M. Szyja, E. A. Pidko, E. J. M. Hensen, R. P. Sijbesma, *Macromolecules* **2011**, *44*, 9187.
- [196] T. Mes, M. M. E. Koenigs, V. F. Scalfani, T. S. Bailey, E. W. Meijer, A. R. A. Palmans, *ACS Macro Lett.* **2011**, *1*, 105.
- [197] J. Adisoejoso, Y. Li, J. Liu, P. N. Liu, N. Lin, *J. Am. Chem. Soc.* **2012**, *134*, 18526.
- [198] J. Rao, E. Paunescu, M. Mirmohades, I. Gadwal, A. Khaydarov, C. J. Hawker, J. Bang, A. Khan, *Polym. Chem.* **2012**, *3*, 2050.
- [199] C. Thomas, F. Peruch, B. Bibal, *RSC Adv.* **2012**, *2*, 12851.
- [200] R. Vaiyapuri, B. W. Greenland, S. J. Rowan, H. M. Colquhoun, J. M. Elliott, W. Hayes, *Macromolecules* **2012**, *45*, 5567.
- [201] A. PrevotEAU, C. Soulié-Ziakovic, L. Leibler, *J. Am. Chem. Soc.* **2012**, *134*, 19961.
- [202] J. Li, C. L. Lewis, D. L. Chen, M. Anthamatten, *Macromolecules* **2011**, *44*, 5336.
- [203] T. Ware, K. Hearon, A. Lonneck, K. L. Wooley, D. J. Maitland, W. Voit, *Macromolecules* **2012**, *45*, 1062.
- [204] M. Jiang, M. Li, M. Xiang, H. Zhou, in *Polymer Synthesis/Polymer-Polymer Complexation, Vol. 146* (Eds.: S. Inoue, S. Jacob, M. Jiang, J. P. Kennedy, M. Li, H. Sugimoto, M. Xiang, H. Zhou), Springer Berlin Heidelberg, **1999**, pp. 121. 978-3-540-65313-4
- [205] K. Dobrosielska, A. Takano, Y. Matsushita, *Macromolecules* **2009**, *43*, 1101.
- [206] W. H. Binder, M. J. Kunz, E. Ingolic, *J. Polym. Sci. A: Polym. Chem.* **2004**, *42*, 162.

7. Literature

- [207] W. H. Binder, D. Machl, *J. Polym. Sci. A: Polym. Chem.* **2005**, *43*, 188.
- [208] E. Ostas, K. Schröter, M. Beiner, T. Yan, T. Thurn-Albrecht, W. H. Binder, *J. Polym. Sci. A: Polym. Chem.* **2011**, *49*, 3404.
- [209] G. E. Moore, *Electronics* **1965**, *38*, 4.
- [210] P. Sigwalt, M. Moreau, *Prog. Polym. Sci.* **2006**, *31*, 44.
- [211] V. Volkis, R. K. Shoemaker, J. Michl, *Macromolecules* **2012**, *45*, 9250.
- [212] J. P. Kennedy, B. Iván, *Designed Polymers by CARBOCATIONIC MACROMOLECULAR ENGINEERING - Theory and Practice*, Carl Hanser Verlag, **1992**.
- [213] J. E. Puskas, G. Kaszas, *Prog. Polym. Sci.* **2000**, *25*, 403.
- [214] J. P. Kennedy, *J. Polym. Sci. A: Polym. Chem.* **1999**, *37*, 2285.
- [215] B. Iván, J. P. Kennedy, V. S., C. Chang, *J. Polym. Sci.: Polym. Chem. Ed.* **1980**, *18*, 3177.
- [216] J. P. Kennedy, R. A. Smith, *J. Polym. Sci.: Polym. Chem. Ed.* **1980**, *18*, 1523.
- [217] J. P. Kennedy, V. S. C. Chang, R. A. Smith, B. Iván, *Polym. Bull.* **1979**, *1*, 575.
- [218] G. Kaszas, M. Györ, J. P. Kennedy, T. Ferenc, *J. Macromol. Sci.-Chem.* **1982**, *18*, 1367
- [219] C. Paulo, J. E. Puskas, S. Angepat, *Macromolecules* **2000**, *33*, 4634.
- [220] J. E. Puskas, M. G. Lanzendorfer, *Macromolecules* **1998**, *31*, 8684.
- [221] J. Feldthusen, B. Iván, A. H. E. Müller, J. Kops, *Macromol. Rapid Commun.* **1997**, *18*, 417.
- [222] M. K. Mishra, C. Charles Chen, J. P. Kennedy, *Polym. Bull.* **1989**, *22*, 455.
- [223] H. Y. Yeong, B. Voit, Y. Li, F. E. Kühn, N. Radhakrishnan, *Macromol. Symp.* **2011**, *308*, 35.
- [224] P.-F. Yan, A.-R. Guo, Q. Liu, Y.-X. Wu, *J. Polym. Sci. A: Polym. Chem.* **2012**, *50*, 3383.
- [225] R. Kumar, P. Dimitrov, K. J. Bartelson, J. Emert, R. Faust, *Macromolecules* **2012**, *45*, 8598.
- [226] S. Ummadisetty, D. L. Morgan, C. D. Stokes, J. J. Harrison, C. G. Campbell, R. F. Storey, *Macromol. Symp.* **2013**, *323*, 6.
- [227] S. Ummadisetty, D. L. Morgan, C. D. Stokes, R. F. Storey, *Macromolecules* **2011**, *44*, 7901.
- [228] D. L. Morgan, C. D. Stokes, M. A. Meierhoefer, R. F. Storey, *Macromolecules* **2009**, *ASAP*.
- [229] K. L. Simison, C. D. Stokes, J. J. Harrison, R. F. Storey, *Macromolecules* **2006**, *39*, 2481.
- [230] S. Hadjikyriacou, R. Faust, *Polym. Mat. Sci. Eng.* **1997**, *76*, 300.
- [231] S. Hadjikyriacou, Z. Fodor, R. Faust, *J.M.S. - Pure Appl. Chem.* **1995**, *32*, 1137
- [232] H. Schlaad, K. Erentova, R. Faust, B. Charleux, M. Moreau, J.-P. Vairon, H. Mayr, *Macromolecules* **1998**, *31*, 8058.
- [233] A. Hanisch, H. Schmalz, A. H. E. Müller, *Macromolecules* **2012**, *45*, 8300.
- [234] A. J. D. Magenau, N. Martinez-Castro, D. A. Savin, R. F. Storey, *Macromolecules* **2009**, *42*, 8044.
- [235] R. F. Storey, C. D. Stokes, J. J. Harrison, *Macromolecules* **2005**, *38*, 4618.
- [236] S. Hadjikyriacou, R. Faust, *Macromolecules* **1999**, *32*, 6393.
- [237] P. De, R. Faust, *Macromolecules* **2006**, *39*, 7527.
- [238] U. Ojha, R. Rajkhowa, S. R. Agnihotra, R. Faust, *Macromolecules* **2008**, *41*, 3832.
- [239] R. Tripathy, U. Ojha, R. Faust, *Macromolecules* **2009**, *42*, 3958.
- [240] D. L. Morgan, N. Martinez-Castro, R. F. Storey, *Macromolecules* **2010**, *43*, 8724.
- [241] D. L. Morgan, R. F. Storey, *Macromolecules* **2009**, *42*, 6844.
- [242] A. J. D. Magenau, T. R. Hartlage, R. F. Storey, *J. Polym. Sci. A: Polym. Chem.* **2010**, *48*, 5505.

7. Literature

- [243] Y. C. Bae, Z. Fodor, R. Faust, *Macromolecules* **1997**, *30*, 198.
- [244] Y. Zhu, R. F. Storey, *Macromolecules* **2012**, *45*, 5347.
- [245] O. Adekunle, F. Herbst, K. Hackethal, W. H. Binder, *J. Polym. Sci. A: Polym. Chem.* **2011**, *49*, 2931.
- [246] B. Iván, J. P. Kennedy, *J. Polym. Sci. A: Polym. Chem.* **1990**, *28*, 89.
- [247] L. Wilczek, J. P. Kennedy, *J. Polym. Sci. A: Polym. Chem.* **1987**, *25*, 3255.
- [248] M. Gyor, H.-C. Wang, R. Faust, *J.M.S. - Pure Appl. Chem.* **1992**, *29*, 639
- [249] W. H. Binder, L. Petraru, T. Roth, P. W. Groh, V. Pálfi, S. Keki, B. Ivan, *Adv. Funct. Mater.* **2007**, *17*, 1317.
- [250] W. H. Binder, M. J. Kunz, C. Kluger, G. Hayn, R. Saf, *Macromolecules* **2004**, *37*, 1749.
- [251] E. F. Knights, H. C. Brown, *J. Am. Chem. Soc.* **1968**, *90*, 5281.
- [252] H. C. Brown, C. Snyder, B. C. S. Rao, G. Zweifel, *Tetrahedron* **1986**, *42*, 5505.
- [253] R. Appel, *Angew. Chem. Int. Ed.* **1975**, *14*, 801.
- [254] M. Ito, K. Koyakumar, T. Ohta, H. Takaya, *Synthesis* **1995**, *1995*, 376.
- [255] F. Herbst, Diploma Thesis, Institute of Chemistry, Martin-Luther-University Halle-Wittenberg, **2009**.
- [256] R. Huisgen, G. Szeimies, L. Möbius, *Chem. Ber.* **1967**, *100*, 2494.
- [257] R. Huisgen, *Pure & Appl. Chem.* **1989**, *61*, 613.
- [258] K. V. Gothelf, K. A. Jørgensen, *Chem. Rev.* **1998**, *98*, 863.
- [259] H. C. Kolb, M. G. Finn, K. B. Sharpless, *Angew. Chem. Int. Ed.* **2001**, *40*, 2004.
- [260] V. V. Rostovtsev, L. G. Green, V. V. Fokin, K. B. Sharpless, *Angew. Chem. Int. Ed.* **2002**, *41*, 2596.
- [261] W. H. Binder, R. Sachsenhofer, *Macromol. Rapid Commun.* **2007**, *28*, 15.
- [262] W. H. Binder, R. Sachsenhofer, *Macromol. Rapid Commun.* **2008**, *29*, 952.
- [263] W. H. Binder, R. Zirbs, "Click" Chemistry in Macromolecular Synthesis, John Wiley & Sons, Inc., **2009**.
- [264] W. H. Binder, F. Herbst, in *McGraw-Hill Yearbook of Science & Technology* (Ed.: D. Blumel), McGraw-Hill, **2011**. 978-0-470-56667-1
- [265] U. Mansfeld, C. Pietsch, R. Hoogenboom, C. R. Becer, U. S. Schubert, *Polym. Chem.* **2010**, *1*, 1560.
- [266] L. Liang, D. Astruc, *Coord. Chem. Rev.* **2011**, *255*, 2933.
- [267] K. Kempe, A. Krieg, C. R. Becer, U. S. Schubert, *Chem. Soc. Rev.* **2012**, *41*, 176.
- [268] V. V. Fokin, K. Matyjaszewski, in *Organic Chemistry – Breakthroughs and Perspectives*, Wiley-VCH Verlag GmbH & Co. KGaA, **2012**, pp. 247.
- [269] M. A. Harvison, A. B. Lowe, *Macromol. Rapid Commun.* **2011**, *32*, 779.
- [270] C. W. Tornøe, C. Christensen, M. Meldal, *J. Org. Chem.* **2002**, *67*, 3057.
- [271] V. Coessens, K. Matyjaszewski, *J. Macromol. Sci., Pure Appl. Chem.* **1999**, *A36(5&6)*, 667.
- [272] V. Coessens, Y. Nakagawa, K. Matyjaszewski, *Polym. Bull.* **1998**, *40*, 135.
- [273] R. Fayt, R. Forte, C. Jacobs, R. Jerome, T. Ouhadi, P. Teyssie, S. K. Varshney, *Macromolecules* **1987**, *20*, 1442.
- [274] www.polymersource.com, see poly(*n*-butyl acrylate) product sheet and references therein, accessed April 07th, **2013**.
- [275] S. Chen, M. Rocher, C. Ladaviere, J.-F. Gerard, F. Lortie, J. Bernard, *Polym. Chem.* **2012**, *3*, 3157.
- [276] J. Bernard, F. Lortie, B. Fenet, *Macromol. Rapid Commun.* **2009**, *30*, 83.
- [277] A. Bertrand, F. Lortie, J. Bernard, *Macromol. Rapid Commun.* **2012**, *33*, 2062.
- [278] O. Altintas, P. Gerstel, N. Dingenouts, C. Barner-Kowollik, *Chem. Commun.* **2010**, *46*, 6291.
- [279] B. D. Mather, J. R. Lizotte, T. E. Long, *Macromolecules* **2004**, *37*, 9331.
- [280] F. Ilhan, M. Gray, V. M. Rotello, *Macromolecules* **2001**, *34*, 2597.

7. Literature

- [281] M. L. Pellizzaro, S. A. Barrett, J. Fisher, A. J. Wilson, *Org. Biomol. Chem.* **2012**, *10*, 4899.
- [282] F. H. Beijer, R. P. Sijbesma, J. A. J. M. Vekemans, E. W. Meijer, H. Kooijman, A. L. Spek, *J. Org. Chem.* **1996**, *61*, 6371.
- [283] H.-J. Schneider, R. K. Juneja, S. Simova, *Chem. Ber.* **1989**, *122*, 1211.
- [284] M. Kunz, Dissertation - Synthese und strukturelle Untersuchungen an supramolekularen Poly(etherketon)-Poly(isobutylene) pseudo-block Copolymeren, TU Wien, Inst. f. Angewandte Synthesechemie,
- [285] T. Mezger, *Das Rheologie-Handbuch*, Vincentz Verlag, **2000**.
- [286] D. Xu, J. L. Hawk, D. M. Loveless, S. L. Jeon, S. L. Craig, *Macromolecules* **2010**, *43*, 3556.
- [287] F. van de Manakker, M. van der Pot, T. Vermonden, C. F. van Nostrum, W. E. Hennink, *Macromolecules* **2008**, *41*, 1766.
- [288] T. Shikata, T. Nishida, B. Isare, M. Linares, R. Lazzaroni, L. Bouteiller, *J. Phys. Chem. B* **2008**, *112*, 8459.
- [289] A. Noro, Y. Matsushita, T. P. Lodge, *Macromolecules* **2008**, *41*, 5839.
- [290] S. M. Aharoni, *Macromolecules* **1986**, *19*, 426.
- [291] T. G. Fox, P. J. Flory, *J. Phys. Chem.* **1951**, *55*, 221.
- [292] K. Kunal, M. Paluch, C. M. Roland, J. E. Puskas, Y. Chen, A. P. Sokolov, *J. Polym. Sci. B: Polym. Phys.* **2008**, *46*, 1390.
- [293] Y. H. Lin, *Macromolecules* **1990**, *23*, 5292.
- [294] H. Gong, M. J. Krische, *J. Am. Chem. Soc.* **2005**, *127*, 1719.
- [295] E. Wisse, A. J. H. Spiering, E. N. M. van Leeuwen, R. A. E. Renken, P. Y. W. Dankers, L. A. Brouwer, M. J. A. van Luyn, M. C. Harmsen, N. A. J. M. Sommerdijk, E. W. Meijer, *Biomacromolecules* **2006**, *7*, 3385.
- [296] A. Dardin, C. Boeffel, H. W. Spiess, R. Stadler, E. T. Samulski, *Acta Polymerica* **1995**, *46*, 291.
- [297] N. Hadjichristidis, S. Pispas, G. Floudas, *Block Copolymer Morphology*, John Wiley & Sons, Inc., **2003**.
- [298] I. W. Hamley, *The physics of block copolymers*, Oxford University Press: Oxford, New York, **1998**.
- [299] H. Hayashi, P. J. Flory, G. D. Wignall, *Macromolecules* **1983**, *16*, 1328.
- [300] A. Vananroye, P. Leen, P. Van Puyvelde, C. Clasen, *Rheol. Acta* **2011**, *50*, 795.
- [301] A. N. Gaikwad, A. Choperena, P. C. Painter, T. P. Lodge, *Macromolecules* **2010**, *43*, 4814.
- [302] R. F. M. Lange, M. V. Gulp, E. W. Meijer, *J. Polym. Sci. A: Polym. Chem.* **1999**, *37*, 3657.
- [303] L. J. Fetters, D. J. Lohse, D. Richter, T. A. Witten, A. Zirkel, *Macromolecules* **1994**, *27*, 4639.
- [304] P. Woodward, D. H. Merino, I. W. Hamley, A. T. Slark, W. Hayes, *Aust. J. Chem.* **2009**, *62*, 790.
- [305] S. D. Tobing, A. Klein, *J. Appl. Polym. Sci.* **2001**, *79*, 2230.
- [306] E. v. Ruymbeke, E. B. Muliawan, D. Vlassopoulos, H. Gao, K. Matyjaszewski, *Eur. Polym. J.* **2011**, *47*, 746.
- [307] M. Antonietti, T. Pakula, W. Bremser, *Macromolecules* **1995**, *28*, 4227.
- [308] E. van Ruymbeke, D. Vlassopoulos, M. Mierzwa, T. Pakula, D. Charalabidis, M. Pitsikalis, N. Hadjichristidis, *Macromolecules* **2010**, *43*, 4401.
- [309] C. Liu, J. He, E. v. Ruymbeke, R. Keunings, C. Bailly, *Polymer* **2006**, *47*, 4461.
- [310] R. D. Andrews, A. V. Tobolsky, *J. Polym. Sci.* **1951**, *7*, 221.
- [311] <http://www.arkema.com>, accessed March 25th, **2013**.
- [312] R. N. Keller, H. D. Wrcoff, L. E. Marchi, in *Inorg. Synth.*, Vol. 2, John Wiley & Sons, Inc., **1947**, pp. 1.

7. Literature

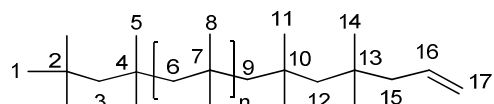
- [313] N. F. Langille, T. F. Jamison, *Org. Lett.* **2006**, *8*, 3761.
- [314] P. C. Srivastava, A. P. Callahan, E. B. Cunningham, F. F. Knapp, *J. Med. Chem.* **1983**, *26*, 742.
- [315] W. H. Binder, C. Kluger, *Macromolecules* **2004**, *37*, 9321.
- [316] E. W. Lindsell, C. Murray, P. N. Preston, T. A. J. Woodman, *Tetrahedron* **2000**, *56*, 1233.
- [317] C. Ammann, P. Meier, A. Merbach, *J. Magn. Reson.* **1982**, *46*, 319.
- [318] R. Deans, G. Cooke, V. M. Rotello, *J. Org. Chem.* **1997**, *62*, 836.
- [319] S. Coca, C. B. Jasieczek, K. L. Beers, K. Matyjaszewski, *J. Polym. Sci. A: Polym. Chem.* **1998**, *36*, 1417.
- [320] H. Ryu, L. R. Subramanian, M. Hanack, *Tetrahedron* **2006**, *62*, 6236.
- [321] M. Kurinovich, J. Lee, *J. Am. Soc. Mass. Spectrom.* **2002**, *13*, 985.

8. Appendix

8.1. Synthesis

Synthesis of allyl-functionalized poly(isobutylene)s (PIB) (5 and 6)

The synthesis was done under a dry atmosphere of nitrogen. All glassware was heated under vacuum and flushed with argon several times before chemicals were weighed in. In a three-neck round-bottom-flask, equipped with mechanical stirrer, gas tap and rubber septum, 2,6-di-*tert*-butylpyridin (DtBP), dimethylacetamide (DMA) and TiCl_4 were added to a solution of dry *n*-hexane and dry dichloromethane (v:v = 60:40). Subsequently, the solution was cooled in a MeOH/ N_2 bath (-80 °C) and the initiator was added. DCCl was prepared as a stock solution in dry *n*-hexane. The polymerization was started by addition of condensed isobutylene (precooled to -80 °C). During the polymerization the reaction temperature was held at -80 °C and the solution was stirred vigorously. After 10 min the reaction was quenched by adding allyltrimethylsilane (ATMS) and the solution was stirred for 20 min, before methanol was added. 20 min later, most of the solvent was removed by means of a rotary evaporator. *n*-Hexane was added till all polymer was dissolved. The polymer was precipitated two times in 10-fold excess of acetone/methanol (2:1). Finally, the polymer was dried at a high vacuum pump to constant weight, yielding PIB-Allyl as a clear, colorless, sticky, viscous liquid.



$^1\text{H-NMR}$ (500 MHz, CDCl_3): δ 5.84 (m, 1H, H_{16}), 5.00 (m, 2H, H_{17}), 2.01 (d, 2H, H_{15} , $^3J_{\text{H,H}} = 7.42$ Hz), 1.42 (s, $n \cdot 2\text{H}$, H_6), 1.11 (s, $n \cdot 6\text{H}$, H_8), 0.99 (s, 15 H, H_{1+5}).

$^{13}\text{C-NMR}$ (125 MHz, CDCl_3): δ 136.1 (C_{16}), 116.7 (C_{17}), 59.5 (C_6), 58.9 (C_3), 58.2 (C_9), 55.8 (C_{12}), 50.3 (C_{15}), 38.2 (C_7), 37.9 (C_4), 37.8 (C_{10}), 35.4 (C_{13}), 32.6 (C_2), 32.4 (C_1), 31.2 (C_8), 31.0 (C_5), 30.8 (C_{11}), 29.2 (C_{14}).

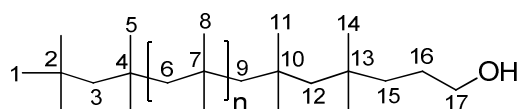


$^1\text{H-NMR}$ (500 MHz, CDCl_3): δ 7.17 (s, 3H, H_{4+6}), 5.84 (m, 2H, H_{24}), 5.00 (m, 4H, H_{25}), 2.01 (d, 4H, H_{23} , $^3J_{\text{H,H}} = 7.40$ Hz), 1.83 (s, 4H, H_9), 1.42 (s, n·2H, H_{14}), 1.11 (s, n·6H, H_{16}).

$^{13}\text{C-NMR}$ (125 MHz, CDCl_3): δ 149.0 (C_5), 148.5 (C_3), 136.1 (C_{24}), 121.2 (C_6), 120.1 (C_4), 116.7 (C_{25}), 59.5 (C_{14}), 59.4 (C_{12}), 59.1 (C_{17}), 58.6 (C_9), 55.8 (C_{20}), 50.3 (C_{23}), 39.0 (C_7), 38.2 (C_{15}), 38.0 (C_{13}), 37.9 (C_{18}), 37.8 (C_{10}), 35.4 (C_{21}), 34.8 (C_2), 32.3 (C_8), 31.6 (C_1), 31.2 (C_{16}), 31.0 (C_{11}), 30.8 (C_{19}), 29.1 (C_{22}).

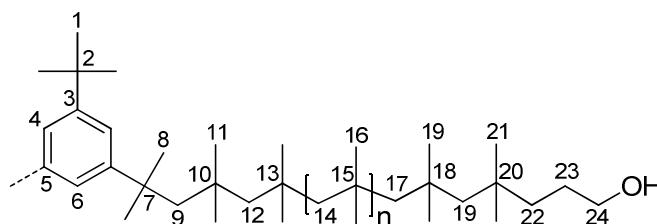
Synthesis of hydroxyl-functionalized poly(isobutylene)s (PIB) (7 and 8)

The Synthesis was done under a dry atmosphere of nitrogen. All glassware was heated under vacuum and flushed with argon several times before chemicals were weighed in. In a three-neck round-bottom flask, equipped with gas inlet tap, glass stopper, septum and magnetic stir bar, allyl-functionalized PIB (5/6) was dissolved in dry THF. The solution was sparged with nitrogen for 15 min. Subsequently, a 9-BBN solution in THF (0.5 M) was added and the solution was stirred for 6 h at room temperature. Afterwards, the solution was cooled in an ice bath (0 °C), and methanol and MCPBA (in portions of 2-4 g) were added carefully. After complete addition the reaction was stirred for 12 h at room temperature. The solution was transferred into a separating funnel and *n*-hexane (half the volume of THF) was added. The organic layer was washed with distilled water, where the pH was adjusted to 9 using K_2CO_3 , three times with a MeOH/ H_2O mixture (v:v = 3:1) and two times with distilled water. The organic layer was dried over NaSO_4 , filtered and the solvent was removed at a rotary evaporator. The crude product was dissolved in *n*-hexane and precipitated in 10-fold excess of methanol. Finally, the polymer was dried in high vacuum to constant weight, yielding hydroxyl-functionalized PIB (7/8) as a clear, colorless, sticky, viscous liquid. For experimental details see **Table 30** (appendix).



$^1\text{H-NMR}$ (500 MHz, CDCl_3): δ 3.62 (t, 2H, H_{17} , $^3J_{\text{H,H}} = 6.71$ Hz), 1.42 (s, 2·nH, H_6), 1.11 (s, 6·nH, H_8), 1.00 (s, 15H, H_{1+5}).

$^{13}\text{C-NMR}$ (125 MHz, CDCl_3): δ 64.0 (C_{17}), 59.5 (C_6), 58.8 (C_3), 58.2 (C_9), 55.6 (C_{12}), 41.5 (C_{15}), 38.2 (C_7), 37.9 (C_4), 37.8 (C_{10}), 34.8 (C_{13}), 32.6 (C_2), 32.4 (C_1), 31.2 (C_8), 30.9 (C_5), 30.8 (C_{11}), 29.4 (C_{14}), 27.8 (C_{16}).



$^1\text{H-NMR}$ (500 MHz, CDCl_3): δ 7.17 (s, 3H, H_{4+6}), 3.61 (t, 4H, H_{24} , $^3J_{\text{H,H}} = 6.70$ Hz), 1.83 (s, 4H, H_9), 1.42 (s, n·2H, H_{14}), 1.11 (s, n·6H, H_{16}).

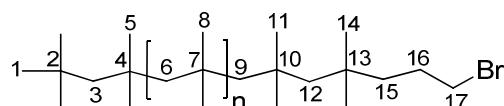
$^{13}\text{C-NMR}$ (125 MHz, CDCl_3): δ 149.0 (C_3), 148.5 (C_5), 121.2 (C_6), 120.1 (C_4), 64.0 (C_{24}), 59.5 (C_{14}), 59.3 (C_{12}), 59.1 (C_{17}), 58.6 (C_9), 55.6 (C_{19}), 41.5 (C_{22}), 39.0 (C_7), 38.2 (C_{15}), 38.0 (C_{13}), 37.9 (C_{18}), 37.8 (C_{10}), 34.8 (C_{20}), 34.8 (C_2), 32.3 (C_8), 31.7 (C_1), 31.3 (C_{16}), 30.9 (C_{11}), 30.8 (C_{19}), 29.4 (C_{21}), 27.8 (C_{23}).

Synthesis of bromine-functionalized poly(isobutylene)s (PIB) (9 and 10)

The Synthesis was done under a dry atmosphere of nitrogen. All glassware was heated under vacuum and flushed with argon several times before chemicals were weighed in. In a two-neck round-bottom flask hydroxyl-functionalized PIB (7/8) and carbon tetrabromide were dissolved in dry DCM. The solution was cooled in an ice bath (0 °C) and triphenylphosphine (TPP) dissolved in dry DCM (1 g TPP in 5 ml DCM) was added dropwise. After the addition was complete the solution was stirred for 12 h at room temperature. The solvent was removed in vacuum and the residue was suspended in *n*-hexane. The precipitate was allowed to set and the supernatant organic layer was removed via pipette. Afterwards, the precipitate was again suspended in *n*-hexane and the organic layer was removed as described. Then, the organic layers were combined and *n*-hexane was evaporated. The crude product was purified by column chromatography (SiO_2 ; *n*-hexane/ethyl acetate = 40:1) yielding bromine-functionalized PIB (9/10) as a clear, colorless, sticky, viscous liquid. For experimental details see **Table 31** (appendix).

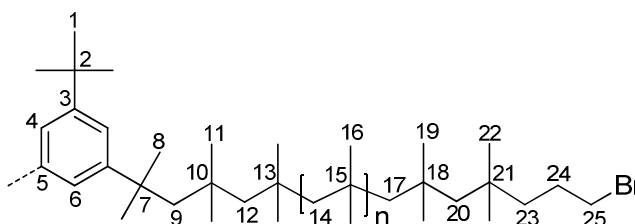
8. Appendix

TLC: *n*-hexane/ethyl acetate = 40:1; $R_f(\text{PIB-Br}) = 0.95$; $R_f(\text{TPP}) = 0$



$^1\text{H-NMR}$ (500 MHz, CDCl_3): δ 3.37 (t, 2H, H_{17} , $^3J_{\text{H,H}} = 6.91$ Hz), 1.42 (s, 2nH, H_6), 1.11 (s, 6nH, H_8), 0.99 (s, 15H, H_{1+5}).

$^{13}\text{C-NMR}$ (125 MHz, CDCl_3): δ 59.5 (C_6), 58.9 (C_3), 58.2 (C_9), 55.7 (C_{12}), 44.1 (C_{15}), 38.2 (C_7), 37.9 (C_4), 37.8 (C_{10}), 34.9 (C_{13}), 34.8 (C_{17}), 32.6 (C_2), 32.4 (C_1), 31.2 (C_8), 30.9 (C_5), 30.8 (C_{11}), 29.4 (C_{14}), 28.2 (C_{16}).



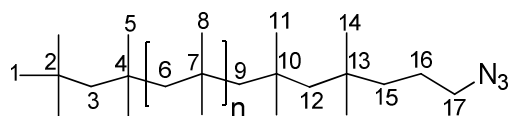
$^1\text{H-NMR}$ (500 MHz, CDCl_3): δ 7.17 (s, 3H, H_{4+6}), 3.37 (t, 4H, H_{25} , $^3J_{\text{H,H}} = 6.91$ Hz), 1.83 (s, 4H, H_9), 1.41 (s, n·2H, H_{14}), 1.11 (s, n·6H, H_{16}).

$^{13}\text{C-NMR}$ (125 MHz, CDCl_3): δ 149.0 (C_3), 148.5 (C_5), 121.2 (C_6), 120.1 (C_4), 59.5 (C_{14}), 59.2 (C_{12}), 59.1 (C_{17}), 58.6 (C_9), 55.7 (C_{20}), 44.1 (C_{23}), 39.0 (C_7), 38.2 (C_{15}), 38.0 (C_{13}), 37.9 (C_{18}), 37.8 (C_{10}), 34.9 (C_{21}), 34.8 (C_2), 34.8 (C_{25}), 32.3 (C_8), 31.6 (C_1), 31.2 (C_{16}), 30.9 (C_{11}), 30.8 (C_{19}), 29.4 (C_{22}), 28.2 (C_{24}).

Synthesis of azide-functionalized poly(isobutylene)s (PIB) (11 and 12)

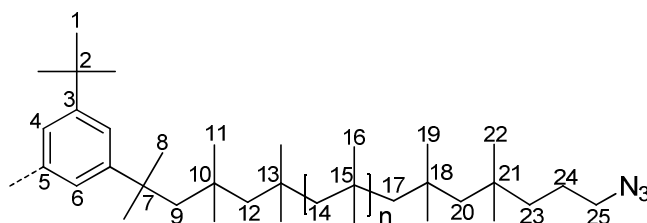
The synthesis was done under a dry atmosphere of argon. All glassware was heated under vacuum and flushed with argon several times before chemicals were weighed in. In a two-neck round-bottom flask, equipped with gas inlet tap, magnetic stir bar and septum, bromine-functionalized PIB (**9/10**) was dissolved in dry THF. Tetrabutylammonium fluoride (TBAF) was added as a 1 M solution in THF. Subsequently, azidotrimethylsilane (TMSA) was added and the solution was heated to 50 °C. The solution was stirred at 50 °C for 5 hours. Afterwards, the solvent was removed in vacuum, the residue was dissolved in *n*-hexane and washed 5 times with distilled water. The organic layer was dried over Na_2SO_4 and filtered. Then, the solvent was removed and the crude product was dried at a high vacuum pump to constant weight, yielding azide-functionalized PIB (**11/12**) as a clear, colorless, sticky, viscous liquid. For experimental details see **Table 32** (appendix).

8. Appendix



$^1\text{H-NMR}$ (500 MHz, CDCl_3): δ 3.23 (t, 2H, H_{17} , $^3J_{\text{H,H}} = 6.94$ Hz), 1.42 (s, n·2H, H_6), 1.11 (s, n·6H, H_8), 0.99 (s, 15H, H_{1+5}).

$^{13}\text{C-NMR}$ (120 MHz, CDCl_3): δ 59.5 (C_6), 58.8 (C_3), 58.2 (C_9), 55.7 (C_{12}), 52.4 (C_{17}), 42.5 (C_{15}), 38.2 (C_7), 37.8 (C_4), 37.8 (C_{10}), 34.9 (C_{13}), 32.6 (C_2), 32.4 (C_1), 31.2 (C_8), 30.9 (C_5), 30.8 (C_{11}), 29.3 (C_{14}), 24.0 (C_{16}).

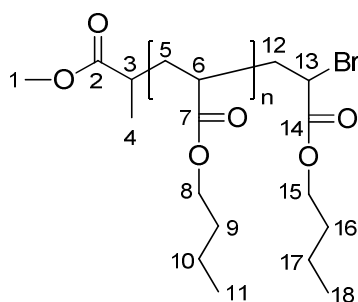


$^1\text{H-NMR}$ (500 MHz, CDCl_3): δ 7.17 (s, 3H, H_{4+6}), 3.23 (t, 4H, H_{25} , $^3J_{\text{H,H}} = 6.95$ Hz), 1.83 (s, 4H, H_9), 1.41 (s, n·2H, H_{14}), 1.11 (s, n·6H, H_{16}).

$^{13}\text{C-NMR}$ (125 MHz, CDCl_3): δ 149.0 (C_3), 148.5 (C_5), 121.2 (C_6), 120.1 (C_4), 59.5 (C_{14}), 59.2 (C_{12}), 59.1 (C_{17}), 58.6 (C_9), 55.7 (C_{20}), 52.4 (C_{25}), 42.5 (C_{23}), 39.0 (C_7), 38.2 (C_{15}), 38.0 (C_{13}), 37.8 (C_{18}), 37.8 (C_{10}), 34.9 (C_{21}), 34.8 (C_2), 32.3 (C_8), 31.6 (C_1), 31.2 (C_{16}), 30.9 (C_{11}), 30.8 (C_{19}), 29.3 (C_{22}), 24.0 (C_{24}).

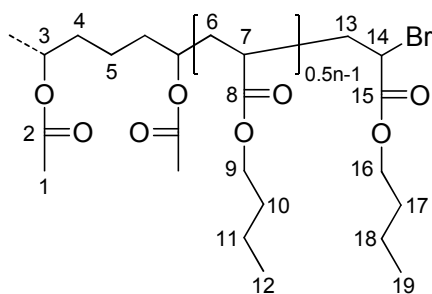
Synthesis of bromine-functionalized poly(*n*-butyl acrylate)s (PnBAs) (13 and 14)

The synthesis was accomplished via a modified method reported by Coessens *et al.*^[272] The Synthesis was done under a dry atmosphere of nitrogen. All glassware was heated under vacuum and flushed with argon several times before chemicals were weighed in. In a Schlenk-tube (50 ml) dNbpy, dry benzene and dry *n*-butyl acrylate were added. Three freeze-pump-thaw-cycles were performed and the solution was allowed to reach room temperature. The Schlenk-tube was transferred into a glove-box and Cu(I)Br was added. Then, the Schlenk-tube was removed from the glove-box and the solution was stirred for 15 min at room temperature, till all the Cu(I)Br was dissolved and the copper(I)-complex was formed (~15 min). Absolute MBPP was added and the solution was heated at 80 °C. The conversion was monitored by removing small sample volumes via syringe (0.1 ml) and conducting a GPC measurement. When the desired molecular weight was reached, the reaction was cooled to room temperature, opened to the atmosphere, THF was added (same volume as reaction volume) and the solution was stirred for 30 min. The resulting green solution was passed through an Al₂O₃-column (neutral), the solvent was removed and a small amount of THF was added. After the polymer was precipitated into a MeOH/water mixture (v:v = 6:4), the crude polymer was dissolved in THF and purified via dialyses (solvent THF; regenerated cellulose dialysis tubings; MWCO 1000) for 2, 4 and 12 h. Finally, the solvent was removed and PnBA-Br (**13/14**) was dried in high vacuum to yield a pale yellow, low viscous liquid. For experimental details see **Table 36** (appendix).



¹H-NMR (400 MHz, CDCl₃): δ 4.15 (t, 2H, ³J_{H,H} = 6.3 Hz, H₁₅), 4.01 (m, n·2H, H_{8,15,13}), 3.60 (s, 3H, H₁), 2.61 (m, 1H, H₃), 2.25 (m, n·1H, H₆), 1.88-1.33 (m, n·6H, H_{5,9,10,12,16,17}), 1.09 (d, 3H, H₄), 0.90 (t, n·3H, ³J_{H,H} = 7.35 Hz, H_{11,18}).

¹³C-NMR (100 MHz, CDCl₃): δ 176.1 (C₂), 174.3 (C₇), 169.1 (C₁₄), 65.7 (C₁₅), 64.3 (C₈), 51.4 (C₁), 41.4 (C₆), 37.2 (C₃), 36.6-34.2 (C_{9,13,16}), 31.8 (C₁₂), 30.5 (C₅), 19.0 (C_{10,17}), 16.6 (C₄), 13.6 (C_{11,18}).

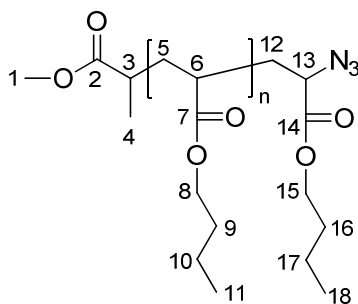


$^1\text{H-NMR}$ (400 MHz, CDCl_3): δ 4.13 (m, 4H, H_{16}), 4.01 (m, $n \cdot 2\text{H}$, $\text{H}_{3,9}$), 3.61 (s, 6H, H_1), 2.26 (m, $n \cdot 1\text{H}$, H_7), 1.87-1.16 (m, $n \cdot 6\text{H}$, $\text{H}_{4-6,10,11,13,17,18}$), 0.90 (t, $n \cdot 3\text{H}$, $^3J_{\text{H,H}} = 7.3 \text{ Hz}$, $\text{H}_{12,19}$).

$^{13}\text{C-NMR}$ (100 MHz, CDCl_3): δ 175.4 (C_2), 174.3 (C_8), 169.2 (C_{15}), 77.2 (C_3), 65.8 (C_{16}), 64.3 (C_9), 51.3 (C_1), 41.3 (C_7), 36.3-34.3 ($\text{C}_{4,10,14,17}$), 31.8 (C_{13}), 30.6 (C_6), 22.6 (C_5), 19.0 ($\text{C}_{11,18}$), 13.6 ($\text{C}_{12,19}$).

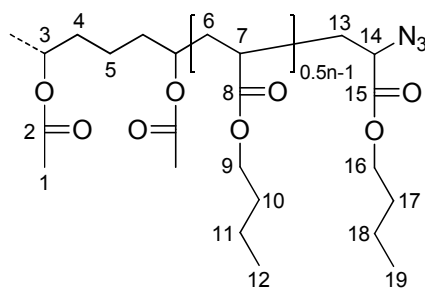
Synthesis of azide-functionalized poly(*n*-butyl acrylate)s (PnBAs) (**15** and **16**)

The synthesis was accomplished via a modified method reported by Coessens *et al.*^[271-272] In a one-neck round-bottom flask (50 ml) PnBA-Br (**13/14**) (1 equ.) was dissolved in DMF (3 mL DMF per 1 g PnBA-Br) and sodium azide (1.5 equ.) was added. The resulting solution was stirred for 5 h at 35 °C. Chloroform was added and the organic layer was washed twice with distilled water, once with Brine and once with distilled water. Then, the organic layer was dried over Na_2SO_4 , filtered and the solvent was removed. Finally, the product was dried in high vacuum to yield PnBA- N_3 (**15/16**) as a pale yellow viscous liquid.



$^1\text{H-NMR}$ (500 MHz, CDCl_3): δ 4.14 (t, 2H, $^3J_{\text{H,H}} = 6.6 \text{ Hz}$, H_{15}), 4.00 (m, $n \cdot 2\text{H}$, H_8), 3.82 (m, 1H, H_{13}), 3.61 (s, 3H, H_1), 2.54 (m, 1H, H_3), 2.25 (m, $n \cdot 1\text{H}$, H_6), 1.88-1.32 (m, $n \cdot 6\text{H}$, $\text{H}_{5,9,10,12,16,17}$), 1.08 (m, 3H, H_4), 0.89 (t, $n \cdot 3\text{H}$, H_{11+18} , $^3J_{\text{H,H}} = 7.4 \text{ Hz}$).

$^{13}\text{C-NMR}$ (125 MHz, CDCl_3): δ 176.1 (C_2), 174.9-174.0 (C_7), 169.8 (C_{14}), 65.7 (C_{15}), 64.7-64.2 (C_8), 60.2 (C_{13}), 51.4 (C_1), 41.3 (C_6), 37.2 (C_3), 36.6-33.8 (C_{9+16}), 31.7 (C_{12}), 30.5 (C_5), 19.0-17.6 (C_{10+17}), 16.7 (C_4), 13.6 (C_{11+18}).



$^1\text{H-NMR}$ (400 MHz, CDCl_3): δ 4.17 (t, 4H, $^3J_{\text{H,H}} = 4.17$ Hz, H_{16}), 4.04 (m, n·2H, $\text{H}_{3,9}$), 3.85 (m, 2H, H_{14}), 3.63 (s, 6H, H_1), 2.27 (m, n·1H, H_7), 1.90-1.19 (m, n·6H, $\text{H}_{4-6,10,11,13,17,18}$), 0.90 (t, n·3H, $^3J_{\text{H,H}} = 7.3$ Hz, $\text{H}_{12,19}$).

$^{13}\text{C-NMR}$ (100 MHz, CDCl_3): δ 175.4 (C_2), 174.4 (C_8), 169.9 (C_{15}), 77.2 (C_3), 65.8 (C_{16}), 64.4 (C_9), 51.4 (C_1), 41.4 (C_7), 36.3-34.0 ($\text{C}_{4,10,14,17}$), 31.8 (C_{13}), 30.6 (C_6), 22.6 (C_5), 19.1 ($\text{C}_{11,18}$), 13.7 ($\text{C}_{12,19}$).

8.1. NMR-titration experiments

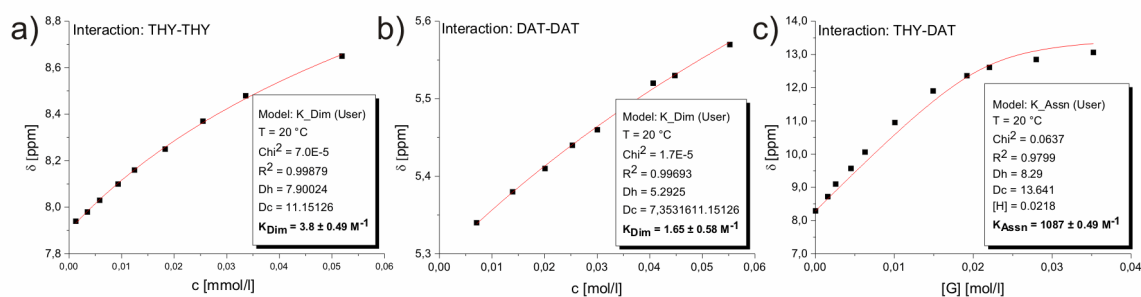


Figure 62. NMR-titration experiments in CDCl_3 for monofunctional PIBs bearing THY or DAT moieties. a) NMR-titration experiment for the THY-THY interaction using PIB-THY-4k (**38a**); b) NMR-titration experiment for the DAT-DAT interaction using PIB-DAT-4k (**41a**); c) NMR-titration experiment for the THY-DAT interaction using PIB-THY-4k (**38a**) and PIB-DAT-4k (**41a**).

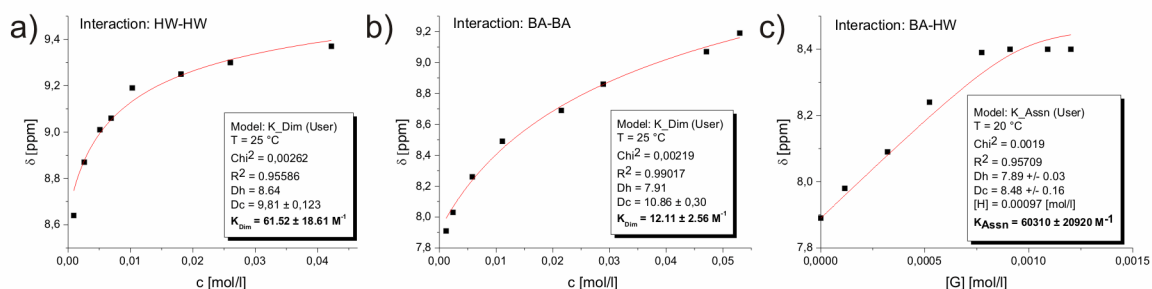


Figure 63. NMR-titration experiments in CDCl_3 for monofunctional PIBs bearing BA or HW moieties. a) NMR-titration experiment for the HW-HW interaction using PIB-HW-4k (**34b**); b) NMR-titration experiment for the BA-BA interaction using PIB-BA-4k (**31b**); c) NMR-titration experiment for the HW-BA interaction using PIB-HW-4k (**34b**) and PIB-BA-4k (**31b**).

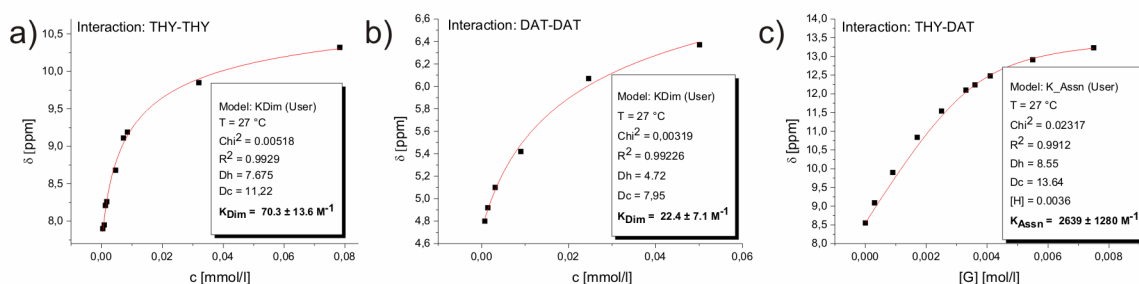


Figure 64. NMR-titration experiments in toluene- d_8 for monofunctional PnBAs bearing THY or DAT moieties. a) NMR-titration experiment for the THY-THY interaction using PnBA-THY-2k (**38a**) b) NMR-titration experiment for the DAT-DAT interaction using PnBA-DAT-2k (**41a**) c) NMR-titration experiment for the THY-DAT interaction using PnBA-THY-2k (**38a**) and PnBA-DAT-2k (**41a**).

8.2. Evaluation of MALDI-TOF-MS measurements & detailed synthesis tables

PIB-DAT-4k (**28a**)

For monofunctional PIB-DAT (**28a**) the best MALDI-TOF-MS spectrum was obtained by ionization with Li-ions (LiTFA:dithranol:analyte = 1:100:10) showing two series, where each series of peaks is separated by ~ 56 Da, the mass of the isobutylene repeating unit (calculated = 56.1 Da). The most intensive signal of the main series at 2050.592 Da can be assigned to a species $[\text{M}\cdot\text{H}]^+$ ($\text{C}_{139}\text{H}_{267}\text{N}_8$; $n = 30$), a value that agrees well with the theoretical m/z value for a species $[\text{M}\cdot\text{H}]^+$ of 2050.117 Da ($\Delta m = 232$ ppm). The most intensive signal of the minor series at 2056.598 Da can be assigned to a species $[\text{M}\cdot\text{Li}]^+$ ($\text{C}_{139}\text{H}_{266}\text{N}_8\text{Li}_1$; $n = 30$), a value that agrees well with the theoretical m/z value for a species $[\text{M}\cdot\text{Li}]^+$ of 2056.126 Da ($\Delta m = 230$ ppm).

PIB-BA₂-Cap (**33**)

For PIB-BA₂-Cap (**33**) the exchange of the acidic CO-NH-CO protons is not possible. Therefore, in contrast to PIB-BA, the MALDI-TOF-MS spectrum of PIB-BA-Cap (**33**) shows only one series, where the series of ions is separated by ~ 56.06 Da, the mass of the PIB repeating unit (calculated 56.06 Da). The most intensive signal of the main series at 2844.550 Da can be assigned to a species $[\text{M}\cdot\text{Ag}]^+$ ($\text{C}_{180}\text{H}_{336}\text{N}_{10}\text{O}_6\text{Ag}_1$; $n = 32$), a value that agrees well with the theoretical m/z value for a species $[\text{M}\cdot\text{Ag}]^+$ of 2844.5406 Da ($\Delta m = 3$ ppm). Furthermore, the calculated isotopic pattern of the main series match well with the observed pattern.

PIB-HW₂-4k (**35a**)

For PIB-HW₂-4k (**35a**) the best spectrum was obtained by ionization with Ag-ions (matrix: DCTB:AgTFA:Analyte = 100:1:10), showing one series, where each series of ions is

8. Appendix

separated by ~56 Da, the mass of the repeating unit (calculated 56.1 Da). The most intensive signal of the main series at 3440.5672 Da can be assigned to a species $[M \cdot Ag_1Li_6Na_1]^+$ ($C_{208}H_{327}N_{20}O_5Ag_1Li_6Na_1$; $n = 25$), assuming the exchange of seven of the amide protons of the Hamilton wedge by other ions,^[250] in good agreement with the theoretical m/z value for a species $[M \cdot Ag_1Li_6Na_1]^+$ ($n = 25$) of 3440.5672 Da ($\Delta m = 30$ ppm). The calculated isotopic pattern matches well with the experimental observed pattern. Although evidenced via 1H -NMR, a series originating from the incomplete functionalized product was not observed in MALDI-TOF-MS measurements, indicating only a small portion of the side-product.

PnBA-N₃-4k (15b)

For PnBA-N₃ **15b** the best spectrum was obtained by ionization with Na-ions (matrix: IAA; matrix:salt:analyte = 100:1:10). The spectrum shows three important series (see **Figure 65**), where each series of ions is separated by ~128 Da, the mass of the repeating unit (calculated 128.17 Da).

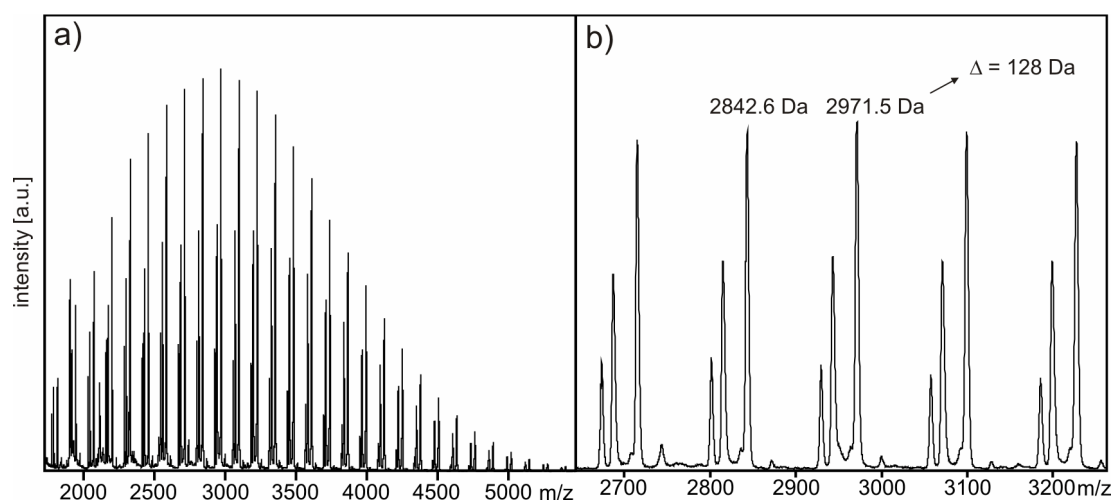


Figure 65. MALDI-TOF-MS spectrum of PnBA-N₃ (**15b**).

8. Appendix

The most intensive signal of the main series at 2971.506 Da can be assigned to a species $[M-N_3\cdot Na]^+$ ($C_{158}H_{271}N_3O_{46}Na_1$; $n = 21$), a value that agrees well with the theoretical m/z value for a species $[M\cdot Na]^+$ ($n = 21$) of 2970.889 Da ($\Delta m = 207$ ppm). For the first minor series the most intensive signal 2942.853 Da can be assigned to a species $[M-N_1\cdot Na]^+$ ($C_{158}H_{271}N_1O_{46}Na_1$; $n = 21$), which is in good agreement with the theoretical m/z value for a species $[M-N_1\cdot Na]^+$ ($n = 21$) of 2942.883 Da ($\Delta m = 10$ ppm). For this series N_2 was released from the azide end group during the ionization process. The most intensive signal of the second minor series at 2801.459 Da can be assigned to a species $[M-H_1\cdot Na]^+$ ($C_{151}H_{261}O_{44}Na_1$; $n = 20$), in good agreement with the theoretical value of 2801.804 Da ($\Delta m = 123$ ppm). Here the azide group was exchanged by a proton during the ionization process. For all series the calculated isotopic patterns match well with the observed patterns (although only visible for low molecular weight peaks).

PnBA-DAT₂-4k (42a)

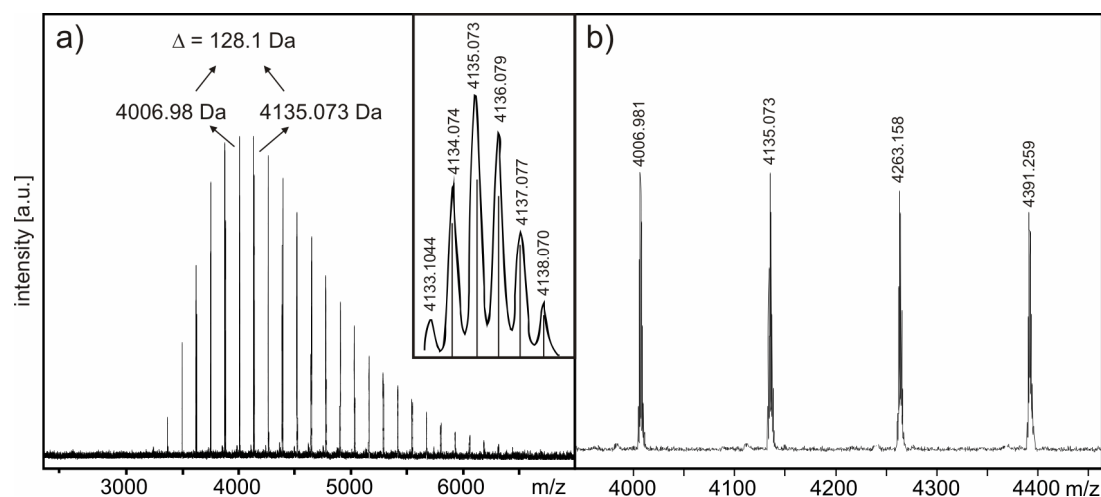


Figure 66. MALDI-TOF-MS spectrum of PnBA-DAT₂ **42a** with $M_n \approx 4000$ Da.

For PnBA-DAT₂-4k (**42a**) the best spectrum was obtained by ionization with Na-ions (matrix: IAA:NaTFA:Analyte = 100:10:1), showing one important series, where each series of ions is separated by ~ 128.1 Da, the mass of the repeating unit (calculated 128.08 Da). The most intensive signal of the main series at 4006.981 Da can be assigned to a species $[M\cdot Na]^+$ ($C_{210}H_{340}N_{16}O_{56}Na_1$; $n = 23$), in good agreement with the theoretical m/z value for a species $[M\cdot Na]^+$ ($n = 23$) of 4007.4211 Da ($\Delta m = 110$ ppm). The calculated isotopic pattern matches well with the observed pattern (see insert in **Figure 66a**).

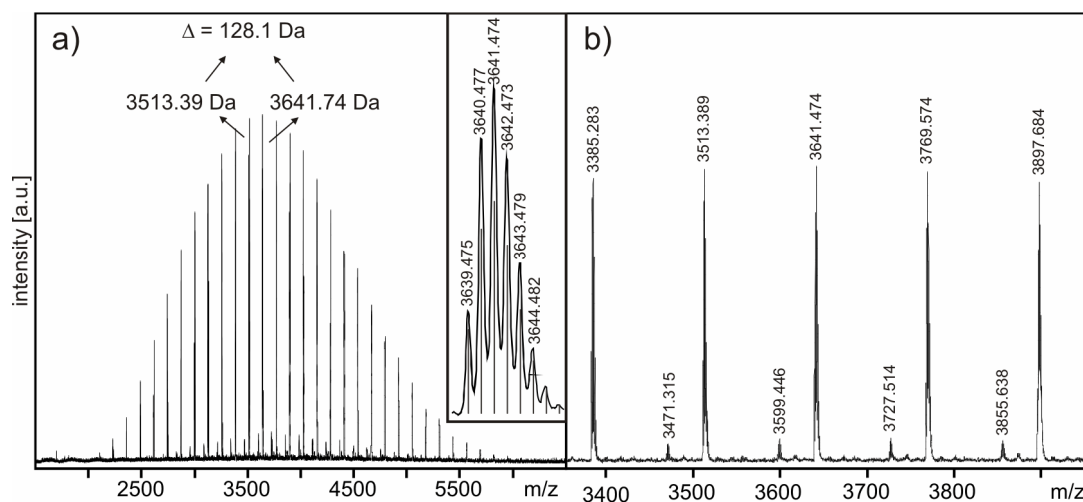
PnBA-THY₂-Cap (40)

Figure 67. MALDI-TOF-MS spectrum of PnBA-THY₂-Cap-4k (40) with $M_n \approx 4000$ Da.

For PnBA-THY₂-Cap (40) the best spectrum was obtained by ionization with Na-ions (matrix: IAA:NaTFA:Analyte = 100:10:1), showing two important series, where each series of ions is separated by ~ 128.1 Da, the mass of the repeating unit (calculated 128.1 Da). The most intensive signal of the main series at 3641.474 Da can be assigned to a species $[M \cdot Na_3]^+$ ($C_{188}H_{308}N_{10}O_{54}Na_3$; $n = 21$), in good agreement with the theoretical m/z value for a species $[M \cdot Na]^+$ ($n = 24$) of 3641.142 Da ($\Delta m = 91$ ppm). Binder *et al.* reported that the acidic $-CO-NH-CO-$ proton of the thymine group can be exchanged during the ionization process, leading to molecule ions bearing, e.g., several sodium atoms, but only one positive charge.^[250] This kind of exchange is not possible for 40 since the $-CO-NH-CO-$ position is blocked with methyl groups ($-CO-NCH_3-CO-$). Kurinovich *et al.* reported for several uracil derivatives, which are very similar to thymine, that beside the N1 and N3 sites (which are both capped in the above mentioned case), the C5 and C6 site of uracil are positions with relatively high acidity as well.^[321] Therefore, one can assume an exchange of the acidic protons of the thymine groups in the C6 position leading to a species $[M \cdot Na_3]^+$. For the first minor series the most intensive signal of the at 3727.514 Da can be assigned to a species $[M \cdot K]^+$ ($C_{194}H_{320}N_{10}O_{56}K$; $n = 22$), whereby only one of the two thymine groups bears the methyl group, indicating incomplete functionalization. Since the integration in 1H -NMR fits well with the expected values (see 5.4.11.) one can assume the content of the monofunctionalized side-product to be negligible small. The theoretical m/z value for a species $[M \cdot K]^+$ ($n = 22$) is 3727.220 Da, a value that agrees well with the signal at 3727.514 Da ($\Delta m = 79$ ppm). The calculated isotopic patterns of the main and first minor series match well with the observed patterns.

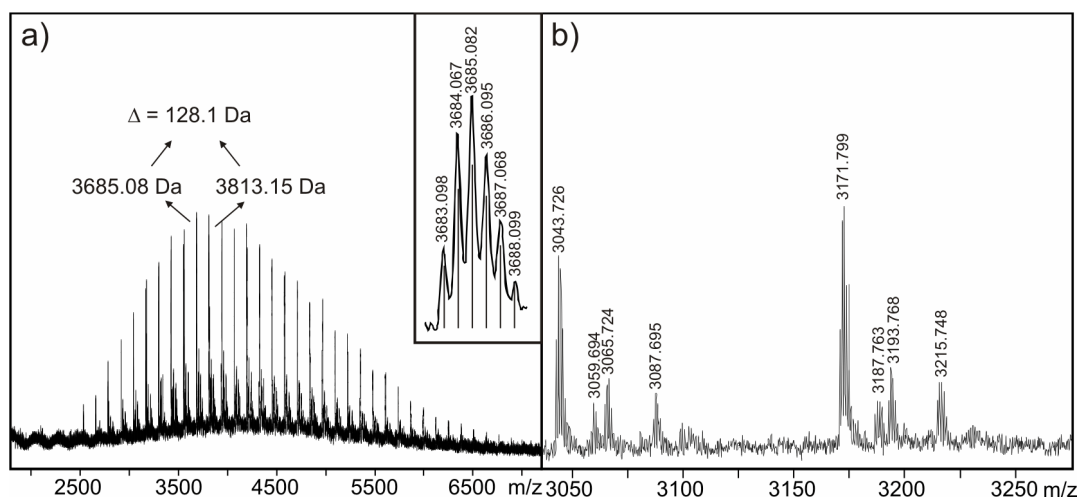
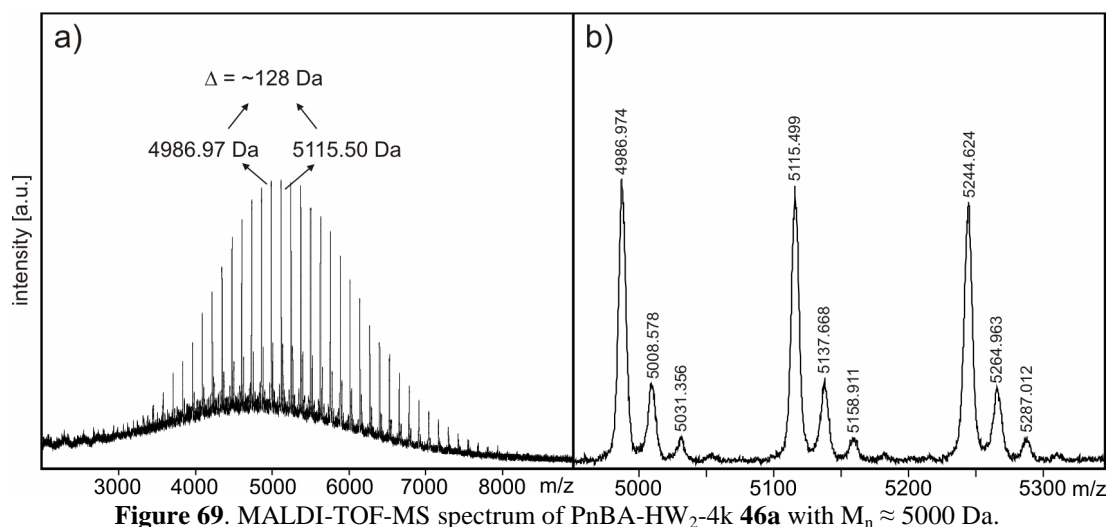
PnBA-BA₂-4k (44a)

Figure 68. MALDI-TOF-MS spectrum of PnBA-BA₂-4k **44a** with $M_n \approx 4000$ Da.

For PnBA-BA₂-4k (**44a**) the best spectrum was obtained by ionization with Na-ions (matrix: IAA:NaTFA:Analyte = 100:10:1). Four important series were visible, where each series of ions is separated by ~ 128 Da, the mass of the PnBA repeating unit (calculated 128.17 Da). The most intensive signal of the main series at 3685.082 Da can be assigned to a species $[M \cdot Na]^+$ ($C_{192}H_{318}N_{10}O_{56}Na_1$; $n = 21$), in good agreement with the theoretical m/z value of 3685.2306 Da ($\Delta m = 40$ ppm). Assuming the exchange of acidic CO–NH–CO protons of the barbituric acid groups, the most intensive peak of the first minor series at 3707.064 Da can be assigned to a species $[M \cdot Na_2]$ ($C_{192}H_{317}N_{10}O_{56}Na_2$; $n = 21$), in agreement with the theoretical m/z value of 3707.2126 Da ($\Delta m = 40$ ppm). For a species $[M \cdot K]^+$ ($C_{192}H_{318}N_{10}O_{56}K_1$; $n = 21$) the theoretical m/z value of 3701.2043 is in good agreement with the experimental value of 3701.058 Da ($\Delta m = 40$ ppm) of the second minor series. The most intensive signal of the third series at 3729.074 Da can be assigned to a species $[M \cdot Na_3]^+$ ($C_{192}H_{316}N_{10}O_{56}Na_3$; $n = 21$), in good agreement with the theoretical m/z value of 3729.1945 Da ($\Delta m = 32$ ppm).

PnBA-HW₂-4k (46a)

For PnBA-HW₂-4k (**46a**) the best spectrum was obtained by ionization with Na-ions (matrix: IAA:NaTFA:Analyte = 100:10:1). Three important series were visible, where each series of ions is separated by ~ 128 Da, the mass of the PnBA repeating unit (calculated 128.17 Da). Assuming the exchange of amide protons of the Hamilton wedge, the most intensive signal of the main series at 4986.974 Da can be assigned to a species $[M \cdot Na_1Li_5]^+$ ($C_{270}H_{411}N_{20}O_{62}Na_1Li_5$; $n = 25$), in good agreement with the theoretical m/z value of 4987.0424 Da ($\Delta m = 14$ ppm). The most intensive signal of the second series at 5264.963 Da can be assigned to a species $[M \cdot Na_2Li_5]^+$ ($C_{284}H_{434}N_{20}O_{66}Na_2Li_5$; $n = 27$), in good agreement with the theoretical m/z value of 5265.1919 Da ($\Delta m = 44$ ppm). For the third series the most intensive peak at 5158.911 Da can be assigned to a species $[M \cdot Na_3Li_5]^+$ ($C_{277}H_{421}N_{20}O_{64}Na_3Li_5$; $n = 26$), in good agreement with the theoretical m/z value of 5159.090 Da ($\Delta m = 35$ ppm).

7. Appendix

Table 29. Experimental details for the synthesis of allyl-functionalized PIBs (PIB-Allyl).

PIB	m _{th} [g]	M _{n(th)} [g/mol]	IB	V(Hex) V(DCM) [ml]	initiator	DMA	DtBP	TiCl ₄	quenching agent	M _{n(GPC)} ^c [g/mol]	M _{n(NMR)} [g/mol]	PDI	yield
5a ^a	15.0	3000	267.0 mmol	229 153	TMPCl (1)	1.91 mmol	1.91 mmol	47.4 mmol	ATMS	3080	3000	1.13	14.4 g
			24.0 ml		5.27 mmol	178 µL	429 µL	5.2 ml	15.8 mmol				96.0 %
			0.7 mol/l		900 µL	5.0 mmol/l	5 mmol/l	124 mmol/l	2.5 ml				
5b ^a	15.0	10000	267.0 mmol	160 107	TMPCl (1)	1.34 mmol	1.34 mmol	30.5 mmol	ATMS	8500	8670	1.10	14.5 g
			24.0 ml		1.52 mmol	124 µL	300 µL	3.3 ml	4.6 mmol				94.8 %
			1 mol/l		260 µL	5 mmol/l	5 mmol/l	114 mmol/l	0.7 ml				
6a ^b	13.0	3000	232.0 mmol	199 132	DCCl (2)	1.66 mmol	1.66 mmol	38.5 mmol	ATMS	2400	2380	1.12	12.4 g
			19.0 ml		4.81 mmol	154 µL	372 µL	4.2 ml	28.9 mmol				95.4 %
			0.7 mol/l		1382.1 mg	5 mmol/l	5 mmol/l	116 mmol/l	4.6 ml				
6b ^b	6.5	10000	116.0 mmol	70 46	DCCl (2)	0.58 mmol	0.58 mmol	10.7 mmol	ATMS	8600	8740	1.16	6.4 g
			9.5 ml		0.67 mmol	54 µL	130 µL	1.2 ml	4.02 mmol				98.6 %
			1 mol/l		192.5 mg	5 mmol/l	5 mmol/l	92 mmol/l	0.7 ml				

^a Monofunctional PIBs; ^b bifunctional PIBs; ^c external calibration with PIB standards.

Table 30. Experimental details for the synthesis of hydroxyl-functionalized PIBs (PIB-OH).

PIB	educt	m _{PIB-Allyl} [g]	M _{n(GPC)} ^b [g/mol]	n _{PIB-Allyl}	V(THF) [ml]	9-BBN	V(9-BBN) 0,5 M [ml]	V(MeOH)	MCPBA	m(MCPBA) 70% purity	M _{n(GPC)} ^c [g/mol]	M _{n(NMR)} [g/mol]	PDI	yield ^d
7a ^a	5a	13.8	3000	4.60 mmol	350	55.2 mmol	110.4	9.0 ml	138 mmol	34.0 g	3000	2950	1.13	13.0 g
				13.1 mmol/l		162 mmol/l		THF:MeOH	394.3 mmol/l					93.8 %
				1 equ.		12 equ.		39	30 equ.					
7b ^a	5b	16.0	8500	1.88 mmol	200	11.3 mmol	22.6	10.0 ml	56.4 mmol	13.9 g	7800	7850	1.12	15.9 g
				9.4 mmol		56.5 mmol/l		THF:MeOH	282.0 mmol/l					99.3 %
				1 equ.		6 equ.		20	30 equ.					

^a Monofunctional PIBs; ^b molecular weight of the allyl-functionalized precursor; ^c external calibration with PIB standards; ^d yield of the transformation step from PIB-Allyl to PIB-OH.

7. Appendix

Table 31. Experimental details for the synthesis of bromine-functionalized PIBs.

PIB	educt	$m_{\text{PIB-OH}}$ [g]	$M_{\text{n(GPC)}}^{\text{b}}$ [g/mol]	$n_{\text{PIB-OH}}$	V(DCM) [ml]	CBr_4	TPP	$M_{\text{n(GPC)}}^{\text{c}}$ [g/mol]	$M_{\text{n(NMR)}}^{\text{c}}$ [g/mol]	PDI	yield ^d
9a ^a	5a	13.01	3000	4.33 mmol	220	26.0 mmol	26.0 mmol	2800	2840	1.12	12.5 g
				19.7 mmol/l		8.62 g	6.82 g				96.2 %
				1 equ.		6 equ.	6 equ.				
9b ^a	5b	15.9	7800	2.04 mmol	200	12.2 mmol	12.2 mmol	7700	8000	1.12	15.7 g
				10.2 mmol/l		4.06 g	3.21 g				98.7 %
				1 equ.		6 equ.	6 equ.				

^a Monofunctional PIBs; ^b molecular weight of the hydroxyl-functionalized precursor; ^c external calibration with PIB standards; ^d yield of the transformation step from PIB-OH to PIB-Br.

Table 32. Experimental details for the synthesis of azide-functionalized PIBs.

PIB	educt	$m_{\text{PIB-Br}}$ [g]	$M_{\text{n(GPC)}}^{\text{b}}$ [g/mol]	$n_{\text{PIB-BR}}$	V(THF) [ml]	TBAF in THF 1M	TMSA	$M_{\text{n(GPC)}}^{\text{c}}$ [g/mol]	$M_{\text{n(NMR)}}^{\text{c}}$ [g/mol]	PDI	yield ^d
11a ^a	9a	12.5	2800	4.46 mmol	200	26.76 mmol	26.76 mmol	2600	2890	1.12	12.01 g
				22.32 mmol/l		26.8 ml	3.6 ml				96.1 %
				1 equ.		6 equ.	6 equ.				
11c ^a	9b	15.7	7700	2.01 mmol	220	6.03 mmol	6.03 mmol	7700	7800	1.11	15.28 g
				9.14 mmol/l		6.0 ml	0.8 ml				97.3 %
				1 equ.		3 equ.	3 equ.				

^a Monofunctional PIBs; ^b molecular weight of the hydroxyl-functionalized precursor; ^c external calibration with PIB standards; ^d yield of the transformation step from PIB-OH to PIB-Br.

7. Appendix

Table 33. Experimental details for the synthesis of 2,6-diaminotriazine-functionalized PIBs (PIB-DAT) via azide/alkyne-“click” reactions.

PIB	educt	$m_{\text{PIB-Azide}}$ [g]	M_{GPC}^c [g/mol]	$n_{\text{PIB-Azide}}$	alkyne	catalyst	TBTA	DIPEA	reaction time [h] power [W] temperature [°C]	solvent [ml]	M_n, GPC^d [g/mol]	PDI ^d	M_n, NMR [g/mol]	yield			
28a^a	11b	0.19	2800	68 μmol	88 μmol	[CuI(P(OEt ₃))]	14 μmol	140 μmol	5 100 90	iP 1.5	- ^e	- ^e	3200	74 mg			
					19.9 mg	7 μmol				W 1.5							
					11.3 mmol/l	19				2.5 mg					7.2 mg	25 μl	T 3
					1 equ.	1.3 equ.				0.1 equ.					0.2 equ.	2 equ.	= 6
28b^a	11a	2.42	2600	930 μmol	1.12 mmol	[CuI(P(OEt ₃))]	186 μmol	1.86 mmol	23 50 90	iP 10	- ^e	- ^e	4000	1.03 g			
					251.2 mg	93 μmol				W 10							
					18.6 mmol/l	19				33.2 mg					98.7 mg	332 μl	T 30
					1 equ.	1.2 equ.				0.1 equ.					0.2 equ.	2 equ.	= 50
29a^b	12a	49.5 mg	3400	15 μmol	32 μmol	[CuI(P(OEt ₃))]	6 μmol	58 μmol	21 50 90	iP 1	- ^e	- ^e	3700	45 mg			
					7.2 mg	3 μmol				W 1							
					3.7 mmol/l	19				1.0 mg					3.1 mg	10 μl	T 2
					1 equ.	2.2 equ.				0.2 equ.					0.4 equ.	4 equ.	= 4
28d^a	11c	1.52	7700	0.20 mmol	0.25 mmol	[CuI(P(OEt ₃))]	0.041 mmol	0.41 mmol	10 50 90	iP 10	- ^e	- ^e	7900	180 mg			
					56.3 mg	0.02 mmol				W 10							
					4.4 mmol/l	19				7.1 mg					21.0 mg	73 μL	T 25
					1 equ.	1.2 equ.				0.1 equ.					0.2 equ.	2 equ.	= 45
28e^a	11c	1.3	7700	0.16 mmol	0.19 mmol	[CuI(P(OEt ₃))]	32 μmol	0.32 mmol	17 50 80	iP 7	- ^e	- ^e	7600	727 mg			
					43.2 mg	16 μmol				W 7							
					5.5 mmol/l	19				5.7 mg					16.9 mg	57 μL	T 15
					1 equ.	1.2 equ.				0.1 equ.					0.2 equ.	2 equ.	= 29

^a Monofunctional PIBs; ^b bifunctional PIBs; ^c molecular weight of the azide-functionalized precursor; ^d external calibration with PIB standards; ^e M_n -values determined via GPC-measurements are considerably underestimated, probably due to interaction of the 2,6-diaminotriazine group with the column material; ^f not possible due to poor resolution of the initiator fragment. Abbreviations: iP = isopropanol; W = water; D = DMSO; T = toluene.

7. Appendix

Table 33. (continuation).

PIB	educt	$m_{\text{PIB-Azide}}$ [mg]	$M_{\text{n(GPC)}}^{\text{c}}$ [g·mol ⁻¹]	$n_{\text{PIB-Azide}}$	alkyne	catalyst	catalyst II	TBTA	DIPEA	reaction time [h] power [W] temperature [°C]	Solvent [ml]	$M_{\text{n(GPC)}}^{\text{d}}$ [g·mol ⁻¹]	PDI ^d	$M_{\text{n(NMR)}}^{\text{f}}$ [g·mol ⁻¹]	yield
28c ^a	11a	68	2600	26 μmol	31 μmol	CuSO ₄ ·5H ₂ O	NaAsc	5.2 μmol	0.1 mmol	17 50 80	iP = 1	- ^e	- ^e	2740	36 mg
					7.0 mg	5 μmol	52 μmol				W = 1.5				
				5.78 mmol/l	19	1.2 mg	10.5 mg	2.8 mg	19 μol		T 2				52.9 %
				1 equ.	1.2 equ.	0.2 equ.	2 equ.	0.2	4 equ.		= 4.5				
28f ^a	11d	89	28600	3.12 μmol	31.2 μmol	[CuI(P(OEt ₃))]	CuBr	0.6 μmol	18.7 μmol	17 100 100	T = 0.5	23500	1.1	- ^f	6.0 mg
					7.0 mg	0.3 μmol	31.2 μmol				W = 0.25				
				3.12 mmol/l	19	0.1 mg	4.5 mg	0.3 mg	3.3 μL		D = 0.25				6.7 %
				1 equ.	10 equ.	0.1 equ.	10 equ.	0.2 equ.	6 equ.		= 1				
30a ^a	11c	688	7700	89.4 μmol	0.11 mmol	[CuI(P(OEt ₃))]	-	17.9 μmol	0.18 mmol	17 25 70	T = 20	6300	1.1	8200	654 mg
					24.7 mg	8.9 μmol					W = 8				
				2.5 mmol/l	21	3.2 mg		9.5 mg	31.9 μL		iP = 8				92.1 %
				1 equ.	1.2 equ.	0.1 equ.		0.2 equ.	2 equ.		= 36				

^a Monofunctional PIBs; ^b bifunctional PIBs; ^c molecular weight of the azide-functionalized precursor; ^d external calibration with PIB standards; ^e M_{n} -values determined via GPC-measurements are considerably underestimated, probably due to interaction of the 2,6-diaminotriazine group with the column material; ^f not possible due to poor resolution of the initiator fragment. Abbreviations: iP = isopropanol; W = water; D = DMSO; T = toluene.

7. Appendix

Table 34. Experimental details for the synthesis of barbituric acid-functionalized PIBs (PIB-BA) via azide/alkyne-“click” reactions.

PIB	educt	m _{PIB-Azide} [mg]	M _{n(GPC)} ^c [g·mol ⁻¹]	n _{PIB-Azide}	alkyne 22	catalyst	catalyst II	TBTA	DIPEA	reaction time [h] power [W] temperature [°C]	solvent [ml]	M _{n(NMR)} [g·mol ⁻¹]	PDI ^d	M _{n(GPC)} ^d [g·mol ⁻¹]	yield		
31a ^a	11b	46	2800	0.017 mmol	22 μmol	[(Ph ₃ P) ₃ CuBr	–	3.4 μmol	0.10 mmol	17 50 90	iP 0.5	3800	1.2	2700	11 mg		
				6.8 mmol/l	4.9 mg	1.7 μmol					W 0.5						
					1 equ.	1.6 mg					1.8 mg					18 μL	T 1.5
						1.3 equ.					0.1 equ.					0.2 equ.	6 equ.
31b ^a	11a	599	2600	0.23 mmol	0.345 mmol	[(Ph ₃ P) ₃ CuBr	CuBr	46 μmol	1.38 mmol	7 50 80	iP 10	3800	1.1	2400	316 mg		
				5.75 mmol/l	76.7 mg	23 μmol	1.74 mmol	W 10									
					1 equ.	21.4 mg	250 mg	24 mg	246 μL		T 20						
						1.5 equ.	0.1 equ.	7.56 equ.	0.2 equ.		6 equ.					= 40	
31c ^a	11c	1000	7700	0.13 mmol	0.16 mmol	[(Ph ₃ P) ₃ CuBr	CuBr	26 μmol	0.78 mmol	17 25 90	iP 4	7000	1.1	6500	554 mg		
				8.13 mmol/l	34.7 mg	13 μmol	1.3 mmol	W 4									
					1 equ.	12.1 mg	186.4 mg	13.8 mg	139 μL		T 8						
						1.2 equ.	0.1 equ.	10 equ.	0.2 equ.		6 equ.					= 16	
31d ^a	11d	945	28600	0.033 mmol	0.13 mmol	[(Ph ₃ P) ₃ CuBr	CuBr	6.6 μmol	33 μmol	17 25 90	iP 5	– ^e	1.1	27200	479 mg		
				1.65 mol/l	30 mg	6.6 μmol	0.33 mmol	W 5									
					1 equ.	6.1 mg	7.3 mg	3.5 mg	59 μL		T 10						
						4 equ.	0.2 equ.	10 equ.	0.2 equ.		10 equ.					= 20	
32a ^b	12b	201	3200	0.063 mmol	0.14 mmol	[(Ph ₃ P) ₃ CuBr	CuBr	12.6 μmol	0.63 mmol	17 25 90	iP 1	4700	1.6	4900	33 mg		
				12.6 mmol/l	30 mg	12.6 μmol	0.063 mmol	W 1									
					1 equ.	11.7 mg	9.0 mg	6.6 mg	112 μL		T 3						
						2.2 equ.	0.2 equ.	1 equ.	0.2 equ.		10 equ.					= 5	
32c ^b	12d	477	13800	0.035 mmol	0.077 mmol	[(Ph ₃ P) ₃ CuBr	CuBr	7 μmol	0.28 mmol	17 25 90	iP 3	14000	1.2	13800	357 mg		
				2.5 mmol/l	17.1 mg	7 μmol	0.35 mmol	W 3									
					1 equ.	6.5 mg	50.20 mg	3.7 mg	50 μL		T 8						
						2.2 equ.	0.2 equ.	10 equ.	0.2 equ.		8 equ.					= 14	

^a Monofunctional PIBs; ^b bifunctional PIBs; ^c molecular weight of the azide-functionalized precursor; ^d external calibration with PIB standards; ^e not possible due to poor resolution of the initiator fragment. Abbreviations: iP = isopropanol; W = water; T = toluene.

7. Appendix

Table 34. (continuation).

PIB	educt	$m_{\text{PIB-Azide}}$ [mg]	$M_{\text{n(GPC)}}^c$ [g·mol ⁻¹]	$n_{\text{PIB-Azide}}$	alkyne 22	catalyst	catalyst II	TBTA	DIPEA	reaction time [h] power [W] temperature [°C]	solvent [ml]	$M_{\text{n(NMR)}}$ [g·mol ⁻¹]	PDI ^d	$M_{\text{n(GPC)}}^d$ [g·mol ⁻¹]	yield			
32e^b	12e	470	29200	16.1 μmol	35.3 μmol	[(Ph ₃ P) ₃ CuBr	CuBr	3.2 μmol	0.13 mmol	17 25 70	iP 2	28400	1.1	26700	256 mg			
				1.15 mmol/l	7.8 mg	3.2 μmol	0.16 mmol				3.2 μmol					23 μL	W 2	
						3 mg	23 mg										T 10	
						1 equ.	2.2 equ.										0.2 equ.	10 equ.
32b^b	12b	635	3200	0.2 mmol	0.738 mmol	[(Ph ₃ P) ₃ CuBr	CuBr	39 μmol	0.2 mmol	17 25 70	iP 15	3900	1.3	4000	443 mg			
				3.3 mmol/l	97.3 mg	39 μmol	0.2 mmol				21 mg					355 μL	W 15	
						37 mg	28.5 mg										T 30	
						1 equ.	2.2 equ.										0.2 equ.	1 equ.
32d^b	12c	589	7600	77.5 μmol	170.5 μmol	[(Ph ₃ P) ₃ CuBr	CuBr	15.5 μmol	775 μmol	17 20 70	iP 10	8700	1.2	7900	466 mg			
				1.9 mmol/l	37.9 mg	15.5 μmol	775 μmol				8.2 mg					13.8 μmol	W 10	
						14.4 mg	111.2 mg										T 20	
						1 equ.	2.2 equ.										0.2 equ.	10 equ.
33a^b	12b	190	3100	59 μmol	alkyne 23	[(Ph ₃ P) ₃ CuBr	CuBr	12 μmol	0.24 mmol	17 25 70	iP 5	3800	1.3	3700	180 mg			
				5.9 mmol/l	0.13 mmol	11.8 μmol	59 μmol				6.3 mg					43 μL	W 5	
						36.2 mg	10.9 mg										8.5 mg	T 10
						1 equ.	2.2 equ.										0.2 equ.	1 equ.

^a Monofunctional PIBs; ^b bifunctional PIBs; ^c molecular weight of the azide-functionalized precursor; ^d external calibration with PIB standards; ^e not possible due to poor resolution of the initiator fragment. Abbreviations: iP = isopropanol; W = water; T = toluene.

7. Appendix

Table 35. Experimental details for the synthesis of Hamilton wedge-functionalized PIBs (PIB-HW) via azide/alkyne-“click” reactions.

PIB	educt	m _{PIB-Azide} [mg]	M _{n(GPC)} ^c [g·mol ⁻¹]	n _{PIB-Azide}	24	catalyst	catalyst II	TBTA	DIPEA	reaction time [h] power [W] temperature [°C]	solvent [ml]	M _{n(NMR)} [g·mol ⁻¹]	PDI ^d	M _{n(GPC)} ^d [g·mol ⁻¹]	yield	
34a ^a	11b	52	2800	0.019 mmol	0.038 mmol	[(Ph ₃ P) ₃ CuBr	CuBr	3.8 μmol	114 μmol	17 50 90	iP 0.5 W 0.5 T 1.5 = 2.5	3330	1.2	3200	49 mg	
				7.6 mmol/l	28.3 g	1.9 μmol	2.0 mg								94.2 %	
				1 equ.	2 equ.	1.8 mg	0.2 equ.								6 equ.	
						0.1 equ.	excess									
34b ^a	11a	581	2600	0.22 mmol	0.396 mmol	[(Ph ₃ P) ₃ CuBr	CuBr	44 μmol	1.32 mmol	9 50 75	iP 10 W 10 T 20 = 40	3470	1.1	2900	463 mg	
				5.5 mmol/l	294.6 mg	22 μmol	1.74 mmol								63.0 %	
				1 equ.	1.8 equ.	20.5 mg	250 mg								23.3 mg	236 μL
						0.1 equ.	7.9 equ.								0.2 equ.	6 equ.
34c ^a	11c	998	7700	0.13 mmol	0.143 mmol	[(Ph ₃ P) ₃ CuBr	CuBr	13 μmol	0.14 mmol	17 25 90	iP 5 W 5 T 15 = 25	8500	1.1	8300	390 mg	
				5.2 mmol/l	106.4 mg	13 μmol	0.13 mmol								39.1 %	
				1 equ.	1.1 equ.	12.1 mg	18.7 mg								6.8 mg	25 μL
						0.1 equ.	1 equ.								0.1 equ.	1.1 equ.
34d ^a	11d	1008	28600	0.035 mmol	0.043 mmol	[(Ph ₃ P) ₃ CuBr	CuBr	7 μmol	71 μmol	17 25 90	iP 3 W 3 T 10 = 16	27700	1.1	25900	71 mg	
				2.2 mmol/l	31.5 mg	3.5 μmol	0.035 mmol								7.0 %	
				1 equ.	1.2 equ.	3.3 mg	5.1 mg								31.5 mg	12 μL
						0.1 equ.	1 equ.								0.2 equ.	2 equ.
35a ^b	12b	606	3200	0.189 mmol	0.397 mmol	[(Ph ₃ P) ₃ CuBr	CuBr	38 μmol	2.27 mmol	17 25 60	iP 10 W 10 T 20 = 40	4900	1.2	4700	384 mg	
				4.7 mmol/l	295 mg	19 μmol	0.189 mmol								43.3 %	
				1 equ.	2.1 equ.	17.5 mg	27 mg								20.2 mg	405 μL
						0.1 equ.	1 equ.								0.2 equ.	12 equ.
35b ^b	12d	284	13800	19.9 μmol	43.8 μmol	[(Ph ₃ P) ₃ CuBr	CuBr	4 μmol	79.6 μmol	17 16 60	iP 3 W 3 T 10 = 16	functionalization only 50 %		99 mg		
				1.2 mmol/l	32.6 mg	19.9 μmol	0.19 mmol							34.0 %		
				1 equ.	2.2 equ.	18.5 mg	28.5 mg							2.1 mg	14 μL	
						1 equ.	10 equ.							0.2 equ.	4 equ.	

^a Monofunctional PIBs; ^b bifunctional PIBs; ^c molecular weight of the azide-functionalized precursor; ^d external calibration with PIB standards. Abbreviations: iP = isopropanol; W = water; T = toluene.

7. Appendix

Table 36. Experimental details for the synthesis of bromine-functionalized PnBAs (PnBA-Br) via ATRP.

PnBA	m_{th} [g]	calculated conversion [%]	$M_{n(th)}$ [g/mol]	benzene [ml]	nBA	initiator	ligand	CuBr	reaction time [h]	M_{GPC}^c [g/mol]	M_{NMR} [g/mol]	PDI ^c	yield
13a^a	3.0	67	2000	5	35 mmol	MBPP	dNbpy	1.50 mmol	8	1800	2000	1.2	2.87 g
						1.50 mmol	3.00 mmol						95.0 %
					5.0 mL	167 μ L	1.23 g	215 mg					
13b^a	15	85	2800	19.7	138 mmol	MBPP	dNbpy	3.75 mmol	9.5	3200	3300	1.2	9.24
						5.36 mmol	7.50 mmol						61.6 %
					19.7 mL	598 μ L	3065 mg	538 mg					
13c^a	15	85	10000	19.7	138 mmol	MBPP	dNbpy	1.05 mmol	20.3	8000	9400	1.1	8.67 g
						1.50 mmol	2.10 mmol						57.8 %
					19.74 mL	167 μ L	858 mg	151 mg					
14a^b	15	90	4000	18.6	130 mmol	DMDBH	dNbpy	2.88 mmol	1.6	3800	4600	1.2	8.56 g
						4.11 mmol	5.75 mmol						57.1 %
					18.6 mL	894 μ L	2351 mg	413 mg					
14b^b	5	60	80000	1.9	65 mmol	DMDBH	dNbpy	0.63 mmol	42	22500	23500	1.1	4.63 g
						63 μ mol	1.26 mmol						92.6 %
					9.3	13.7 μ L	513.0 mg	90.0 mg					

^a Monofunctional PnBAs; ^b bifunctional PnBAs; ^c external calibration with PS standards.

7. Appendix

Table 37. Experimental details for the synthesis of thymine-functionalized PnBAs (PnBA-THY) via azide/alkyne-“click” reactions.

PnBA	educt	$m_{\text{PnBA-Azide}}$ [mg]	$M_n(\text{GPC})^c$ [g·mol ⁻¹]	$n_{\text{PnBA-Azide}}$	alkyne 17	catalyst	TBTA	DIPEA	reaction time power temperature	solvent [ml]	M_{GPC}^d [g/mol]	M_{NMR} [g/mol]	PDI ^d	yield
38a ^a	15a	310	1900	0.163 mmol	0.196 mmol	[(Ph ₃ P) ₃ CuBr 16.3 μmol	32.6 μmol	0.489 mmol	16 h 20 W 55 °C	THF 10	1800	2250	1.2	293 mg
				16.3 mmol/l	32.1 mg	15.2 mg	17.0 mg	87 mL						87.4 %
				1 equ.	1.2 equ.	0.1 equ.	0.2 equ.	3 equ.						
38b ^a	15b	1009	3200	0.315 mmol	0.378 mmol	CuBr 31.5 μmol	63.0 μmol	0.945 mmol	17 h 20 W 55 °C	THF 30	3300	3900	1.2	695 mg
				10.5 mmol/l	62.1 mg	4.5 mg	33.4 mg	169 μL						65.6 %
				1 equ.	1.2 equ.	0.1 equ.	0.2 equ.	3 equ.						
38c ^a	15c	1000	8000	0.125 mmol	0.163 mmol	CuBr 25 μmol	25 μmol	0.375 mmol	16 h 20 W 55 °C	THF 30	8700	10300	1.1	566 mg
				4.2 mmol/l	26.7 mg	3.6 mg	13.3 mg	67 μmol						55.1 %
				1 equ.	1.3 equ.	0.2 equ.	0.2 equ.	3 equ.						
38d ^a	15b	1062	3200	0.331 mmol	0.662 mmol	[CuI(P(OEt ₃))] 66 μmol	66 μmol	0.993 mmol	17 h 30 W 55 °C	THF 20	3100	3900	1.2	473 mg
				16.5 mmol/l	108.7 mg	23.5 mg	35.0 mg	177 μL						44.5 %
				1 equ.	2 equ.	0.2 equ.	0.2 equ.	3 equ.						
39a ^b	16a	1130	3500	0.323 mmol	0.969 mmol	CuBr 65 μmol	65 μmol	1.29 mmol	17 h 20 W 55 °C	THF 20	3000	4600	1.2	753 mg
				16.2 mmol/l	159.1 mg	9.3 mg	34.5 mg	230 μL						61.9 %
				1 equ.	3 equ.	0.2 equ.	0.2 equ.	4 equ.						
39b ^b	16b	1980	22800	0.087 mmol	0.35 mmol	CuBr 87 μmol	17 μmol	0.35 mmol	17 h 20 W 55 °C	THF 10	24100	26900	1.1	259 mg
				8.7 mmol/l	57.1 mg	12.5 mg	9.2 mg	62 μL						12.9 %
				1 equ.	4 equ.	1 equ.	0.2	4 equ.						

^a Monofunctional PnBAs; ^b bifunctional PnBAs; ^c molecular weight of the azide-functionalized precursor; ^d external calibration with PS standards.

7. Appendix

Table 38. Experimental details for the synthesis of 2,6-diaminotriazine-functionalized PnBAs (PnBA-DAT) via azide/alkyne-“click” reactions.

PnBA	educt	$m_{\text{PnBA-Azide}}$ [mg]	$M_{\text{n(GPC)}}^{\text{c}}$ [g·mol ⁻¹]	$n_{\text{PnBA-Azide}}$	alkyne 21	catalyst	TBTA	DIPEA	reaction time power temperature	solvent [ml]	$M_{\text{GPC}}^{\text{d}}$ [g/mol]	M_{NMR} [g/mol]	PDI ^d	yield				
41a ^a	15a	310	1900	0.163 mmol	0.196 mmol	CuBr	33 μmol	0.49 mmol	16 h 20 W 55 °C	THF 15	1400	2300	1.2	194 mg				
						49 μmol												
				10.9 mmol/l	49.9 mg	7.0 mg	17.3 mg	87 μL										
				1 equ.	1.2 equ.	0.3 equ.	0.2 equ.	3 equ.										
41b ^a	15b	1032	3300	0.313 mmol	0.626 mmol	[CuI(P(OEt ₃))]	63 μmol	0.94 mmol	17 h 30 W 55 °C	THF 20	2000	3800	1.2	490 mg				
						63 μmol												
				15.7 mmol/l	160.0 mg	22.3 mg	33.4 mg	168 μL										
				1 equ.	2 equ.	0.2 equ.	0.2 equ.	3 equ.										
41c ^a	15c	1070	8000	0.133 mmol	0.266 mmol	[CuI(P(OEt ₃))]	27 μmol	0.40 mmol	17 h 30 W 55 °C	THF 20	8600	10900	1.1	600 mg				
						27 μmol												
				6.7 mmol/l	68 mg	9.5 mg	14.1 mg	71 μL										
				1 equ.	2 equ.	0.2 equ.	0.2 equ.	3 equ.										
42a ^b	16a	1165	3500	0.333 mmol	1.00 mmol	CuBr	66.7 μmol	1.33 mmol	16 h 20 W 55 °C	THF 20	1700	4600	1.3	796 mg				
						0.333 mmol												
				16.7 mmol/l	255.3 mg	47.8 mg	35.3 mg	237.8 μL										
				1 equ.	3 equ.	1 equ.	0.2 equ.	4 equ.										
42b ^b	16b	2004	22800	0.87.9 μmol	0.35 mmol	CuBr	17.6 μmol	0.352 mmol	17 h 20 W 55 °C	THF 15	25500	29600	1.1	490 mg				
						35.2 μmol												
				5.9 mmol/l	89.4 mg	5.0 mg	9.3 mg	62 μL										
				1 equ.	4 equ.	0.4 equ.	0.2 equ.	4 equ.										

^a Monofunctional PnBAs; ^b bifunctional PnBAs; ^c molecular weight of the azide-functionalized precursor; ^d external calibration with PS standards.

7. Appendix

Table 39. Experimental details for the synthesis of barbituric acid-functionalized PnBAs (PnBA-BA) via azide/alkyne-“click” reactions.

PnBA	educt	$m_{\text{PnBA-Azide}}$ [mg]	$M_n(\text{GPC})^c$ [g·mol ⁻¹]	$n_{\text{PnBA-Azide}}$	alkyne 22	catalyst	TBTA	DIPEA	reaction time power temperature	solvent [ml]	M_{GPC}^d [g/mol]	M_{NMR} [g/mol]	PDI ^d	yield			
43a	15b	1018	3300	0.308 mmol	82.2 mg	CuBr	62 μ mol	0.924 mmol	17 h 20 W 55 °C	THF 12	2700	3400	1.2	651.0 mg			
				25.7 mmol/l	0.37 mmol	0.308 mmol								44.2 mg	32.9 mg	165 μ L	60.0 %
				1 equ.	1.2 equ.	1 equ.								0.2 equ.	3 equ.		
43b	15c	1066	8000	0.133 mmol	35.6 mg	CuBr	27 μ mol	0.399 mmol	17 h 20 W 55 °C	THF 12	9400	10200	1.2	790.0 mg			
				11.1 mmol/l	0.16 mmol	0.133 mmol								19.1 mg	14.3 mg	71.2 μ L	72.5 %
				1 equ.	1.2 equ.	1 equ.								0.2 equ.	3 equ.		
44a	16a	1005	3500	0.287 mmol	191.3 mg	CuBr	86 μ mol	1.15 mmol	17 h 20 W 55 °C	THF 15	4700	4700	1.2	590 mg			
				19.1 mmol/l	0.861 mmol	0.287 mmol								41.2 mg	45.6 mg	205 μ L	53.2 %
				1 equ.	3 equ.	1 equ.								0.3 equ.	4 equ.		

^a Monofunctional PnBAs; ^b bifunctional PnBAs; ^c molecular weight of the azide-functionalized precursor; ^d external calibration with PS standards.

7. Appendix

Table 40. Experimental details for the synthesis of Hamilton wedge-functionalized PnBAs (PnBA-HW) via azide/alkyne-“click” reactions.

PnBA	educt	$m_{\text{PnBA-Azide}}$ [mg]	$M_{n(\text{GPC})}^c$ [g·mol ⁻¹]	$n_{\text{PnBA-Azide}}$	alkyne 24	catalyst	TBTA	DIPEA	reaction time power temperature	solvent [ml]	M_{GPC}^d [g/mol]	M_{NMR} [g/mol]	PDI ^d	yield
45a	15c	597	9800	0.061 mmol	0.064 mmol	CuBr 0.061 mmol	0.012 mmol	0.183 mmol	17 h 20 W 55 °C	THF 8	10200	10800	1.1	152.0 mg
				7.6 mmol/l	47.6 mg	8.8 mg	6.3 mg	33 µL						23.7 %
				1 equ.	1.05 equ.	1 equ.	0.2 equ.	3 equ.						
45b	15b	930	3400	0.274 mmol	0.273 mmol	CuBr 0.274 mmol	54.8 µmol	0.822 mmol	17 h 20 W 55 °C	THF 12	4200	4000	1.1	412.0 mg
				22.8 mmol/l	203.0 mg	40.0 mg	30.7 mg	147 µL						36.4 %
				1 equ.	1 equ.	1 equ.	0.2 equ.	3 equ.						
46a	16a	795	4300	0.185 mmol	0.389 mmol	CuBr 0.185 mmol	74 µmol	0.74 mmol	17 h 20 W 55 °C	THF 7	5800	5500	1.1	610.0 mg
				26.4 mmol/l	289 mg	26.5 mg	39.3 mg	134 µL						57.0 %
				1 equ.	2.1 equ.	1 equ.	0.4 equ.	4 equ.						

^a Monofunctional PnBAs; ^b bifunctional PnBAs; ^c molecular weight of the azide-functionalized precursor; ^d external calibration with PnBA standards.

8.3. List of publications

Herbst, F.; Schröter, K.; Gunkel, I.; Gröger, S.; Thurn-Albrecht, T.; Balbach, J.; Binder, W. H., **Aggregation and Chain Dynamics in Supramolecular Polymers by Dynamic Rheology: Cluster Formation and Self-Aggregation.** *Macromolecules* **2010**, *43* (23), 10006-10016.

Herbst, F.; Schulz, M.; Binder, W. H., **Ordentlich dynamisch: Supramolekulare Polymere.** *Nachr. Chem.* **2010**, *58* (7-8), 734-739.

Binder, W. H.; Enders, C.; Herbst, F.; Hackethal, K., **Synthesis and Self-Assembly of Hydrogen-Bonded Supramolecular Polymers.** In *Complex Macromolecular Architectures: Synthesis, Characterization and Self Assembly*, Hadjichristidis, N.; Hirao, A.; Tezuka, Y.; Du Prez, F., Eds. Wiley-VCH: **2011**.

Binder, W. H.; Herbst, F., **Click chemistry in polymer science.** In *McGraw-Hill Yearbook of Science & Technology*, Blumel, D., Ed. McGraw-Hill: **2011**.

Adekunle, O.; Herbst, F.; Hackethal, K.; Binder, W. H., **Synthesis of nonsymmetric chain end functionalized polyisobutylenes.** *J. Polym. Sci. A: Polym. Chem.* **2011**, *49* (13), 2931-2940.

Zare, P.; Stojanovic, A.; Herbst, F.; Akbarzadeh, J.; Peterlik, H.; Binder, W. H., **Hierarchically Nanostructured Polyisobutylene-Based Ionic Liquids.** *Macromolecules* **2012**, *45* (4), 2074-2084.

Pulamagatta, B.; Ostas, E.; Herbst, F.; Struth, B.; Binder, W. H., **Shear induced structure orientation in norbornene block copolymers: In situ Rheo-SAXS investigations.** *Eur. Polym. J.* **2012**, *48* (6), 1127-1134.

Binder, W. H.; Schunack, M.; Herbst, F.; Pulamagatta, B., **Biomimetic Principles in Macromolecular Science.** In *Bioinspiration and Biomimicry in Chemistry*, Swiegers, G., Ed. Wiley-VCH: **2012**.

Herbst, F.; Seiffert, S.; Binder, W. H., **Dynamic supramolecular poly(isobutylene)s for self-healing materials.** *Polym. Chem.* **2012**, *3* (11), 3084-3092.

(This article has been identified as a 'Paper-of-the-week' for Polymer Chemistry. The article has been highlighted on the blog of Polymer Chemistry.)

Hackethal, K.; Herbst, F.; Binder, W. H., **Synthesis and clustering of supramolecular "graft" polymers.** *J. Polym. Sci. A: Polym. Chem.* **2012**, *50* (21), 4494-4506.

Herbst, F.; Döhler, D.; Michael P.; Binder, W. H., **Self-healing polymers via supramolecular forces.** *Macromol. Rapid Commun.* **2013**, *34* (3), 203-220.

7. Appendix

Herbst, F.; Binder, W. H., **Self-healing polymers via supramolecular, hydrogen bonded networks**. In *Self Healing Polymers*, Binder, W. H., Ed. Wiley-VCH: **2013**.

Herbst, F.; Binder, W. H., **Comparing solution and melt-state association of hydrogen bonds in supramolecular polymers**. *Polym. Chem.* **2013**, 4, 3602-3609.

Danksagung

Ich bedanke mich bei meinem Betreuer Prof. Dr. Wolfgang H. Binder für die Überlassung des interessanten Themas, die vielen fruchtbaren Diskussionen und Anregungen sowie die Möglichkeit die Arbeit selbst mitgestalten zu können.

Bei der gesamten Arbeitsgruppe bedanke ich mich für die angenehme Arbeitsatmosphäre. Besonders danke ich meinen Kollegen aus dem Büro und Labor 3.03 für die schöne Zeit, auch weit über die Laborarbeit hinaus. Auch gilt mein herzlicher Dank den „3 Säulen der Arbeitsgruppe“ (Susanne Tanner, Anke Hassi und Normen Diedrich) für die unermüdliche Hilfe durch die Übernahme unzähliger kleiner und großer Aufgaben.

Bei der gesamten Arbeitsgruppe um Prof. Dr. Thomas Thurn-Albrecht bedanke ich mich für die angenehme Kooperation und die ertragreichen Diskussionen. Besonderer Dank gilt dabei Dr. Klaus Schröter für die zahlreichen Hilfestellungen und anschaulichen Erklärungen. Auch danke ich Dr. Ilja Gunkel und M.Sc. Tingzi Yan für die Durchführung der SAXS-Messungen.

Dr. Sebastian Seiffert danke ich für die fruchtbare Zusammenarbeit im Rahmen der Publikation in Polym. Chem.

Prof. Dr. Sybrand van der Zwaag und Ph.D. Ranjita Bose danke ich für die Durchführung der DMA-Untersuchungen.

Bei der Arbeitsgruppe „NMR“ um Dr. Dieter Ströhl und der Arbeitsgruppe von Prof. Dr. Jochen Balbach, besonders seinem Mitarbeiter Stefan Gröger, bedanke ich mich für die Anfertigung der NMR-Spektren.

Bei meiner Familie, meinen Freunden und den Teamkollegen der Saalebiber bedanke ich mich für immerwährende Unterstützung und das entgegengebrachte Verständnis.

Bei meiner Frau Sabine Herbst bedanke ich mich für die unzähligen kleinen und großen Dinge, die zum Erfolg dieser Arbeit beigetragen haben.

Lebenslauf

Dipl. Chem. Florian Herbst

Werrastraße 18

D-06122 Halle

Herbst.Florian@gmx.de

geboren am 10.12.1984 in Halle (Saale)

verheiratet, keine Kinder

Staatsangehörigkeit: deutsch



Berufserfahrung

seit 04 / 2013

DOMO Caproleuna GmbH

wissenschaftlicher Mitarbeiter im Bereich Entwicklung und Qualitätskontrolle (www.domochemicals.com)

10 / 2009 – 03 / 2013

Universität Halle

wissenschaftlicher Mitarbeiter in der Arbeitsgruppe von Prof. Wolfgang H. Binder (Makromolekulare Chemie); Promotion auf dem Gebiet der supramolekularen Polymere

Studium

08 / 2009

Abschluss der Diplomarbeit (Prädikat: *sehr gut*)
Gesamtnote: 1,1

10 / 2008 – 08 / 2009

Anfertigung der Diplomarbeit in der Arbeitsgruppe von Prof. Wolfgang H. Binder (Makromolekulare Chemie)

10 / 2007 – 09 / 2008

Vertiefungsstudium im Bereich
„Makromolekulare Chemie/Polymerchemie“

10 / 2004 – 09 / 2007

Grundstudium Chemie an der
Martin-Luther-Universität Halle-Wittenberg

Schule

09 / 1995 – 07 / 2004

Abitur am Frieden-Gymnasium in Halle

09 / 1991 – 07 / 1995

Grundschule „Frieden“ in Halle

Eigenständigkeitserklärung

Hiermit erkläre ich an Eides statt, dass ich die vorliegende Arbeit selbstständig und ohne fremde Hilfe verfasst habe. Andere als die angegebenen Quellen und Hilfsmittel wurden nicht benutzt und die den benutzten Werken wörtlich oder inhaltlich entnommenen Stellen wurden als solche kenntlich gemacht.

Halle, den

Florian Herbst